UNIVERSITÀ DEGLI STUDI DI TRIESTE

Università Ca'Foscari Venezia

UNIVERSITÀ DEGLI STUDI DI TRIESTE

E

UNIVERSITÀ CA' FOSCARI DI VENEZIA

XXXVII CICLO DEL DOTTORATO DI RICERCA IN CHIMICA

Chirality effects on peptide dynamic covalent libraries

Settore scientifico-disciplinare: **CHIM/06**

DOTTORANDA
Erica Scarel

COORDINATORE
PROF. Enzo Alessio

SUPERVISORE DI TESI
PROF. Silvia Marchesan

CO-SUPERVISORE DI TESI
PROF. Silvano Geremia

ANNO ACCADEMICO 2023/2024

“I peptidi sono come i maiali. Non si butta via niente”

“*Peptides are like pigs. Everything is used but the oink."*

Table of contents

Table of contents 3
List of abbreviations 8
Abstract 9
Riassunto 10
Chapter 1: General introduction 11
1.1 – Supramolecular chemistry 11
1.1.1 – Self-assembly and non-covalent interactions 12
1.2 – Peptide self-assembly 14
1.2.1 – Short-peptide hydrogels as nanostructured materials 16
1.2.2 – Cyclopeptide nanotubes 19
1.3 – Dynamic-covalent chemistry and self-assembly 24
1.3.1 – Thiol/disulfide exchange reaction 25
Chapter 2: Aim of the project 31
Chapter 3: Dynamic-covalent libraries of Cys-Phe-Cys 34
3.1 – Tripeptide synthesis 34
3.2 – Kinetic studies of Cys-Phe-Cys DCL 35
3.3 – Hydrogel characterisation 39
3.4 – Identification of the DCL gelator 43
Chapter 4: Homochirality and nanotubes 47
4.1 – Introduction and main results 47
4.2 – NMR investigation of cyclic dimers 48
4.2.1 – Antiparallel cyclic dimer ROESY 50
4.2.2 – Parallel cyclic dimer ROESY 51
4.3 – Single-crystal XRD of cyclic dimers 53

4.3.1 – Antiparallel cyclic dimer....55
4.3.2 – Parallel cyclic dimer....58
4.4 – Comparison between antiparallel and parallel cyclic dimer....60
Chapter 5: Heterochiral cyclic dimers....62
5.1 – DLL antiparallel cyclic dimer....62
5.1.1 – DLL Antiparallel cyclic dimer ROESY....63
5.1.2 – DLL antiparallel cyclic dimer XRD....64
5.2 – LDL antiparallel cyclic dimer....66
5.3 – LDL antiparallel cyclic trimer from crystallisation trials on the pentamer....69
5.4 - LLD antiparallel cyclic dimer....73
5.4.1 – LLD antiparallel cyclic dimer ROESY....73
5.4.2 – LLD antiparallel cyclic dimer XRD....75
5.5 – LLD parallel cyclic dimer....82
5.6 – Heterochiral dimers comparison....83
Chapter 6: Conclusions....86
Chapter 7: Materials and methods....88
7.1 – Solid-phase peptide synthesis....88
7.1.1 – General strategy....88
7.1.2 – Loading of the C-terminal residue....88
7.1.3 – Fmoc deprotection....89
7.1.4 – Couplings....89
7.1.5 – Cleavage from the resin....89
7.1.6 – Loading calculation....90
7.1.7 – Colorimetric test....91
7.2 – Peptide purification....93
7.2.1 – General sample preparation....93
7.2.2 – HPLC Semipreparative gradients....93
7.3 – Peptide characterisation....95

7.3.1 – LCMS characterisation 95
7.3.2 – NMR characterisation 96
7.4 – Kinetic studies 96
7.5 – Large-scale libraries. 96
7.5.1 – Cyclic peptides purification 97
7.6 – LDL cyclic pentamer amplification 100
7.7 – LDL cyclic pentamer esterification 100
7.7.1 – LDL cyclic pentamer methyl ester purification 100
7.7.2 – LDL cyclic pentamer methyl ester characterisation 101
7.8 – Macrocycles NMR characterisation 102
7.9- Circular dichroism characterisation 102
7.9.1 –Cyclic dimers 102
7.9.2 – LDL cyclic pentamer 103
7.10 – Crystallisation experiments 103
7.10.1 – LLL and LLD stereoisomers 103
7.10.2 – DLL stereoisomer 104
7.10.3 – LDL stereoisomer 104
7.11 – Transmission electron microscopy (TEM) 104
7.12 – Single crystal analysis (XRD) 105
7.12.1 – LLL, LLD stereoisomers and LDL antiparallel cyclic trimer 105
7.12.2 – DLL antiparallel cyclic dimer 105
7.12.3 – LDL antiparallel cyclic dimer 106
Appendix 107
A.1 – General compound structures 107
A.2 – Tripeptide spectroscopic data 108
A.2.1 – L-Cys-L-Phe-L-Cys 108
A.2.2 – D-Cys-L-Phe-L-Cys 110
A.2.3 - L-Cys-D-Phe-L-Cys 113

A.2.4 – L-Cys-L-Phe-D-Cys 115
A.3 – Tripeptide HPLC traces 118
A.4 – LCMS kinetic studies data 119
A.4.1 – L-Cys-L-Phe-L-Cys kinetic in H_2O 120
A.4.2 – D-Cys-L-Phe-L-Cys kinetic in H_2O 121
A.4.3 – L-Cys-D-Phe-L-Cys kinetic in H_2O 122
A.4.4 – L-Cys-L-Phe-D-Cys kinetic in H_2O 123
A.5 – Cyclic peptides HPLC traces 125
A.5.1 – LLL dynamic library 125
A.5.2 – DLL dynamic library 126
A.5.3 – LDL dynamic library 126
A.5.4 – LLD dynamic library 127
A.6 – Cyclic dimers NMR characterisation 127
A.6.1 – LLL antiparallel cyclic dimer 127
A.6.2 – LLL parallel cyclic dimer 129
A.6.3 – DLL antiparallel cyclic dimer 130
A.6.4 – LLD antiparallel cyclic dimer 132
A.6.5 – LLD parallel cyclic dimer 134
A.7 – LDL Cyclic pentamer methyl ester mass spectrometry 136
A.7.1 – LCMS characterisation 136
A.7.2 – ESI-TOF characterisation 138
A.8 – Circular dichroism 140
A.8.1 Cyclic dimers 140
A.8.2 Cyclic pentamer 141
A.9 – Crystallisation experiments 142
A.9.1 – LLL stereoisomers 142
A.9.2 – DLL antiparallel cyclic dimer 143
A.9.3 – LDL antiparallel cyclic dimer 143

A.9.4 – LLD antiparallel cyclic dimer 143
A.9.5 – LDL antiparallel cyclic trimer 144
A.10 – XRD data 144
A.10.1 – LLL stereoisomers 144
A.10.2 – DLL antiparallel cyclic dimer 145
A.10.3 – LDL antiparallel cyclic dimer 145
A.10.4 – LLD antiparallel cyclic dimer 146
A.10.5 – LDL antiparallel cyclic trimer 147
References 148

List of abbreviations

BB	borate buffer
Cys	cysteine
DCC	dynamic covalent chemistry
DCM	dichloromethane
DIC	N,N'-diisopropylcarbodiimide
DL	dynamic library
DMF	dimethylformamide
DMSO-d_6	deuterated dimethylsulfoxide
FA	formi acid
Fmoc	fluorenylmethoxycarbonyl
HPLC	high-performance liquid chromatography
LCMS	liquid-chromatography mass spectrometry
MeCN	acetonitrile
MeOH	methanol
NMR	nuclear magnetic resonance
Phe	phenylalanine
$SOCl_2$	thionil chloride
SPPS	solid-phase peptide synthesis
TCEP	tris-(2-Carboxyethyl)phosphine hydrochloride
TFA	trifluoroacetic acid
TIPS	triisopropylsilane
UV	ultraviolet radiation
XRD	X-ray diffraction

Abstract

Peptides are a class of biomolecules that has attracted a lot of interest in different scientific fields, thanks to their biocompatibility and potential to self-assemble into supramolecular structures in water. In particular, cyclopeptides composed of α-amino acids have been intensively studied for their ability to stack into supramolecular nanotubes, which are held together by intermolecular hydrogen bonding. The intense research efforts in this area have unravelled the design rules for self-assembly in terms of stereoconfiguration, and amino-acidic composition. However, an extensive investigation on this class of compounds requires a synthetic effort that is not trivial. Dynamic covalent chemistry (DCC) thus offers an appealing alternative to classical chemical synthesis, to yield cyclopeptides from linear building blocks that are simpler to synthesise. In this way, the reagents can combine into a dynamic covalent library (DCL). Furthermore, the formation of covalent bonds under thermodynamic equilibrium can be used together with the self-assembly process, as a possible route to discover new suprastructures, thanks to the self-templating effect.

A set of Cys-Phe-Cys tripeptide stereoisomers was synthesised to study their ability to undergo DCC in alkaline water, through thiol/disulfide exchange. The stereoisomerism impacted the DCC leading to the formation of diverse cyclic oligomers, and it allowed to shed light on key differences between the homochiral, and the heterochiral DCLs. Cyclic oligomers were purified by reverse-phase HPLC, and characterised by NMR and single-crystal XRD. A particular stereoconfiguration enabled the DCL to self-assemble into a hydrogel composed of only one macrocycle at the thermodynamic equilibrium. The analysis on the supramolecular material by rheology, circular dichroism, and transmission electron microscopy revealed the presence of an anisotropic and elongated supramolecular structure, compatible with the presence of nanotubes whose diameter could correspond to the size of its macrocyclic building block. This compound had a similar conformation in solution at different pH values, but it was able to self-assemble into hydrogels only in the zwitterionic form.

Overall, this study demonstrated how an appropriate choice of amino acid stereoconfiguration on simple tripeptides can be a strategic design tool towards diverse cyclic structures and, in specific cases, to yield DCLs that eventually converge into a main gelator product. This research work thus laid the basis to easily access a new class of self-assembling cyclopeptides that could find various applications in materials science, and beyond.

Riassunto

I peptidi sono una classe di biomolecole in grado di attrarre molto interesse in diversi campi scientifici, grazie alla loro biocompatibilità e alla possibilità di assemblare in superstrutture in acqua. In particolare, i ciclopeptidi composti da α-amino acidi sono stati intensivamente studiati per la loro abilità di assemblare in nanotubi supramolecolari, i quali sono tenuti assieme da interazioni di legame idrogeno. L'intensiva ricerca in questa area ha elucidato le regole del design del loro auto-assemblaggio in termini di stereoconfigurazione e composizione amino-acidica. Tuttavia, uno studio estensivo di questa classe di composti richiede uno sforzo sintetico non banale. La chimica dinamica covalente offre quindi un'alternativa interessante alla classica sintesi consentendo di produrre ciclopeptidi da mattoncini lineari molto più semplici da sintetizzare. In questo modo, i reagenti si combinano in una libreria dinamica covalente. Inoltre, la formazione di legami covalenti sotto equilibrio termodinamico in concomitanza all'autoassemblaggio possono essere usati come possibile strada per scoprire nuove suprastrutture, grazie all'effetto di autoreplicazione.

Un set di stereoisomeri tripeptidici Cys-Phe-Cys sono stati sintetizzati per studiare la loro abilità di reagire covalentemente in acqua alcalina attraverso lo scambio tiolo/disolfuro. Lo stereoisomerismo ha influito sulla chimica dinamica portando alla formazione di diversi oligomeri ciclici e ha permesso di fare luce sulle differenze chiave tra la libreria omochirale e quelle eterochirali. Gli oligomeri ciclici sono stati purificati con la cromatografia ad alta prestazione a fase inversa e caratterizzati da RMN e diffrazione a raggi X. Una particolare stereoconfigurazione ha permesso alla libreria di auto assemblarsi in un idrogel composto da un solo macrociclo all'equilibrio termodinamico. L'analisi del materiale supramolecolare da reologia, dicroismo circolare e microscopia a trasmissione elettronica ha rivelato la presenza di una struttura anisotropica allungata compatibile con la presenza di nanotubi, i quali il diametro potrebbe corrispondere alla taglia del mattoncino macrociclico. Questo composto ha conformazioni simili a diversi pH ma è in grado di auto assemblarsi solo quando si trova in forma zwitterionica.

Riassumendo, questo studio dimostra come una scelta appropriata della stereoconfigurazione degli amino acidi su semplici tripeptidi può essere strategica nel progettare diverse strutture cicliche e in casi specifici, ottenere librerie in grado di convergere verso un gel composto da un unico prodotto. Questa ricerca pone quindi le basi per accedere facilmente ad una nuova classe di ciclopeptidi auto assemblanti che possono trovare varie applicazioni nella scienza di materiali e oltre.

Chapter 1: General introduction

1.1 – Supramolecular chemistry

Traditional organic chemistry was born in the late 19th century in the efforts to isolate and synthesise characteristic compounds from living organisms. This, for a long time, was a difficult task and speculations that organic compounds do not follow the laws of chemistry as inorganic compounds was something real. At the end of the 19th century, the theory that the synthesis of organic compounds was possible only by living organisms started to be challenged by several reported syntheses of organic compounds. One well-known example is the *myth of Whöler* and the synthesis of urea.[1] During the early 20th century, organic synthesis was explored in such a manner that the attention for the formation of covalent bonds to get complex molecules was the main focus of the discipline. After the '50s, for sure no *theory of vitalism* was still alive but instead, the great discoveries of the newborn field of molecular biology highlighted the necessity to study complex systems composed by more molecules. One of the most famous stories of that decade, is the race on the discovery of the DNA double-helix structure. Different research groups were trying to rationalise how two polymeric strands composed by phosphosugars, pyrimidine and purine bases, paired through non-covalent interactions.[2,3] Shortly thereafter, during the '60s, the pioneering work of Pedersen, Lehn and Cram on crown ethers, cryptands, and other host-guest systems put the bases for the modern supramolecular chemistry.[4] In chemistry, the focus started then to shift from the strong and often irreversible covalent bonds, towards weaker non-covalent interactions.[5]

Supramolecular chemistry is often defined as the "*chemistry beyond the molecule*" because it focuses on two or more molecules which interact together *via* non-covalent interactions.[6] This ensemble is called *supramolecular structure*, and the peculiarity is that it does not only still possess the properties of the single building blocks, but also it acquires properties that emerge from the ensemble. Nature offers plenty of examples of supramolecular structures, such as the DNA-double helix, cell membranes, virus capsids, and so on. It is clear at this point that the complexity of the living beings must reside in a concert of many molecules, which interact *via* non-covalent interactions, thus creating complex supramolecular machineries that are able to perform tasks that are otherwise difficult for single molecules.

Supramolecular chemistry is not only biology-related, but it also opens to a wide range of technological applications from medicine to electronics.[7–9] Nature is a great source of inspiration for the design of novel smart systems in which the synthetical effort in the lab is ideally minimal. The

synthesis of large molecules is difficult, expensive and time consuming. Supramolecular structures can spontaneously form just by mixing the building blocks in solution. In this way, it is possible to break down large objects into small molecules that are easier to synthesise, so that they organise into complex architectures through weak interactions.

From a thermodynamical point of view, classic supramolecular chemistry studies the formation of molecular complexes at the thermodynamic equilibrium.[10] Non-covalent interactions are weak and can be formed and broken easily, relative to the stronger covalent bonds. Two or more molecules can reach a thermodynamic minimum interacting with each other and forming a supramolecular structure. If more than one arrangement is possible, thus more thermodynamic local minima exist. On the one hand, given an activation energy that is not too high at the desired conditions, the system can explore reversibly the different possibilities reaching at the end the lowest thermodynamic minimum. On the other hand, it is possible to kinetically trap a supramolecular structure through the exploration of suitable conditions. If the activation energy is too high, the structure will not reach the lowest energy basin of the thermodynamic equilibrium, and it can persist for a long period of time.[11] Thermodynamic control enables suprastructures to form and disassemble reversibly, and this gives to the system the possibility to explore, correct and be templated by other molecules. The latter is an interesting concept since the possibility to shift the thermodynamic minimum towards another supramolecular entities allows to adapt the systems to the set conditions.[12]

1.1.1 – Self-assembly and non-covalent interactions

Host-guest chemistry refers to at least two molecules that bind *via* non-covalent interactions to form a supra structure. Host and guest have different sizes; the latter is smaller, and in some suprastructures it can be encapsulated. In nature, several examples of host-guest systems exist, such as receptors and their ligands. However, it is possible to achieve such complexes even with molecules of the same size. In this case, the phenomenon is called self-assembly.[13] It is defined as two or more molecules of a comparable size that interact through weak interactions to form a supramolecular entity. In equilibrium self-assembly, molecules spontaneously organise in discrete complexes held by directional non-covalent interactions.

Directionality of the weak interactions and pre-organisation of the functional groups on the building blocks are key to design well-defined supramolecular complexes. Metal coordination[14,15] and hydrogen bonds[16,17] are two tools to achieve directionality, and the latter allow to work with organic molecules alone. Hydrogen bonding is a powerful tool in the design of supramolecular

objects; acceptors and donors can be easily available in diverse functional groups. In organic solvent, hydrogen bonds guide the system towards self-assembly. The solvent competition is negligible and complex architectures such as capsules, cages, and spheres are possible in solution.[18,19] On the other hand, water as a solvent is a good competitor in hydrogen bond formation, and the control over the geometry and organisation of the complex is more challenging.[20]

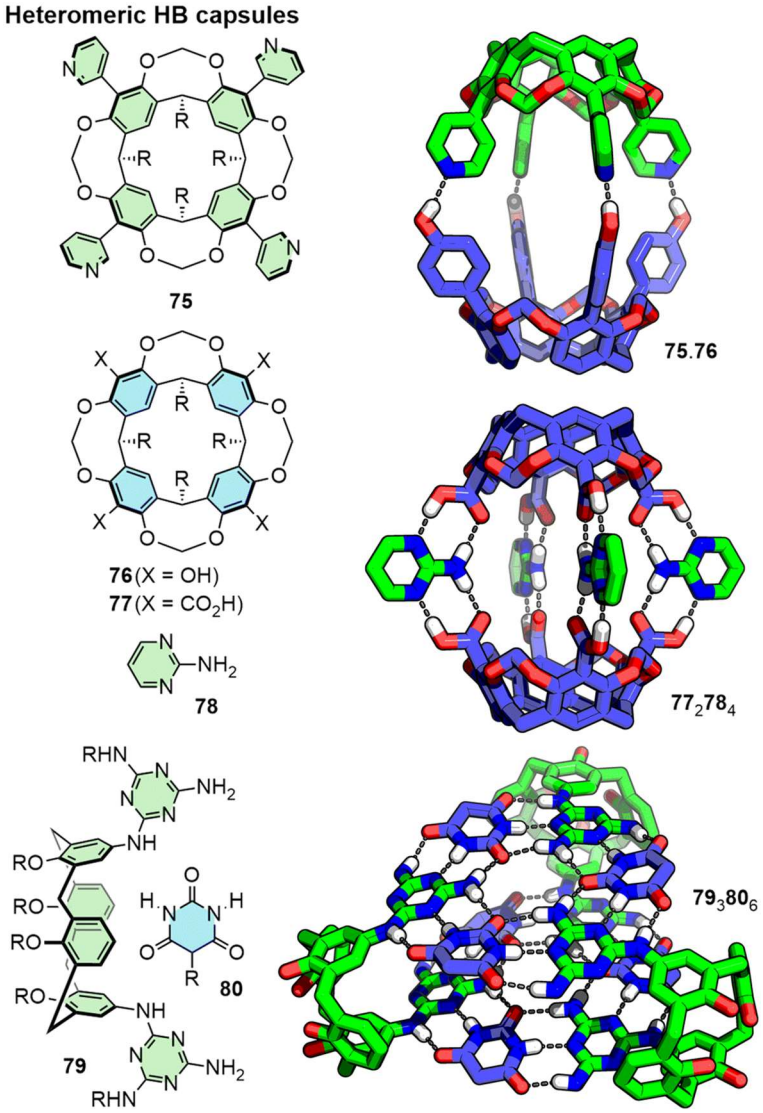

Figure 1: Supramolecular capsules self-assembled *via* hydrogen bond. These three examples highlight the importance of the directionality of the hydrogen bond donor/acceptors functional groups and the pre-organisation of the building-blocks in the design of supramolecular structures. Reproduced from Ref. 19 with permission from the Royal Society of Chemistry.

However, working with organic molecules in water presents an advantage. Hydrophobic moieties such as benzylic aromatic rings and long hydrocarbon chains, have the tendency to segregate to minimise the hydrophobic surface in contact with polar water. Hydrophobic compounds in water are accommodated in solvent cavities. Such cavities are energetically expensive and for this reason,

phase separation may occur.[21] In host-guest chemistry this is commonly observed when hydrophobic cavities in the host are filled with water, and a hydrophobic guest displaces the solvent to form the host-guest complex. This effect is called the hydrophobic effect.[22] From a thermodynamic point of view, this process can be entropically or enthalpically favoured, depending on specific conditions. An entropic gain occurs as solvent molecules are released from confined spaces to become part of the bulk solvent. An enthalpic gain can occur when new interactions are established as a result of solvent release.

Amphiphilic molecules are constituted by both hydrophobic and hydrophilic regions. The segregation tendency of the hydrophobic domains gives rise to superstructures, which reach sizes that are orders of magnitude bigger than their individual components, such as micelles and hydrophobic bylayers.[23] A powerful strategy to design self-assembled systems in water combines molecular components that are able to establish a hydrogen-bond network, with the presence of hydrophobic moieties in the building blocks. This is commonly employed in peptide- and lipid-based supramolecular chemistry. Amphiphilic superstructures interact easily with cell membranes, thus they attracted a lot of interest in therapeutics and antimicrobial drug discovery.[24–26]

1.2 – Peptide self-assembly

Peptides are polymers and oligomers composed of amino acids. Alpha-amino acids are quaternary chiral carbons linked to an amine group, a carboxylic acid, a hydrogen atom and a side chain which is characteristic of the amino acid. There are twenty different sidechains for the proteogenic amino acids, and they are commonly found in the primary structure of proteins. The amino-acidic nature ranges from simple hydrophobic sidechains composed of hydrocarbons, to polar groups such as alcohols, amines, and carboxylic acids.[27] For this reason, amino acids themselves constitute a diverse toolbox for supramolecular chemistry.

Amino acids are polymerised through the formation of an amide bond between the amine and the carboxylic acid of the alpha-carbon. The polymeric chain is called backbone and by itself it is already a scaffold that can engage in hydrogen-bond interactions, thanks to the dual role of the amide groups as donor and acceptor, leading to several secondary structures such as α-helices, β-sheets, and so on.[28–30] Since the backbone is the same in every peptide, what makes the difference in the assembly behaviour is the nature of the sidechain along the sequence. The backbone itself and the two termini of the peptide strand are hydrophilic, and they can interact with water through hydrogen bonds. The

sidechains can be either hydrophilic or hydrophobic and particular amino-acidic sequences can give an amphiphilic character to the peptide.[31]

Characteristic secondary structures found in proteins are available also for short peptides, albeit with some limitations. For instance, length of helices depends also on the amino-acidic sequence, and specific sequences stabilises even short motifs. Several factors influence the stability of an helix[32], but the general reason of such a structure is that the enthalpy of the hydrogen-bond network along the helix must be more advantageous over the entropic cost of an ordered structure. For this reason, several amino acids are required. Another notable secondary structure is the β-sheet motif. Two peptide strands can engage in a backbone-backbone hydrogen-bond interaction to fold in an elongated supramolecular structure, where the two peptide strands run in opposite or same direction (Figure 2).[33] Long β-sheets are not flat but twisted. The running direction of the strands is pivotal to the topology of this secondary structure, which can be identified as parallel or antiparallel. The amino-acidic sequence can promote or inhibit the formation of β-sheet motifs, since also the sidechains are involved in the stabilisation of this supramolecular structure.[34] Furthermore, β-sheets can be formed by one or more peptide chains. In the first case, the strand is folded to pair two segments of itself that can be also distant in the primary structure. The second case is a supramolecular assembly of more strands held together by the hydrogen-bond network. The latter case is interesting in nanotechnology because it is possible to develop β-sheet like topologies with short peptides. Amyloid fibres are composed by proteins or peptides in which a β-sheet secondary structure links several strands orthogonal to the axis of the fibre.[35] Short peptides can also be organised in amyloid-like structures and they are exploited in materials and technological applications.

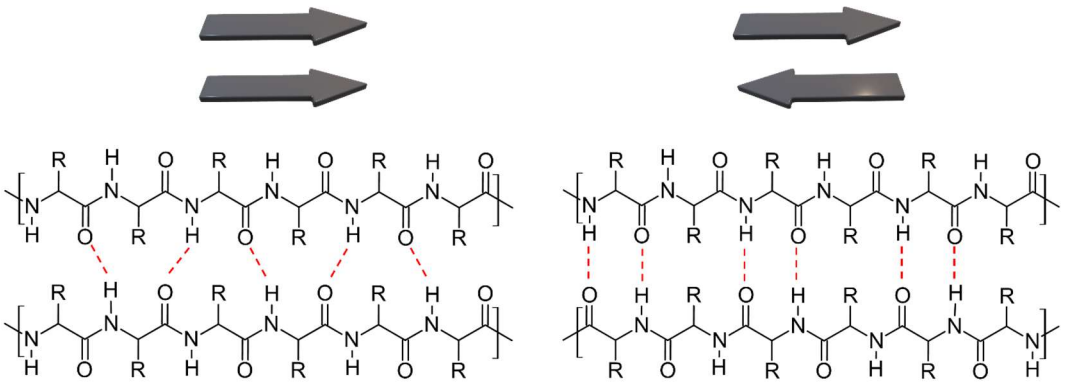

Figure 2: Parallel and antiparallel β-sheet motif. The two peptide strands run in different directions.

Amino acids are chiral molecules; thus, they exist as pairs of enantiomers. Living systems developed a preference for L- homochiral protein and peptides. The mechanism which selected the L-enantiomer over the D- is still debated.[36] Several studies have been conducted on the symmetry breaking and the chiral amplification of one specific enantiomer.[37,38] As far as we know, what is significant at the moment is the difference between the heterochiral and the homochiral world. Heterochiral peptides are diastereomers of the homochiral related sequences. Thus, their physical and chemical properties differ even if the amino-acidic sequence is the same, and stereoconfiguration is another design element that adds to the toolbox of supramolecular chemistry. This is not surprising, since switching from an L- to a D-amino acid along a peptide sequence means changing the spatial organisation of the sidechains. Therefore, the possibilities to design peptide supramolecular systems are expanded.

1.2.1 – Short-peptide hydrogels as nanostructured materials

Ultrashort-peptides (2-5 amino acids) are versatile building blocks in supramolecular chemistry. Several self-assembled peptide nanostructures are reported in literature such as fibres, nanotubes, nanoribbons, nanotapes, vesicles, and so on.[39,40] Depending on the amino-acidic sequence, it is possible to design self-assembling motifs for supramolecular structures in water or organic solvent. In the previous section, the discussed supramolecular structures were characterised by the enclosing directionality of non-covalent interactions leading to discrete nanocontainers such as cages and capsules. It is possible to build supramolecular structures considering an "open" pre-organisation of the functional groups of building blocks in which the assembly process drives the system towards the constitution of a material, such as fibres and fibrillar hydrogels. There is intensive research on peptide supramolecular hydrogels since they span a wide range of applications from biology to electronics.[41–43] The prediction of assembling motifs is still challenging, and hydrogels are nowadays discovered by trial and error experiments. The aggregation propensity of homochiral tripeptides has been investigated through molecular dynamics simulation, to predict their ability to form hydrogels, but this task is still challenging, and only a few gelling sequences were experimentally obtained from an initial search over 8,000 combinations of natural L-amino acids in trimers.[44]

Hydrophobic heterochiral short peptides have been demonstrated to be very good hydrogelators relative to their homochiral diastereomers. A single steroinversion allows to build supramolecular gelling structures in water.[45] The reason is the different spatial organisation of the sidechains. For example, syndiotactic stereoconfiguration enables isotactic super-order of

hydrophobic sidechains, enabling an amphipathic conformation whereby there is a net segregation between hydrophobic and hydrophilic components on opposing sides of the peptide molecules (Figure 3).

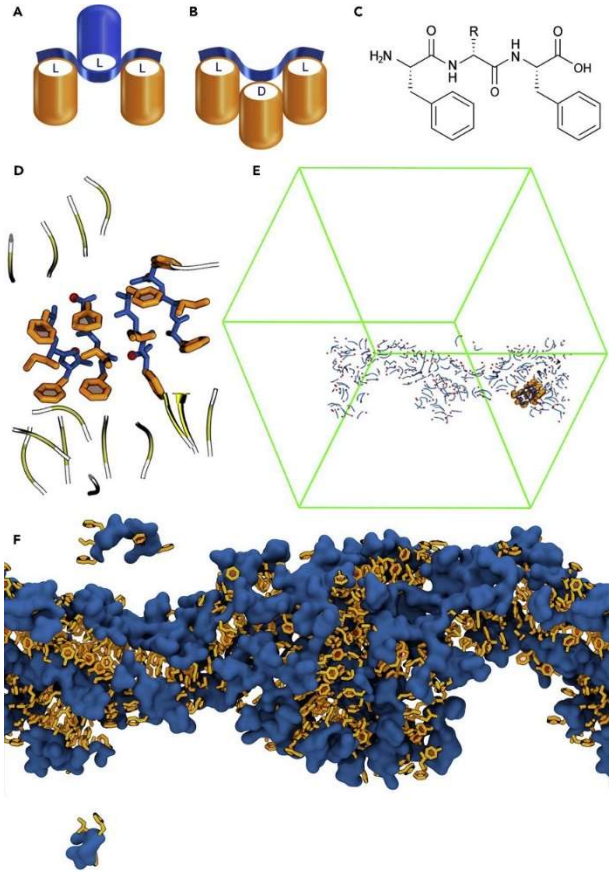

Figure 3: Self-assembly of LDL heterochiral hydrophobic tripeptides in water. A) Classical design of self-assembling L-peptides is based on alternation of hydrophilic (blue) and hydrophobic (gold) amino acids to create amphiphilic conformers. B) Heterochiral design of syndiotactic stereochemistry for hydrophobic sequences is proposed as an alternative strategy leading to isotactic sidechains spatial organisation to yield amphiphilic conformers. C) Self-assembling Phe-Xaa-Phe sequences, where Xaa is an aliphatic amino acid (R = *i*-Pr, *n*-Pr, *i*-Bu, *s*-Bu, *n*-Bu). D-F) The isotactic spatial organisation of the three hydrophobic sidechains creates a hydrophobic surface (gold) which collapses in the inner part of the supramolecular and amphiphilic fibre. The peptides are assembled through hydrogen bonds in a β-sheet motif (D). Reproduced from Ref. 45 with permission from Elsevier.

These heterochiral tripeptides self-assemble into fibres which can cross-link through non-covalent interactions to form self-supporting hydrogels. Gels are materials characterised by specific viscoelastic properties and elevated solvent content. They can be characterised by rheology, measuring the elastic (G') and viscous modulus (G") of the supramolecular material. When G' > G" the system is in a gel state. Since the fibres are held by weak interactions, it is often possible to observe thermoreversibility and self-healing abilities. Transmission microscopy analysis (TEM) reveals the presence of the supramolecular fibres in the gel matrix, and it is possible to measure the

diameter and the length of these supramolecular objects (Figure 4). Other characterisation techniques of these supramolecular materials can be used. For instance, if the peptide assembles in an amyloid superstructure, fluorescence assays, such as the thioflavin-T test can reveal the presence of this particular supramolecular motif.

It is possible to downscale building blocks to dipeptides and still observe a self-assembling ability. Heterochiral dipeptides with the general sequence Phe-Xaa (Xaa = Val, Ile, Leu and Nle) are hydrogelators.[46–49] However, if the alkylic side-chain of the second amino acid is not bulky enough, hydrogelation does not occur as in the case of norvaline (Nva) dipeptides.[50] These minimalistic sequences have been investigated through molecular dynamics screening the heterochiral couples of Phe-Xaa and Xaa-Phe stereoisomers. The conformational analysis highlighted a different distribution of conformations at room temperature for the hydrogelators. All screened dipeptides visited two main conformations at room temperature: with hydrophobic sidechains what were either "folded" at low energy, or "stretched" at higher energy. Folded conformers coincided with those found in single-crystal XRD structures of the peptides. At room temperature hydrogelators can access more easily the "stretched" conformers which are different compared to the folded ones found in the crystalline solid-state.

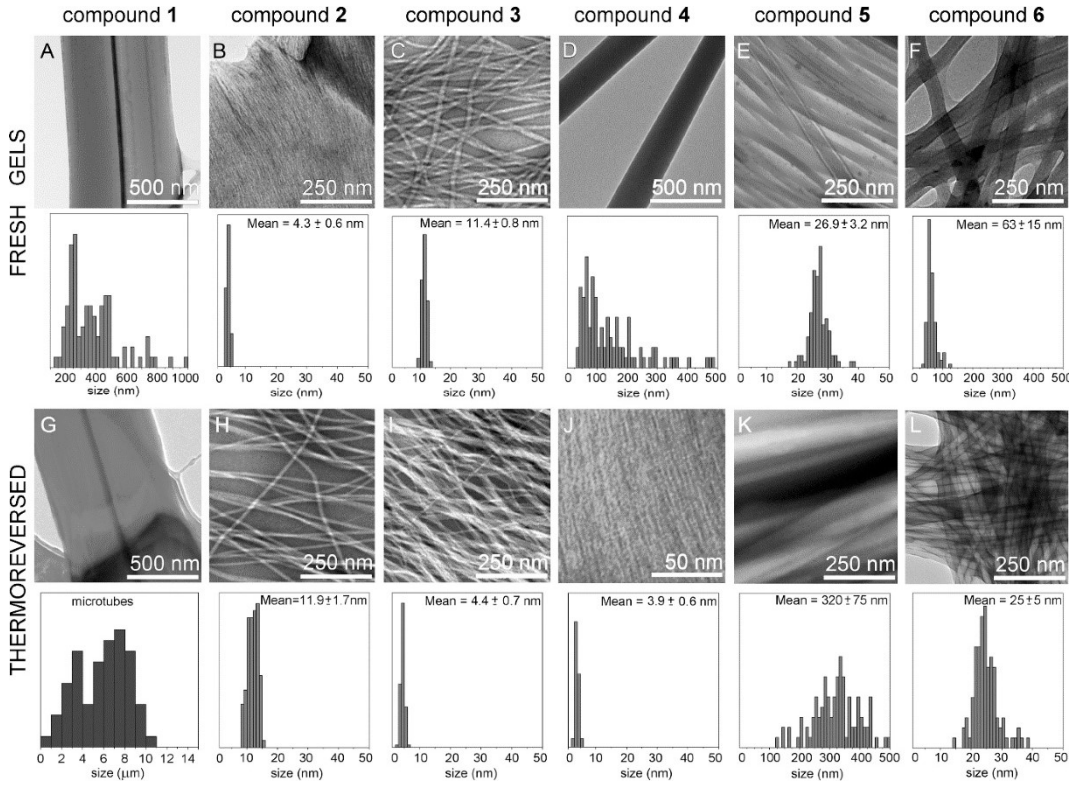

Figure 4: TEM images of diphenylalanine halogenated dipeptide before and after the thermoinversion experiment. Halogenation of the phenylalanine ring allows to tailor the size of the supramolecular fibres. Compound: 1) L-Phe-L-Phe, 2) D-Phe-L-Phe, 3) D-(2F)-Phe-L-Phe, 4) D-(3F)-Phe-L-Phe, 5) D-(4F)-Phe-L-Phe, 6) D-(4I)-Phe-L-Phe. Reproduced from Ref. 56 with permission from American Chemical Society.

The investigation highlighted also that Nva dipeptides at room temperature prefer the folded conformer found in the XRD analysis, thus leading to crystals as opposed to gels.[51] Furthermore, Phe plays an important role in the self-assembly process, since aliphatic heterochiral dipeptides of the Leu-Xaa series (Xaa = Ala, Val, Leu, or Ile) which are devoid of Phe, do not self-assemble into hydrogels.[52]

Phenylalanine is an amino acid with a benzylic sidechain; thus this residue can engage in π-π stacking and CH-arene interactions. The Phe-Phe motif has been identified as the minimal assembling motif in the β-amyloid structures found in the brain of patients with Alzheimer's disease.[53] Furthermore, this minimalistic building block has been intensively studied as a scaffold for several supramolecular assemblies.[54] The role of π-π interactions as a driving force in the assembly process has been widely investigated on Phe and peptides capped with the fluorenylmethyloxycarbonyl (Fmoc) protecting group at the N-terminus.[55,56] Since aromatic rings play a central role in the assembly process, different studies on the modification of the aromatic moiety have been conducted to tailor the supramolecular structures. In particular, heterochirality enabled the establishment of *intra*molecular aromatic interactions at the expense of *inter*molecular ones, thus yield homogenous 4-nm wide nanotubes (Figure 4 B) composed of two D-Phe-L-Phe peptide layers, as opposed to heterogeneously sixed microtubes for L-Phe-L-Phe (Figure 4 A).[57] Halogenation has also been proven to be an effective strategy to tune the supramolecular morphology of the fibres, thus regulating the π-π interactions of the Phe aromatic ring between building blocks (Figure 4).[58,59] In the case of the heterochiral X-Phe-Phe halogenated motif, the presence of the fluorine atom on the N-terminal aromatic ring allowed to tailor the size of the supramolecular fibres, narrowing their diameter distribution (Figure 4, panels C, E, I, J).[57]

1.2.2 – Cyclopeptide nanotubes

Supramolecular nanotubes are a class of self-assembled materials in which macrocycles are stacked along the axis of the super structure. Peptide macrocycle nanotubes have been investigated since the late ’80s. Peptide supramolecular nanotubes are classified following the type of amino acid. The four main classes of building blocks are alternate LD α-amino acids, β-amino acids, sorted α/γ-amino acids, and ε-amino acids (Figure 5). All these categories share the same design concept: nanotubes are stacked *via* hydrogen bonding in a β-sheet like motif and amino-acidic sidechains point outwards. The latter feature allows to functionalise the nanotube surface by selecting specific amino acids that also shield the hydrogen-bond network of the tube from solvent interaction.[60]

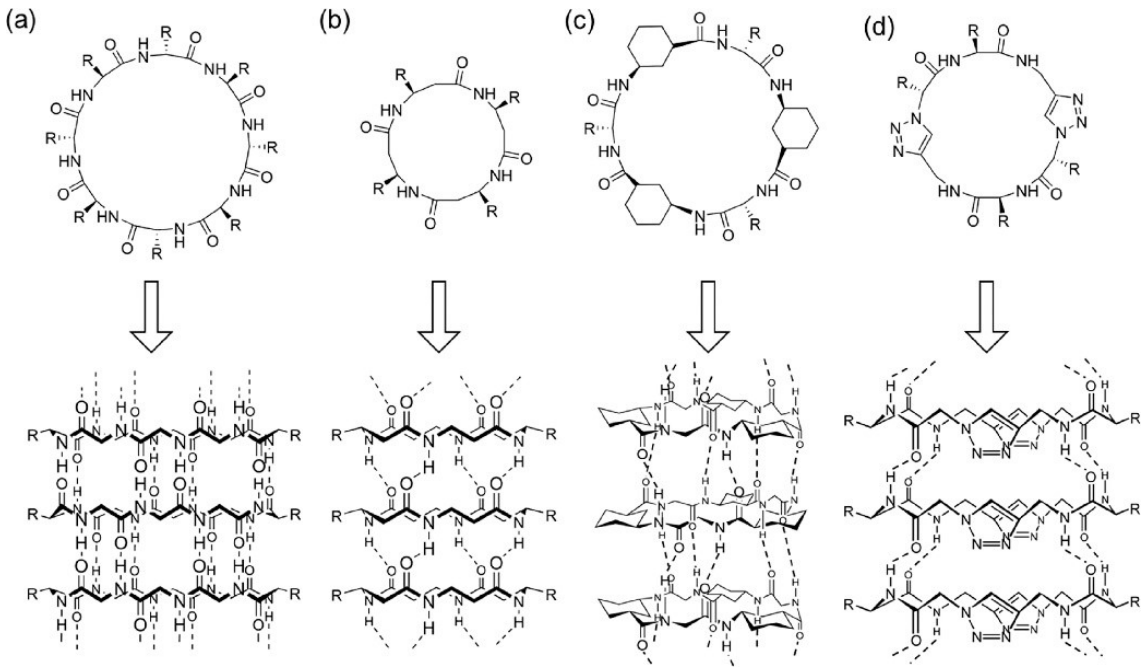

Figure 5: Classes of cyclic peptide and examples of their hydrogen bond network in the nanotubular assembly. a) LD-alternate α-amino acids, β-amino acids, α/γ-amino acids, ε-amino acids. Reproduced from Ref. 59 with the permission from American Chemical Society.

The conceptualisation of the α-amino acid nanotubes started around the ’70s and during the late ’80s experimental studies were carried out to demonstrate the predicted structures. Cyclic peptides with an even number of amino acids with an alternate L and D chirality are expected to stack *via* hydrogen bonds, through the backbone amide groups and all the side chains should point radially outside the nanotube cylinder. The predictions were confirmed by Lorenzi[61] and Ghadiri[62] and their collaborators through the synthesis of several heterochiral cyclic peptides and their analyses. The first cyclopeptide nanotubes were composed of the same hydrophobic amino acid (cyclo-[L-Val-D-Val]$_n$, cyclo-[L-Leu-D-Leu]$_n$, cyclo-[L-Phe-D-Phe]$_n$, n = 2,3,4), but they were insoluble in most organic solvents. In the ’90s Ghadiri and co-workers took into account the problem of the lateral adhesion and conceptualised an amphiphilic peptide sequence: cyclo-[L-Gln-D-Ala-L-Glu-D-Ala]$_2$. The role of the glutamic acid was to prevent the lateral adhesion in alkaline conditions, due to the Coulombic repulsion of the negative charges between tubes. This allowed to later crystallise the compound slowly lowering the pH with trifluoroacetic acid. The role of the amino acid nature was also investigated through the series of cyclo-[L-Gln-D-Xaa]$_4$ (Xaa = Ala, Val, Leu and Phe).[63] These cyclopeptides stacked into nanotubes as expected, and the cryo-EM, FT-IR, electron diffraction and molecular dynamics analyses highlighted a tighter packing for Leu and Phe sequences. Therefore, the character of the side chain is important for the lateral adhesion of the nanotubular structures. All these

four cyclopeptides stacked into an antiparallel β-sheet motif through the backbone amide functional groups.

The variables to be taken into account in the design of nanotubes with α-amino acids are then summarised in the number of amino acids (they must be an even number), and the type of sidechain for the later adhesion. However, even if larger macrocycles have been investigated (10 and 12 amino acids),[64] cyclo-octapeptides have been reported as the easiest ones to characterise, thus making them popular in the literature. The reason is that the solid-state characterisation is important, but it is difficult to characterise precisely the non-covalent interaction between the macrocycles, when compounds do not crystallise. Characterisation in solution allows to study in detail how macrocycles interact. In solution, studies were performed through the synthesis of special cyclopeptides in which the amide groups of the L- (or D-) amino acids are methylated.[65,66] Given the syndiotactic stereoconfiguration, the alternation of methyl groups prevents the hydrogen-bond interaction as donor of one side of the macrocycle. Thus, macrocycles dimerise, and the stacking process stops at this level, allowing to study the hydrogen-bond pattern by NMR. Cyclopeptides with 10 and 12 amino acids were reported to fail the dimerisation process whereas octa-peptides easily formed dimers in solution.[67] N-methylated supramolecular dimers and XRD structures of crystallised nanotubes highlighted a preference to stack in the antiparallel β-sheet motif. Parallel β-sheet motifs have been also discovered, and in the case of the two macrocycles cyclo-[L-Asp-D-Leu-L-Lys-D-Leu]$_2$ and cyclo-[L-Asp-D-Ala-L-Lys-D-Ala]$_2$ the different β-sheet interaction was attributed to the steric hindrance of the Leu residue compared to Ala.[68] In solid state, the Ala macrocycle stacked in a parallel β-sheet motif. The importance of the steric hindrance was again highlighted through the investigation of cyclo-[L-Gln-D-Tle-L-Gln-D-Tle]$_2$ (Tle = *tert*-leucine). This macrocycle failed to assemble when enantiopure, due to the steric clash of the *tert*-leucine, but it is possible to obtain a nanotube as a racemate.[69] Racemate studies are also important to study the preferred β-sheet interaction, through the dimerisation of the N-methylated macrocycles. Enantiopure cyclo-octapeptides assembled in antiparallel β-sheet, whereas racemates preferred parallel β-sheets. These two populations were distinguishable by NMR, and it was possible to calculate their ratio. Racemates of cyclo-[L-Leu-D-^{Me}Leu]$_3$ and cyclo-[L-Phe-D-^{Me}Ala]$_3$ highlighted a preference for the antiparallel β-sheet motif.[70]

The Perrier group reported the characterisation of a set of cyclo-octapeptide nanotubes which were able to cross-link to hierarchically self-assemble into hydrogels.[71] This result expands the possible use of peptides for supramolecular gel materials. A series of cyclic peptides with the general formula cyclo-[D-Leu-L-Xaa]$_4$ have been investigated in water and organic solvent to determine their ability to gel. This design took into account the easier synthesis and characterisation of cyclic octa-peptides, and the presence of alternate Leu residues as promoters for lateral adhesion. Next, they

synthesised different derivatives with tryptophan, lysine, glutamic acid, and cysteine. Lysine was tested both protected, and as a free base. The best design turned out to be an even substitution with tryptophan and an ionic amino acid (Lys, Glu and Lys with a ionic protecting group). Three cyclo-octapeptide hydrogelators were discovered, and they have been tested in different pH conditions. The hydrogelation occurred only when the nanotube was charged. The pH was adjusted using HCl and NaOH although the role of the counterion in the supramolecular assembly was not investigated. This study demonstrated the possibility to develop a cyclic peptide which is able to hierarchically assemble into a supramolecular hydrogel, highlighting the importance of the building blocks in the bottom-up design approach (Figure 6).

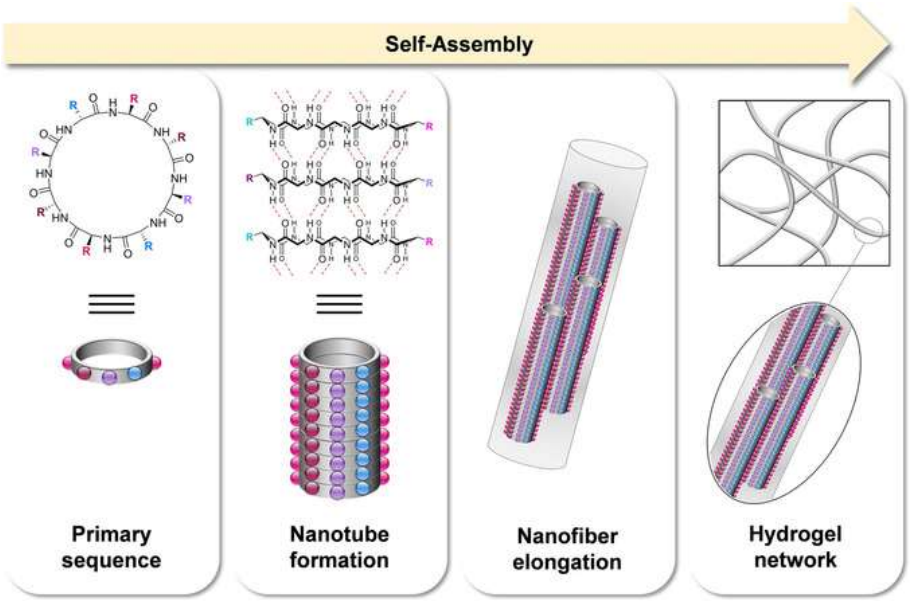

Figure 6: Schematical representation of cyclic peptide hierarchical assembly. The cyclopeptide stack in a nanotubular supramolecular structured held by hydrogen bond and then further assemble in nanofiber and eventually in a hydrogel. Reproduced from Ref. 70 with the permission from John Wiley and Sons.

β-cyclopeptides and α/γ-cyclopeptides are design alternatives to the traditional syndiotactic stereoconfigured α-cyclopeptides. The advantage of β-peptides is the resistance against enzymatic proteolysis, thus it is possible to develop nanotubes that perdure in biological conditions. Chirality again plays a role and different stereoconfiguration is another option. For β-amino acid cyclopeptides, SSSS, SRSR and SSRR diastereomers are all able to assemble into supramolecular nanotubes, and they adopt different hydrogen-bond networks.[72] This is due to the more flexible nature of the β-cyclopeptides. Homochiral β-cyclopeptides prefer a parallel β-sheet like motif for the stacking, in comparison with the alternate LD α-cyclopeptides. However, dimeric studies through the N-

methylation are not possible due to the directionality of the amide hydrogens that prevents the dimerization if methylated. For this reason, these cyclopeptides have been not deeply investigated.

A new class of cyclopeptides is composed by an even number of alternate α and γ-amino acids.[73] The design is peculiar: the γ-amino side chain is closed in a 6 or 5 membered ring on the backbone.[74] This allows to place rigid groups in the macrocycle and due to the different cyclic side chain angle, it is possible to influence the diameter of the final macrocycle. Furthermore, the presence of the 5 and 6 membered rings on the backbone opens the possibility to functionalise the inner surface of the tubes, thanks to the CH_2 group of the cycle that points inwards the supramolecular cavity. For this reason, this is an emerging class of peptide nanotubes which offers space to introduce both structural and functional properties.[75,76]

Cyclopeptide synthesis follows two different possible strategies: in solid state[77] or in solution.[78] Solid-state cyclopeptide synthesis is performed as a standard peptide synthesis procedure, except for anchoring the C-terminal amino acid through a side chain group instead of traditional C-terminal carboxylic acid. Thus, at the end of the synthesis, the cyclisation can be performed in solid state by deprotecting the C-terminus and by reacting it with the N-terminal amine group. This is a convenient strategy, but it is limited to cyclopeptides in which there is at least one amino acid with a suitable functional group for the anchoring onto the resin. All other sequences are synthesised in solution. The peptide is grown in solid state, and then cleaved with all the side chain groups protected. Then the cyclisation is performed in solution at high dilution to prevent oligomerisation. Finally, the sidechain protecting groups are removed. This implies a more complex orthogonal strategy of protecting groups. With both strategies, the synthesis is not trivial and can be problematic for specific peptide sequences.

Amino acid	**Number of A.A units**	**Chirality**	**Stacking β-sheet motif**	**Internal diameter range [nm]**	**Functionalisable?**
α	4, 6, 8, 10, 12	Alternate L and D	Antiparallel preferred	0.74 – 1.3 (8 – 12 res)	Only external surface
β	3, 4, 6	SSSS, SRSR, SSRR	Parallel for SSSS	0.26-0.27 (4 res)	Only external surface
α/γ	4, 6, 8, 10, 12	L, D and S, R	Antiparallel (α-α and γ-γ interaction) Parallel (α-γ interaction)	γ-five membered ring: 0.1 – 1.7 (4 - 12 res)	Both sides

Table 1: Main features of cyclopeptide nanotubes of the three different classes: α, β and α/γ.

1.3 – Dynamic-covalent chemistry and self-assembly

As previously introduced in **section 1.1**, traditional organic chemistry focusses on the synthesis of molecules through the formation of irreversible covalent bonds. This requires a set of conditions to avoid the formation of byproducts, which can lower the yield of the reactions, and often the use of a catalyst favours a particular thermodynamic path. In supramolecular chemistry, these synthesised organic molecules can be employed as building blocks for complex supramolecular structures which assemble through non-covalent interactions. The organisation of the molecules is driven by a thermodynamic equilibrium, which gives the system the possibility to proof-read and correct the assembly because of the reversibility of the weak interactions. The concept of binding reversibly two molecules can be transferred also onto the realm of covalent bonds. There is a class of reversible reactions in which covalent bonds are formed and broken, in such a manner that it is possible to establish a thermodynamic equilibrium between reactants and products. In line of principle, if one or more building blocks are equipped with more than one of these functional groups, more combinations of the reactants are possible. Thus, under thermodynamic control the reaction can explore the formation of different products, and the system will select the best product for those specific conditions. This field of chemistry is called dynamic-covalent chemistry (DCC) and it is a powerful tool for the discovery of new compounds.[79]

Several reactions are reported in literature as suitable for DCC. Popular examples include imines, esters, thiol/disulfide exchange, olefins and boronic acids as functional groups which are able to undergo a thermodynamic equilibrium.[80] The mixture of products which forms in a DCC reaction is called dynamic-covalent library (DCL). In line of principle, DCC at the thermodynamic equilibrium means that covalent bonds are formed and broken reversibly. This is an advantage in terms of exploration of new compounds, but a disadvantage when it is time to isolate a specific compound for the characterisation. If the isolated compound is at the same conditions of the DCC reaction it will re-equilibrate in the DCL. This is a general concept, but every DCC reaction has specific features that allow to bypass this issue. For example. the imine exchange reaction is a powerful tool widely used in supramolecular chemistry, but imines re-equilibrate when isolated from their DCL. This problem can be overcome with the reduction of the imine bond with a hydrogenation to form a stable amine,[81] or through metal coordination to yield discrete cages.[82] In the case of olefin metathesis, the DCC reaction requires a catalyst for the exchange of the olefinic partners. When the catalyst is removed, the reaction stops, allowing the isolation of the compounds without the re-equilibration issue.[83] The thiol/disulfide exchange reaction is another example of a powerful reaction in which it is possible to isolate the DCL products after the complete oxidation of the thiols. This will occur spontaneously by

exposing the system to the atmospheric oxygen; thus, the system composition will be frozen even if it did not reach the thermodynamic equilibrium.[84]

DCC has a lot in common with self-assembly, the main difference is the nature of the interaction. In both cases, two molecules bind reversibly but since the energy of a covalent bond is greater than the energy of a weak interaction, this is reflected in higher activation energies for DCC systems. The dynamic-covalent library (DCL) equilibrates more slowly than the self-assembly process, and days if not weeks can be required to reach the thermodynamic equilibrium. Furthermore, the dynamic library can adapt to the environment conditions. Therefore, it is possible to template specific products. DCC was born as a tool for ligand discovery.[85] The idea was to let the system build the best ligand for a receptor. Different building blocks are allowed to react to form a DCL and if one of the products binds to the receptor, it will be stabilised, thus shifting the thermodynamic equilibrium towards its formation. In this way, the receptor acts as a templating agent, and the selected ligand emerges from the mixture. With the same principle, it is possible to amplify products from DCL, by inserting specific template agents in the reaction mixture.

In general, supramolecular chemistry and DCC can be combined together for the design of complex systems. The formation of a supramolecular structure composed by the library products provide a template agent, and the assembly process will shift the equilibrium of the library towards the supramolecular building block. Therefore, it is possible to develop new supramolecular structures with a minimal synthetic effort, thanks to this feedback effect from the self-assembled system that is able to self-synthesise its own building blocks. The study of these complex systems where DCC and self-assembly are mixed together is called systems chemistry.[86] This is a relatively recent field of chemistry, in which it is possible to study complex chemical systems and the emergence of properties, which are not just the sum of the contributions of the single building blocks, but are characteristic of the overall ensemble.

1.3.1 – Thiol/disulfide exchange reaction

Thiols are organic compounds characterised by the presence of a sulfur atom bonded to a carbon and a hydrogen. Thiols are isoelectronic to alcohols since oxygen and sulfur are in the same group of the periodic table, but the latter has a specific and different chemistry. Thiols can be transformed into several different functional groups ranging from alkylated compounds (*e.g.,* sulfurs and sulfonium salts) to different oxidised sulfur compounds (*i.e.*, sulfenic acids, sulfoxides, sulfones, sulfonic acids).[87,88] Mild oxidation of thiols leads to the formation of a sulfur-sulfur bond. This

oxidation product is called disulfide, and it is quite popular in chemistry and biology. Disulfides are common in proteins where cysteine (Cys) residues are oxidised to increase the macromolecule stability and rigidity in the folding process.[89,90]

On one hand, the oxidative conditions are easy to achieve since atmospheric oxygen acts as an oxidant, and thiols are readily oxidised in mild conditions in alkaline water. Thus, disulfides offer an easy way to bind two organic molecules through a sulfur-sulfur bond. The thiolate ion is the species that is oxidised in water and at low pH it is possible to slow down the oxidation rate. The optimal pH for a rapid oxidation rate is pKa dependent with thiols with electron withdrawing groups having lower pKa than alkylic thiols such as Cys.[91] On the other hand, preventing the oxidation reaction in solution is difficult since an inert atmosphere is required (nitrogen or argon) and the solvent must be degassed from dissolved oxygen. Furthermore, thiol oxidation in water is very sensitive to the presence of metal traces, thus high purity is mandatory for solvents to ensure minimum amount or absence of metallic impurities.[92]

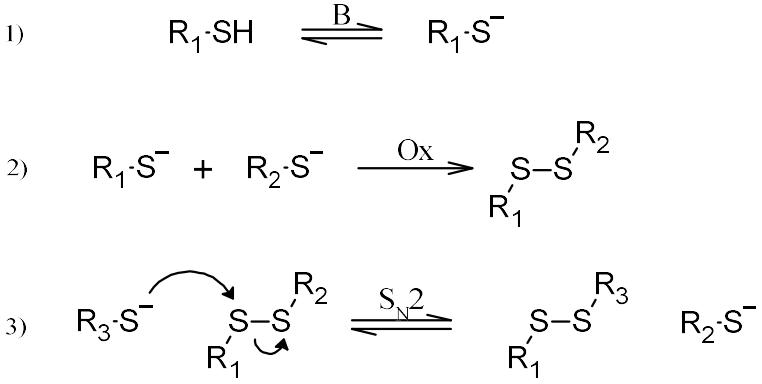

Figure 7: Thiol/disulfide exchange reaction scheme. 1) Thiols are deprotonated in alkaline water. 2) Thiolates spontaneously oxidise when exposed to atmospheric oxygen. 3) The thiol/disulfide exchange reaction can be described as a S_N2 reaction where thiols and disulfides exchange partners continuously.

Disulfides can be reduced again as thiols under reducing conditions. Since disulfides are present in proteins, the interest in disulfide reduction spun from to the study of proteins, and several reducing agents were developed for this purpose.[93] In particular, organic phosphines are an interesting class of reducing agents and tris-(2-carboxyethyl)phosphine hydrochloride (TCEP) is very popular due to its stability to air, solubility in water, and odourlessness, and solid nature for ease of handling.

Thiol/disulfide exchange is a robust reaction used in DCC, and it is based on the presence of these two molecular species in solution. This reaction happens spontaneously in alkaline water at room temperature. Thiolates are oxidised to disulfides over few days, and in this window of time, remaining thiolates react with the disulfides in an exchange reaction via S_N2 mechanism (Figure 7).

However, the real mechanism is still debated[94] but as an approximation it can be described as a nucleophilic substitution in which the transition state is a non-linear trinuclear sulfur complex with a delocalised negative charge.

Intramolecular thiol/disulfide exchange reaction in peptides is influenced by steric and strain effects of the peptide chain. Therefore, this reaction on peptides might have a preference for specific products which are influenced by the overall conformation of the peptide.[95] In DCC, this reaction is very popular and several studies have been published starting from the '90s. The design of the building blocks which participate in this reaction must be carefully taken into account. Non-covalent interactions can guide the system towards a specific compound of the library. Therefore, the strategic use of hydrogen-bond donor/acceptor functional groups, and of aromatic moieties which can contribute to amplify a product through the hydrophobic effect in water are useful tools in the design of the reactants.[96]

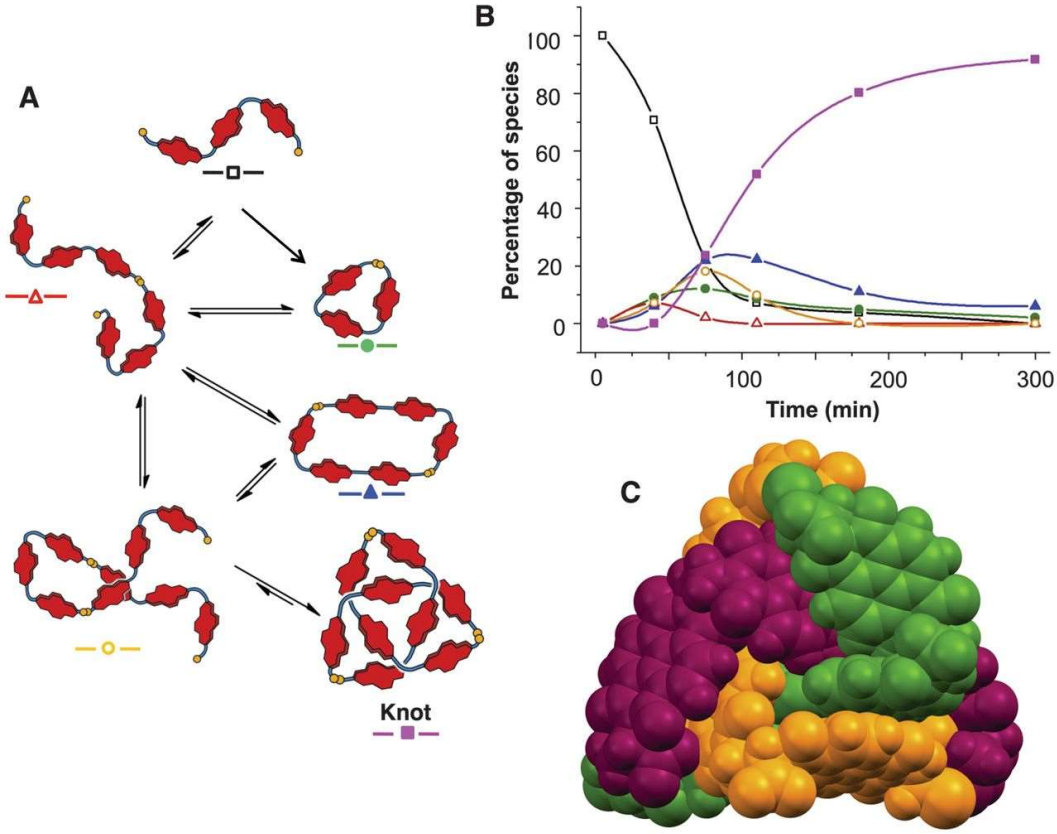

Figure 8: Dynamic-covalent library of a single building block which is able to fold in a trimeric knot. The hydrophobic collapse of the trimer at high ionic strength amplifies this particular topology. A: Schematic representation of the DCC. B) Percentage area of chromatographic peaks vs time. C) Space-filling model of the trefoil knot. Reproduced from Ref. 100 with the permission from The American Association for the Advancement of Science.

The combination of supramolecular chemistry and DCC led to the discovery of several interesting compounds and structures with non-trivial topologies. Sander's group reported a DCL composed by two thiolate units able to form different macrocycles. The presence of a specific guest shifted the thermodynamic equilibrium towards a specific macrocycle that acted as a host. In this way, different guests templated different receptors from the same library.[97] Furthermore, Sander's group developed a single building block composed by three flat aromatic domains connected through two carbon atoms and with two cysteine residues as termini to enable the DCC reaction. This single building block spontaneously formed a trimeric molecular knot thanks to the self-hydrophobic collapse of the aromatic moieties (Figure 8).[98] To prove the importance of the hydrophobic collapse, higher ionic strength led to an amplification of this complex structure at the expense of the monomeric and dimeric macrocycles.

Traditional dynamic-covalent chemistry studies the library composition at the thermodynamic equilibrium but it is also possible to select new compounds and structures under kinetic control. Otto's group developed a family of pseudopeptides composed by a peptide chain functionalised at the N-terminus with a dithiol aromatic group. The general design of this compound allows to form macrocycles composed by the aromatic dithiol units, whereas the peptide chains point radially outside the macrocycle ring. The selected amino-acidic sequence favours the stacking of the macrocycles through a β-sheet motif (Figure 9). The DCL of this compound was studied under three different conditions: no agitation, shacking and stirring. Surprisingly the different mechanical stimuli led to the amplification of different products.[99] This DCL formed macrocyclic oligomers and the peptide chains could interact through non-covalent interactions stabilising a specific oligomer. Therefore, the supramolecular structure acted as a template agent for its own building block. The rate of the propagation of a specific oligomer was influenced by the number of its own supramolecular structures available: since the stacking of these macrocycles formed a fibre, the active growth site was on the tip of the fibre. Thus, the mechanical stimulus broke the fibres and generated more active fibre tips. Agitation and stirring broke different supramolecular structures and led to the amplification of two different oligomers from the DCL. This is an example of DCL under kinetic control. The design of this dithiol aromatic core has been proven to be a very robust scaffold for thiol/disulfide exchange in systems chemistry. The possibility to functionalise and change the amino-acidic sequence of the building block opened the way to a wide range of possible studies in which supramolecular chemistry and DCC are combined to develop complex systems. For instance, the non-covalent interactions of the peptide chains can influence the conformation of the dithiol aromatic ring macrocycle, and they can drive the system towards the formation of foldamers with low symmetry, instead of the previously reporter stacked fibres.[100]

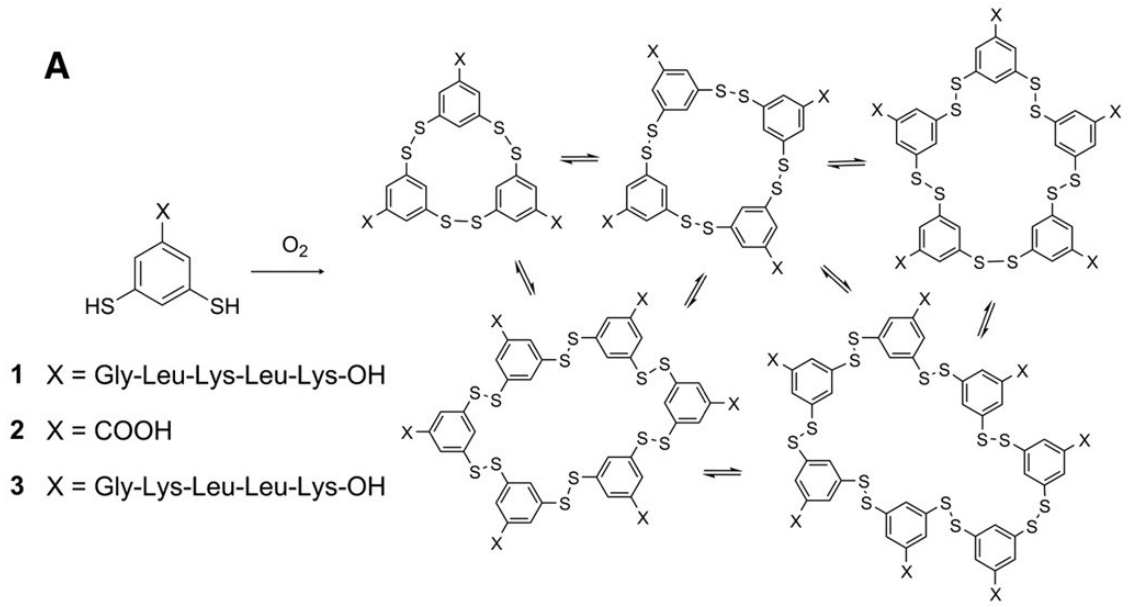

Figure 9: Design of the aromatic dithiol pseudopeptide. Compound 1 displays a β-sheet promoting peptide sequence. DCL of compound 1 responds to the different mechanical stimulus amplifying specific oligomers depending on the applied stimulus. Reproduced from Ref. 99 with the permission of The American Association for the Advancement of Science.

Out-of-equilibrium self-assembly (or dissipative self-assembly) is another interesting research field that focusses on supramolecular structures that are assembled outside of the thermodynamic equilibrium. This is peculiar since the self-assembled structure has a life-time, and the thermodynamic equilibrium is composed of the disassembled building blocks. In nature, the most famous example of such a structure is tubulin, the cytoskeleton protein of eukaryotic cells.[101] These nanotubular structures are formed transiently by self-assembly of the proteins activated by GTP. An enzyme hydrolyses GTP to GDP and promote the disassembling of the supramolecular structure. Therefore, the overall system can be imagined as the supramolecular structure is fuelled by GTP, and it exists so long as sufficient energy sustains the assembly. The same concept can by transferred to DCC: disulfides can be reduced as thiols using a reducing agent and an oxidant will keep oxidising thiols to disulfides. Otto's group demonstrated the possibility to study the competition of two supramolecular structures for a common building block. in an out-of-equilibrium kinetic regime.[102] An aromatic dithiol pseudopeptide derivative is oxidised in a DCL containing trimers, tetramers and hexamers. Trimers are the thermodynamic product since they emerge as the dominating compound thanks to the self-assembly in fragile fibres, whereby the number of fibril tips plays a role in the propagation of these particular superstructures, as discussed above. TCEP reduces the disulfides back to thiols but the rate of this reaction is dependent on the size of the self-assembled fibre. Thus, the trimer is reduced faster than the hexamer. With a constant supply of TCEP and sodium perborate (as oxidant), it was possible to create a kinetic regime in which the dominant product was the hexamer

in contrast with the already proven thermodynamic product, the trimer. When the supply of TCEP and perborate was stopped, the trimer became once again the dominant compound of the DCL. Therefore, this is an out-of-equilibrium system fuelled by TCEP and perborate, and the cyclic hexamer is assembled through a dissipative self-assembly regime. Another example is the competition for two replicators for a common building block, in which one of the two replicators is amplified faster than the other but in the end the second will prevail. It is clear that the second replicator is the thermodynamic product of the DCL, and when it starts to replicate, the first replicator decreases in concentration. With a constant supply of fresh building blocks the system is kept outside the equilibrium and this favours the first replicator which is the kinetic product. When the supply of building blocks is stopped, the second replicator grows in concentration towards the thermodynamic equilibrium.[103]

DCC can also be exploited to form supramolecular hydrogels. Hydrogels form through the cross-linking of fibres as previously introduced, and the cross-link can be physical or chemical. Physical cross-linking occurs through the non-covalent interactions between fibres, and this is the typical case for supramolecular gels obtained from the self-assembly of short peptides. Chemical cross-linking is obtained through covalent bonding between fibres. An example of this process was reported by Otto's group using an orthogonal DCC approach.[104] The well-known fibres created by the stacking of the aromatic dithiol pseudopeptide macrocycles were functionalised so as to display a second functional group, suitable for DCC. The peptide chain was equipped with a hydrazone group at the C-terminus that was able to participate in hydrazone/imine exchange reaction with an aldehydic partner. The linker was a dialdehyde connecting the hydrazone of two fibres trough the formation of an imine bond. After a few minutes since the addition of a specific dialdehyde linker, gelation occurred, and the reversible nature of the linkage was proven by adding hydroxylamine to the gel. This compound formed more stable imines than hydrazones, and thus, after several hours since the addition, hydrogels were disassembled.

Chapter 2: Aim of the project

Peptides are versatile building blocks in supramolecular chemistry, and several supramolecular structures for various applications are reported in literature. Short peptides are easy to synthesise in solid phase and they can be considered green building blocks since they are composed by amino acids that do not persist in the environment and are inherently biocompatible. It is possible to synthesise sequences choosing among the 20 proteogenic amino acids, and even more, considering the plethora of non-natural analogues that are commercially available. Furthermore, since amino acids are chiral, the design of the building blocks can be tailored based on selected combinations of stereoconfiguration too. There is a solid literature on synthetic procedures and characterisation methods of these compounds, therefore it is really convenient to design supramolecular building blocks with this class of simple biomolecules. Lastly, since peptides are found in living organisms, there is also the possibility to exploit these molecules and their materials for bio-applications.

Cyclic peptides can stack in nanotubular supramolecular structures *via* hydrogen-bonding and several design concepts have been introduced in the previous chapter. The state-of-the-art pertaining peptide nanotubes composed by α-amino acids offers a clear picture: cyclic peptides must have syndiotactic stereoconfiguration at the α-carbon and present an even number of amino acids. It has also already been demonstrated that it is possible to develop a hierarchical assembly in which cyclic peptides stack into nanotubes, and which eventually yield supramolecular hydrogels. Furthermore, DCC is a well-known tool for the discovery of new compounds and even new supramolecular structures. The possibility to design a system able to self-synthesise its own building-block is intriguing. Even in this case, it has already been demonstrated that it is possible to build a hierarchical system in which one of the supramolecular objects assembles into a hydrogel.

Considering all these concepts, the aim of this project was the exploration of stereoconfiguration effects on all possible combinations of L- and D-amino acids in minimalistic tripeptide sequences suitable for DCC, and ideally prone to self-assembly, and potentially hydrogelation. The selected sequence was Cys-Phe-Cys (Figure 10), so that Cys at both termini could engage in disulfide linkages, and Phe residues could prompt hydrophobic collapse in water. This peptide sequence will be studied in all its possible diastereomer permutation (*i.e.,* LLL, DLL, LDL and LLD), excluding enantiomers (*i.e.,* DDD, LDD, DLD and DDL) that are expected to display the same supramolecular behaviour as their mirror images.

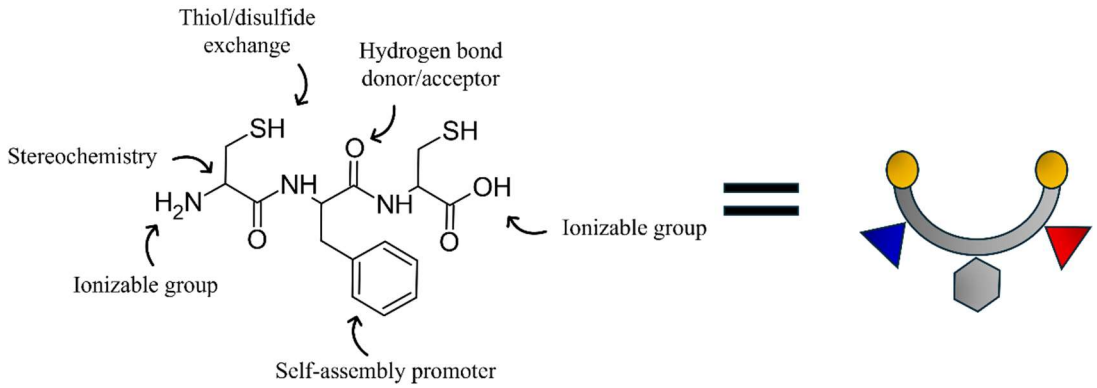

Figure 10: Design concept of the tripeptide. This short sequence presents most of the features described in chapter 1 for self-assembled materials and dynamic covalent systems.

Peptides will be dissolved in alkaline water and their DCL will be characterised through LC-MS, NMR and XRD, if suitable crystals can be obtained. Every library will be composed of cyclic peptides and their ability to self-assemble in supramolecular structures will be evaluated (Figure 11). The macrocycles will be similar to the alternate LD α-cyclopeptides but due to the different starting diastereomer, this project will aim to investigate the role of the chirality in the DCL and its influence on the assembly. Therefore, the DCC is exploited to avoid the difficult synthesis of all the possible combinations of chirality and leave the system select the best building-block for a self-assembled superstructure. This approach will shed light on other possible stereochemical configurations for the assembling cyclic peptides, thus expanding the knowledge on these systems. The peptide building block contains an odd number of amino acids, therefore it will be possible to observe cyclo-peptides with an odd or even number of total amino-acids to challenge the well-known design rule of Lorenzi and Ghadiri group. Cysteine is a strategical residue for two reasons: the first one has been already mentioned above about the DCC. The second one is the presence of the C and N termini of the peptide which do not participate in the DCC. Thus, the cyclopeptides will display three different functional groups radial to the ring: one aromatic ring, one amine group and one carboxylic acid. In this way the system will be pH sensitive, and it will be possible to control the lateral adhesion by varying pH conditions. However, it is worth nothing that, as a consequence of the presence of these two polar groups, the peptide strand has a direction even in the macrocycle. Therefore, the formation of more cyclopeptide isomers will be possible, depending on the direction of the different peptide strands in the macrocycle (Figure 11), thus posing an additional challenge in terms of structural elucidation.

This project will provide the basis for the study of this family of short peptides and their hierarchical assembly for future applications. The goal is to evaluate the influence of the chirality and compare the main difference between homochiral and heterochiral peptides when the system is able

to evolve spontaneously and select its own building blocks, potentially providing new insights that are relevant to the origins of life and emergence of homochirality.

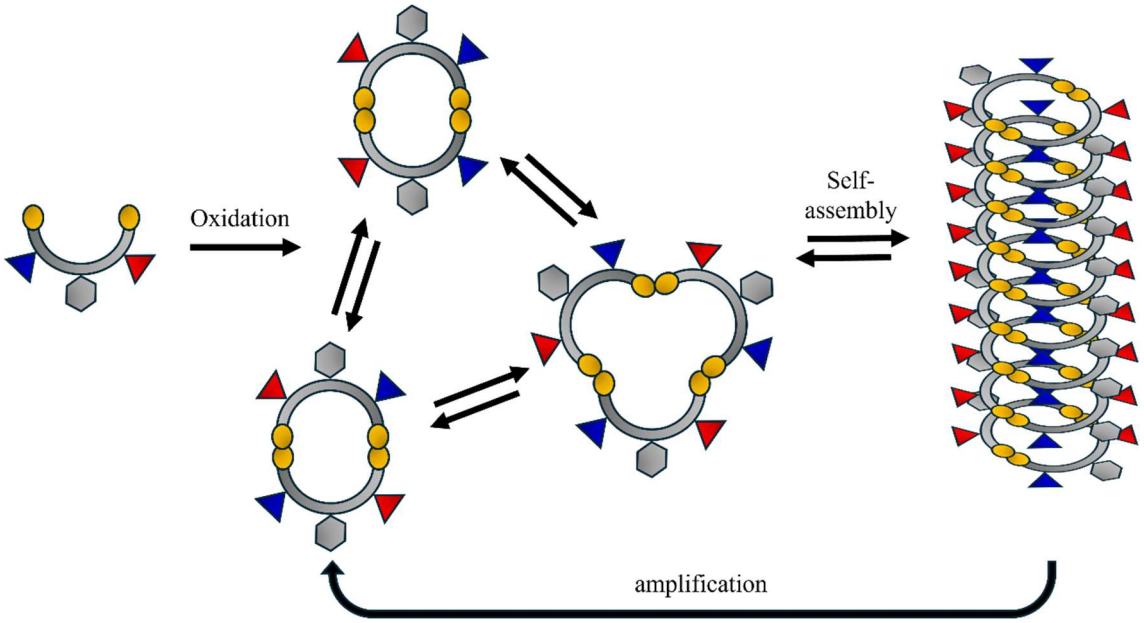

Figure 11: Overall project scheme. The peptide is oxidised in alkaline water in order to form a dynamic-covalent library of macrocycles through thiol/disulfide exchange. The possible self-assembly of a nanotubular structure may template its own building block shifting the thermodynamic equilibrium of the DCL.

Chapter 3: Dynamic-covalent libraries of Cys-Phe-Cys

3.1 – Tripeptide synthesis

All four tripeptide stereoisomers (*i.e.,* Cys-Phe-Cys with stereoconfiguration LLL, DLL, LDL and LLD) were synthetised in solid phase (SSPS) following a Fmoc-protecting group strategy. The synthesis requires inert atmosphere (argon) to avoid the possible oxidation of cysteine (Cys) during the last deprotection step. Cys was protected with the trityl group, which is stable in alkaline conditions, thus ensuring an orthogonal protection strategy combined with the Fmoc group. Peptides were synthesised on the solid support 2-chloro-trityl chloride resin to minimise the risk of C-terminal Cys epimerisation, thanks to the resin steric hinderance.[105] The epimerization is an acid/base reaction, thus, to reduce the formation of byproducts, weaker bases are recommended during all SPPS. For this reason, the weaker 2,4,6 – trimethylpyridine (collidine) was used in place of the traditional DIPEA during the loading step, which was carried out after resin activation with thionyl chloride ($SOCl_2$).

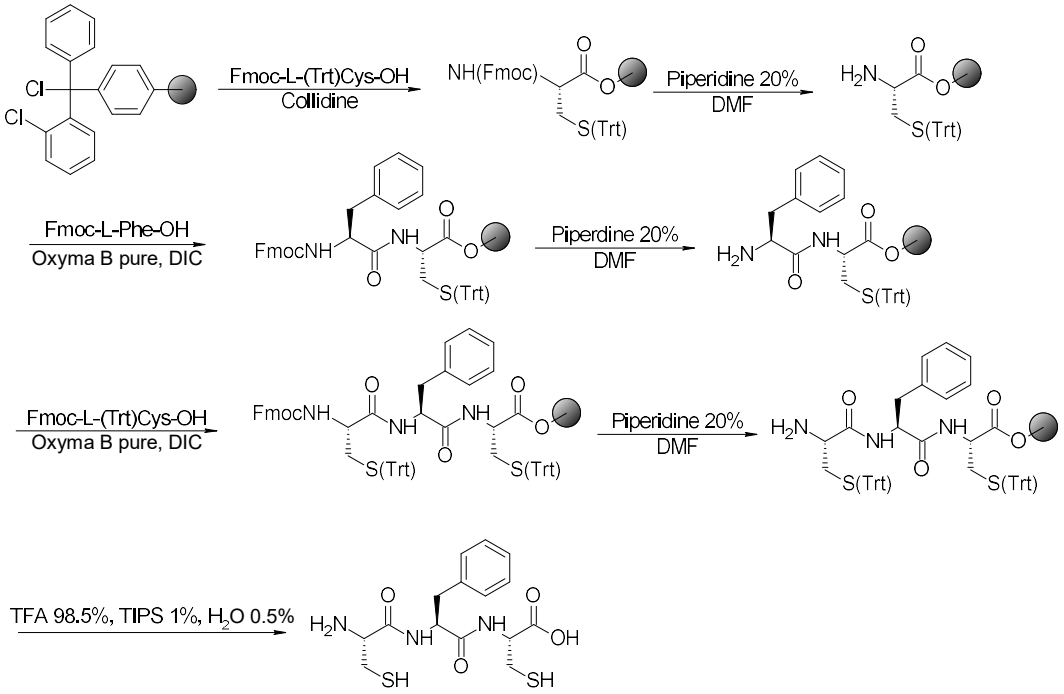

Figure 12: SPPS scheme. All four tripeptides were synthetised following this scheme. In figure is represented the synthesis of the homochiral Cys-Phe-Cys tripeptide.

After the loading reaction, the synthesis scheme was composed by alternate steps consisting of Fmoc- protecting group removal and coupling with the next Fmoc-amino acid along the peptide sequence (Figure 12). Different coupling reagents were tested: HBTU and HOAt in the presence of collidine, HCTU and collidine, or Oxyma B and DIC. The latter option gave a good yield, and it is commercially available at reasonable cost and delivery time. Therefore, all the tripeptides were synthesised with these two coupling agents. Deprotections of the Fmoc group were performed following the standard protocol with 20% piperidine in DMF. The last synthetic step is the cleavage of the anchored peptide from the resin. This was performed with a cleavage cocktail composed of 98.5% trifluoroacetic acid (TFA), 1% triisopropyl silane (TIPS) and 0.5% water. The TFA cleaves the peptide from the resin and deprotects the Cys sidechain, removing the trityl group. TIPS and water act as scavengers for the reactive carbocations which form during the cleavage.

The reaction crude was then evaporated under argon flow to remove the TFA and, then the peptides were purified by reverse-phase chromatography. The reverse-phase HPLC was carried out using a mobile phase composed of a mixture of water and acetonitrile, and when the crude was dissolved in this solvent mixture (see chapter 7), the high content of water precipitated highly hydrophobic impurities, such as the byproducts of the trityl group deprotection. During this process, 0.1 equivalents of TCEP were added to the solvent mixture in order to create a reducing environment to prevent oxidation of the thiols and reduce any oxidised Cys. Samples were centrifuged and filtered to obtain a clear solution for the HPLC. The collected fractions were then freeze-dried, and a white-fluffy powder was obtained for all the four diastereomers. Peptides were characterised by LC-MS and NMR (^{1}H-NMR and H-H COSY) and their identity and purity were confirmed (A.2 – Tripeptide spectroscopic data).

3.2 – Kinetic studies of Cys-Phe-Cys DCL

The ability of the four tripeptides to form DCLs was monitored every 24 hours by LC-MS. Each peptide was dissolved at 20 mM in alkaline milli-Q water (with a resistivity >18 M Ω cm) buffered with sodium borate (100 mM, pH 8.5). The solubility of all the four stereoisomers increased above pH 8.0, thanks to the Cys sidechain deprotonation that lowered the tripeptides hydrophobicity. At pH 8.5, all peptides were completely dissolved, and that moment was considered the starting time of the kinetic study. The DCLs were stored at room temperature inside glass vials, and no agitation or stirring was used during the kinetic study. For LC-MS analyses, samples were diluted with acetonitrile (0.05 % TFA) to reach pH ~ 2 and stop the thiol/disulfide exchange reaction.

The kinetic study was carried out for 96 hours, and it revealed that a complete thiolate oxidation had occurred after 72 hours for all the four stereoisomers (A.4 – LCMS kinetic studies data). In the first 24 hours it was possible to detect very low concentrations of linear dimers as intermediate products and eventually only cyclic compounds were present after 72 hours. Considering all the possible combinations, three linear dimers are possible: head-to-tail, tail-to-tail and head-to-head. Cyclic dimers are the main compounds for all the DCLs after 96 hours followed by cyclic trimers (Figure 13). Traditional cyclopeptides are composed by amino acids connected only by amide bonds, therefore there is only one peptide strand closed on itself. The peptide strands in these macrocycles can be combined in different directions thanks to the sulfur-sulfur bond. For this reason, there are two possible cyclic dimers. This complexity increases with the oligomer size of the DCL products (see A.1 – General compound structures for all the possible combinations). Dimers can form as parallel or antiparallel isomers considering the direction of the two peptide strands. Since the peptide sequence and thus the polar and hydrophobic groups are the same for all the four tripeptide stereoisomers, is interesting to notice how the chirality influences the ratio between these two compounds in every library (Figure 14).

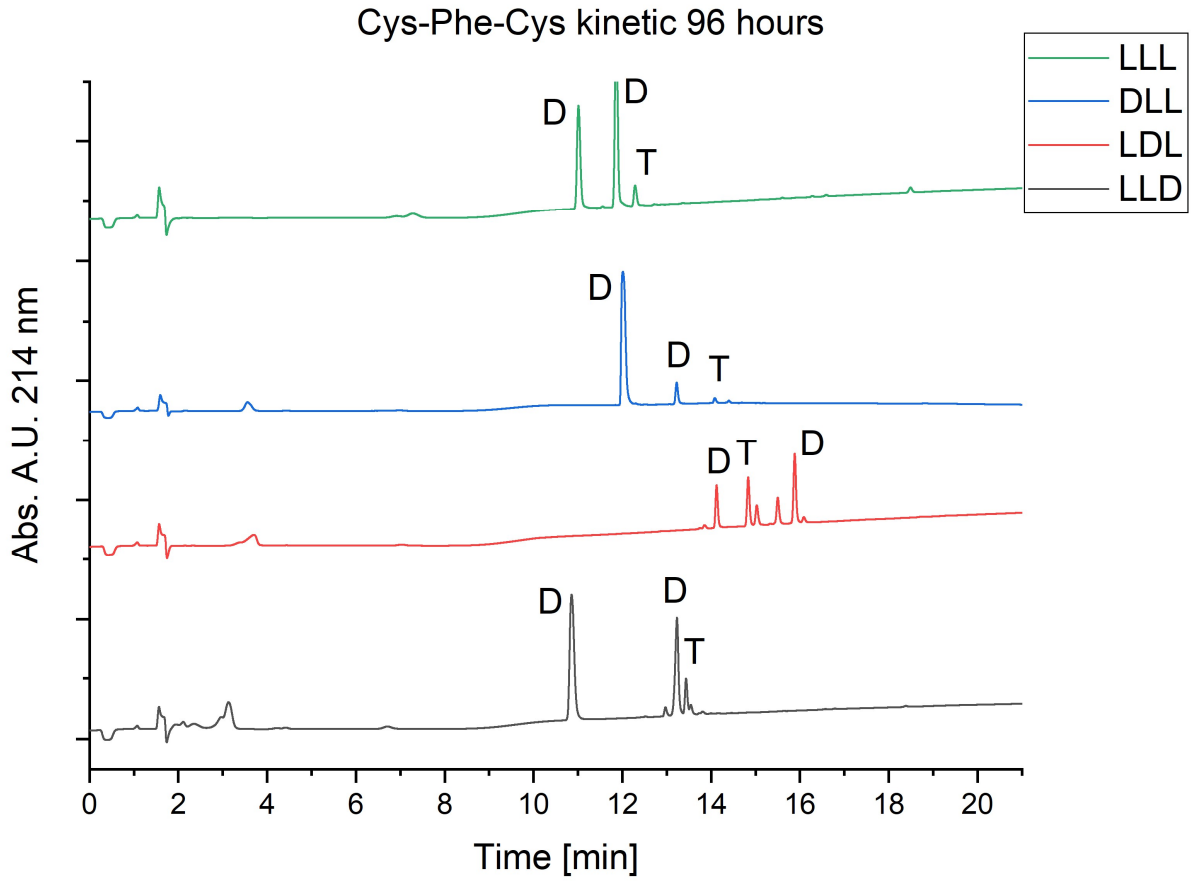

Figure 13: Analytical chromatograms of the four Cys-Phe-Cys stereoisomers after 96 hours. Main products are labelled with: D = dimer, T = trimer.

The different stereoconfiguration acts on the macrocycle strain and on the possible intramolecular non-covalent interactions. It is interesting to note the diversity of stereoconfigured compounds that it is possible to synthesise with this strategy.

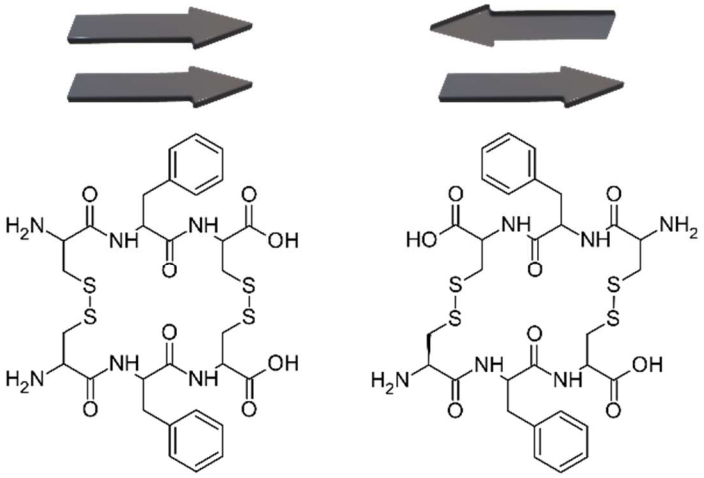

Average chromatogram area % [96h]		
Chirality	**Parallel (%)**	**Antiparallel (%)**
LLL	54.4	37.6
DLL	9.4	83.6
LDL	18.3	32.0
LLD	25.6	45.4

Figure 14: General molecular structures for parallel and antiparallel cyclic dimer. The average chromatogram area % is reported for all the tripeptide stereoisomers highlighting the influence of the chirality on the formation of these two products.

LC-MS analysis allowed to identify the molecular size of the different oligomers, but a deeper investigation was needed to distinguish oligomers with the same size. This investigation was conducted by NMR and XRD (see next chapters) after the purification of the dimers from their DCLs by reverse-phase HPLC. The first difference between the homochiral and the three heterochiral libraries is the nature of the main product. In the case of the homochiral library, the parallel dimer is the favourite one, whereas in the heterochiral libraries the balance is shifted in favour of the antiparallel product and in the case of the DLL stereoisomer this effect is the most pronounced: more than 80% of the library is composed by the cyclic antiparallel dimer. Cyclic dimers can form from the oxidation of linear dimers, or generally by the continuous thiol/disulfide exchange reaction. Considering the simple oxidation process, three possible linear dimers can form, and their oxidation will lead to the formation of the relative cyclic compounds. Head-to-head and tail-to-tail linear dimers will both contribute to the formation of the parallel cyclic dimer, whereas the head-to-tail isomer contributes to the antiparallel product. However, the concentration of these three linear products was very low and often undetectable by LC-MS, whereas the cyclic dimers formed rapidly, and they accumulated before the complete consumption of the monomer. It is hard to formulate a firm conclusion on the reaction mechanism without the structures of the linear dimers and their kinetic data, although the structural investigation on the cyclic dimers by XRD provided interesting insights.

Cyclic dimers are small enough to engage in intramolecular hydrogen bonding between the two peptide strands. The stereoconfiguration can favour or not this possible non-covalent interaction. Therefore, considering the weak interactions and the ring strain, it is possible that the different ratios of parallel/antiparallel dimers are governed by these factors. This hypothesis is supported by the thermodynamic equilibrium of the different DCLs. The composition of the libraries reached a plateau in 72 hours and further reactivation of the libraries by 0.01 equivalents of TCEP (as a reducing agent) did not change the overall composition for the LLL, DLL and LLD stereoisomers.

The LDL library was more interesting. The antiparallel cyclic dimer was the main product of the library, and it reached its maximum concentration within 24 hours. After that time, it started to decrease its concentration, with the concomitant increase of higher-order oligomers (Figure 15). After 72 hours, the reaction ended due to the complete oxidation of the thiols. Therefore, to investigate the thermodynamic equilibrium of the library, and not kinetically trapped products, a TCEP solution was added to reactivate the thiol/disulfide exchange reaction. The solution increased in viscosity and after two reactivation steps with TCEP (0.01 equivalents every 24 hours), the DCL formed a self-supporting hydrogel. Unfortunately, the supramolecular gel did not allow to investigate its composition by LC-MS. Lowering the pH of the gel from 8.5 to 7.0 or even more towards acidic pH values, strengthened the self-assembled gel, and even then, samples were diluted considerably, it was not possible to detect molecules in the LC-MS chromatogram because of the presence of insoluble aggregates.

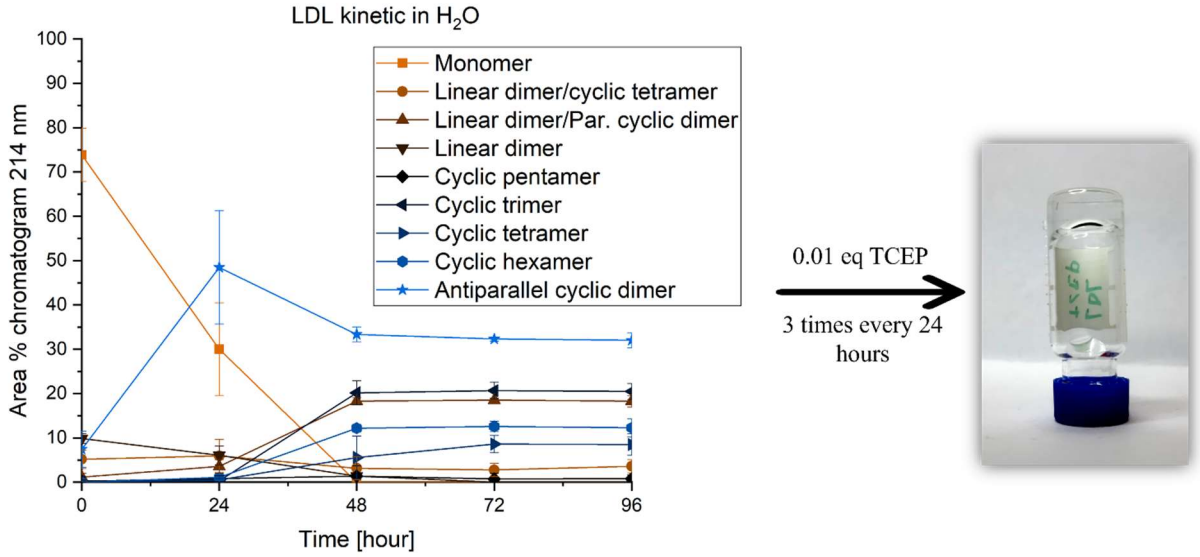

Figure 15: Average percentage area for the LDL stereoisomer DCL (experiments were performed in triplicates). The antiparallel cyclic dimer reached a maximum concentration around 24 hours and then it started to decrease. After 96 hours, 0.01 equivalents of TCEP were added every 24 hours to reactivate the library. After two TCEP additions, the system assembled in a self-supporting hydrogel.

3.3 – Hydrogel characterisation

Chapter 1 mentioned that Ghadiri, Lorenzi and co-workers highlighted the importance of the lateral adhesion when cyclopeptides assemble in nanotubes. Ghadiri demonstrated that a polar residue such as the glutamate allowed to prevent the precipitation of the nanotubes in alkaline environment, thanks to the Coulombic repulsion between the anionic assembled nanostructures. In this project, cyclic oligomers present an amine and a carboxylic acid for every peptide strand of the macrocycle. Therefore, the gel was tested in acidic, neutral, and alkaline conditions, to investigate the influence of pH on hydrogelation. From a macroscopic point of view, at pH 8.5 and 7.0, the system was a self-assembled hydrogel. At pH 12.0, the system disassembled into a clear solution, whereas at pH 1.0 it was disassembled too, aggregates were present (Figure 16, A). Therefore, there is a different level of supramolecular interactions when the system is positively or negatively charged.

The system was then characterised by circular dichroism. Since the concentration of the gel was too high for correct data acquisition even with the shortest pathlength available (*i.e.,* 0.1 mm), all the samples were diluted 1:2 with milli-Q water. From the macroscopical point of view, the gel existed only in neutral or nearly neutral pH. Nevertheless, the circular dichroism spectra show almost the same features, regardless of the sol or gel state (Figure 16, B). According to the literature (chapter 1), cyclic peptide assembles in nanotubes at different pH conditions, but the lateral adhesion is sensitive to these conditions if charged polar groups are present in the amino-acidic sequence. Therefore, this CD investigation opens to the hypothesis of a nanotubular structure able to hierarchically assembly in a self-supporting hydrogel when the Columbian repulsion is minimised by the pH value.

Peptides secondary structures are distinguishable at the circular dichroism and in literature are available theoretical and experimental data. The β-sheet motif is characterised by a minimum at 220 nm followed by a maximum at 195 nm.[106,107] These two signals are generated by electronic transitions of the peptide backbone. In particular, the amide group absorbs UV with the following electronic transitions: $\pi \rightarrow \pi^*$ and $n \rightarrow \pi^*$. The circular dichroism spectrum is sensitive to the conformation of the peptide. Therefore, these two transitions change in intensity and in wavelength according to the peptide secondary structure. The peptide responsible for the gel formation showed a minimum around 200 nm suggesting a random coil conformation. Cyclopeptides composed by syndiotactic stereoconfiguration are expected to self-assembly in nanotubes through the formation of an antiparallel β-sheet motif. This circular dichroism investigation highlights a different situation. However, in literature all the self-assembling cyclic peptides are composed by an even number of amino acids. This DCC system can generate also peptides with an odd number of amino acids.

Therefore, in this case new compounds can form with different features compared to the well-known family reported in literature.

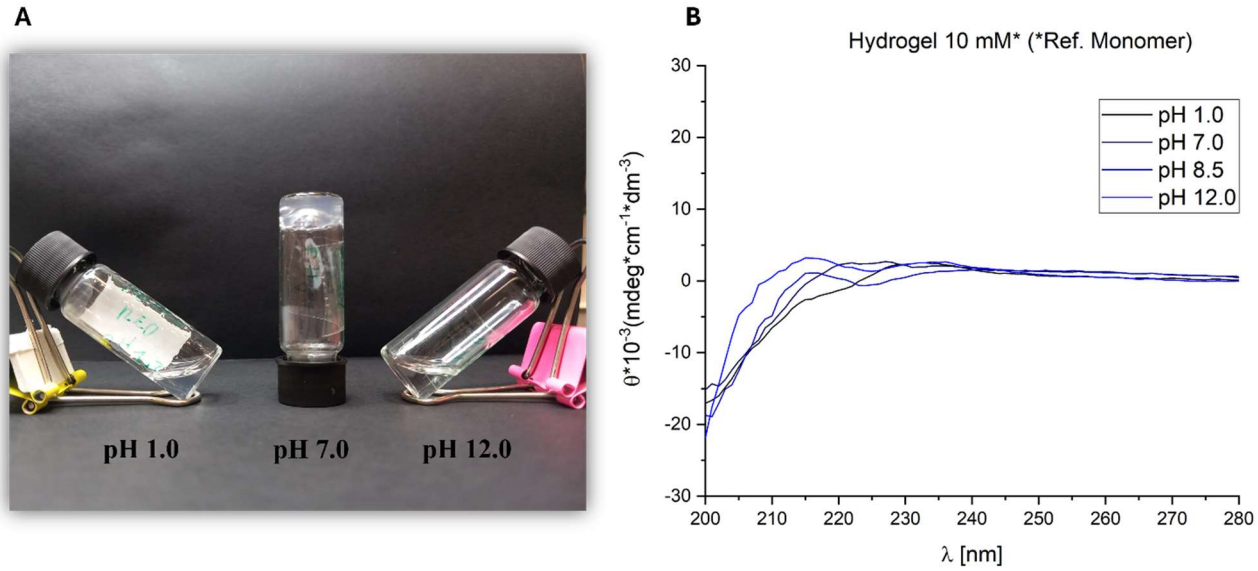

Figure 16: A: Tube inversion test for the self-assembled material at different pH values. From left to right: pH 1.0 solution with aggregates, pH 7.0 self-supporting hydrogel, pH 12.0 clear solution, **B:** Circular dichroism of the self-assembled material. Due to the high UV absorption, samples were diluted 1:2, and then the CD spectra were collected at 25 °C. The different pH does not affect the molecular conformation of the building block but the hydrogel forms only at pH 7.0 and 8.5.

It is thus possible that the pH influences the last step of the hierarchical assembly. One possibility is that the cyclopeptidic molecules stack into nanotubes at all the tested pH conditions, while their lateral association could be regulated by the Coulombic repulsion yielding a self-supporting hydrogel. However, further analyses, such as microscopy at the nanoscale, are needed to verify this hypothesis.

Hydrogels were investigated by rheology too, to ensure their gel nature at pH 8.5 and 7.0. Gels were prepared before loading their samples onto the instrument, and then they were carefully transferred with a pipette onto the rheometer plate. This process resulted in a stress that partially disrupted the material, and during the time sweep experiment (Figure 17) it was possible to observe the recovery of the gel over time. The viscoelastic properties of the two tested gels were similar, except for the kinetics of the self-assembly, which was faster at pH 7.0 and its trend appears indicating a two-step process. We inferred that the supramolecular interactions between the zwitterionic cyclopeptides are favoured at pH 7.

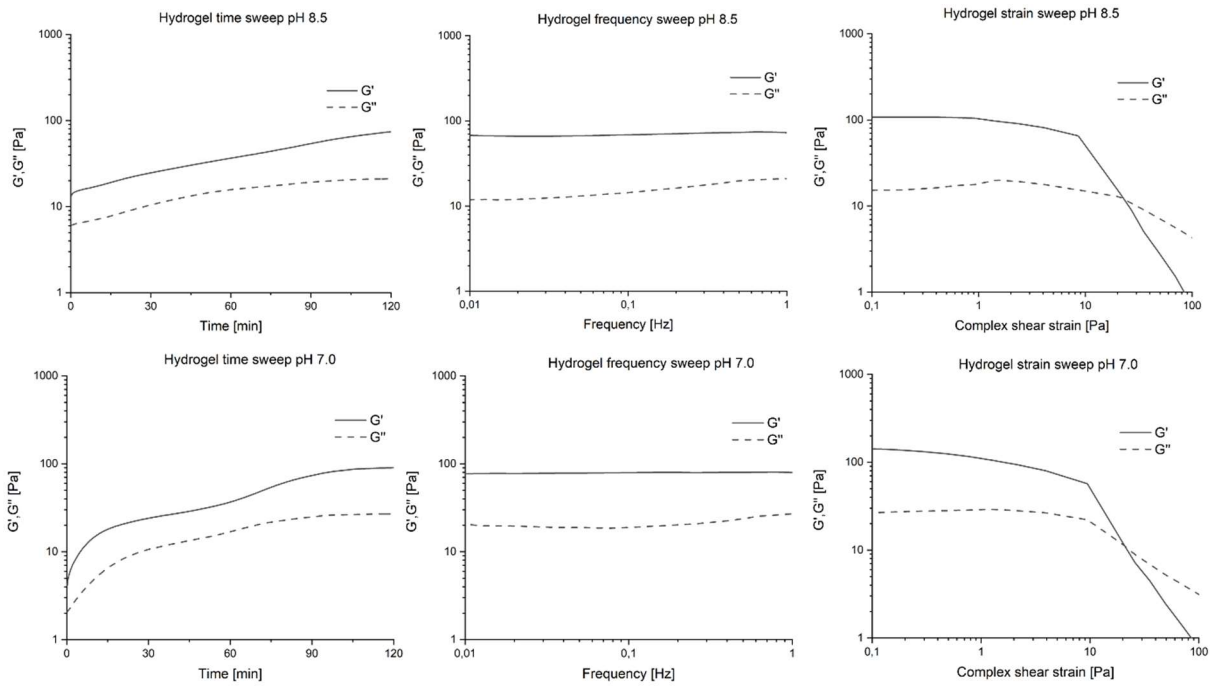

Figure 17: Rheology investigation on the hydrogel at different pH. Solid line: G' elastic modulus, dotted line: G" viscous modulus.

It is also worth noting that the rheological analyses were explorative and aimed at confirming the gel nature of the material. They were carried out on samples obtained from the DCL. In the future, further optimisation of the conditions yielding gels, for instance changing peptide concentration or buffer, could open the way to soft materials with faster kinetics and enhanced viscoelastic properties.

The hydrogel was then characterised by transmission electron microscopy (TEM) at pH 8.5 to verify the presence of nanotubes or other nanostructures. The gel was dried on the grids and stained with a sodium phosphotungstate solution (2%). TEM analyses revealed the presence of nanomorphologies compatible with supramolecular nanotubes (Figure 18). The average diameter of the nanostructures was ~2 nm and considering the size range of cyclic oligomers, the elongated structures could be composed by stacked single molecules. However, further investigation is needed to ensure the presence of these supramolecular structures at different pH values. This will shed light on the hierarchical assembly mechanism and the importance of the elongated structures in the gelation process.

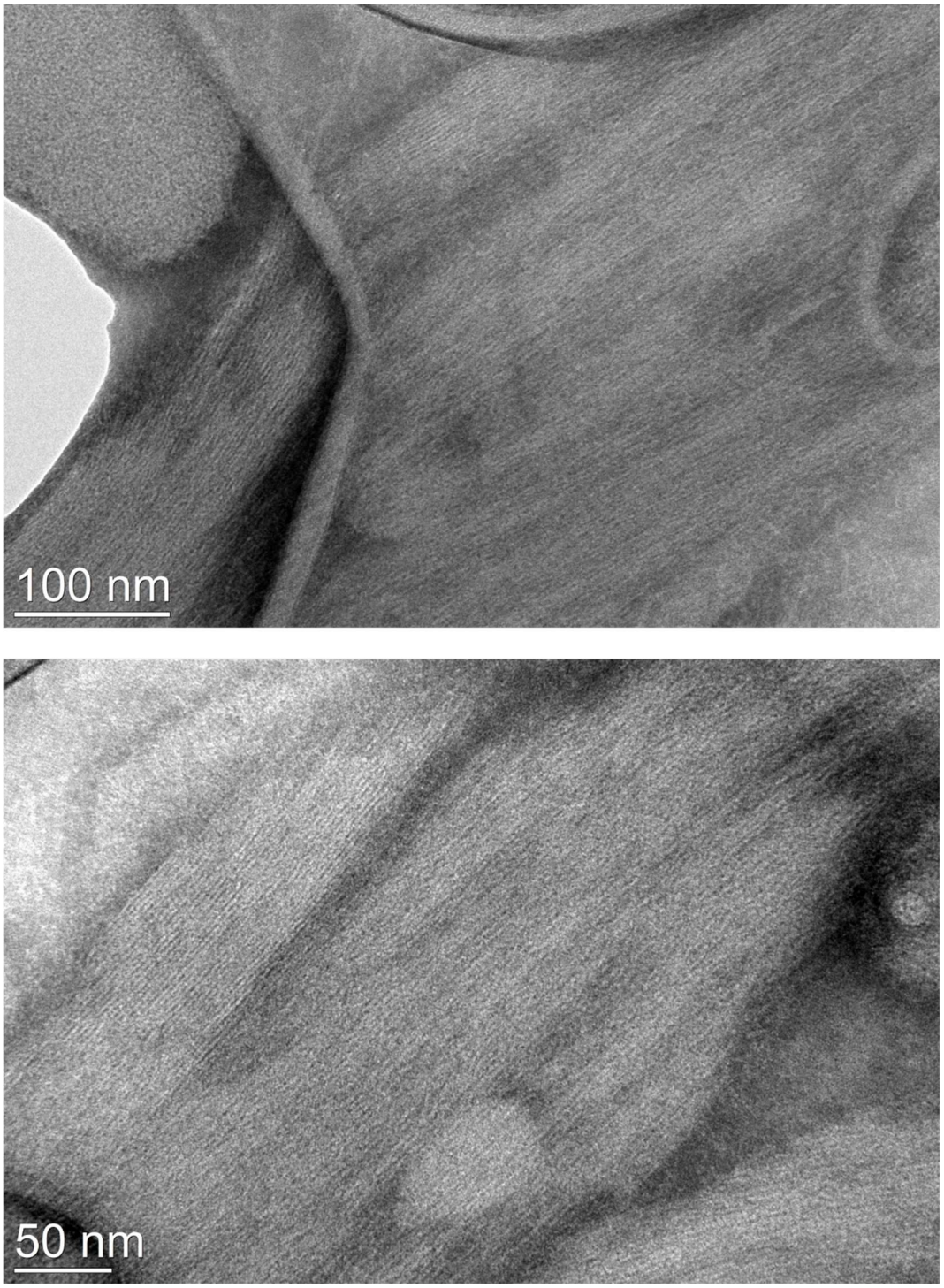

Figure 18: TEM images of the hydrogel. The mesh of the lacey grid is visible in the picture. The elongated structures present a diameter around 2 nm.

3.4 – Identification of the DCL gelator

As previously mentioned, LC-MS analyses did not allow to establish the molecular nature of the gelator(s) due to the manifest insolubility at the pH values compatible with the available equipment. It is worth noting the LC-MS mobile phase was acidic due to the presence of 0.1% of formic acid, and at these conditions the two ionizable groups (*i.e.*, the N- and C-termini) of the DCL components were protonated. In particular, the cationic ammonium group was expected to increase the cyclopeptides' solubility. A derivatisation strategy on the C-terminus was thus taken into account to change the physico-chemical properties of these compounds. In particular, esterification with methanol was undertaken by virtue of the simplicity of the reaction.

A few attempts were conducted to identify suitable reaction conditions. The hydrogel was freeze-dried, and the esterification reaction was performed in methanol, acting both as the solvent and the reactant, and being easy to remove under reduced pressure, thanks to its low boiling point. The esterification was performed with an acid catalyst. In the first attempt, TFA was used as catalyst for the reaction to enable a simple work-up by evaporation. A first trial was performed at 45 °C dissolving the peptide as 50 mM in methanol and adding TFA to reach a final concentration of 0.5 M of acid. A second trial was performed with the similar conditions under reflux. Both reactions lasted 4 hours but the esterification degree was low. In literature, a possible route for peptide esterification with $SOCl_2$ was suggested for compounds with disulfide bonds, such as oxidised glutathione.[108] A new esterification batch was thus carried out using the literature conditions. The peptide was dissolved in methanol (8 mM) and reacted with $SOCl_2$ in a ratio of 1:20 for 4 hours. This procedure proved successful, and the methyl ester derivatisation of the library was achieved. The esterification suppressed the gelation behaviour of the system, and the overall solubility was still low. The characterisation by LC-MS was possible only changing the mobile phase of the instrument as MeOH/H_2O instead of MeCN/H_2O. The LC-MS analysis revealed the presence of one main product, corresponding to a cyclo-pentamer pentamethyl ester, followed by the cyclopentamer tetramethyl-ester as minor product (Figure 19, A). This analysis thus confirmed that the favoured thermodynamic product of the DCL after the reactivation with TCEP was a single compound corresponding to the mass of a cyclic pentamer, which was able to hierarchically assemble into a hydrogel. Unfortunately, this analysis did not allow the identification of which isomer formed. The combinations of five peptide strands in a cyclic peptide indeed leads to three possible combinations: a full antiparallel isomer with all the peptides connected in a head-to-tail fashion, a single inverted strand, and a head-to-tail trimer connected to a head-to-tail dimer (Figure 19, B). All these possible compounds present a syndiotactic stereoconfiguration of the monomer, but not of the overall peptide sequence along the

cycle, and likely with isotacticity for the phenyl rings that could potentially stack and engage in hydrophobic interactions,

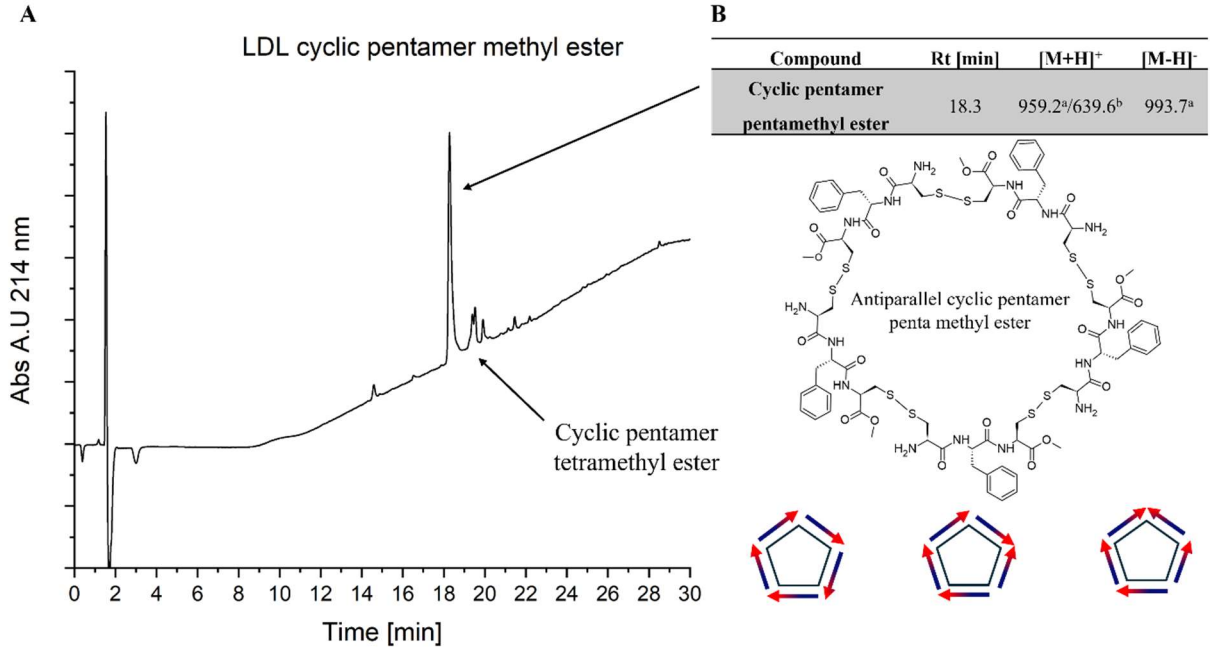

Figure 19: LC-MS analysis of the esterification product. A) The chromatography and the mass spectrometry revealed the identity of the self-assembling building block selected by the DCL: a cyclic pentamer. B) A model for the antiparallel cyclic pentamer is reported in the picture as an example. The isomerism of the product was not determined by LC-MS and further investigations are required to elucidate the covalent connectivity of the isomer, thus the direction of each monomer in the cycle.

The cyclic pentamer pentamethyl ester was purified by reverse-phase HPLC using the same mobile phase of the LC-MS analysis with the idea to characterise it by NMR, but due to its insolubility in all the available deuterated solvents, all the acquired spectra were not informative, and no signals could be clearly detected. To further confirm the identity of the product, an ESI-TOF accurate-mass spectrum of the purified compound was thus acquired (Figure 20). The analysis confirmed the identity of the product, in agreement with the LC-MS data. The ESI-TOF spectrum clearly showed the molecular ion of the cyclic pentamer pentamethyl ester with its isotopical pattern. The simulated pattern for such a molecule confirmed the experimental data obtained by LC-MS and ESI-TOF. However, residual peaks of dimers' and trimers' methyl esters were detected too, even after the HPLC purification. The origin of these signals, however is unclear, since they originate from one single peak at the HPLC, and ESI-TOF is not expected to lead to fragmentation. However, it is a more sensitive technique compared to the LC-MS (quadrupole filter), and we cannot exclude that is able to detect small impurities that are not clearly visible in the LC-MS trace, or that the small amounts of dimers and trimers originate from the cyclopentamer.

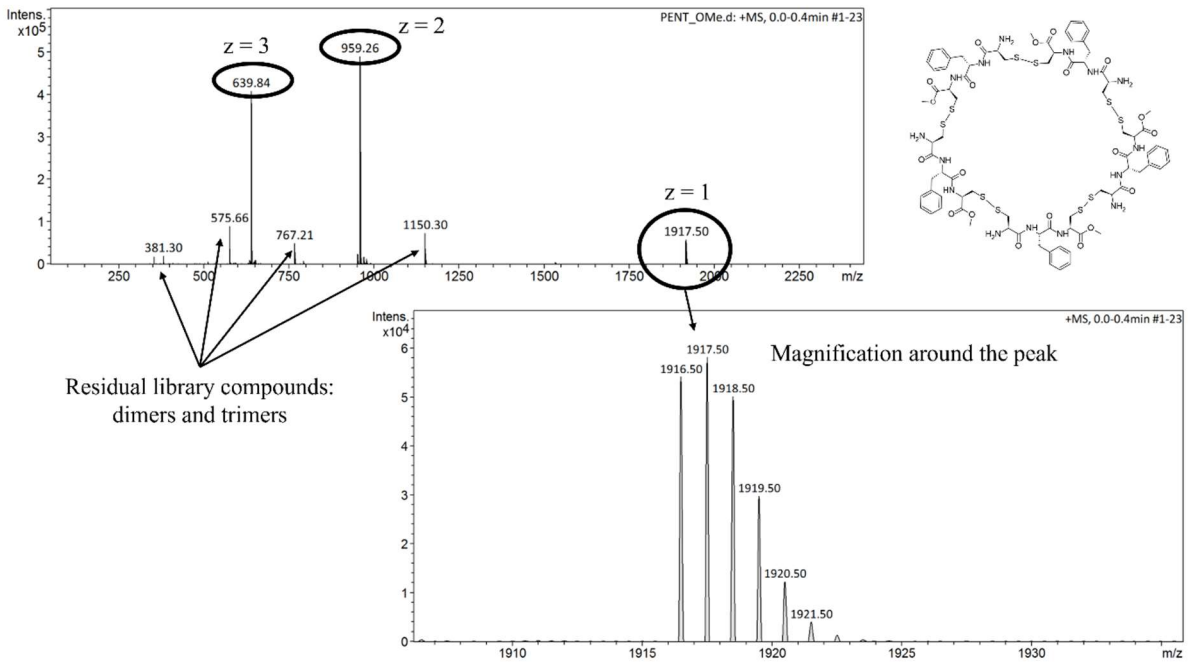

Figure 20: ESI-TOF mass spectrum of the purified cyclic pentamer pentamethyl ester. The spectrum confirmed the data of the LC-MS analysis with z = 2,3 and in this case, it was possible to observe even the signal with z = 1. The analysis of the isotopical pattern confirmed the molecularity of the product. In the mass spectrum it was possible to observe also signals of byproducts such as dimers and trimers methyl ester as impurities with the same retention time of the cyclic pentamer.

The characterisation at molecular and supramolecular level demonstrated that the system was able to self-synthesise its own building block during the DCC reaction. This molecule underwent hierarchical assembly in elongated supramolecular structures that were visible in the TEM micrographs discussed above. The anisotropic nanomorphology was compatible with the presence of nanotubes arising from the stacking of single molecules of the cyclopentamer, although further investigations are needed to confirm this hypothesis beyond any doubt. This compound was able to further assemble into a supramolecular hydrogel at pH 8.5 and 7.0. Even without the isomerism determination of the three possible cyclic pentamers, it is possible to draw some conclusions comparing these results with the literature. This cyclic pentamer is composed by fifteen amino acids divided in five syndiotactic peptide strand units connected by sulfur-sulfur bonds. This is the first reported case of a cyclic peptide arising from syndiotactic monomers and with an overall odd number of amino acids able to self-assemble in this fashion. The classical rules for cyclopeptides that stack into nanotubes require an even number of amino acids to efficiently establish a β-sheet antiparallel stacking interaction, therefore this present case is a notable exception. The experimental CD showed a signature that was different from the β-sheet, which is quite interesting, considering that the cyclic pentamer is a new type of building block that could thus assemble through a different hydrogen bonding pattern. Furthermore, in this project four tripeptide stereoisomers have been tested at the

same conditions and the LDL isomer was the only one that was able to form oligomers that were larger, compared to the cyclic dimers found in all the other three DCLs. This again underlines the role of amino acid chirality and the importance of the stereoconfiguration in the design of smart materials.

Chapter 4: Homochirality and nanotubes

4.1 – Introduction and main results

The evolution of the homochiral DCL is peculiar compared with the three heterochiral libraries. As introduced in chapter 3, the homochiral library was composed mainly by two cyclic dimers which were present in relatively similar quantities (54.4% *vs* 37.6%). In the library a cyclic trimer was also present at low concentration. The LC-MS analysis was not sufficient to fully characterise these compounds, and for this reason, the library was prepared on a larger scale to isolate its single components. After 96 hours, the library solution was freeze-dried, and then redissolved in the HPLC mixture composed of water and acetonitrile with 0.05 % TFA. The pH was monitored with the pH-meter to ensure the suitability of the solution with the HPLC mobile-phase acidic conditions. The three main components of the library were successfully separated, and their LC-MS analysis was performed once again to compare the retention time and the mass spectrum with the library data. The identity of the three compounds was confirmed, and the chromatograms showed a high purity for all the three collected fractions (A.5.1 – LLL dynamic library).

The yield of the cyclic trimer after the purification was too low to investigate this compound by NMR, and because of this, crystallisation trials were attempted to get a single crystal suitable for XRD. Unfortunately, no single crystals formed at the tested conditions, but instead the compound self-assembled in what appeared as a membrane or a hydrogel in the presence of the Zn^{2+} cation at pH 7.0 (Figure 21, B).

Instead, cyclic dimers, were purified in higher quantities and therefore they were investigated by ^{1}H-NMR, TOCSY, and ROESY. The mono-dimensional NMR spectrum with its relative TOCSY spectrum allowed to recognise the signals of the three different amino acids. For both compounds, these spectra showed a symmetric conformation and only proton chemical shifts were different for the two compounds. ROESY experiments were performed to distinguish the two isomers through the spatial proximity of the protons. Parallel and antiparallel dimers are different, due to the different directionality of the peptide strands. Thus, the parallel-dimer disulfides bind the two C-termini on one side, and the two N-termini on the other side of each peptide strand. In the case of the antiparallel dimer, the disulfide bridge binds in both cases the N- and C-terminal Cys sidechains. Such a difference between the two dimers is important, since the ROESY experiment could help to distinguish these two possible situations. Unfortunately, no characteristic cross-peaks were detected, and the two compounds were still not distinguishable by NMR. Because of this, crystallisation trials

were performed on these compounds and crystals were obtained for both of them. The cyclic dimers' chemical structure has thus been fully characterised by single-crystal XRD.

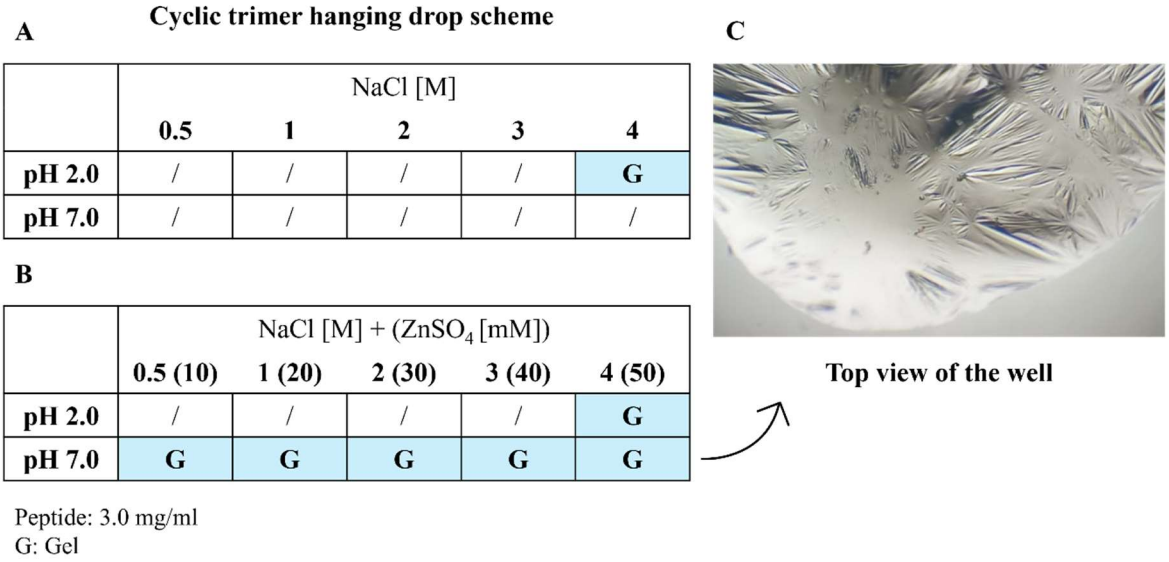

Figure 21: Crystallisation trials for the purified LLL cyclic trimer. A) Hanging drop experiment at acidic and neutral pH with increasing ionic strength (NaCl). In acidic pH, and at high ionic strength (NaCl 4M), the compound self-assembled in what appeared like a membrane or hydrogel. B) Hanging drop scheme with the same parameters of A and the presence of $ZnSO_4$ at different concentrations. At pH 7.0, the compound self-assembled in a material that appeared like a membrane or a hydrogel in all the tested conditions. C) Optical microscope picture of the material formed in the B hanging drop experiment.

4.2 – NMR investigation of cyclic dimers

The two cyclic dimers have been characterised by NMR with the following techniques: ^{1}H-NMR, TOCSY (A.6 – Cyclic dimers NMR characterisation) and ROESY. The latter is a useful technique that allows to observe the spatial proximity of two NMR-active nuclei. The ROESY technique is based on the nuclear Overhauser effect (NOE). This effect enhances the NMR signal of an observed nucleus through the saturation of a neighbour nucleus in spatial proximity (< 5 Å). This is due to the cross-relaxation of the perturbed populations of the spin system through dipole-dipole interaction.[109] This means that the effect can be observed also for nuclei which are not close in terms of number of sigma bonds, but they are just close in space. This is a very useful technique to determine the conformation of organic molecules, thanks to the structural information obtained from the enhanced signals.[110] The signal is inversely proportional to the sixth power of the distance between the observed, and saturated nucleus. Thus, it is possible to measure distances between nuclei with this technique. The NOE effect can be positive or negative depending on the relaxation mechanism

involved in the process. This depends on the size of the molecule and on its correlation time. Low-viscosity solvents and small molecules produce a positive NOE signal, whereas polymers and big molecules produce a negative effect. The molecular tumbling rate in solution is an important parameter that regulates the magnitude of the NOE, and it is correlated with the mobility and molecular size in solution. There is a molecular-size range in which the NOE change sign, and therefore it is close to 0. In this case, NOE in mono-dimensional NOE and NOESY (*i.e.,* the bidimensional version of the technique) can be undetectable. This is the case for molecules in the range of 500-1000 Da. Considering the size of these cyclic macrocycles (738.91 Da), these molecules fell in the critical region for the NOESY technique.

The rotating frame NOE (ROE or ROESY) is a technique that allows to overcome this problem to study the NOE of medium-size molecules. The technique does not have the same dependence on the molecular tumbling rate as NOESY (Figure 22). On one hand, the ROE signal magnitude is always positive, and it is possible to explore the region of the medium sized molecules where the NOE signal magnitude is close to 0. On the other hand, the NOE for large molecules shows a higher absolute magnitude than the ROE. Therefore, the choice of the technique is crucial and must be carefully evaluated.

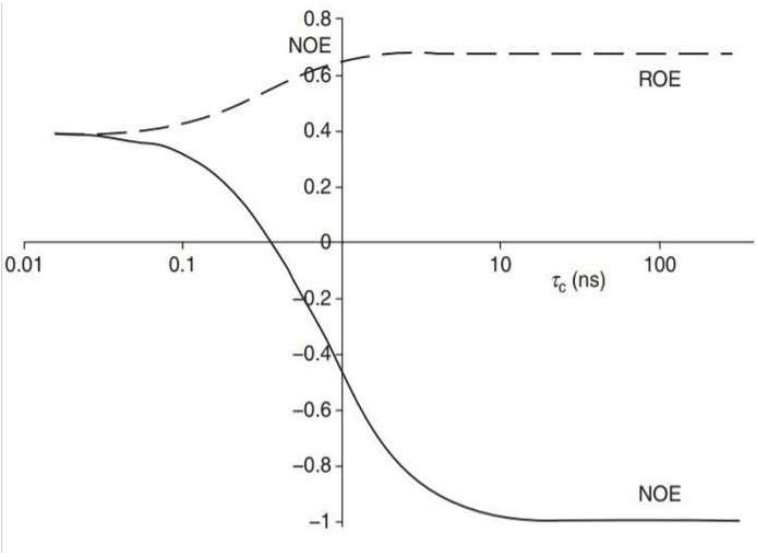

Figure 22: Signal magnitude for NOE and ROE in function of the molecular tumbling rate. The ROE is always positive whereas the NOE is positive for small molecules (fast tumbling rate) and negative for large molecules (slow tumbling rate). Reproduced from Ref. 110 with the permission from Elsevier.

Another crucial parameter for these techniques is the mixing time. This is the time in which the magnetization is transferred between the two nuclei. On one hand, a short mixing time does not allow a proper magnetisation transfer and therefore the NOE (or ROE) can be undetectable. On the other

hand, too-long mixing times can relax the nucleus and again the NOE (or ROE) can be undetectable. Therefore, the mixing time depends on case by case. Furthermore, the mixing time for NOESY and ROESY are different. The ROE builds up faster than the NOE. Therefore, a shorter mixing time might be appropriate for this technique. However, it is possible to have an estimation of the mixing time range in the following table adapted from ref 109:

Size of the molecule	NOESY [ms]	ROESY [ms]
Small (< 500 Da)	400-500	200-300
Medium (500-1000 Da)	200-400	70-200
Large (>> 1000 Da)	100-200	35-70

Table 2: Mixing times expressed in milliseconds for NOESY and ROESY considering the three classes of molecular size.

However, it is important to consider also the instrumental features. A *Varian Innova* 400 MHz NMR instrument was used to acquire the ROESY spectra in this thesis. The instrument manual discourages the use of long mixing times, because due to the energy transferred to the sample, the probe can be damaged during long acquisitions. Considering all these elements, for the cyclic dimers investigation mixing times of 150 and 200 ms were selected; the latter gave the best results.

Another interesting feature of ROESY compared to NOESY is the possibility to distinguish cross-peaks of exchanging protons. The ROESY diagonal peaks have opposite phase compared to the ROE cross-peaks, thus enabling their clear identification. Exchanging protons can be seen as well in ROESY, but the phase of these signals is the same of the diagonal. Therefore, it is possible to distinguish cross-peaks from ROE and from exchanging protons. In NOESY, all the cross-peaks have the same phase.

4.2.1 – Antiparallel cyclic dimer ROESY

The antiparallel cyclic dimer was dissolved in deuterated water, and the compound was investigated by ^{1}H NMR, TOCSY (A.6 – Cyclic dimers NMR characterisation), and ROESY (Figure 23). All the ROESY cross-peaks gave the same information of the TOCSY experiment; therefore, it was only possible to detect the proximity of the well-known connected protons of the molecule. The conformation of the macrocycle in D_2O at the tested conditions did not reveal crucial ROE signals. Therefore, the macrocycle is indistinguishable from the parallel dimer in this ROESY experiment. The spectrum helped in the signal assignation as well as the TOCSY because it was possible to

observe the cross-peaks relative to the Phe residue. The aromatic ring is a closed spin system, and in the TOCSY spectrum, no cross-peaks were detectable between the aromatic ring and the beta protons of its sidechain. In the ROESY spectrum it was possible to observe the spatial proximity of the Phe beta protons to the aromatic ring and thus it was possible to distinguish clearly the signals of this amino acid from the others.

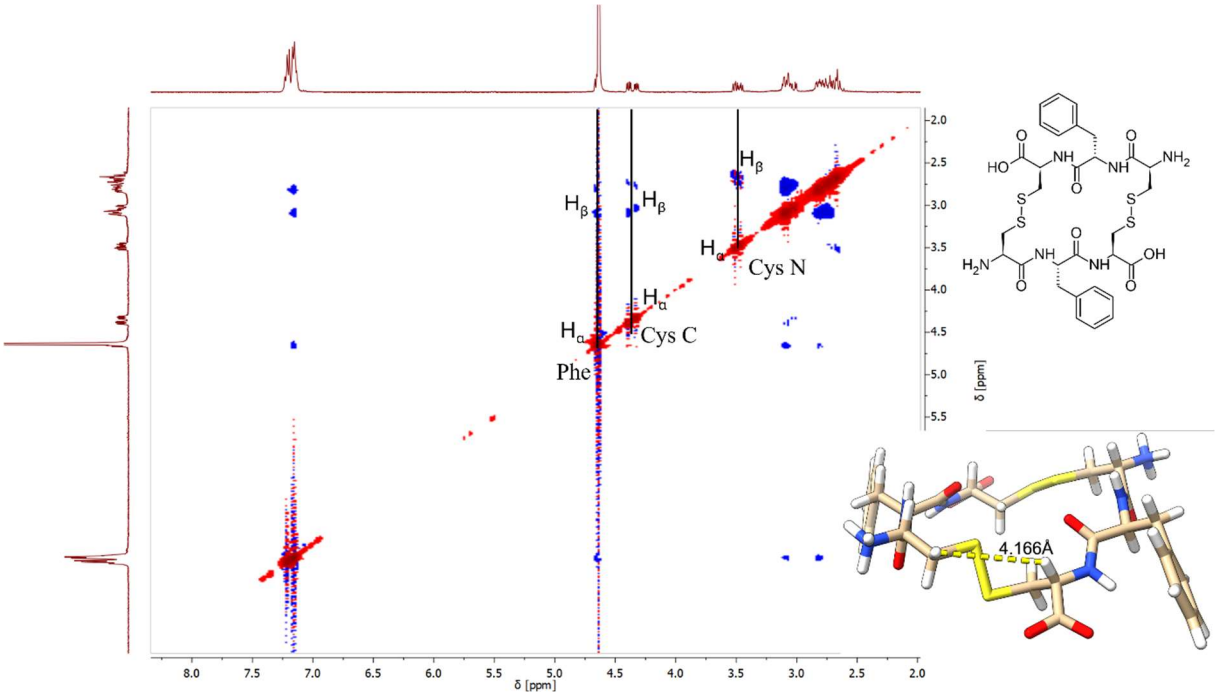

Figure 23: NMR ROESY 400 MHz of LLL antiparallel cyclic dimer in D_2O (mixing time 200 ms). A pictorial representation made by Avogadro software, and rendered by Chimera software is shown as inset in the bottom-right corner to illustrate the scope of the experiment. The intention of the model is to highlight a possible NOE effect between the N-terminal and C-terminal Cys residues.

A conceptual model was created with Avogadro software, and then rendered with Chimera software to illustrate the scope of the ROESY experiment. Antiparallel cyclic isomers are characterised by the disulfide bond between the C-, and the N-terminal Cys sidechain. In line of principle, the proximity of these two amino acids, thanks to the sulfur-sulfur bond, makes these isomers good candidates for the ROESY investigation. However, in this case no cross-peaks were observed, and therefore it was not possible to characterise this isomer by the ROESY technique.

4.2.2 – Parallel cyclic dimer ROESY

The parallel cyclic dimer was dissolved in DMSO-d_6 because in this solvent it is possible to observe the amide protons. The previous isomer was found to be insoluble in DMSO and deuterated

water was the only possible choice. The parallel cyclic dimer instead dissolved in DMSO, and it was possible to acquire its ^{1}H-NMR, TOCSY (A.6 – Cyclic dimers NMR characterisation) and ROESY spectrum (Figure 24). As in the previous case, mono-dimensional NMR combined with TOCSY allowed to characterise the spin systems of the three amino acids. Even in this case, the molecule appeared symmetric, and the relative intensity of the signals highlighted only three amino acids. The compound was then studied by ROESY as well, but even this time no characteristic cross-peaks were detectable (Figure 24). Therefore, for the couple of LLL cyclic dimers, the NMR investigation did not allow to distinguish between the two isomers.

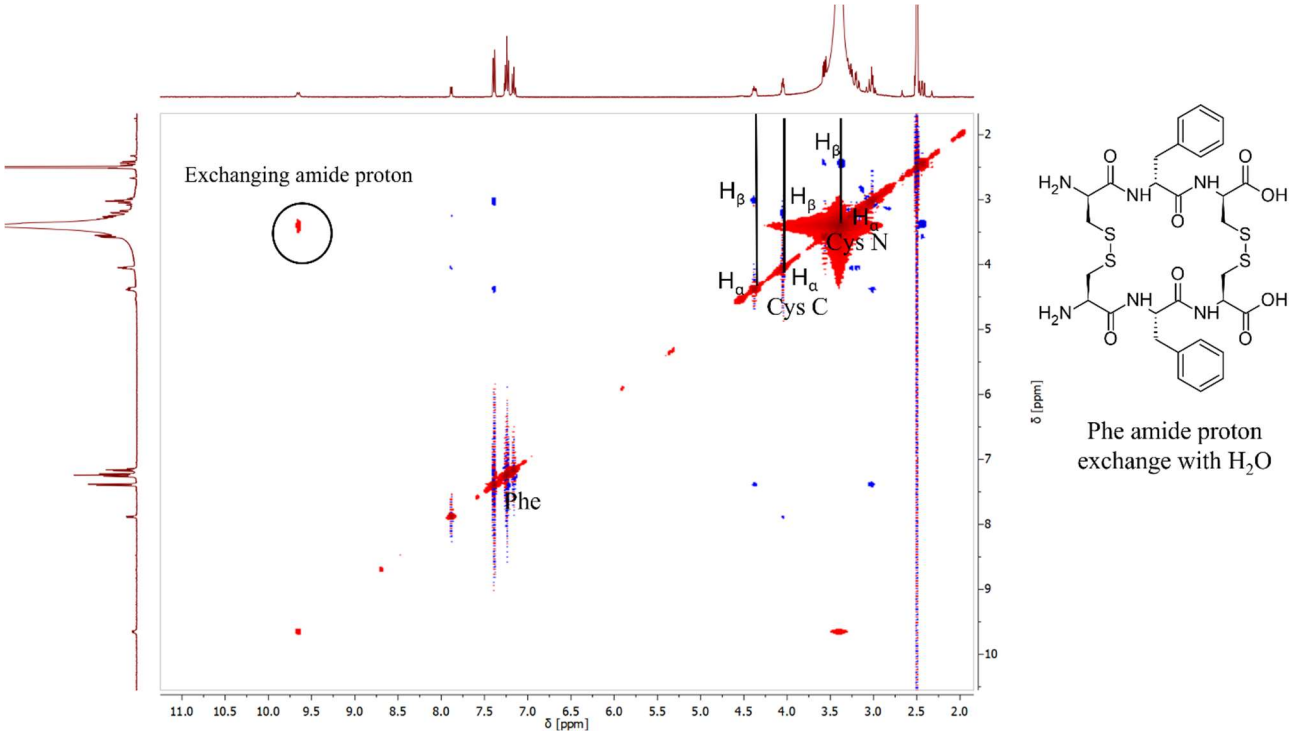

Figure 24: NMR ROESY 400 MHz of LLL parallel cyclic dimer in DMSO-*d*$_6$ (mixing time 200 ms). Phe amide proton exchange with water.

The ROESY spectrum showed a cross-peak with the same phase of the diagonal peaks for one amide group. The Phe amide proton exchanges with water present in the solvent, as highlighted by the position and the phase of the cross-peak shown in Figure 24. Unfortunately, it was not possible to compare this result with the previous ROESY experiment, since amides are not visible in D_2O, but still, it is an interesting detail. This exchanging proton could suggest that this amide group is not involved in intramolecular hydrogen-bonding, thus opening the possibility to stack this compound in nanotubes through inter-molecular H-bonds. The parallel cyclic dimer is the main compound of this library, and the absence of this intramolecular interaction is interesting considering that it could be decisive in the dimer stabilisation during the DCC. Thus, it is possible that both homochiral cyclic

dimers lack this possible non-covalent interaction and, this might explain the difference between this library and the three heterochiral DCL. Anyway, further characterisation and analyses are required to confirm this hypothesis.

4.3 – Single-crystal XRD of cyclic dimers

The NMR analysis did not allow to distinguish the two isomers, although it provided some insights on the conformations of these two molecular species. The antiparallel dimer adopts a conformation in which N-Cys and C-Cys are distant, and no cross-peaks were detectable by ROESY between these two terminal amino acids. The parallel dimer in DMSO showed an exchanging amide proton, opening the possibility for inter-molecular hydrogen bonding as described in traditional cyclopeptide nanotubes.

The isomerism of both cyclic dimers were determined by single-crystal XRD. Compounds were crystallised by the hanging drop technique. Crystallisation trials in organic solvents were attempted as well, but both dimers were insoluble. Hanging drop is a vapour-diffusion method for the crystallisation of molecules in aqueous solution, and it is a well-known technique in protein crystallography.[111] In this technique, the peptide is dissolved in undersaturation conditions (Figure 25, ii), and then the system is allowed to equilibrate through vapour diffusion. The setup of the experiment requires the use of a larger volume solution with a crystallising agent called *reservoir,* and a smaller volume peptide solution forming a drop. The *reservoir* could be a saline solution with a particular ionic strength and therefore a certain vapour pressure. The peptide solution is obtained dissolving the peptide in undersaturation conditions and then diluting this solution 1:2 with the *reservoir.* The saline concentration of the *reservoir* is orders of magnitude higher than the peptide concentration, therefore the system can be described just in terms of saline concentration. At the start of the experiment, the two solutions are placed in a close environment and allowed to equilibrate. The *reservoir* possesses a double concentration of salts compared to the peptide solution. Therefore, the two solutions are not in equilibrium since they have different vapour pressures. The thermodynamic equilibrium is reached through the solvent evaporation from the peptide solution towards the *reservoir*. This rises the concentration of the saline content in the peptide drop and when the vapour pressure of the two solutions is equal, the evaporation stops.

From the peptide point of view, the process is described in Figure 25, ii. The evaporation of solvent from the peptide solution leads to higher concentration of both the peptide and the saline content (the adjustable parameter).

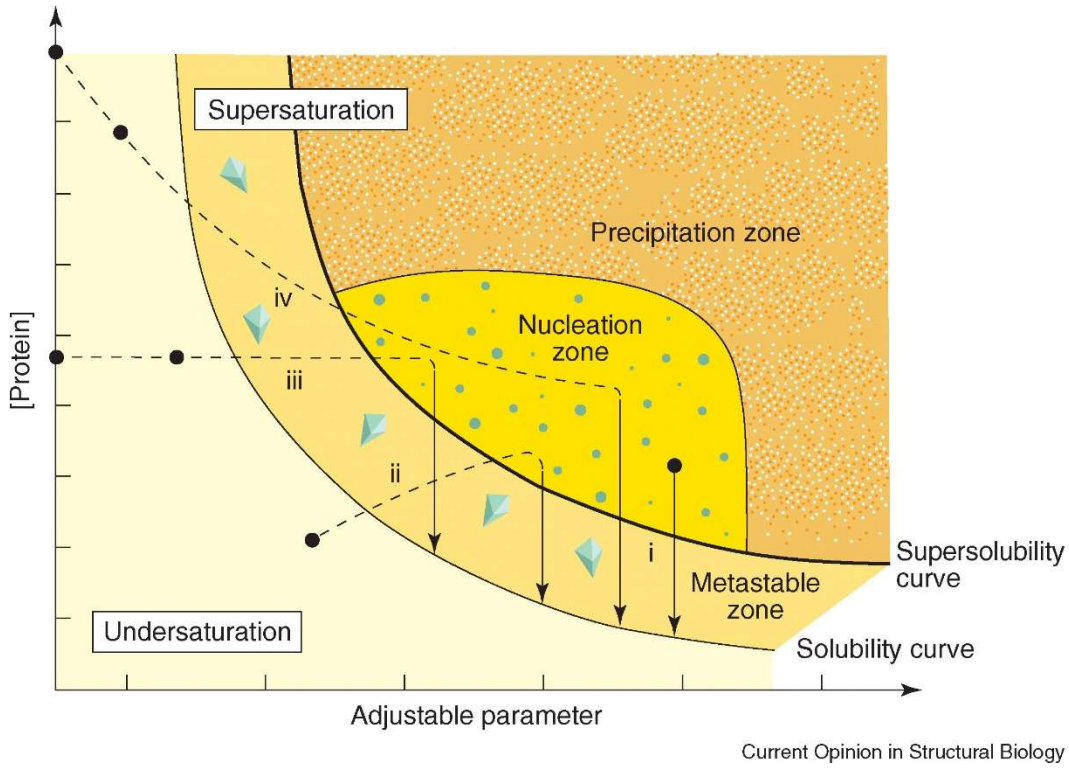

Figure 25: Solubility of a generic protein/peptide in function of an adjustable parameter. For instance, this parameter can be the ionic strength. Different crystallisation paths are represented: (i) Batch. (ii) Vapour diffusion. (iii) Dialysis. (iv) Free-interface diffusion (FID). Reproduced from Ref. 111 with the permission from Elsevier

The peptide enters the metastable zone which is the ideal situation for the crystal growth. When the nucleation zone is reached, the crystallisation starts, and it causes a decrease in peptide concentration from the solution. Crystals grow in the metastable zone and the process stops when the peptide concentration reaches the solubility curve. It is important to set the starting parameters to avoid the precipitation zone. It is also important to reach the nucleation zone to trigger the crystallisation process. The vapour diffusion regulates the kinetics of the evaporation, thus it is possible to grow few larger crystals even with difficult peptides, instead of powders. The temperature must be constant during the whole experiment.

Both cyclic dimers were crystallised successfully with this technique, and all the details are reported in appendix (A.9.1 – LLL stereoisomers). It was possible to acquire XRD data and solve two crystallographic structures: one for the antiparallel dimer and one for the parallel dimer. The antiparallel dimer crystallised at acidic and neutral pH yielding different shapes of crystals (Figure 26, panels A and B). The crystalline habit is very different between these two conditions and since nanotubes are expected to crystallise when the Coulombic repulsion between the suprastructure is

minimised by the pH, the needle-shape at pH 7.2 was in agreement with this prediction. The XRD structure in acidic conditions is still under elaboration.

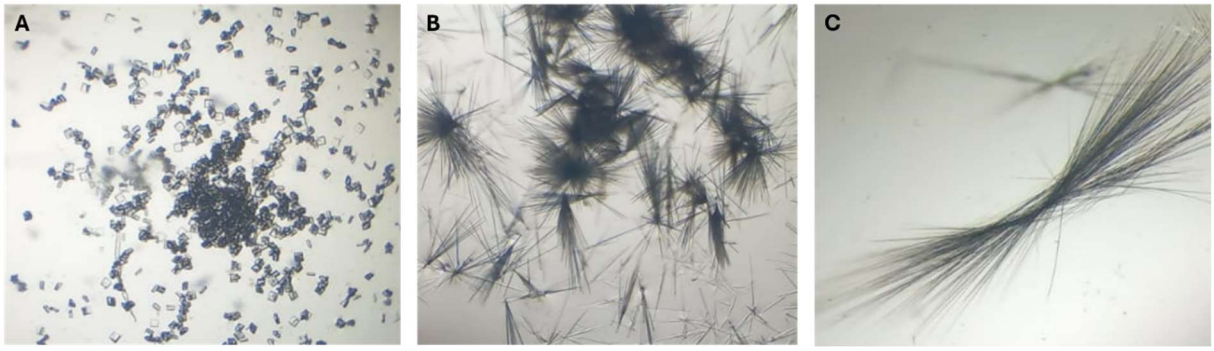

Figure 26: Optical microscope images of crystals obtained in the hanging drop experiment. A) Antiparallel dimer at pH 1.2, cubic-shaped crystals. B) Antiparallel dimer at pH 7.2. needle-shaped crystals. C) Parallel dimer at pH 7.2, needle-shaped crystals. These crystals were very flexible and only few diffracted.

The parallel dimer crystallised only in neutral pH, and most of the crystallisation batches were composed by non-diffracting fibres. The crystals obtained at pH 7.2 were thin and flexible (Figure 26, panel C) and only few of them diffracted. Data collection was obtained only for one small thicker crystal after a long search in the middle of flexible fibres. The diffraction was lost quickly during the data collection, and for this reason, the redundancy of the data was not high.

4.3.1 – Antiparallel cyclic dimer

The compound crystallised in the monoclinic crystal system with the spacegroup C2. Several crystals were collected but the resolution was always limited at 0.9 Å. The compound crystallised with a 2-fold symmetry axis in the centre of the macrocycle and therefore only one peptide strand is present in the asymmetric unit with four water molecules. No counterions were detected, and the peptide is zwitterionic as expected from the crystallisation conditions. Macrocycles are stacked in nanotubes *via* hydrogen bond (Figure 27, B). The cavity of the macrocycle is too narrow to accommodate solvent molecules, and all the water molecules are packed outside the nanotube. The water fills the cavities between nanotubes due to the open conformation of the Phe rings. It is peculiar that even though the aromatic rings are surrounded by water, they do not appear disordered. Peptides stack via hydrogen bonding between amide groups reproducing a parallel β-sheet pattern (Figure 28, A). The conformation of the backbone is close to the zig-zag conformation and the Phe residue shows

torsional angles close to 180°. Nanotubes are connected by salt bridges between the macrocycle carboxylate and ammonium group, and they are slightly staggered between each other (Figure 28, B).

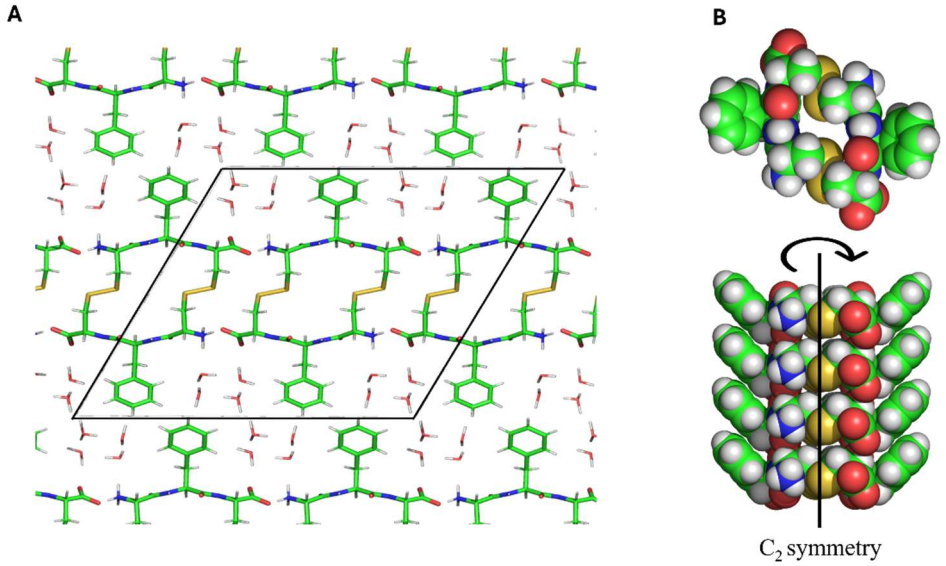

Figure 27: A) LLL antiparallel dimer zwitterion unit cell, view along the *b* crystallographic axis. B) space filling model of the macrocycle with the top and side view of the nanotube. The macrocycle cavity is too narrow to be filled with water. Green: carbon, blue: nitrogen, red: oxygen. yellow: sulfur, white: hydrogen.

The large cavities between the Phe rings are filled with water. The solvent molecules are organised through a hydrogen-bond network which involves also the carboxylate and the ammonium groups of the peptide (Figure 29). The macrocycles are related to each other via a 2-fold rotational axis which falls in the middle of the water cavity. It is interesting to note that peptides and the oxygen atom of water molecules are related by this symmetry, but not the hydrogen-bond network. The water in the asymmetric unit shows a slight disorder. This is due to the presence of two possible hydrogen-bond networks. The water can be divided into two clusters: cluster A and cluster B. Their oxygen atoms respect the 2-fold symmetry axis. The water molecule close to the rotational axis of the cluster A interacts with its symmetry related copy in cluster B. However, because of the symmetry, two hydrogens should point towards each other, and this is not chemically possible. The rationalisation of the network leads then towards two different hydrogen-bond networks in which two water molecules are not symmetrically equivalent. In Figure 29 it is possible to observe that the green and blue water molecules are rotated differently in the two clusters. In network A, the blue water points towards the Phe ring, whereas in the network B this molecule interacts with the green water that is then rotated towards the other cluster connecting the two networks.

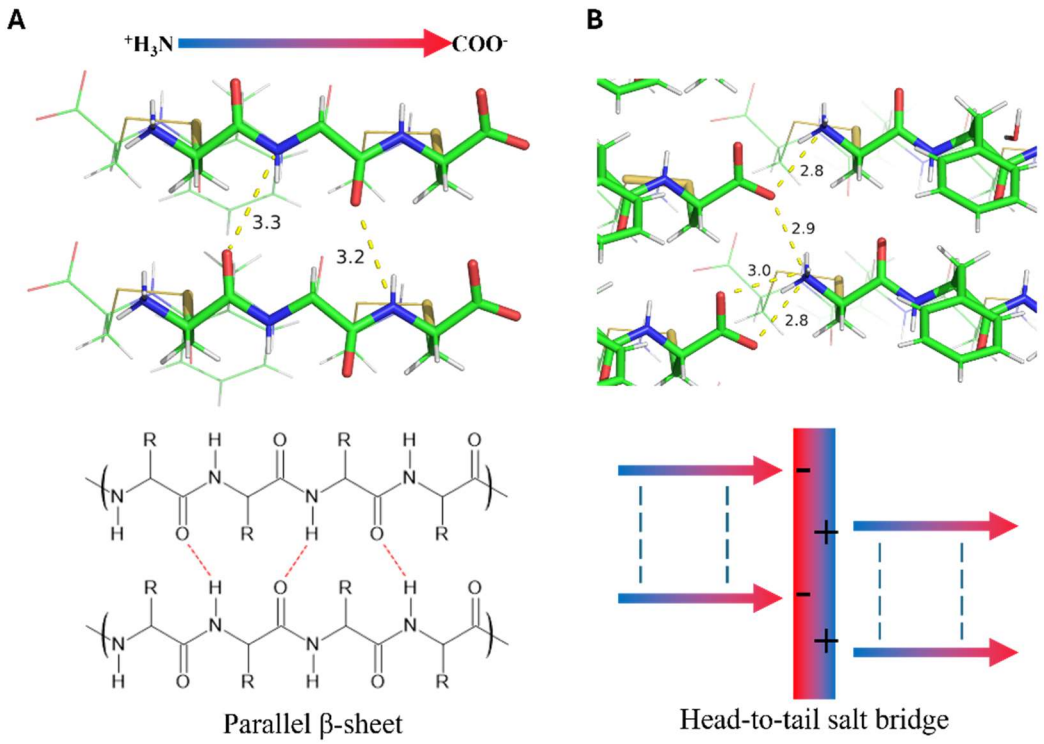

Figure 28: Nanotube hydrogen-bond interactions. A) amide hydrogen-bond stacking between macrocycles. Macrocycles interact with a parallel beta-sheet pattern. B) Salt bridges between nanotubes. Backbones are represented in sticks and wire. Phe aromatic ring in figure A is omitted for clarity.

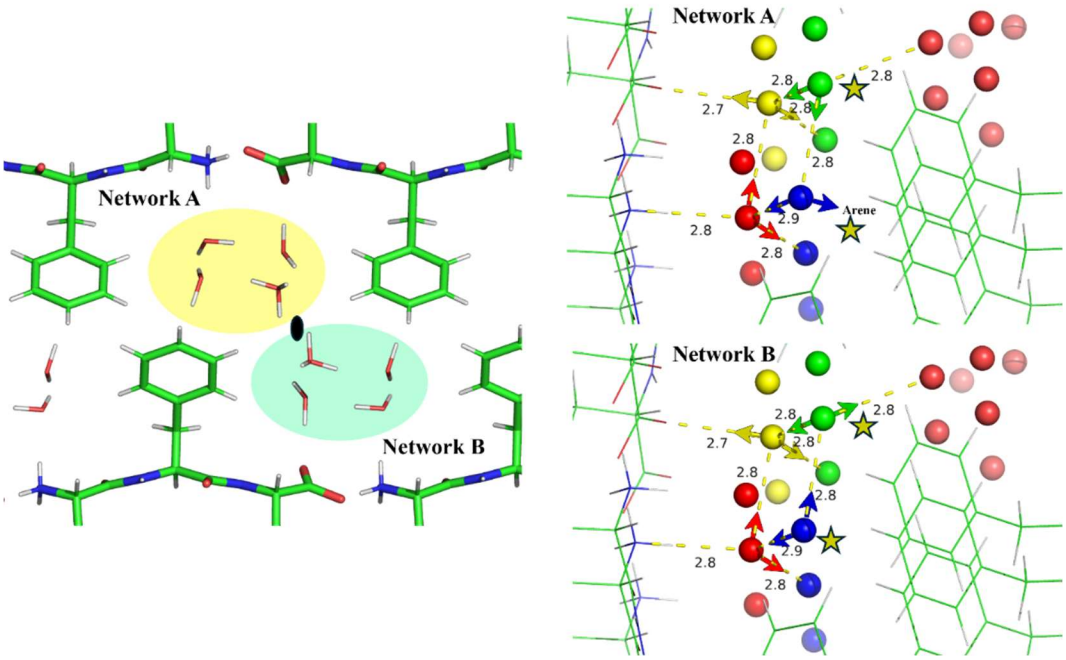

Figure 29: Solvent packing in the cavity. The black oval is placed on the C_2 symmetry axis (left image). The hydrogen-bond network (right image) can be represented as two clusters, which are not related by symmetry. Water molecule oxygens are coloured in green, blue, yellow, and red to show the disposition along the column. Yellow stars denote their differing orientation. Hydrogens are represented with arrows to depict the hydrogen bond network.

4.3.2 – Parallel cyclic dimer

The parallel dimer crystallised in the orthorhombic crystal system with the space group $P2_12_12_1$. The asymmetric unit is composed by the macrocycle and disordered water molecules. In the model, there are five water molecules (two inside the cavity and three between the macrocycles) with an overall occupancy of 1.5. This disorder could explain why the crystal diffracted only at 0.9 Å of resolution. The overall packing shows one independent macrocycle stacked in nanotubes along the *a* crystallographic axis (Figure 30, A), and disordered water in the nanotube cavity, and between nanotubes. The peptide crystallised as a zwitterion, and no counterions are present in the crystal as expected from the crystallisation conditions (pH 7.2). The space-filling model of the nanotube highlights the cavity created by the macrocycle (Figure 30, B). The parallel dimer, compared to the antiparallel isomer, displays two different sides of the nanotube: one composed by two carboxylate groups and the other with two amine groups. In this case, the conformation is not symmetric as in the previous crystal structure, and the two peptide strands have different dihedral angles.

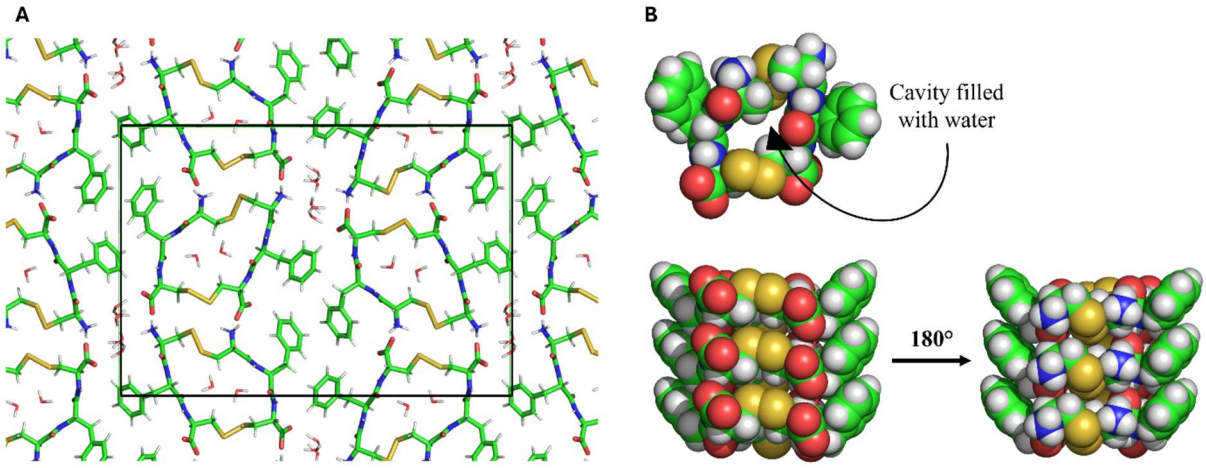

Figure 30: A) LLL parallel cyclic dimer crystal packing along the *a* crystallographic axis. Water between the nanotubes is disordered and there are three possible positions from one water molecule. B) Space-filling model of the macrocycle. The cavity is filled with water (omitted). Nanotube side-view of the carboxylate and ammonium face. Green: carbon, blue: nitrogen, red: oxygen. yellow: sulfur, white: hydrogen.

The nanotube is formed by peptides' stacks *via* hydrogen-bonds, forming a parallel β-sheet motif as in the case of the antiparallel dimer (Figure 31, left). The macrocycle can be split into two peptide strands: considering the nanotube stack, strand 1 is bonded through hydrogen bond to another strand 1, and the same is true for strand 2. The cavity of the nanotube is filled with water. Two possible positions were found analysing the electron density map. The occupancy of the two water molecules is low (0.2 and 0.3). The inner cavity of the tube is hydrophobic considering the presence of the two

sulfur atoms and the absence of polar groups. According to the electron density map, it is possible that the two water molecules point their hydrogen atoms towards the carbonyls involved in the stacking between macrocycles and sulfur lone pairs. All these details suggest that water is loosely bound inside the macrocycle, and it is possible that solvent might flow inside the supramolecular structure.

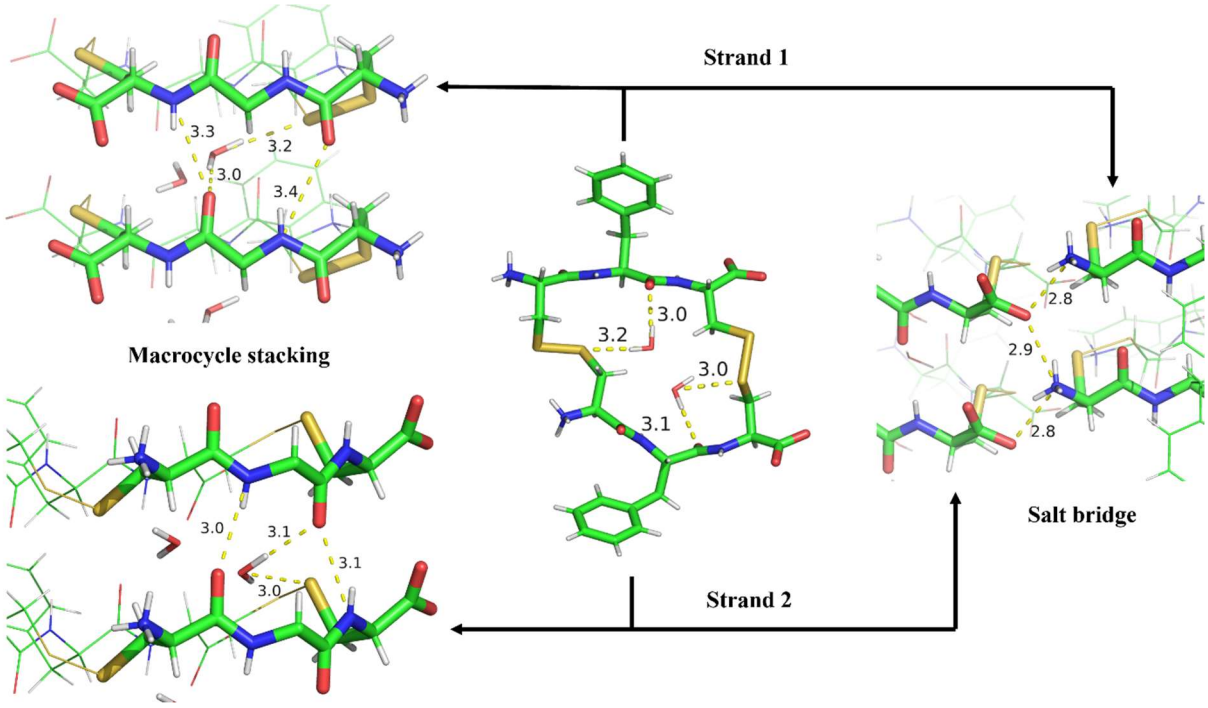

Figure 31: Hydrogen bond network of the macrocycle. Left: stacking along the nanotube. The macrocycle interacts through a parallel β-sheet pattern. Two water molecules are trapped inside the hydrophobic cavity of the macrocycle. The solvent interacts *via* hydrogen-bonding. The first water molecule interacts with the strand 1 through the Phe carbonyl and a sulfur lone pair. The second water molecule interacts with the strand 2 through the N-Cys carbonyl and another sulfur lone pair. The two water molecules are isolated from the rest of the solvent inside the cavity. Right: salt bridges between nanotubes. The head-to-tail interaction is an alternate strand 1/strand 2 interaction between COO- and NH_3^+. Nanotubes are staggered and one ammonium group interacts with carboxylates from two different macrocycles of the neighbour tube.

Nanotubes are packed through salt bridges between ammonium and carboxylates (Figure 31, right). The ammonium side of the nanotube interacts with the carboxylate side of another nanotube, and the tubes relative position is staggered. Thus, ammonium and carboxylates groups are zipped along the nanotube axis. Phe aromatic rings are stacked in hydrophobic domains between layers of salt-bridged nanotubes. Due to the size of the macrocycle compared with the Phe aromatic ring, this leads to alternating hydrophobic domains constituted by aromatic rings, and disorder water columns. The disordered water bridges the polar groups between layers of macrocycles. In the asymmetric unit, three positions were found for water molecules according to the electron density map and the overall

occupancy is 1.0 (0.5, 0.25, 0.25). This could be another detail that might explain the low resolution of the data collection. Crystals, as discussed above, were very flexible, and similar to fibres. Considering the nanotube packing and the disordered water pockets between nanotubes, this might be the reason of the flexibility of the solid state.

4.4 – Comparison between antiparallel and parallel cyclic dimer

In conclusion, both macrocycles were studied by ROESY and single-crystal XRD. The NMR study did not allow to assign the correct isomerism for the two compounds. The two XRD structures highlighted the reason: the α-protons from N- and C-terminal Cys are too far away from each other, because of the conformation of the macrocycle (> 7 Å), and no ROE is detectable for both isomers. The β-protons of the two Cys sidechains should be close enough, but since ROESY did not detect any signal, this fact suggests that the conformation in solution is different compared to the solid state. Both macrocycles stack into nanotubes *via* hydrogen bonds. The antiparallel dimer forms a *C2* symmetric nanotube, and the two peptide strands have the same conformation, whereas the parallel dimer nanotube has no symmetry (Figure 32, A). In solid state, no intramolecular hydrogen bonding was observed for either isomer, and this might explain the results of the kinetics study. Nanotubes were observed at pH 7 and the crystallisation trials in alkaline pH highlighted a higher solubility for both isomers (A.9.1 – LLL stereoisomers). Thus, the self-assembly did not occur at alkaline pH and the two macrocycles were formed in the DCL without a template effect or possible intramolecular hydrogen-bonding. This might explain the high relative percentage of both isomers for the homochiral library.

As a consequence of the running direction of the peptide strands in the macrocycle, the antiparallel dimer has a *C2* rotational axis which relates the two peptide strands. A parallel isomer is formed turning upside-down one of the two peptide strands and, for this reason, the macrocycle lost the *C2* symmetry. A possible symmetric parallel dimer could be obtained combining an LLL strand with a DDD. In this case, the two strands will be related by a mirror plane and a possible symmetric structure could be obtained. In the parallel cyclic dimer, the strand 2 is tilted compared to the strand 1 and, to the antiparallel dimer too (Figure 32, B and C). The parallel dimer symmetry observed by ROESY could be due to the fast interconversion between different conformations in solution.

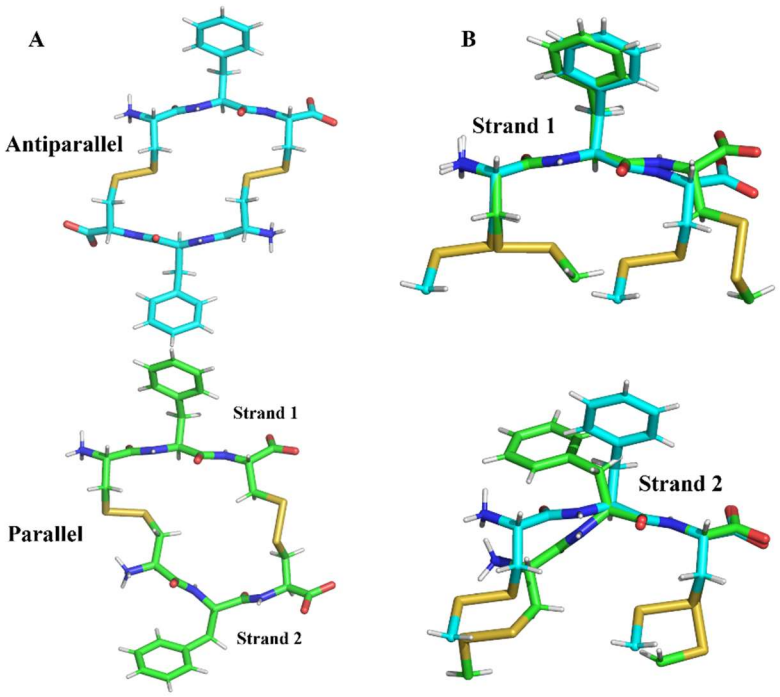

C

Peptide	Phe φ	Phe ψ
Antiparallel	-156.4	160.1
Parallel str. 1	-160.4	172.9
Parallel str. 2	-134.6	130.5

Figure 32: A) Antiparallel (cyan) and parallel (green) homochiral cyclic dimers. The two strands of the antiparallel dimer are related by C2 symmetry, and they share the same conformation. Parallel dimer is not symmetric, and the two strands have different torsional angles. B) Overlap of the strand of antiparallel dimer (cyan) with the two different strands of the parallel dimer (green). C) Table of the Phe torsional angles for the three different strands.

Chapter 5: Heterochiral cyclic dimers

All the three heterochiral libraries were characterised by NMR and XRD, where possible, as in the case of the homochiral library. All XRD structures were solved at the beamline XRD1 of the Elettra synchrotron facility in Trieste. The procedure was almost the same of the previous chapter: a large-scale library was prepared, and after 96 hours the library was purified by reverse-phase HPLC. Then, the obtained compounds were characterised by LC-MS, ^{1}H-NMR, TOCSY, CD, and the correct isomerism was attributed by ROESY, and single-crystal XRD analyses. All the antiparallel dimers were characterised successfully by ROESY, and single-crystal XRD. Heterochiral cyclic dimers are distinguishable by ROESY, and single-crystal XRD confirmed the NMR results. Single crystals suitable for XRD were successfully grown for LDL and DLL stereoisomers in batch using a mixture of organic solvent and water, whereas the LLD stereoisomer was crystallised by the hanging-drop technique. It was also possible to crystallise the LDL antiparallel cyclic trimer as host/guest complex using the cyclic pentamer gel as a crystallisation matrix. In total, five different crystal structures were obtained, and the influence of the stereoisomerism on the DCC was elucidated.

5.1 – DLL antiparallel cyclic dimer

The DLL DCL was the easiest one to characterise since it evolved towards one main compound: the antiparallel cyclic dimer (83.6 %). The effect of the stereoisomerism in this library is drastic. The antiparallel cyclic dimer grew fast, and it was also demonstrated to be the thermodynamic product. Reactivation of the library with TCEP did not change the overall equilibrium. For this reason, the purification of this compound from the large-scale library was easy, considering the quantity of available product and its retention time. The antiparallel dimer was characterised by LC-MS, CD, ^{1}H-NMR, TOCSY, ROESY and single-crystal XRD. The rest of the library was composed by the other cyclic dimer, and two cyclic trimers. However, it was possible to obtain only the second cyclic dimer as a second pure fraction. The two cyclic trimers were purified together in the same fraction, and considering their amount and the close retention time, it was not possible to perform further purifications. The parallel cyclic dimer was characterised only by LC-MS (A.5.2 – DLL dynamic library). Its quantity was too low for a NMR study, and with the small amount of pure compound, some crystallisation trials were performed in batch using a mixture of water and organic solvent, but unfortunately the compound did not crystallise.

5.1.1 – DLL Antiparallel cyclic dimer ROESY

The compound was dissolved in DMSO-d_6, and then it was fully characterised by ^{1}H-NMR, TOCSY and ROESY (A.6.3 – DLL antiparallel cyclic dimer). The combination of the monodimensional spectrum with TOCSY allowed the correct assignation of the different NMR signals. The compound was studied by ROESY to shed light on its isomerism. For this heterochiral dimer, a characteristic ROE cross-peak allowed to assign the correct isomerism (Figure 33). As discussed in the previous chapter, parallel and antiparallel dimers differ in the connection of the disulfide bridge: in the case of the parallel isomer, the bridge is formed by the same amino acid (for instance, two C-terminal Cys), and in the case of the antiparallel isomer by different amino acids (*i.e.,* N-terminal Cys with C-terminal Cys). Therefore, a ROE signal could be detectable between the two Cys residues if the stereoconfiguration and the conformation allows it. In the case of the homochiral dimers, the steroconfiguration orients the Cys α-protons too far away for ROE (> 7 Å). In line of principle, the switch of the stereoconfiguration in DLL or LLD should enable to investigate these compounds with ROESY, in contrast to the homochiral LLL.

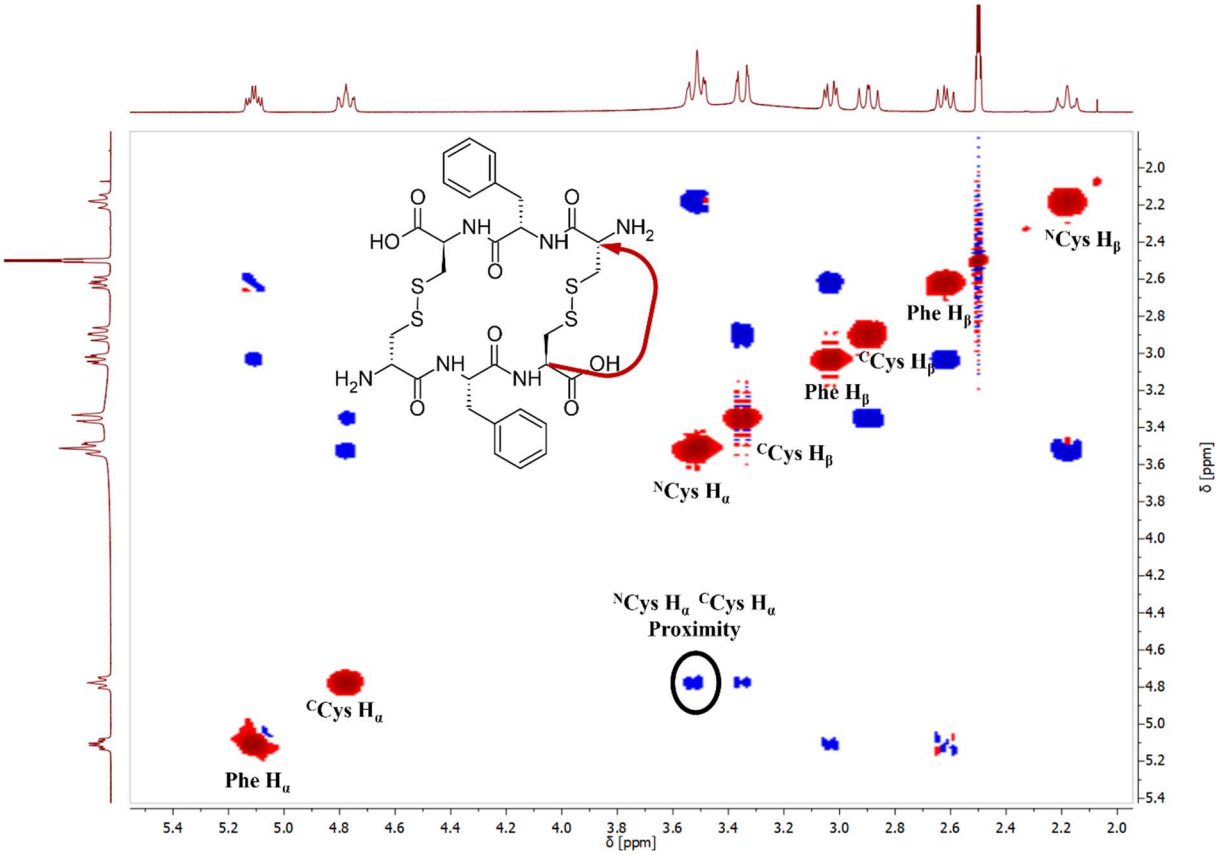

Figure 33: DLL antiparallel cyclic dimer NMR ROESY (400 MHz, DMSO-d_6). Particular of alfa and beta protons region: a ROE cross-peak highlights the spatial proximity of the two alfa protons of N-Cys to C-Cys revealing the isomerism of the compound.

Figure 33 shows the ROESY spectrum of the DLL antiparallel dimer in the α/β proton region. The two α-protons of N- and C-terminal Cys are close enough in space, so that a cross peak is visible in the spectrum. This cross peak allows to establish the isomerism of the compound and, as a consequence, also the isomerism of the other cyclic dimer. This result was later confirmed by single-crystal XRD.

5.1.2 – DLL antiparallel cyclic dimer XRD

The compound was crystallised in batch with a mixture of water and 1-butanol at pH 7.1 (A.9.2 – DLL antiparallel cyclic dimer). The data collection and elaboration were performed by Prof. De Zorzi.

The compound crystallised in the monoclinic crystal system in the space group *C2*. The asymmetric unit is composed by four macrocycles (2 asymmetric and 2 symmetric), and disordered water. No counterions are present in the crystal packing and the peptide crystallised as a zwitterion as expected from the pH value of the crystallisation experiment. Several macrocycles form a hydrophobic pocket along the *c* crystallographic axis. The surface of the pocket is constituted by aromatic rings (Figure 34, A).

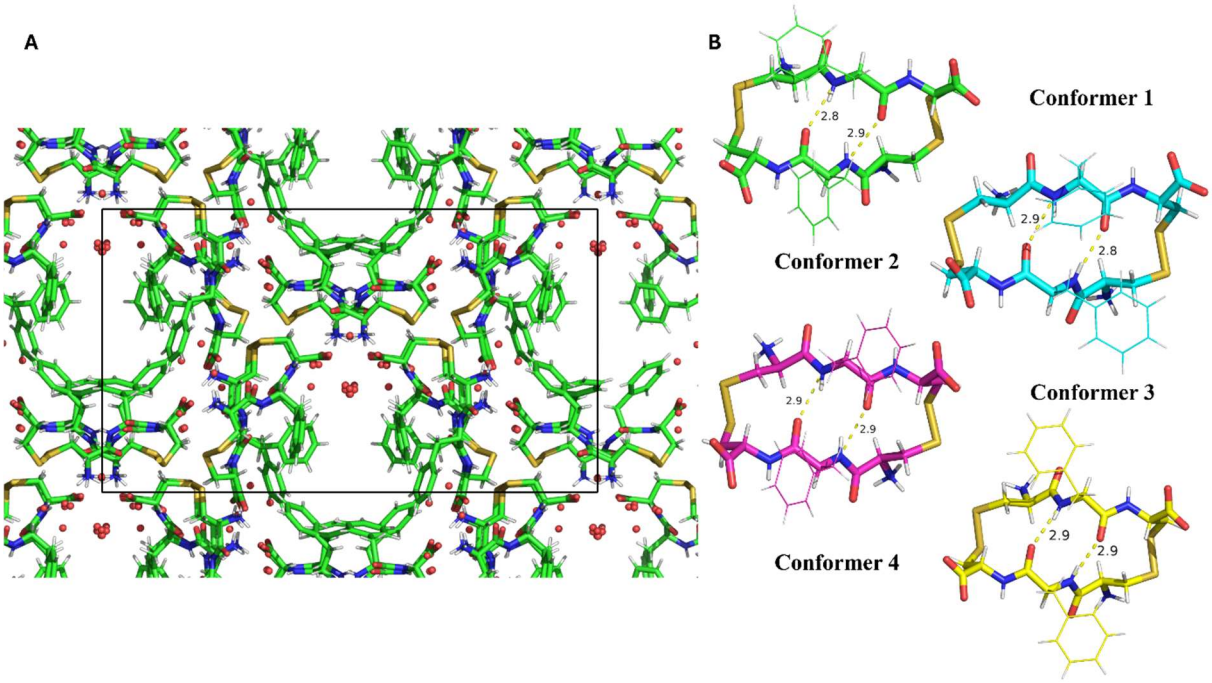

Figure 34: A) DLL antiparallel cyclic dimer crystal packing along the *c* crystallographic axis. B) the four different conformers of the asymmetric unit. All the conformers engage in intramolecular hydrogen bonding between Phe amide groups. Peptides are represented as stick models and disordered water as spheres. Green: carbon, blue: nitrogen, red: oxygen. yellow: sulfur, white: hydrogen. In panel B, Phe sidechains are represented with the wire model.

This hydrophobic pocket is filled with solvent, but the electron density map is not interpretable, therefore it is possible that it is filled with water and/or 1-butanol. The four conformers of the antiparallel dimer form intramolecular hydrogen bonding between the Phe amide groups (Figure 34, B). Conformers 1 and 2 are asymmetric whereas conformers 3 and 4 are symmetric and a *C2* rotational axis relate the two peptide strands (Figure 35). The superimposition of the four macrocyclic rings reveals that the conformation of the backbone is very similar for all the four conformers. The difference between these four macrocycles is related to the conformation of the Phe sidechain. The heterochiral steroisomerism enabled the intramolecular hydrogen bonding. This is an interesting detail compared to the homochiral counterpart in which all amide groups prefer intermolecular hydrogen bonding, and can thus stack in nanotubes. This intramolecular interaction stabilises the macrocyclic ring to a specific conformation, and the overall crystal packing is obtained adapting the position of Phe sidechains. For all the four conformers it is possible to notice the spatial proximity of the Cys α-protons. The stereoconfiguration and the conformation of the backbone orients all the four Cys α-protons inwards the macrocyclic ring. This detail was observed in the ROESY experiment too.

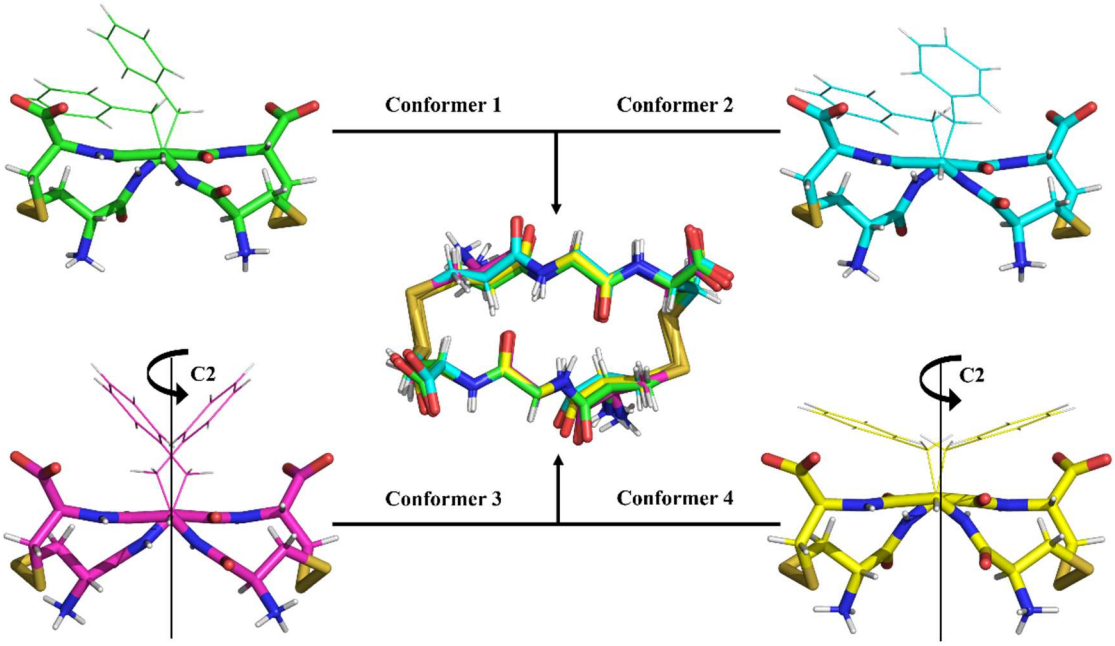

Figure 35: The four conformers of the asymmetric unit. The backbone conformation is very similar for all the four structures. The four peptide differs in the phenylalanine ring rotamers. Conformers 1 and 2 are asymmetric whereas conformers 3 and 4 are symmetric. A C2 rotational axis relates the two strands of the macrocycle.

Macrocycles interact *via* hydrogen bonds forming salt bridges between the N- and C-terminal residues. Disordered water is also present in three different salt-bridge sites (Figure 36). The hydrogen bond network is quite complex to visualise since it involves several macrocycles and water molecules.

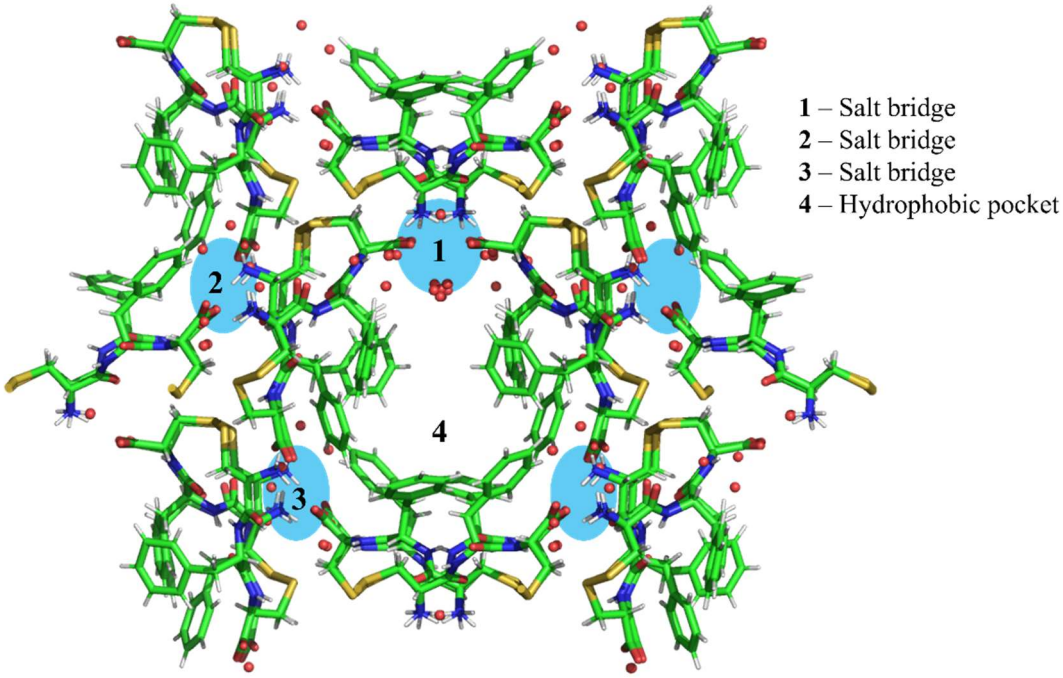

Figure 36: Peptides interact through salt bridges and hydrogen bonding with the solvent. The overall hydrogen bonding network is complex, and difficult to represent. Three distinct salt-bridge sites are present in the crystal packing.

5.2 – LDL antiparallel cyclic dimer

A large-scale LDL library was prepared to isolate its components by reverse-phase HPLC. The task was challenging. since this library presented many compounds distributed in a narrow range of retention times. For this reason, the purification strategy was focused on the isolation of the most abundant compound: the antiparallel cyclic dimer. This molecule reached its highest concentration in 24 hours, and then it started to be consumed by further evolution of the library. For this reason, the large-scale library was freeze-dried after 24 hours. The dimer was successfully isolated from its DCL, and characterised by LC-MS (A.5.3 – LDL dynamic library). The compound crystallised fast in batch using a mixture of methanol and water. Therefore, since its isomerism was determined by single-crystal XRD, no ROESY spectrum was acquired on this compound.

The data collection and elaboration were performed by Prof. De Zorzi. The compound crystallised in the monoclinic crystal system with the space group *C2*. The asymmetric unit is

composed by two independent macrocycles and disordered solvent molecules. The overall number of water molecules in the model is 14, and 7 of them show full occupancy, whereas all the rest have 0.5 of occupancy. There is also a methanol molecule with an occupancy of 0.5 in the asymmetric unit. No counterions were detected and the peptide crystallised as a zwitterion. The peptide crystallised in an alternate hydrophobic/hydrophilic layer along the *c* crystallographic axis (Figure 37, A). The two independent conformers engage in intramolecular hydrogen bonding between the Phe amide groups (Figure 37, B). The superposition of the two macrocycle rings highlighted a similar conformation for both the conformers. Phe sidechains display different rotamers for the two conformers, and this is the main difference between them.

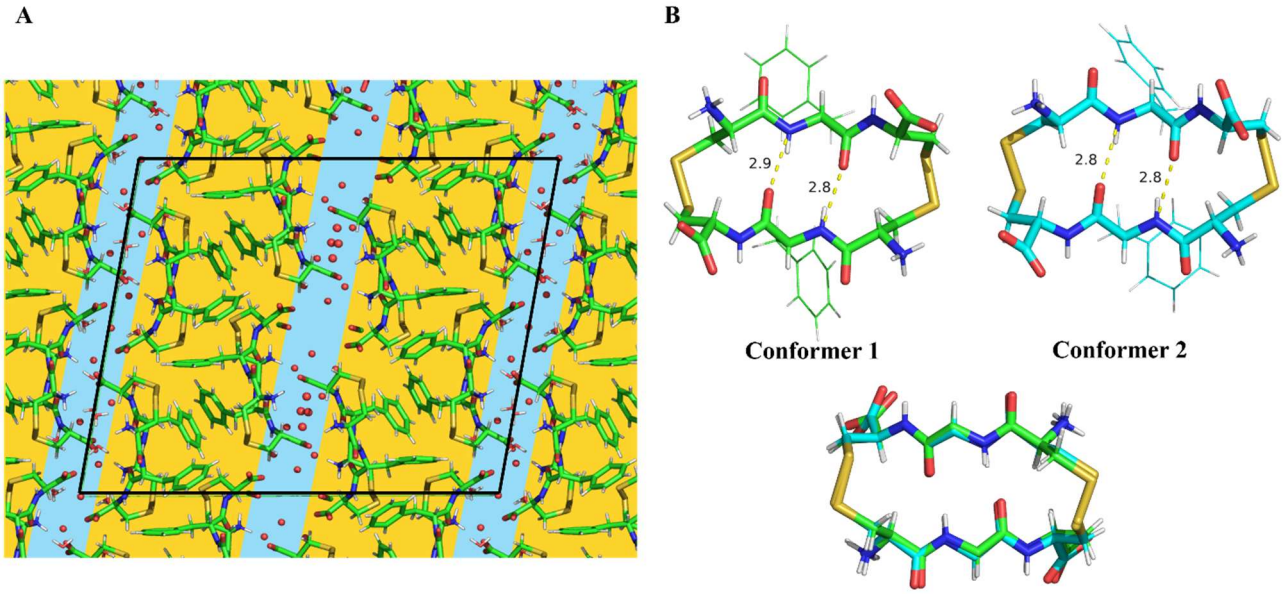

Figure 37: A) LDL antiparallel cyclic dimer crystal packing along the *b* crystallographic axis. B) The two independent conformations of the macrocycle. In both cases, Phe amide group engages in intramolecular hydrogen-bonding. Peptides are represented as stick models and disordered water as spheres. Green: carbon, blue: nitrogen, red: oxygen. yellow: sulfur, white: hydrogen. In panel B, Phe sidechains are represented with the wire model.

The stereoconfiguration is responsible for the amphiphilic character of the peptide. The two Phe aromatic rings point towards the same side of the macrocycle as well as the sulfur bridges creating a hydrophobic surface. Ammonium and carboxylates groups instead are projected on the other side of the macrocycle ring creating a hydrophilic surface (Figure 38, A). This observation is supported by the layered crystal packing. Both conformers are packed in hydrophobic layers constituted by the hydrophobic sides of the macrocycle whereas the hydrophilic faces interact with the solvent layer composed of water (Figure 38, B). The LC-MS analysis of its DCL highlighted the higher hydrophobicity of this compound compared to all the other peptides formed in the reaction. This finding is peculiar since this cyclic dimer was more hydrophobic than larger oligomers of the library.

The hydrophilic layers are composed by disordered solvent molecules which bridge the peptide macrocycles. The dimer interacts with the solvent through hydrogen-bonding interaction, and the peptide layers are packed forming salt bridges between N- and C-termini.

This compound reached the maximum concentration within 24 hours in the DCL, and then it started to be consumed. The library evolved in a self-supporting gel after the reactivation, and the analysis on the gelator building block revealed the evolution into a cyclic pentamer. Unfortunately, no experimental data are available on how the cyclic pentamer formed in solution, since with the LC-MS analysis it was not possible to follow the further evolution of the system. The conformation of this cyclic dimer however is interesting. The position of the disulfide bridges compared to the previous stereoisomer, is peculiar. The charged termini of the macrocycle lied on the other side of the ring, and this might influence the reactivity of the disulfide in the exchange reaction. In all other cases, a charged group was found on the same side of the sulfur bridge.

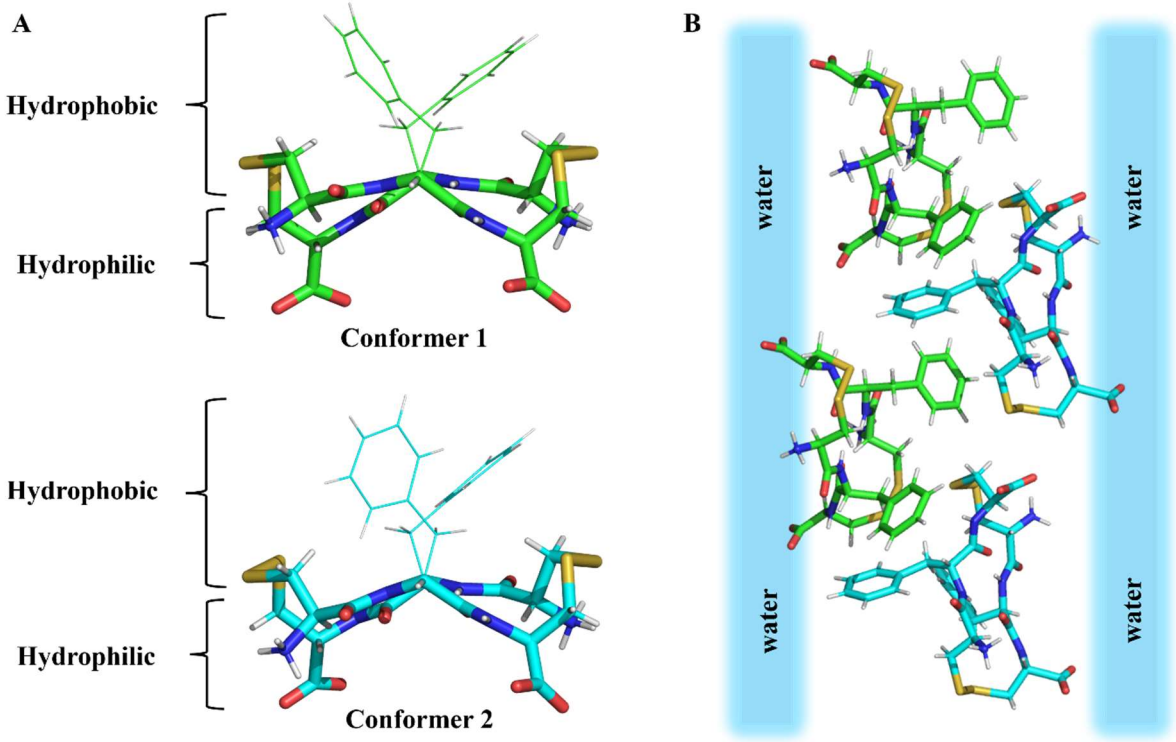

Figure 38: A) The two independent conformers of LDL antiparallel cyclic dimer. The stereoconfiguration and the conformation of the macrocycle create a hydrophobic surface composed by aromatic rings and sulfur atoms. B) The two amphiphilic conformers crystallised in alternate hydrophobic/hydrophilic layers.

5.3 – LDL antiparallel cyclic trimer from crystallisation trials on the pentamer

Several attempts have been conducted to crystallise the cyclic pentamer. Unfortunately, none of them worked. The crystallisation trials were conducted in batch with organic solvent, and with the hanging drop method too, in aqueous solution. The hydrogel was freeze-dried into a white powder. This powder was insoluble in every tested organic solvent, and water was the only possible solvent for this molecule. Because of this limited solubility, the hanging drop method provided the best approach to find the crystallisation conditions. The compound was then tested at different pH values, different ionic strengths, and in presence of different metals or organic molecules (A.9.5 – LDL antiparallel cyclic trimer). The persistency to form a material that appeared like a gel was very strong and the system was in solution state only in alkaline pH above 12. In all the other cases, the compound self-assembled to a solid gel-like material, and crystals from buffers and salts were instead obtained. The drop composed by NaCl 0.6 M, $ZnSO_4$ 30 mM and pH 7.0 yielded two crystals (Figure 39). The drop showed the presence of what appeared to be gel, thus the cyclic pentamer was still self-assembled in a hydrogel. The two crystals found in the gel matrix were collected as single crystals for XRD, and the solved structure revealed an LDL antiparallel cyclic trimer. In crystallisation technology, gels are used to favour the crystallisation of guest compounds.[112] It is possible that the presence of the cyclic pentamer gel matrix favoured the crystallisation of the small impurity composed by the antiparallel cyclic trimer. In section 3.4, the ESI-TOF spectrum showed the presence of a trimeric impurity (Figure 20). It is possible that the crystals obtained from this hanging drop experiment were relative to that impurity.

A

Cyclic pentamer hanging drop scheme

Guest	NaCl [M]				
10-50 mM	**0.2**	**0.4**	**0.6**	**0.8**	**1.2**
Urea	G	G	G	G	G
NH_4^+	G	G	G	G	G
$ZnSO_4$	G	G	**G +C**	G +C	G +C
$AuCl_3$	G	G	G + C*	C*	C*

*Gold borate crystals

B

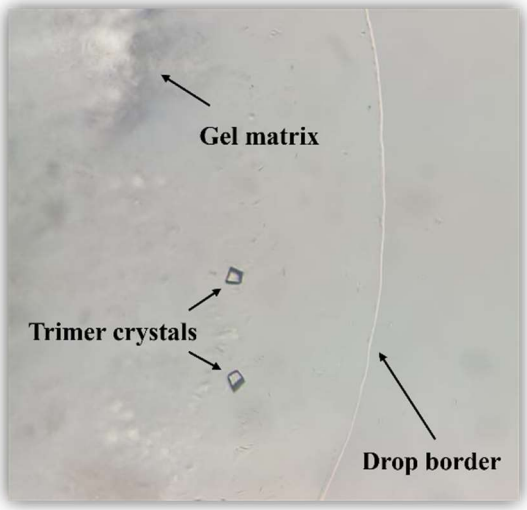

Figure 39: A) Cyclic pentamer hanging drop scheme at pH 7.0. Columns: different NaCl molar concentration. Rows: different guest concentration from 10 to 50 mM. G: gel, C: trimer crystal, C*: gold borate crystal. B) Top view of the hanging drop with $ZnSO_4$ 30 mM and NaCl 0.6 M. In the picture is visible the cyclic pentamer gel and two cyclic trimer single crystals.

The antiparallel cyclic trimer crystallised in the trigonal crystal system with the space group *R3*. The asymmetric unit is composed by one peptide strand, two zinc ions both on a *C3* rotational axis, a chloride ion on a *C3* rotational axis and two water molecules. The peptide crystallised as a zinc complex with all the three amines and the three carboxylates deprotonated. The packing is quite complex to describe, and in this paragraph, several details will be described separately. The macrocycle forms a host/guest system in which all the three N-terminal Cys coordinate a zinc ion with an octahedral geometry (Figure 40). The macrocycle is dissymmetric, and the three peptide strands are related by a *C3* rotational axis. The octahedral complex is distorted, this is due to the Cys bite-size of 78.8°. Cys coordinates the metal with the N-termini amine group and its carbonyl. Therefore, the geometry is influenced by the connectivity of the organic molecule. The metal complex is chiral and only the Λ enantiomer is present in the crystal.

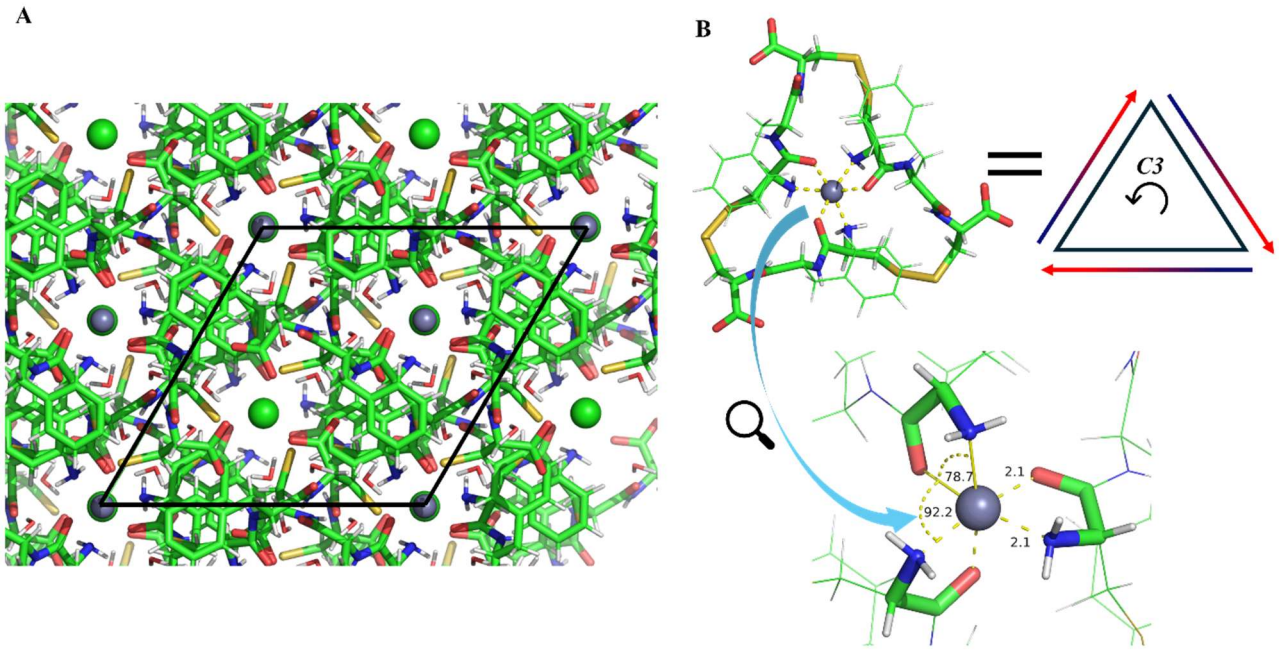

Figure 40: A) LDL antiparallel cyclic trimer crystal packing along the c crystallographic axis. B) The macrocycle zinc complex. The three peptide strands are related by a *C3* rotational axis. Thus, the three peptide strands share the same conformation. The Zinc is coordinated with an octahedral geometry by the three N-termini Cys with the amine and carbonyl group. The geometry is slightly distorted due to the Cys bite-size of 78.7°. Peptide and water molecules are represented as stick models, zinc and chloride ions as spheres. Green: carbon, blue: nitrogen, red: oxygen. yellow: sulfur, white: hydrogen, grey: zinc, lime: chlorine. In panel B, Phe sidechains are represented with the wire model.

A second crystallographic independent zinc ion is present in the crystal packing. The carboxylates of the C-terminal Cys are coordinated to this second zinc ion. Even in this case, there is a *C3* symmetry and three carboxylates from three different macrocycles are coordinated to the same zinc ion (Figure 41, A). This fact makes the system a MOF (metal Organic Framework) in which

every macrocycle is connected to other macrocycles through zinc ions. This second zinc ion completes its tetrahedral coordination by a chloride ion. The electron density map shows a two-position disorder of this metal ion with a opposite orientation of the apical chlorine ligand of the tetrahedron. (Figure 41, B). In one case, the electron density map suggested the presence of an additional water molecule weakly interacting with the zinc ion in trans to the chlorine ligand, however the geometry of the complex can still be considered tetrahedral. The occupancy of the two zinc ions is close to 0.5 each.

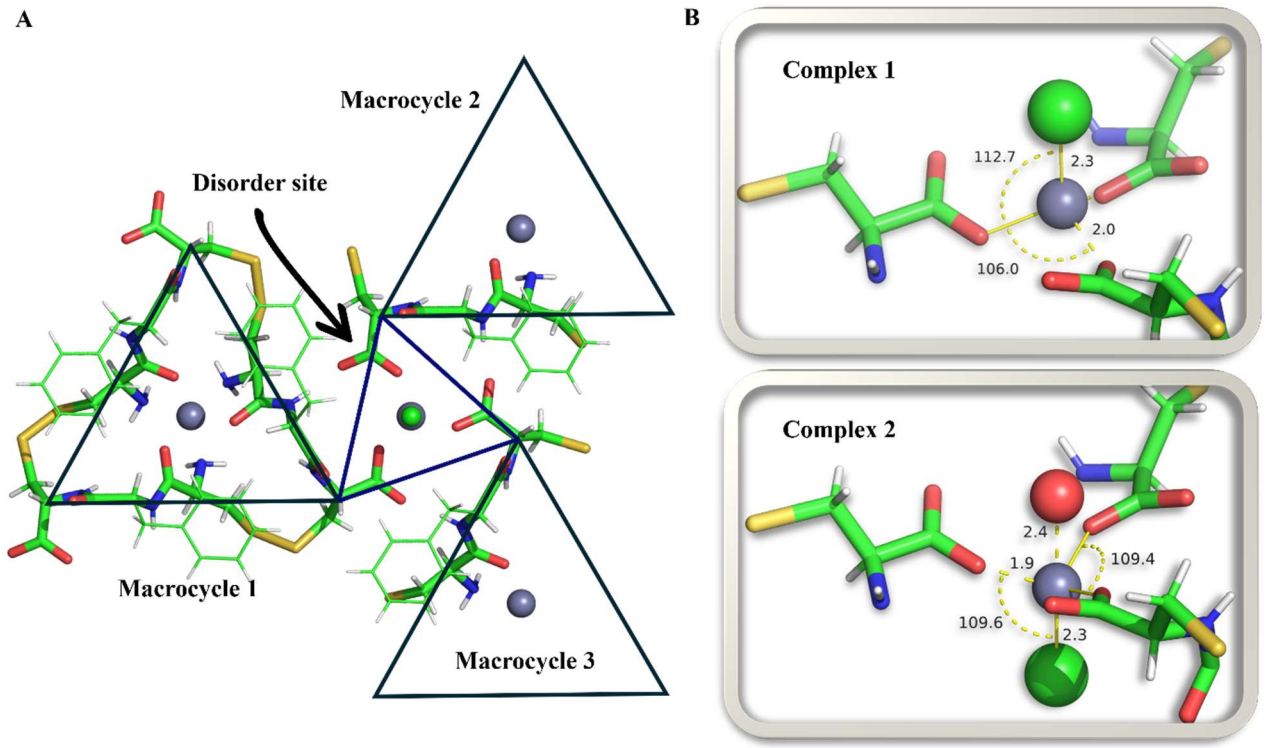

Figure 41: A) The carboxylates of the macrocycle form another zinc complex making the crystal a supramolecular polymer. The zinc complex between macrocycles is disordered, and the electron density map highlighted two possible situations. B) The two different occupancies for the zinc ion. In both cases, the metal forms a tetrahedral complex with three carboxylates from three different macrocycles and a chloride ion. In complex 2, the electron density map showed the presence of a water molecule close to the zinc ion. However, the coordination geometry of the complex is a perfect tetrahedra, therefore the water is not coordinated to the zinc ion.

The conformation of the peptide strand is very different when compared to the cyclic dimer series. In particular, the comparison with the LDL antiparallel cyclic dimer of the previous section shows different torsional angles (Figure 42). The geometry of the trimeric strand is influenced by the metal coordination of both Cys residues and also to the different macrocyclic nature. The Phe ψ torsional angle shows a difference of almost 70° if compared to the two independent macrocycles found in the LDL antiparallel cyclic dimer crystal (Figure 42, B). No intramolecular hydrogen bonds are present in the trimer. The two amide groups lie in two orthogonal planes, and they are involved

in intermolecular hydrogen bond interactions. Two full occupancy water molecules are present in the asymmetric unit, and macrocycles are packed as layers bridged by these water molecules (Figure 43, A). The hydrogen bond network is reproduced by the *C3* rotational axis along the zinc-chloride metal complex. The first water molecule engages in hydrogen bonding interaction with the chloride ion of the metal complex and the C-terminal Cys carboxylate (Figure 43, B). The same carboxylate is coordinated to the zinc ion; therefore, the water molecule forms a "closed" network with the peptide and the metal complex. The second water molecule engages in hydrogen bonding interaction with the lone pair of the previous water molecule, and with a Phe carbonyl of one macrocycle of the upper layer. This molecule acts as a bridge between the two macrocyclic layers. The layer bridge is formed also by a second hydrogen bond interaction formed by the amide group of the C-terminal Cys of the lower layer with the same Phe carbonyl aforementioned.

A

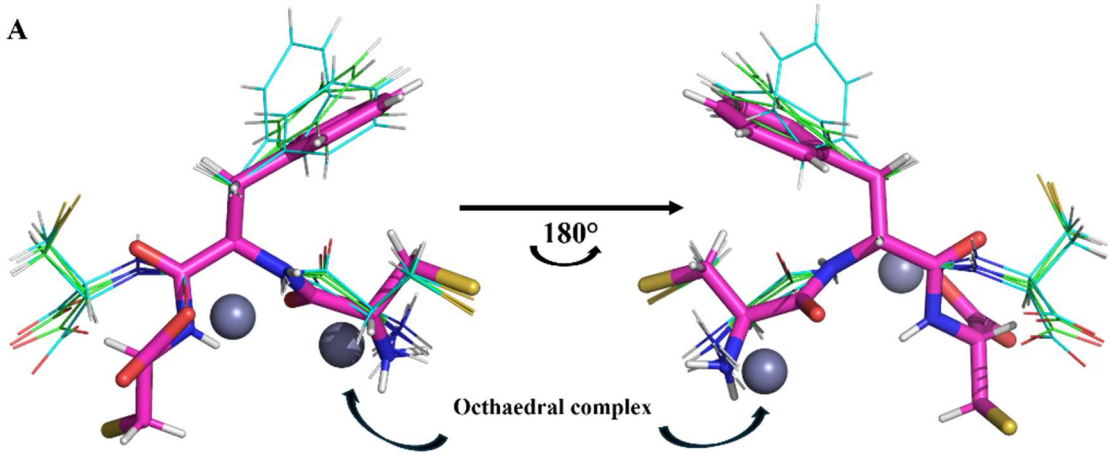

B

	Peptide	Phe φ	Phe ψ
Cyclic dimer	Conf. 1 strand 1	140.6	-147.0
	Conf. 1 strand 2	134.4	-144.8
	Conf. 2 strand 1	123.8	-141.2
	Conf. 2 strand 2	146.3	-155.9
	Trimer	105.3	-20.8

Figure 42: A) LDL antiparallel cyclic trimer strand comparison with LDL antiparallel cyclic dimer strands. The trimer strand is rotated with the view along the Phe α-carbon front and back. Purple: trimer, green: dimer conformer 1, cyan: dimer conformer 2. B) Torsional angles of the represented models. C-terminal Cys is rotated more than 70° compared to the dimers strand. The two trimer amide groups lie on two orthogonal planes.

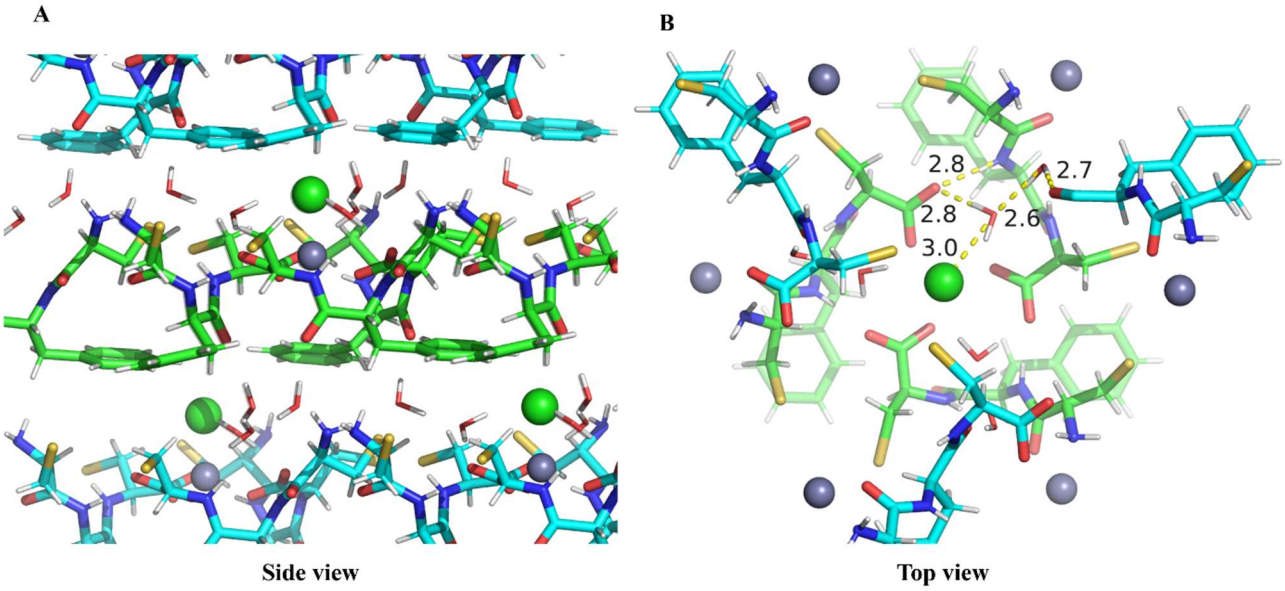

Figure 43: A) Layer packing of the cyclic trimers. The two layers are separated by few water molecules which connect the zinc-chloride complex to the Phe carbonyls of the upper layer. B) The layer top view. Water molecules engage in hydrogen bonds, and connect the two macrocyclic layers. One water molecule interacts with the chloride ion and the C-termini Cys carboxylate in a closed network. The other water molecule bridges the previous water molecule to the Phe carbonyl of the upper layer. The same carbonyl is also involved in a hydrogen bond interaction with the amide group of the C-termini Cys of the lower layer.

5.4 - LLD antiparallel cyclic dimer

Once again, a large-scale library was prepared to purify and separate the compound of this last DCL. The main compounds of the library were, also in this case, cyclic dimers. The antiparallel cyclic dimer was easy to separate from the DCL since it fell in an isolated part of the chromatogram. Two fractions were collected: one with the antiparallel cyclic dimer and one with the rest of the library which was distributed in a narrow range of retention time. The mixture of this second HPLC fraction was then separated with a second HPLC method, and also the parallel dimer was isolated successfully and characterised by LC-MS (A.5.4 – LLD dynamic library). The two compounds were studied by ^{1}H-NMR, TOCSY, ROESY, CD, and the antiparallel cyclic dimer was crystallised, and its XRD structure was solved.

5.4.1 – LLD antiparallel cyclic dimer ROESY

The compound was dissolved in DMSO-d_6, and characterised by ^{1}H-NMR, TOCSY, and ROESY. As in the previous sections, the identity of the different protons was assigned by the mono-

dimensional NMR spectrum combined with the TOCSY (A.6.4 – LLD antiparallel cyclic dimer). The isomerism of the compound was determined by the ROESY spectrum. As in the case of the DLL antiparallel dimer, the α-protons of N- and C-terminal Cys were in spatial proximity (Figure 44). The ROESY spectrum showed a cross-peak characteristic of the antiparallel isomerism, and this allowed to identify the compound. This result was later confirmed by single-crystal XRD.

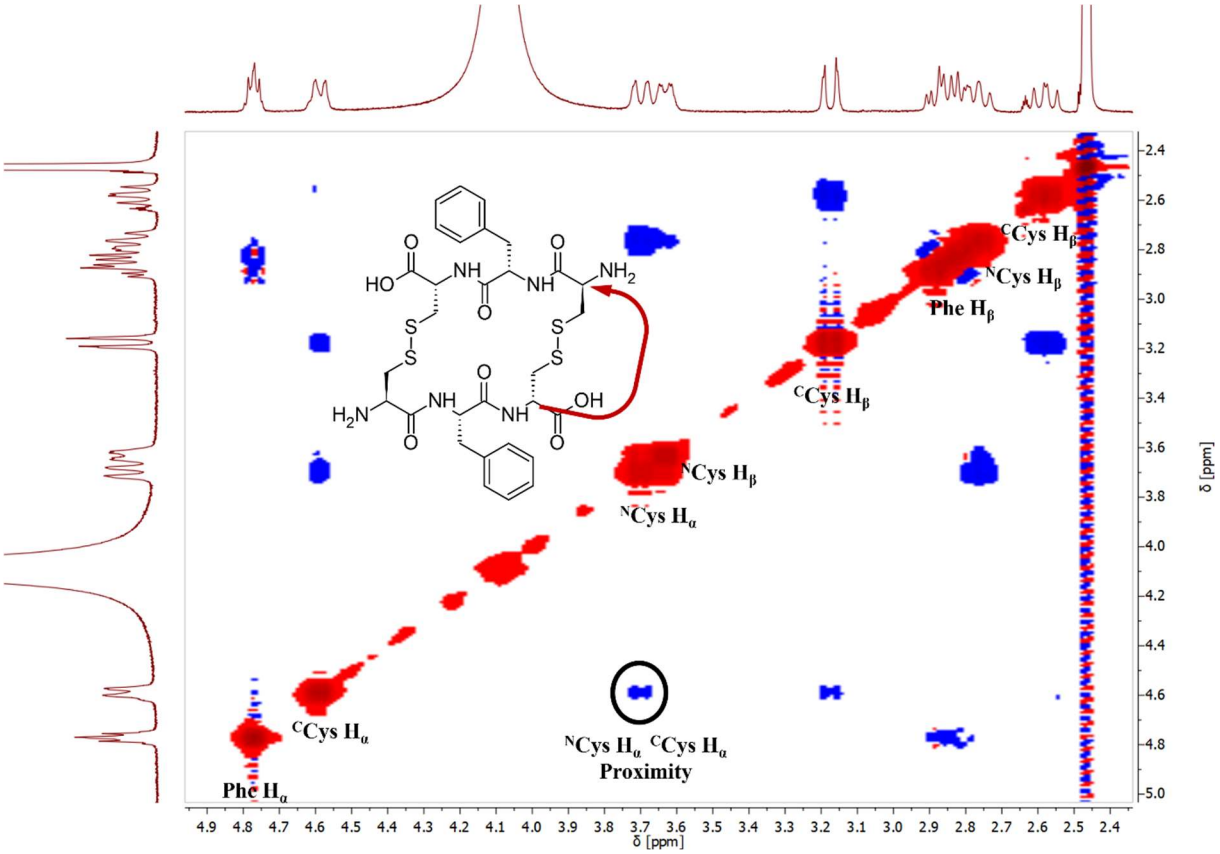

Figure 44: Particular of the α- and β-protons region of LLD antiparallel cyclic dimer NMR ROESY (400 MHz, DMSO-*d*6)

This is an interesting result considering the previous study on the DLL antiparallel cyclic dimer. The two peptide strands are arranged in both cases in opposite directions, and the difference is the different chirality on both Cys residues. The DLL isomer was the most abundant compound of its DCL, and it reached the relative concentration of 83.6%. The LLD DCL was more balanced in terms of cyclic dimers, and the antiparallel product reached the relative concentration of 45.4%. It is worth noting that the different stereoisomerism enabled also the synthesis of larger oligomers. In the LLD DCL, traces of a cyclic pentamer were detected by the LC-MS study, whereas the DLL tripeptide stops at the size of cyclic trimers (A.4 – LCMS kinetic studies data). The ROESY spectrum of LLD antiparallel cyclic dimer showed the proximity of the α-protons of the Cys residues as in the case of the DLL stereoisomer. Thus, the two protons point inwards the macrocyclic ring in both cases and it

is possible that the two stereoisomers shared some conformational features in solution. But still, the DCL outcome was completely different, and a deeper investigation was needed to compare the two stereoisomers.

5.4.2 – LLD antiparallel cyclic dimer XRD

The peptide was crystallised by the hanging-drop technique screening different pH and ionic strength values. The macrocycle yielded crystals at acidic, and neutral pH too (Figure 45). Two XRD structures were solved for this compound in different protonation states according to the crystallisation experiment.

Hanging drop scheme

	NaCl [M]					
	0.1	**0.5**	**1.0**	**2.0**	**3.0**	**4.0**
pH 2.2	C	C	/	C	C	C^A
pH 7.2	C^B	/	/	/	/	/
pH 12.0	/	/	/	/	/	/

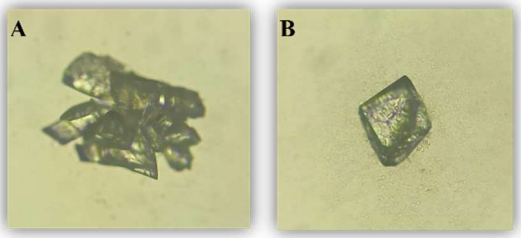

Figure 45: LLD antiparallel cyclic dimer hanging drop scheme, and optical microscope image of the two chosen crystals for XRD.

Crystal A: The macrocycle crystallised in acidic aqueous solution in the monocline crystal system with the space group $P2_1$. The asymmetric unit is composed by two independent macrocycles, five water molecules and two chloride counterions. The overall electric charge of the macrocycle is +1, and one of the C-termini Cys residue is protonated. The crystal packing is complex to visualise, but along the (1 0 1) direction it is possible to observe the macrocycles packed in columns and divided by water channels (Figure 46, A). Chloride counterions are packed inside the water channels, and one of the two counterions shows an occupancy of 0.8. The disorder of the chloride site shows the presence of a TFA anion with an occupancy of 0.2 in place of the chloride and two water molecules (Figure 46, B).

The two independent macrocycles display a different conformation between each other. In both cases, there is an intramolecular hydrogen bond interaction between the Phe amide groups, but in conformer 1 there is only one non-covalent interaction (Figure 47). The reason is the different φ torsional angle (-65.8) which orients the amide group almost orthogonal to the macrocycle plane. The superimposition of the two conformers reveals similar conformations for the macrocycle rings despite the amide group rotation (Figure 48).

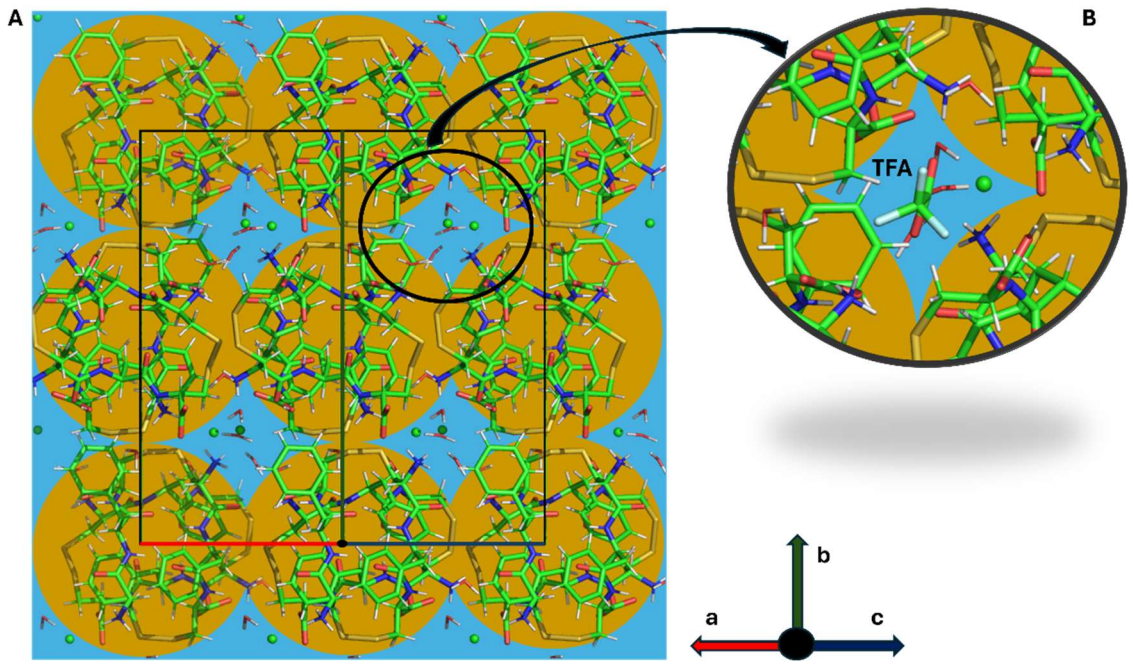

Figure 46: A) LLD antiparallel cyclic dimer crystal packing along (1 0 1) direction. B) Peptide counterions are packed inside water channels. Chloride was found as counterion, and in one of the two occupancy sites, a disorder shows the presence of a TFA anion instead the chloride with an occupancy of 0.2. Peptide, TFA, and water molecules are represented as stick models, chloride ions are represented as spheres. Green: carbon, blue: nitrogen, red: oxygen. yellow: sulfur, white: hydrogen, green lime: chlorine, pale light blue: fluorine.

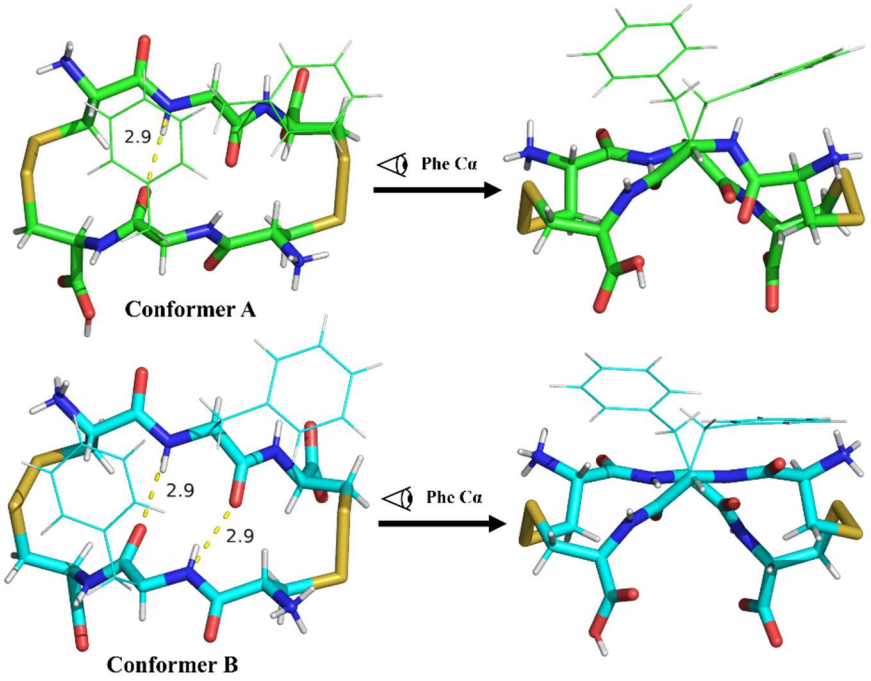

	Phe Φ	Phe Ψ
Conformer A	-65.8	154.4
	-142.5	130.2
Conformer B	-149.3	156.3
	-152.5	131.0

Figure 47: Independent LLD antiparallel cyclic dimer conformers. Conformer A: Phe amide engages in one intramolecular hydrogen bonding interaction. Conformer B: in this case, the macrocycle forms two intramolecular hydrogen bonding interactions. Phe sidechain is presented with the wire model.

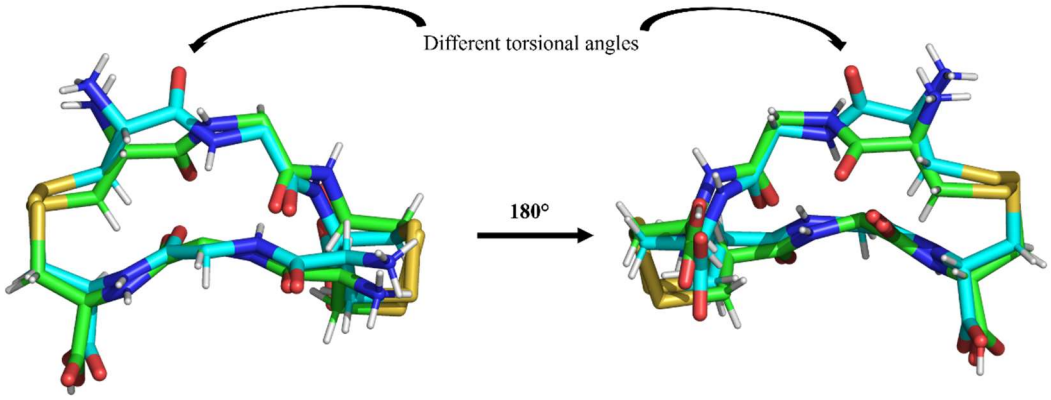

Figure 48: Superimposition of the two independent macrocycles. The amide group formed by Phe and N-terminus Cys is rotated for conformer B, and the peptide cannot form a second intramolecular hydrogen bond. Phe sidechain is omitted for clarity.

Macrocycles are stacked in columns *via* hydrogen bonding interaction, and salt bridges between N- and C-terminal Cys residues (Figure 49). The two independent conformers are stacked in an alternate disposition interacting through the termini polar groups. In each macrocycle, only one C-terminal residue is protonated; therefore, the overall electric charge of each dimer is +1. A water molecule acts as a bridge between the carboxylic acid of the cyan macrocycle, and the green macrocycle ammonium group Figure 49. The two chloride ions are bridged by a water molecule and connects the ammonium group of the cyan macrocycle with the C-terminal NH amide group of the green macrocycle. To better visualise the peptide columns, the peptides are coloured also in grey and purple Figure 49.

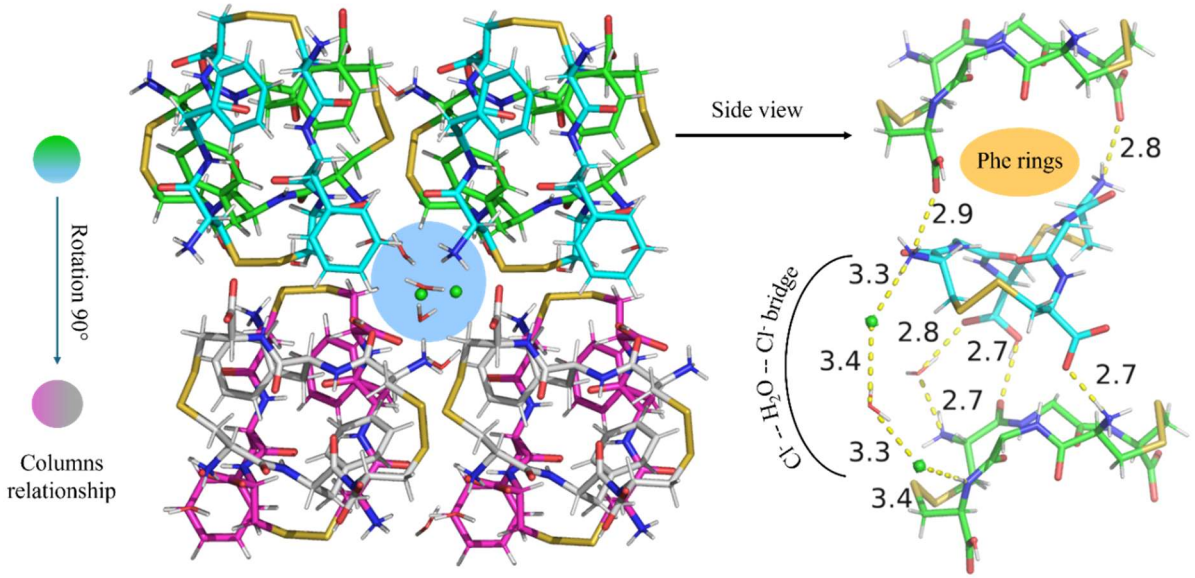

Figure 49: Non-covalent interactions between macrocycles. In every column there are the two conformers alternatively stacked to each other. To better visualise the disposition, the two conformers are painted with different colour: green and cyan for the first column and violet and grey for the second. The different colour highlights the different rotation of the columns by 90°. It is possible to observe several hydrogen bonds between the termini of the peptide, chlorine ions and water molecules along the column.

The columns are packed according to the previous description, but they are rotated by 90° between each other. Because of this, the water channel between the four peptide columns is difficult to describe due to the amount of hydrogen bonding interaction with the different disposition of the two macrocycles. In Figure 50, three panels describe all the non-covalent interactions present in the water channel.

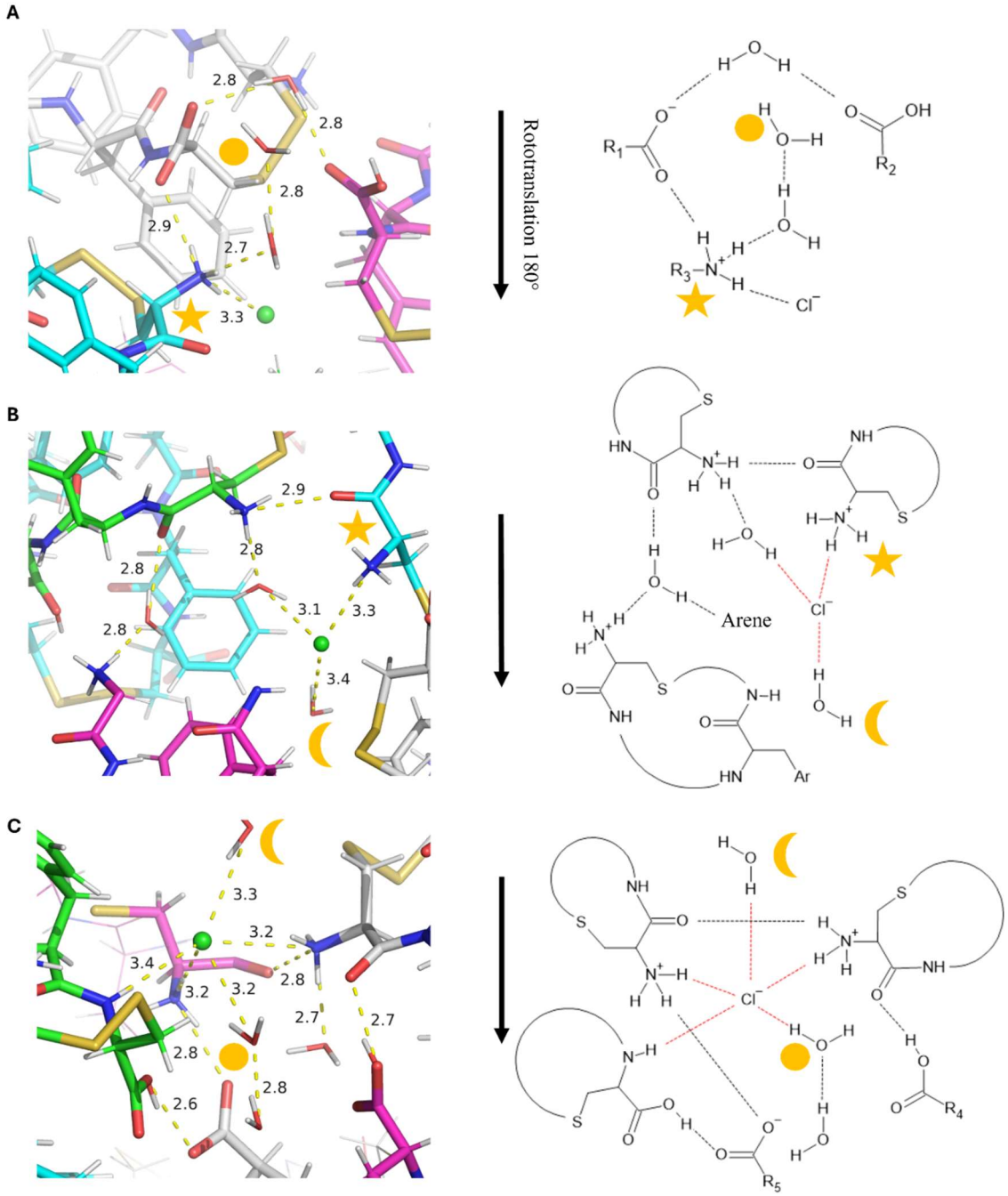

Figure 50: Inside the water channel. The description is split into three images due to the overcrowding of the non-covalent interactions. A) The yellow circle represents the starting water molecule of the channel, which is the same present in figure C. Likewise, the same ammonium group is denoted by a yellow star in the three panels, and the same water molecule by a yellow moon. B) The first chloride coordination site. The ammonium is the reference point between figure A and B. The view is also rotated of almost 180°. One water molecule points towards the aromatic ring as a donor in a OH-π interaction. C) The second chloride coordination site. The water molecule highlighted with the yellow circle is the same of figure A, thus the channel is repeated by symmetry along the crystal.

On the left of the figure, a schematic representation describe the XRD model. The three panels are roto-translated by 180° for clarity reasons due to the overcrowd of macrocycle functional groups. The main features of the water channel are: two chloride ions, five ammonium groups, and two carboxylates. The overall charge is 0 considering an extra carboxylate group that is not involved in the water channel description but it salt-bridges one of the ammonium groups as previously described.

Figure 50 panel B, describes the first chloride coordination site. The analysis of the electron density map reveals a disorder on that coordination site in which TFA ion is present with an occupancy of 0.2 instead of the chloride ion and two water molecules. The non-covalent interactions involved are described in Figure 51.

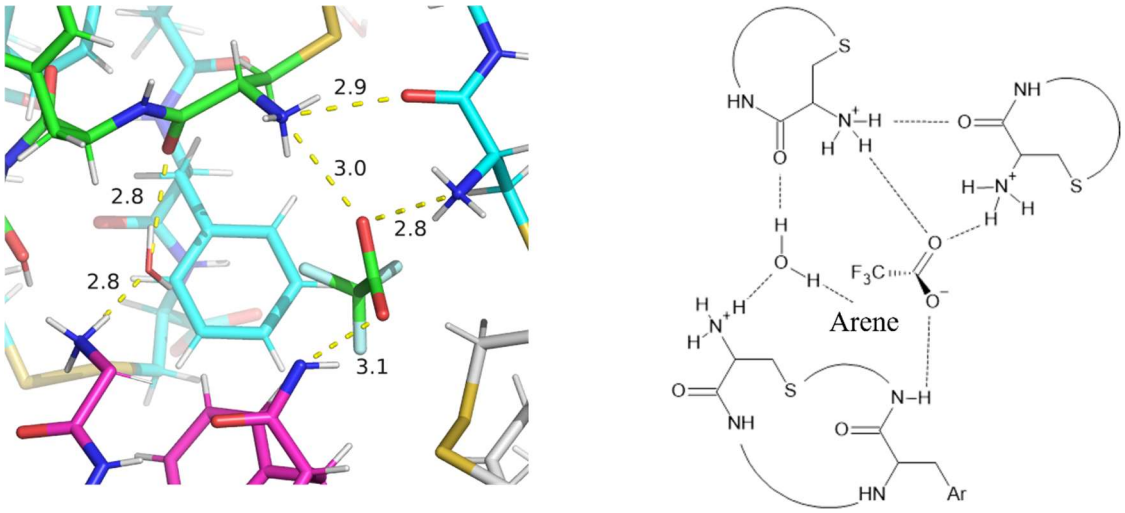

Figure 51: Alternative packing of the first chloride site. The view is the same of the previous figure and displays how the TFA ion interacts without changing the overall packing. The TFA ion substitutes two water molecules and one chloride ion.

The TFA replaces the chloride ion, and it bridges two ammonium groups from two different peptide columns. Furthermore, the TFA anion engage in a hydrogen bonding interaction with the amide group of the purple macrocycle. This interaction is not observed for the chloride ion when it is present in the water channel.

Crystal B: The macrocycle crystallised in the trigonal crystal system with the space group $P3_2$. The crystal was twinned by merohedry, and the diffraction pattern appeared at higher symmetry, therefore the diffraction spots were initially integrated and merged with the space group $P3_221$. During the structure refinement, the twin law was identified by SHELXLe as the following rotation matrix: (010 100 00-1). The scaling process was repeated with the space group $P3_2$. The final structure refinement gives as fractional contribution of the twin components (BASF) the value of 0.425(2). The asymmetric unit is composed by two independent macrocycles, six water molecules with full

occupancy, and three disordered water molecules with 0.3, 0.2, and 0.2 occupancies. The peptide crystallised as zwitterion and no counterions are present in the crystal packing. Thus, the overall electric charge of the macrocycle is 0. The macrocycles are packed in columns which are rotated by 90° respect to each other (Figure 52, A). Columns are separated by the water molecules which act as bridges between the peptides.

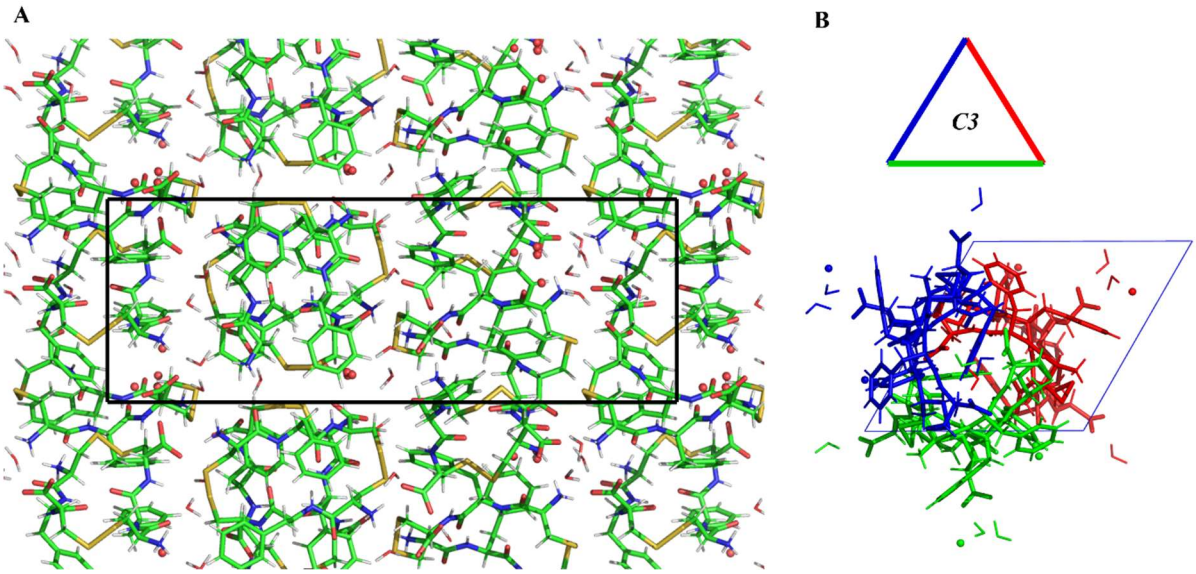

Figure 52: A) LLD antiparallel cyclic dimer crystal pacing along the *b* crystallographic axis. B) View of the along the *c* crystallographic axis, and the asymmetric unit related by the 3_2 screw axis. Peptide and water molecules are represented as stick models. Green: carbon, blue: nitrogen, red: oxygen. yellow: sulfur, white: hydrogen.

Phe amide groups engage in intramolecular hydrogen bonding in both the independent conformers (Figure 53, A). The superimposition model of the two macrocycles displays a similar conformation for one peptide strand, but different torsional angles are present in the second strand (Figure 53, B). The different conformation is reflected also in the hydrogen bond distances in which for the conformer B, one interaction is weaker compared to the other (Figure 53, A).

Peptides are packed forming salt bridges between the N- and C-termini of Cys residues and several hydrogen bond interactions with water molecules. The overall interaction can be represented as a cluster of eight Cys from eight different macrocycles (four N- and four C-termini, Figure 54). For simplicity, in Figure 54 this cluster is split in two subgroups with different colours. The green cluster is composed by four salt bridge interactions which involves two N- and two C-terminal Cys residues. One water molecule acts as a bridge between the two carboxylates. Another disordered water molecule bridges the green cluster to the cyan cluster interacting with the ammonium and carbonyl groups of the Cys residue of the green cluster, and an ammonium group and a water molecule of the cyan cluster. The green and cyan cluster are composed by the same number of Cys residues,

but the latter has more water molecules involved in the network. Only one salt bridge is present in the cyan cluster, and all the other interactions are hydrogen bonds between water molecules and terminal polar groups.

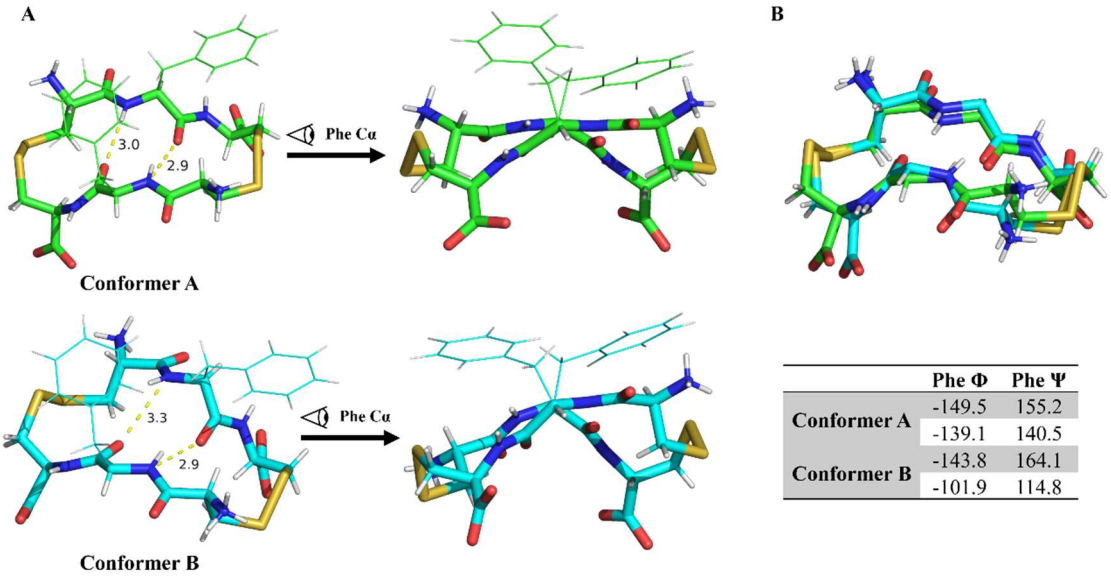

	Phe Φ	Phe Ψ
Conformer A	-149.5	155.2
	-139.1	140.5
Conformer B	-143.8	164.1
	-101.9	114.8

Figure 53: Intramolecular hydrogen bonding interaction between Phe amide groups. In this case, conformer B presents a weaker hydrogen bond interaction (3.3 Å) compared to conformer A.

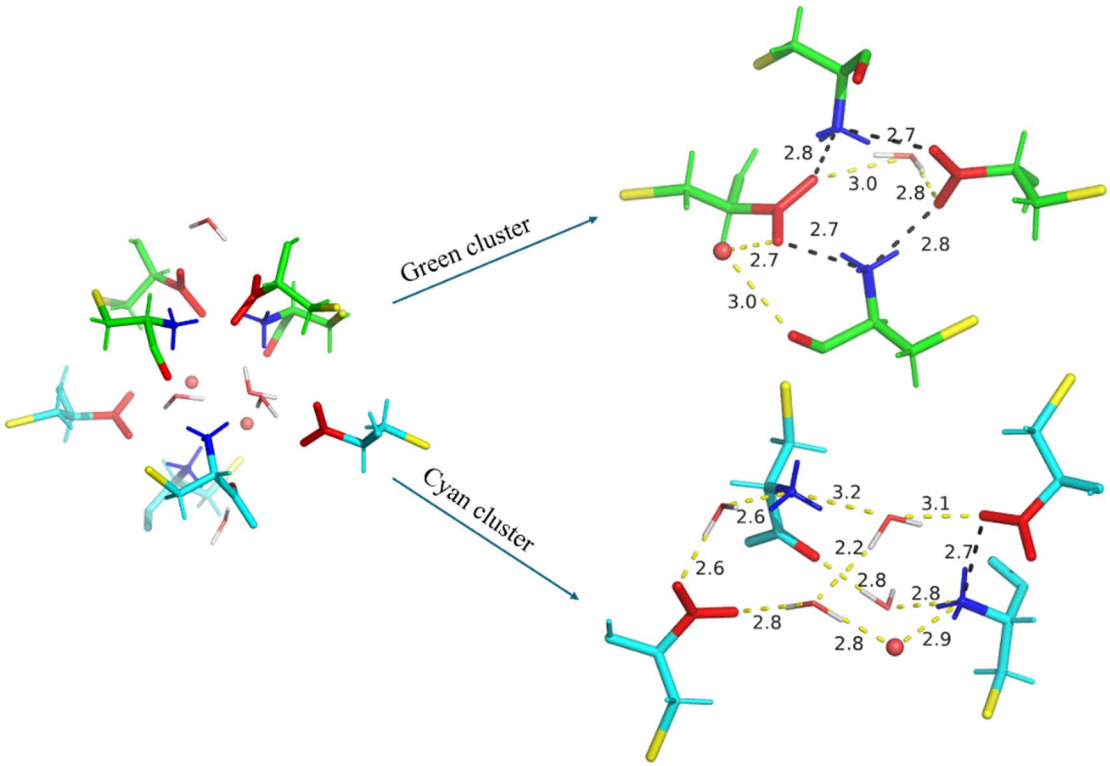

Figure 54: The hydrogen bond network is composed by eight Cys residues, and seven water molecules. For simplicity, Cys are divided into two subgroups, green and cyan, and their interactions are analysed separately. The cluster is represented with stick models with the following colours: blue: ammonium, red: carboxylates, carbonyls, and oxygen, yellow: sulfur, green and cyan: Cys skeletons. Hydrogen bonds are represented with dashed lines: Black: salt bridge, yellow: hydrogen bond.

5.5 – LLD parallel cyclic dimer

The compound was characterised by LC-MS, and NMR. Crystallisation trials were performed as well but no crystals were obtained in the tested conditions. The isomerism was determined as the consequence of the previous results on the antiparallel isomer.

The peptide was dissolved in DMSO-d_6, but its solubility was low. The NMR spectra were acquired as well, and the ^{1}H-NMR and TOCSY allowed the assignation of the different NMR signals despite the low solubility. The signal/noise ratio was not high, and several signals were difficult to interpret by the mono-dimensional spectrum alone. The ROESY investigation helped in the identification of the Phe residue thanks to the proximity of the aromatic ring to its sidechain (Figure 55). However, no characteristic ROE peaks were detected. This was expected since this is the parallel isomer. No exchanging cross-peaks were observed between the amide groups and the water present in the solvent. Therefore, it is possible that also in this stereoisomer Phe amide groups are involved in intramolecular, the hydrogen bond interactions.

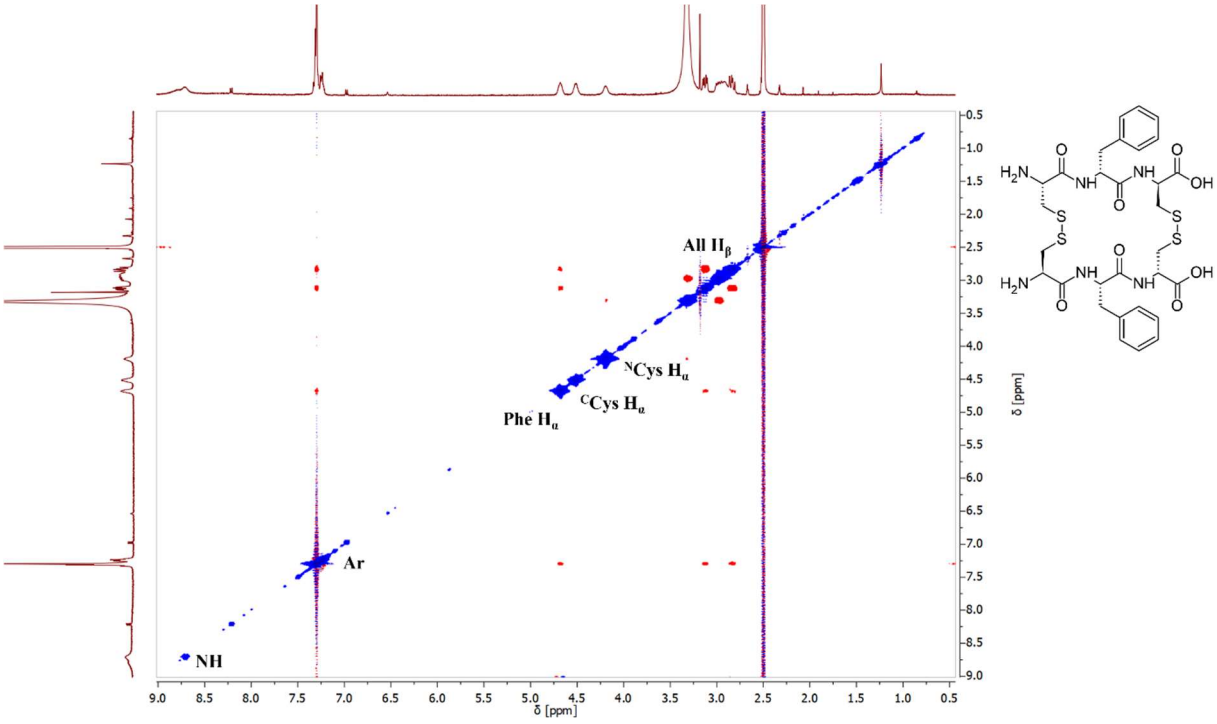

Figure 55: LLD parallel dimer NMR ROESY (400 MHz, DMSO-d_6).

Several crystallisation trials were performed by the hanging drop technique. Unfortunately, no crystals formed in the experiments. The peptide was tested at two different concentrations, pH values and ionic strength (Figure 56). The compound precipitated in almost all the crystallisation

trials probably due to its high hydrophobicity. At acidic pH instead, it formed a self-assembled suprastructure which was similar to a vesicle under the optical microscope investigation.

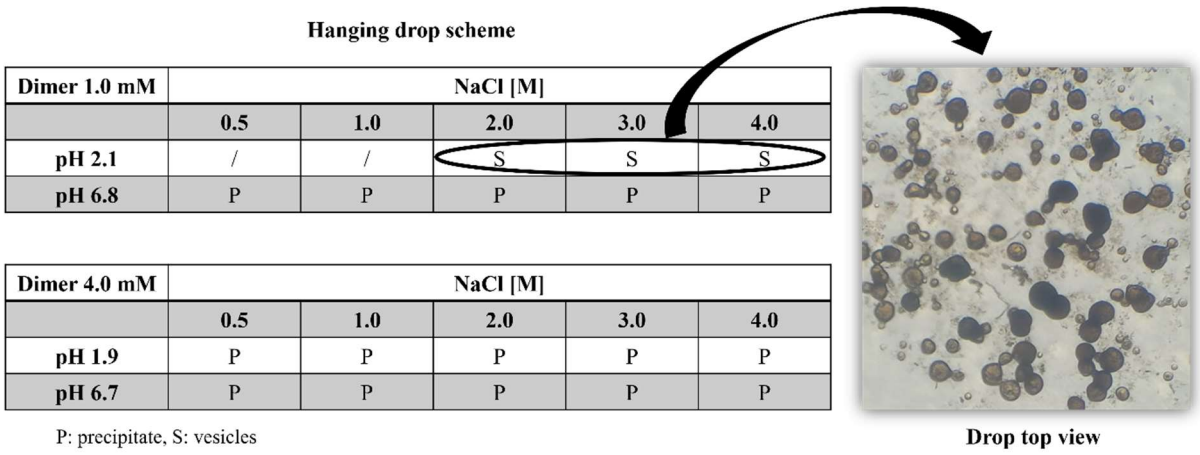

Dimer 1.0 mM	NaCl [M]				
	0.5	1.0	2.0	3.0	4.0
pH 2.1	/	/	S	S	S
pH 6.8	P	P	P	P	P

Dimer 4.0 mM	NaCl [M]				
	0.5	1.0	2.0	3.0	4.0
pH 1.9	P	P	P	P	P
pH 6.7	P	P	P	P	P

P: precipitate, S: vesicles

Figure 56: LLD parallel cyclic dimer hanging drop scheme. The compound precipitated in almost all the crystallisation drops. At low concentration in acidic media, the peptide self-assembled in a suprastructure simile to a vesicle.

5.6 – Heterochiral dimers comparison

All the heterochiral antiparallel dimers were studied by single-crystal XRD in their zwitterionic form. In all cases, the macrocycles form intramolecular hydrogen bond interactions between Phe amide groups, and none of them stacked into nanotubes as in the case of the homochiral stereoisomers. This is the main difference between the homochiral and the heterochiral libraries. The intramolecular hydrogen bond interactions, and the stereoisomerism favoured always the antiparallel cyclic dimer as the main product in the case of heterochiral stereoisomers whereas for the homochiral library it was the opposite. Comparing the different stereoisomers, it is possible to distinguish a different spatial organisation of the functional groups (Phe aromatic ring, carboxylates and ammoniums). DLL and LLD stereoisomers are constituted by the presence of both Phe sidechains on the same side of the ring (Figure 57). The difference between these two stereoisomers is the inversion of the carboxylate and ammonium groups. This is not surprising considering the double stereoinversion of both Cys residues. For some reason, this double stereoinversion enabled a different DCL composition, and the DLL stereoisomer prefers the antiparallel cyclic dimer over all the other possible isomers of its DCL. In the case of LLD stereoisomer instead, the antiparallel cyclic dimer is still the most abundant compound of the DCL but with a lower concentration compared to the DLL stereoisomer. However, the LLD stereoisomer was found to crystallise with two different macrocyclic conformations. The second conformer had a different disposition of one of the two ammonium group,

thus creating a particular situation. The ammonium group points outward the macrocyclic ring resembling more to the LDL stereoisomer functional group disposition. The LDL stereoisomer differs among the other heterochiral stereoisomer because it displayed an amphiphilic distribution of functional groups. The two Phe sidechain are alone on the upper side of the cycle whereas all the four polar charged groups are on the lower side.

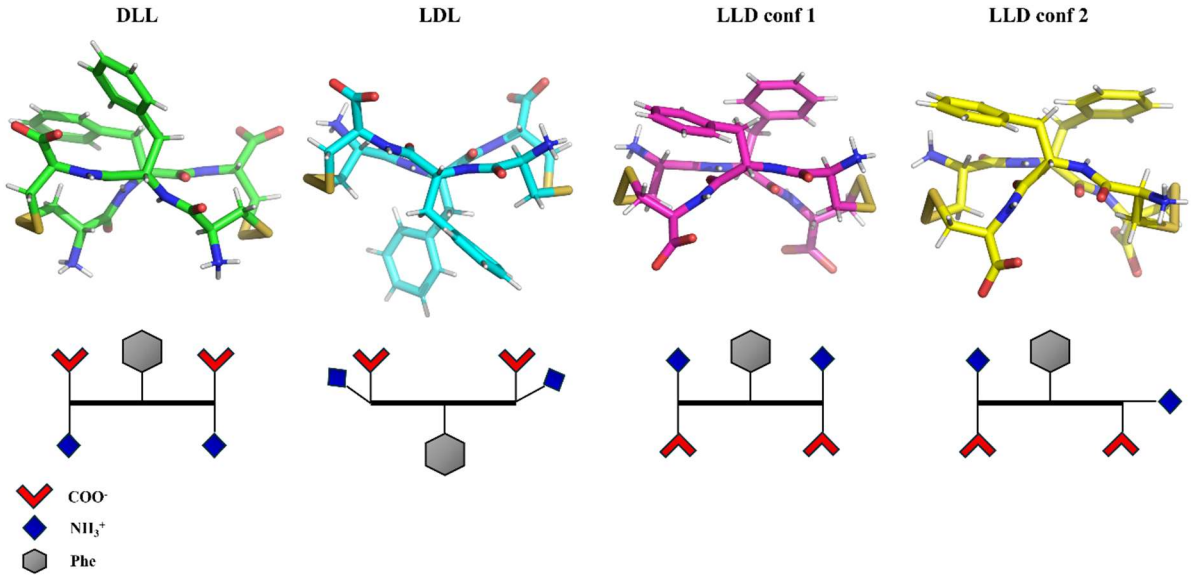

Figure 57: Heterochiral antiparallel cyclic dimers comparison. DLL and LDL had also more independent conformers in their XRD models, but since the main difference was the rotation of the Phe sidechain, only one of them was selected for the comparison. For LLD the macrocycle ring showed different conformations, and because of this both the independent macrocycles were reported. Peptides are represented with the stick model. Green, cyan, purple and yellow lime: carbon, red: oxygen, blue: nitrogen, yellow: sulfur, white: hydrogen. A schematic representation of the dimers is reported to highlight the spatial distribution of the lateral groups respected to the two macrocyclic faces.

The presence of these charged groups around the disulfide bridge could influence the thiol/disulfide exchange reaction. The LDL antiparallel cyclic dimer was the most abundant compound of its DCL, as well as for the other heterochiral DCLs, but it was later consumed by the formation of a higher oligomer able to self-assemble in a supramolecular structure. Since its peculiar conformation is stabilised as well by intramolecular hydrogen bonding interactions, it is possible that this particular functional group distribution favours the further evolution of the system towards larger oligomers. Without the structure of the cyclic pentamer, it is hard to draw a firm conclusion on the reactivity of this library. It is worth noting that the LDL library evolved into the cyclic pentamer, and the LLD library showed also the presence of a small amount of a cyclic pentamer. The second conformer of the LLD antiparallel cyclic dimer showed a conformation with one side of the ring similar to the LDL

stereoisomer. Further studies are required to shed light on the remaining cyclic structures, and the mechanism of the cyclic pentamer formation.

Chapter 6: Conclusions

A series of Cys-Phe-Cys diastereomers was synthesised in solid-phase, purified by reverse-phase HPLC, freeze-dried, and characterised by LC-MS, ^{1}H-NMR, H-H COSY. Their ability to undergo thiol/disulfide exchange in alkaline water was studied by LC-MS, and several macrocycles formed for each DCL. All the libraries were composed mainly by two cyclic dimers, and cyclic trimers too. The directionality of the peptide strand increased the complexity of the products, which differed not only in size, but also in isomerism (*i.e.*, parallel or antiparallel).

The LLL homochiral library showed a preference for the parallel dimer as the main DCL product, whereas all the three heterochiral DCLs yielded the antiparallel dimer as the dominating compound. A deeper investigation by NMR ROESY and single-crystal XRD allowed to assign the correct isomerism to each dimeric compound. The analysis also revealed an intriguing difference between the homochiral, and the three heterochiral systems. Homochiral cyclic dimers stacked into nanotubes in the crystal form, and their conformation and stereoisomerism favoured the intermolecular hydrogen bonding, whereas heterochiral diastereomers preferred intramolecular hydrogen bonding, and they did not stack into nanotubes. Solid-state comparison of the three heterochiral antiparallel dimers revealed the influence of the stereoconfiguration on their conformation and packing ability. The three different functional groups (*i.e.*, aromatic ring, ammonium, and carboxylate) were disposed on the two sides of the macrocycle according to their stereoisomerism thus enabling different physico-chemical properties, such as amphiphilicity in the case of the heterochiral LDL cyclic dimer. The LLL, DLL, and LLD tripeptide stereoisomers reached a thermodynamic equilibrium within 96 hours, and reactivation of their DCLs did not lead to further changes. Instead, the LDL stereoisomer showed a further evolution after reactivation with a reducing agent (TCEP), and the system self-assembled into a self-supporting hydrogel, as confirmed by rheology. The identification of the gelator was conducted through the derivatisation of its DCL in methyl esters after it had reached the thermodynamic equilibrium. The LC-MS, and ESI-TOF analyses of the main product revealed a cyclic pentamer. Even though its covalent connectivity (*i.e.*, parallel or antiparallel strand combinations) is still unclear, TEM analysis revealed anisotropic elongated suprastructures in the gel constituted by this compound. Therefore, considering these results, it is possible that the cyclic pentamer underwent stacking *via* hydrogen bonding interaction to form nanotubes, and the physical cross-link of these supramolecular tubes led to the formation of a hydrogel. Rheology and circular dichroism supported this hypothesis highlighting the stability range of the gel in the zwitterionic region and showing similar CD spectra for the compound from acidic to alkaline pH (1.0-12-0).

In conclusion, this project aimed to study the influence of amino-acidic stereoconfiguration on a DCC reaction for each one of four tripeptide diastereomers, and on their possible ability to self-assemble into supramolecular structures. The data described in this thesis unravelled fine details of steroisomerism great impact on the DCL products, and on their ability to self-organise into nanotubes and hydrogels. The LDL stereoisomer was able to self-synthesise its own cyclopentamer that hierarchically assembled into a supramolecular hydrogel, whereas homochirality was found to offer a convenient stereoconfiguration yielding supramolecular nanotubes as crystals in water. In the future, it would be interesting to explore different experimental conditions, such as ionic strength and pH, to verify the gelling ability of the homochiral dimers as potentially pH-responsive materials, exploiting the different ionisation state of their termini.

The discovery of the host/guest system composed by the LDL antiparallel cyclic trimer with zinc, opens the possibility to template the macrocycles during the DCC reaction using different metals or guests as templating agents, thus expanding the possible formation of new compounds for future applications. Furthermore, the threefold symmetry of the macrocycle offers an intriguing building block for hierarchical structures of various topologies. For instance, a second metal could coordinate the carboxylate groups that protrude from the vertices, or synthesis of differing compounds that replace the carboxylates with other coordinating functionalities could further expand the realm of architectural possibilities. Therefore, this research project not only provided a milestone to understand and control DCLs from heterochiral linear tripeptides, but also opened many future possibilities to guide the DCLs towards different directions.

Chapter 7: Materials and methods

7.1 – Solid-phase peptide synthesis

7.1.1 – General strategy

All the tripeptides were synthetised by solid-phase peptide synthesis under inert atmosphere (argon) from the C- to the N-terminal residue following a Fmoc protection strategy. Cysteine thiols were orthogonally protected with the acid-labile trityl protecting group. Compounds were synthetised on a 2-chloro-trityl chloride resin (100-200 mesh, crosslinked 1% divinylbenzene, loading 1.6 mmol/g). The resin choice has been done considering the molecular weight of the target peptide and to avoid the epimerisation of the C-terminal cysteine residue during the synthesis.[113] This resin swells in dichloromethane (DCM) and dimethylformamide (DMF), therefore these two solvents were used in all the steps of the SPPS. Coupling steps were performed with Oxyma B Pure and N,N'-diisopropylcarbodiimide (DIC) as coupling agents and Fmoc protecting groups were removed by piperidine. Peptides were cleaved by trifluoroacetic acid (TFA) based cleavage cocktail in concomitance with the deprotection of the cysteine residues.

7.1.2 – Loading of the C-terminal residue

Resin was left dry under vacuum for 20 min before use. All the glassware was kept in oven at 75 °C and then cooled down under argon flow to prevent water condensation since this resin is moisture sensitive. A proper amount of resin was weighted and placed inside a glass reactor vessel. This reactor was connected to the argon line in order to guarantee an inert atmosphere during all the synthetic operations. The resin was swelled in DCM for 20 minutes and then activated with $SOCl_2$ in a ratio of 100 µl for 1 gram of resin in DCM for 1 hour. This operation is necessary to activate the possible alcohol derivatives of the resin. After that time, the resin was washed with DCM and DMF.
The C-terminal Fmoc-protected residue was dissolved in DMF at the stoichiometric ratio of 1.6 mmol for 1 gram of resin. The loading reaction was carried out adding the amino acid solution to the resin with the weak base collidine (2,4,6-trimethyl-piperidine, 0.9 ml for 1 gram of resin). Usually, SPPS loading and couplings require DIPEA as a base. Cysteine is sensitive to strong bases and for this

reason a weaker base was used. At the end of the reaction, the resin was washed with DCM and DMF. The resin was then capped with MeOH in DCM (0.5 ml of MeOH for 1 gram of resin) in order to prevent byproducts from the unreacted resin sites. For the loading calculation see **section 7.1.6.**

7.1.3 – Fmoc deprotection

All the Fmoc deprotection steps have been done as follows: a solution of piperidine 20% in DMF was prepared and used in the deprotection reaction. Fmoc is well known to react with piperidine forming a benzofulvene-piperidine adduct. This deprotection product is detectable with the UV spectroscopy at λ 301 nm and it is possible to quantify the loading of the first amino acid as described in **section 7.1.6**. After every coupling step and the first loading, the Fmoc deprotection have been done adding the piperidine solution to the resin. The system was left react for 7 minutes, after that time, a fresh piperidine solution replaced the old one for further 7 minutes. At the end, the resin was then washed with DCM and DMF. The reaction was monitored via colorimetric tests as described in **section 7.1.7** to confirm the presence of the free N-terminal amine group.

7.1.4 – Couplings

The peptide chain was growth coupling a new Fmoc-protected amino acid with the free amine of the growing chain anchored to the resin. The peptide equivalents were determined by the loading calculation described in **section 7.1.6**. Oxyma B Pure and DIC were used as coupling agents and in a stoichiometry of 3 equivalents referred to the peptide chain. The Fmoc-amino acid (3 equivalents) was weighted together with the Oxyma B Pure and dissolved in DMF. The solution was then added to the resin followed by the DIC. The reaction was left react for 1 hour and 30 minutes. After that time, the resin was washed with DMC and DMF and the reaction was monitored via colorimetric tests as described in **section 7.1.7** to ensure that all the free N-terminal amines reacted with the new Fmoc-amino acid.

7.1.5 – Cleavage from the resin

After the last Fmoc-removal, the peptide chain is ready to be cleaved from the resin. This reaction occurs in a mild acidic cocktail mainly composed by trifluoroacetic acid (TFA). During this step, the cysteine trityl protecting groups are also removed. The cleavage cocktail was composed as follows:

Cleavage cocktail:

- 7.0% TFA
- 2.5% DCM
- 1.0% TIPS (triisopropyl silane)
- 0.5 % H_2O

TIPS and water are scavengers for the possible carbocation formation during the cleavage reaction. In particular, trityl removed by TFA is an equilibrium reaction and the carbocation can re-alkyl the cysteine thiol. To avoid this, TIPS is recommended to react irreversibly with the trityl cations.[114]
The cleavage was added to the resin and left under argon flow for 1 hour and 30 minutes, After that time, the liquid phase was collected in a round bottom flask. The resin was washed for further 15 minutes each with a fresh cleavage cocktail and then with DCM. All the liquid phases were collected in the same round bottom flask and the solution was then evaporated under argon flow to get the reaction crude.

7.1.6 – Loading calculation

The amount of C-terminal amino acid loaded on the resin is calculated monitoring the benzofulvene-piperidine byproduct of the Fmoc deprotection. After the loading reaction, few milligrams of resin (around 5 mg) were placed in an Eppendorf tube and left dry overnight. The dry resin was then weighted and 1 ml of 20% piperidine solution in DMF was added to the Eppendorf (see **section 7.1.3**). The resin was shacked for 20 minutes and after that time centrifuged at 15000 rpm for 5 minutes. 100 ul of the supernatant were then diluted in DMF (10 ml final volume, dilution 1:100) and the UV absorbance at 301 nm was measured.[115]

The loading was calculated with the following formula:

$$substitution\left(\frac{mmol}{g}\right) = \frac{101 * Abs_{301nm}}{7.8 * m_{resin}}$$

This formula is derived from:

$$SFmoc\ \left(\frac{mmol}{g}\right) = \frac{Abs_{301nm} * 10^6 mmol * mol^{-1} * mg * g^{-1} * V * D}{\varepsilon * m_{resin} * l}$$

Where:

- SFmoc = Fmoc substitution [mmol/g]
- ε = Molar absorption coefficient at 301 nm [7800 L mol^{-1} cm^{-1}]
- 10^6 mmol mol^{-1} mg g^{-1} conversion factor
- V = volume of the solution [l]
- D = dilution factor
- l = optical path length of the cell [cm]

7.1.7 – Colorimetric test

SPPS synthetic steps cannot be monitored with traditional organic chemistry techniques because of the presence of the resin. Different essays have been developed to detect the presence of free primary amines bound to the resin. All the synthetic steps in the SPPS are characterised by the presence or the removal of the Fmoc protection groups, thus the N-terminal amine group could be either protected or free depending on the step. Evaluate the presence of the free aminic group is essential to follow the outcome of every synthetic step.
In this work, two different colorimetric tests have been used to ensure the end of every reaction. The chloranil and bromophenol test are both colorimetric test which can detected the presence of a free primary amine bound to the resin colouring the beads in blue.[116]

Positive test: blue beads
Negative test: uncoloured beads

The bromophenol solution is prepared dissolving 5 mg in 10 ml of DMF (0.05%). To perform the test, a few amounts of beads are placed in an Eppendorf tube and mixed with some drops of the bromophenol solution. The presence of the free amine turns the colour of the beads from yellowish to blue (Figure 58).[117]

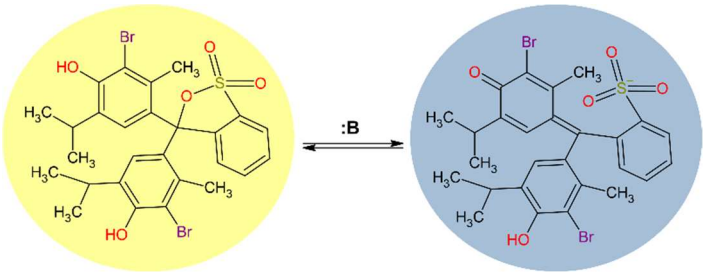

Figure 58: Molecular structure of bromophenol. When deprotonated, its colour shift from yellow to blue.

The reaction is an acid/base reaction. For this reason, it is possible to observe a colour shift towards blue even if the Fmoc group is still bound to the N-terminal. This could happen when other amines are present in the system. For instance, when the resin is not properly washed from the piperidine solution, the colorimetric test tube could turn from yellow to greenish/blue.

The chloranil test consist in an aromatic nucleophilic substitution which leads to a blue peptide/chloranil adduct.[118] The test is performed adding two solutions in an Eppendorf with few beads.

Solution 1: 0.2 ml of acetaldehyde in 10 ml of DMF (solution 2%)

Solution 2: 189 mg of chloranil in 10 ml of DMF (solution 2%)

The presence of the free amine is detected by the blue colour shift of the beads (Figure 59). The acetaldehyde ensures the reactivity towards primary amines which is the case for a N-terminal amine group.[119]

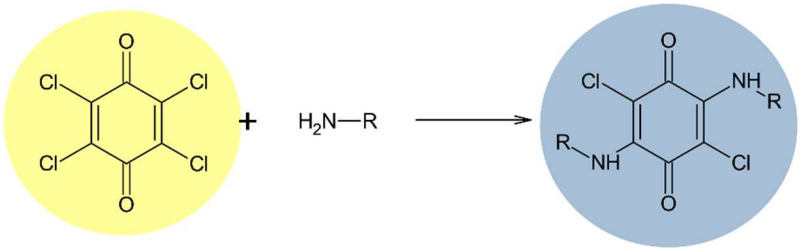

Figure 59: Chloranil reaction in presence of a primary amine. The colour of the solution turns from yellow to blue.

This test is more reliable than the bromophenol because the latter could give false positive results.

7.2 – Peptide purification

All the synthetised peptides were purified by reverse-phase HPLC (*1260 Agilent infinity*) equipped with a gradient quaternary pump (*G1311B*), C-18 semipreparative column (*Kinetex, 5 μm, 100 Å, 250 x 10 mm, Phenomenex*) and photodiode array detector (*G1315C*). The mobile phase was a mixture of water and acetonitrile with 0.05% TFA.

7.2.1 – General sample preparation

All crudes obtained by the evaporation of the cleavage cocktail were dissolved first in acetonitrile and then a proper amount of water was added carefully reaching the desired ratio of MeCN/H_2O according to **section 7.2.2**. 0.1 equivalents of tris-(2-Carboxyethyl)phosphine hydrochloride (TCEP) were dissolved in the water part of the mixture to prevent oxidation of the thiols to disulfides.
All crudes dissolved in MeCN and after the water addition, a white precipitate formed. This precipitate is composed of impurities of the cleavage and the reacted trityl protecting groups. For this reason, all samples were centrifugated at 15000 rpm for 10 minutes and the filtered with a 0.45 μm PTFE syringe filters.

7.2.2 – HPLC Semipreparative gradients

Purification of all the peptides was optimised in order to find the best gradient in terms of speed and precision.

General parameters:

- Column temperature: 35 °C
- Mobile phase flow: 3.0 ml/min
- Sample injection: 900 μl
- Draw and injection speed: 900 μl/min (low viscosity)
- UV-detector: 214 and 254 nm

L-Cys-L-Phe-L-Cys and D-Cys-L-Phe-L-Cys:

Sample preparation: the crude was dissolved in 85/15 H_2O/MeCN with 0.05% TFA and 0.1 eq of TCEP.

Chromatographic method:

t = 0 min	15% MeCN
t = 2 min	15% MeCN
t = 17 min	25% MeCN
t = 18 min	95% MeCN
t = 20 min	95% MeCN

The purified compound was collected in a falcon tube and then freeze-dried. The peptide was obtained as a white fluffy powder.

L-Cys-D-Phe-L-Cys:

Sample preparation: the crude was dissolved in 80/20 H_2O/MeCN with 0.05% TFA and 0.1 eq of TCEP.

Chromatographic method:

t = 0 min	20% MeCN
t = 2 min	20% MeCN
t = 13 min	70% MeCN
t = 14 min	95% MeCN
t = 27 min	95% MeCN

The purified compound was collected in a falcon tube and then freeze-dried. The peptide was obtained as a white fluffy powder.

L-Cys-L-Phe-D-Cys:

Sample preparation: the crude was dissolved in 70/30 H_2O/MeCN with 0.05% TFA and 0.1 eq of TCEP.

Chromatographic method:

t = 0 min	25% MeCN
t = 2 min	25% MeCN
t = 8 min	45% MeCN
t = 10 min	95% MeCN
t = 15 min	95% MeCN

The purified compound was collected in a falcon tube and then freeze-dried. The peptide was obtained as a white fluffy powder.

7.3 – Peptide characterisation

All peptides were characterised by LCMS and NMR. The LC module has been already described in **section 6.2** except for the analytical column (*Phenomenex LUNA C-18, 5 µm, 100 Å, 150 x 2 mm*). Mass spectra were collected on an *Agilent 6120 ESI-quadrupole* system in *fast scan mode* (mass range 100-2000, solvent delay 2 min, scan speed 5200 u/sec, threshold 150). NMR spectra were acquired on a *Varian innova* instrument (400 MHz).

7.3.1 – LCMS characterisation

General sample preparation: compounds were dissolved at 1 mg/ml in 50/50 H_2O/MeCN 0.1% formic acid (FA) and filtered with a 0.2 µm PTFE syringe filter.

Chromatographic method:

t = 0 min	5% MeCN
t = 20 min	95% MeCN
t = 21 min	95% MeCN

Samples were analysed in positive and negative mode.

7.3.2 – NMR characterisation

Several solvents were tried in order to achieve the best concentration for the NMR experiments. Dimethylsulfoxide-d_6 (DMSO) has been identified as the best solvent in terms of compounds solubility and possibility to observe the amide protons.

General sample preparation: 2 mg of peptide were dissolved in 750 µl of DMSO-d_6 and placed in an NMR tube suitable for 400 MHz.

General scan parameters: All mono-dimensional ^{1}H-NMR were collected at 25 °C with 32 scans and relaxion time of 1 second in the spectral window from 0 to 14 ppm.
H-H COSY experiments were collected at 25 °C with 200 scans and 2 scans for t_1 increment.

7.4 – Kinetic studies

The libraries evolution was followed over time by LCMS analysis with the same parameters described in **section 7.3**. Libraries were analysed every 24 hours starting from t_0 until 96 hours (five days). Chromatograms acquired on λ 214 nm were then integrated manually with the Agilent software and the percentage area was plotted over time.

Library preparation: The tripeptide was dissolved in buffered water (100 mM borate buffer, pH 8.5) to reach the final concentration of 20 mM. The pH value was monitored by a pH-meter and tuned with a small amount of NaOH 1M. Every time point was analysed diluting 100 µl of the library with 100 µl of MeCN, the pH was lowered with FA to the final value of 2.0. Finally, the sample was filtered with 0.45 µm PTFE syringe filter.

7.5 – Large-scale libraries.

Large-scale libraries were prepared according to procedure in **section 7.4** in order to isolate and characterise the library main products. For L-Cys-L-Phe-L-Cys, D-Cys-L-Phe-L-Cys and L-Cys-L-Phe-D-Cys, the library was left react for 72 hours and then freeze-dried. In the case of L-Cys-D-Phe-

L-Cys instead, the library reacted for 24 hours and then was freeze-dried in order to get the higher quantity of main product possible.

7.5.1 – Cyclic peptides purification

All the large-scale libraries were purified by reverse-phase HPLC with the same instrumental parameters described in **section 7.3.**

L-Cys-L-Phe-L-Cys library:

13 mg of library were dissolved in 4 ml 75/15 H_2O/MeCN 0.05% TFA and then filtered with 0.45 μm PTFE syringe filter.

Chromatographic method:

t = 0 min 15% MeCN
t = 2 min 15% MeCN
t = 15 min 30% MeCN
t = 16 min 95% MeCN
t = 18 min 95% MeCN

Three fractions were collected in falcon tubes and then freeze-dried.

Compound	Rt [min]	Mass [mg]
Antiparallel cyclic dimer	9.0-10.5	3.58
Parallel cyclic dimer	10.5-12.5	1.46
Cyclic trimer	13.5-14.5	0.37

D-Cys-L-Phe-L-Cys library:

40 mg of library were dissolved in 5 ml 80/20 H_2O/MeCN 0.05% TFA and then filtered with 0.45 μm PTFE syringe filter.

Chromatographic method:

t = 0 min 15% MeCN

t = 2 min 15% MeCN

t = 20 min 40% MeCN

t = 22 min 95% MeCN

t = 25 min 95% MeCN

Three fractions were collected in falcon tubes and the freeze-dried.

Compound	Rt [min]	Mass [mg]
Antiparallel cyclic dimer	11.8-14.5	20.99
Parallel cyclic dimer	15.3-16.0	1.39
Cyclic trimer	16.8-17.5	0.78

L-Cys-D-Phe-L-Cys library:

13 mg of library were dissolved in 85/15 H_2O/MeCN 0.05% TFA and then filtered with 0.45 μm PTFE syringe filter.

Chromatographic method:

t = 0 min 20% MeCN

t = 2 min 20% MeCN

t = 18 min 55% MeCN

t = 19 min 95% MeCN

t = 20 min 95% MeCN

One fraction was collected in falcon tube and the freeze-dried. All other fractions were always more than one product.

Compound	Rt [min]	Mass [mg]
Antiparallel cyclic dimer	13.6-14.0	4.56

L-Cys-L-Phe-D-Cys library:

20 mg of library were dissolved in 90/10 H_2O/MeCN 0.05% TFA and then filtered with 0.45 μm PTFE syringe filter.

Chromatographic method antiparallel dimer:

t = 0 min 10% MeCN
t = 2 min 10% MeCN
t = 17 min 25% MeCN
t = 20 min 37% MeCN
t = 22 min 95% MeCN
t = 24 min 95% MeCN

Two fractions were collected in falcon tubes and then freeze-dried. The first fraction was the antiparallel dimer, the second fraction all the rest of the library together. This fraction was then repurified with a second method.

Compound	Rt [min]	Mass [mg]
Antiparallel cyclic dimer	13.4-15.6	8.05

The second fraction of the previous purification was freeze-dried and then redissolved in 90/10 H_2O/MeCN 0.05% TFA and then filtered with 0.45 μm PTFE syringe filter.
A total amount of 15 mg obtained from different large-scale libraries were dissolved in 4 ml of HPLC solvent mixture.

Chromatographic method parallel dimer:

t = 0 min 10% MeCN
t = 2 min 10% MeCN
t = 13 min 85% MeCN
t = 14 min 95% MeCN

Two fractions were collected in falcon tubes and then freeze-dried.

Compound	Rt [min]	Mass [mg]
Parallel cyclic dimer	10.3-10.8	5.19

7.6 – LDL cyclic pentamer amplification

A large-scale LDL library was prepared according to **section 7.5**. After 72 hours, a concentrated TCEP stock solution was added to the system in order to reach the final concentration of TCEP of 0.2 mM (library concentration 20 mM referred to monomer). The TCEP was added in a catalytical amount of 1:100 referred to monomer concentration. TCEP was added every 24 hours for 5 days. After the first day the library self-assembled in a hydrogel. The following days, TCEP was added after disassembling the gel vortexing the vial. The pH of the solution was monitored with the pH-meter through all the five days. The gel formed at pH 8.5.

7.7 – LDL cyclic pentamer esterification

The hydrogel prepared according to **section 7.6** was freeze-dried. The glassware was kept in the oven at 75 °C and then cooled down under argon flow to prevent water condensation. 30 mg of peptide powder were suspended in 10 ml of MeOH in a round bottom flask and stirred in an ice bath for 20 min. After this time, 120 µl of $SOCl_2$ were added slowly and the reaction was left overnight. The day after, gases were vented with argon flow and then 120 µl of $SOCl_2$ were added to the system. The reaction was kept under argon overnight again and the day after the solvent was removed by rotavapor to get an amber sticky oil.

7.7.1 – LDL cyclic pentamer methyl ester purification

The product was purified by reverse-phase HPLC with almost the same parameters of **section 7.2**. The mobile phase was composed by methanol and water with 0.05% TFA. Due to the higher pressure in the system generated by the different viscosity of MeOH/H_2O compared to MeCN/H_2O, the flow was set at 2.5 ml/min.

Sample was dissolved in 70/30 H_2O/MeOH 0.05% TFA and the solution was kept in ice bath to prevent a possible hydrolysis of the methyl esters. The solution was filtered with 0.45 µm PTFE syringe filter and purified with the following method:

t = 0 min 30% MeOH

t = 2 min 30% MeOH

t = 22 min 95% MeOH

t = 24 min 95% MeOH

The fractions were diluted with water to reduce the amount of MeOH below the 30% and then freeze-dried.

7.7.2 – LDL cyclic pentamer methyl ester characterisation

The esterification product was analysed by LCMS and by ESI-TOF mass spectrometry. For the LCMS, the setup was the same of **section 7.3** but again MeCN was switched with MeOH in the mobile phase.

Sample was dissolved in 50/50 H_2O/MeOH with 0.1% FA and then filtered with 0.2 µm PTFE syringe filter.

Chromatographic method:

t = 0 min 5% MeOH

t = 20 min 95% MeOH

t = 30 min 95% MeOH

The same sample was analysed by ESI-TOF (*ESI-micrOTOF-Q instrument*) with the following parameters:

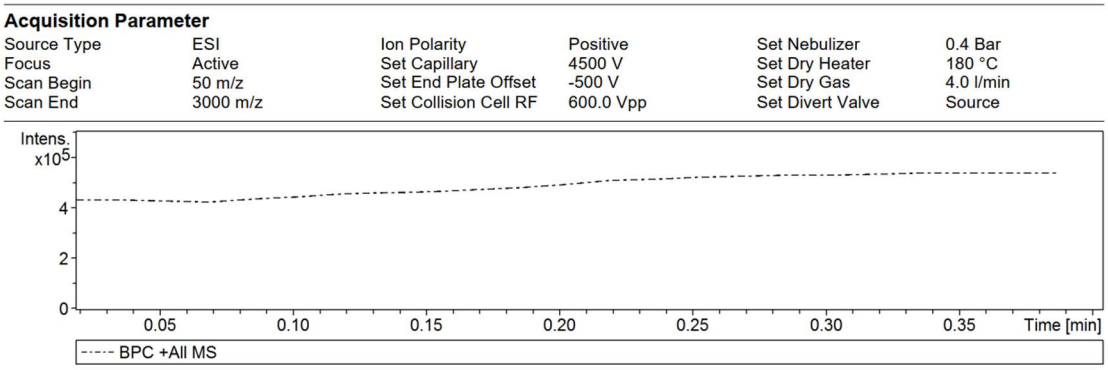

7.8 – Macrocycles NMR characterisation

Purified macrocycles were studied by TOCSY and ROESY NMR in order to gain structural information about their isomerism. The NMR spectrometer was the same of **section 7.3.**

TOCSY parameters:

- Scans for t_1 increments 4
- t_1 increments 200
- Spinlock pattern Clean MLEV17
- Spinlock duration 80 ms

ROESY parameters:

- Scans for t_1 increments 16
- t_1 increments 200
- Spinlock pattern TROESY
- Spinlock mixing time 200 ms

7.9- Circular dichroism characterisation

All CD spectra were acquired on a *JASCO J185 spectropolarimeter* with the following parameters:

- Temperature 25 °C
- Spectral width: 185-280 nm
- Step size 1 nm
- Scan speed 100 nm/min
- DIT 1 s
- Band width 2 nm

7.9.1 –Cyclic dimers

Purified compounds were dissolved in milli-Q water and the pH was tuned with NaOH 1 M to reach the final value of 7.0 and the final concentration of peptide of 1 mM. Peptide solutions were placed in a 0.1 mm quartz cuvette.

7.9.2 – LDL cyclic pentamer

The self-assembled library was diluted 1:2, and then the pH was tuned with NaOH and HCl 1.0 M to reach the desired value. The resulting solution/gel was transferred in a 0.1 mm quartz cuvette for the data acquisition.

7.10 – Crystallisation experiments

7.10.1 – LLL and LLD stereoisomers

Macrocycles were dissolved in milli-Q water at the desired final concentration and then the pH was tuned by NaOH or HCl 1M. Crystallisation reservoirs were prepared as NaCl solutions with different concentration. Drops were prepared by mixing 3 µl of the macrocycle solution with 3 µl of the reservoir solution and then they were placed on the center of a plastic cover slip (22x22 mm, 0.157 mm thickness). The multiwell plate was prepared with the different reservoir solutions and with a thin film of vacuum grease on the edges of the well to ensure a proper sealing with the plastic cover slip as a cap.

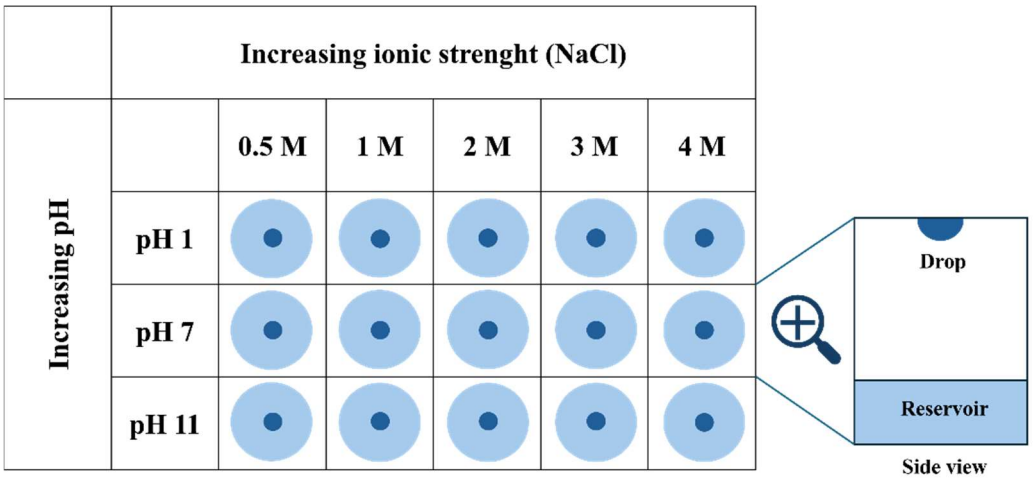

Figure 60: Hanging drop general scheme. Light blue: NaCl solution reservoir, blue: drop solution obtained mixing 3 µl of the macrocycle solution and 3 µl of the reservoir. On the right, side view of one of the hanging drop wells.

7.10.2 – DLL stereoisomer

LDL antiparallel cyclic dimer was dissolved in water at 20 mM and the pH was tuned with the pH-meter at 7.0. The solution was tested under optical microscope mixing 2 µl with a same amount of an organic solvent (methanol, ethanol, 2-propanol, 1-butanol). The drops with precipitate or crystals were reproduced in large-large scale to get the crystals.

7.10.3 – LDL stereoisomer

The antiparallel cyclic dimer was dissolved in methanol and then placed in a vapour diffusion closed system with a second solution of water/methanol. The evaporation of methanol from the dimer solution led to the crystallisation of the compound.

7.11 – Transmission electron microscopy (TEM)

TEM images were collected by Dr. Slavko Kralj from Jožef Stefan Institute in Ljubljana (Slovenia) on a *Jeol, JEM 2100* instrument at 100 kV.

Sample preparation: The LDL cyclic pentamer gel was prepared according to **section 7.6.** A lacey grid (300 mesh, 100 micron) was placed in the ozone cleaner (*UV-ozone Procleaner*) for 5 minutes. After that time, 2 µl of gel were placed on the top of the grid and dried carefully with a tiny piece of paper. After 5 minutes, 2 µl of phosphotungstate stain solution was added at the top of the grid. The sample was left dry overnight in a vacuum chamber.

Phosphotungstate stain solution: A 2% phosphotungstate solution in water was prepared dissolving the phosphotungstate in milli-Q water. Then, the pH was tuned adding NaOH 1M to reach the desired value. The solution was centrifugated at 15000 rpm for 10 minutes and the supernatant was filtered with 0.2 µm syringe filter.

7.12 – Single crystal analysis (XRD)

7.12.1 – LLL, LLD stereoisomers and LDL antiparallel cyclic trimer

All compounds were loaded on cryo-loops and cryoprotected in NHV oil (Jena bioscience, Germany). All crystals were analysed at Elettra synchrotron XRD1 beamline (Trieste, Italy). Loops were loaded on the goniometer and cooled down to 100 K by a nitrogen stream. The data collection was performed with the rotating crystal method (λ 0.7 Å) and diffraction images were collected every 0.5° of rotation for a total of 720 images.

Reflections were indexed and integrated by XDS package,[120] and the space group was determined by POINTLESS.[121] Phase was obtained with SHELXT[122] by direct methods and the model was then refined by SHELXL[123] using the SHELXle GUI.[124] Water molecules were placed analysing the maps and the distances between the neighbour atoms with COOT.[125] Refinement was conducted by full-matrix least-square method on F^2 and thermal parameters were refined anisotropically except for hydrogen atoms which were added at the geometrically calculated positions. The final model was then validated by PLATON.[126]

7.12.2 – DLL antiparallel cyclic dimer

A stick-shaped single crystal of the peptide was collected with a loop, cryoprotected by dipping the crystal in glycerol and stored frozen in liquid nitrogen. The crystal was mounted on the diffractometer at the synchrotron Elettra, Trieste (Italy), beamline XRD1, using the robot present at the facility. Temperature was kept at 100 K by a stream of nitrogen on the crystal. Diffraction data were collected by the rotating crystal method using synchrotron radiation, wavelength 0.70 Å, rotation interval 1°/image, crystal-to-detector distance of 85 mm. A total of 270 images were collected to increase redundancy of data. Reflections were indexed and integrated using the XDS package, space group C2 was determined using POINTLESS, and the resulting data set was scaled using AIMLESS. Phase information were obtained by direct methods using the software SHELXT [4]. Refinements cycles were conducted with SHELXL-14 [4], operating through the WinGX GUI [5], by full-matrix least-squares methods on F2. Unit cell parameters and scaling statistics are reported in Table 2. The asymmetric unit contains six molecules of the peptide, 11 molecules of water in positions at full occupancy and 4.5 water molecules in 9 positions at partial occupancy. Hydrogen atoms of the

peptide were added at geometrically calculated positions and refined isotropically, with thermal parameters dependent on those of the attached atom. During refinement, geometric constrains were applied on distances and angles of two phenyl moieties. All the atoms, except the hydrogen atoms, within the asymmetric unit have been refined with anisotropic thermal parameters. Disordered solvent molecules present in the channels of the structure were too difficult to be modelled, but their contribution was taken into account using the SQUEEZE/PLATON procedure. Residual electron densities corresponding to 196 electrons/cell were found in the voids of the crystal, corresponding to 14% of the cell volume. Refinements using reflections modified by the SQUEEZE procedure behaved well and R-factors were reduced from 11% to 9%.

7.12.3 – LDL antiparallel cyclic dimer

A stick-shaped single crystal of the peptide was collected with a loop, cryoprotected by dipping the crystal in glycerol and stored frozen in liquid nitrogen. The crystal was mounted on the diffractometer at the synchrotron Elettra, Trieste (Italy), beamline XRD1, using the robot present at the facility. Temperature was kept at 100 K by a stream of nitrogen on the crystal. Diffraction data were collected by the rotating crystal method using synchrotron radiation, wavelength 0.70 Å, rotation interval 1°/image, crystal-to-detector distance of 85 mm. A total of 180 images were collected. Reflections were indexed and integrated using the XDS package, space group *C2* was determined using POINTLESS and the resulting data set was scaled using AIMLESS. Phase information were obtained by direct methods using the software SHELXT. Refinements cycles were conducted with SHELXL-14, operating through the WinGX GUI, by full-matrix least-squares methods on F2. Unit cell parameters and scaling statistics are reported in Table 1. The asymmetric unit contains two circular dimers of the compound, 7 water molecules at full occupancy, 7 water molecules at 50% statistical occupancy and a methanol molecule at 50% occupancy. Hydrogen atoms were added at geometrically calculated positions and refined isotropically, with thermal parameters dependent on those of the attached atom, except for the hydrogen atoms of the water molecules that were refined with restraints on the bond distance and angle, using the DFIX and DANG card of the SHELXL-14 software. During refinement, geometrical restraints were applied on distances, angles or thermal parameters of the compound in regions of the structure with poor electron density. All the atoms at full occupancy, except the hydrogen atoms, within the asymmetric unit have been refined with anisotropic thermal parameters.

Appendix

A.1 – General compound structures

Compound	Chemical formula	Molecular weight [g/mol]
Monomer	$C_{15}H_{21}N_3O_4S_2$	371.47
Cyclic monomer	$C_{15}H_{19}N_3O_4S_2$	369.45
Cyclic dimer	$C_{30}H_{38}N_6O_8S_4$	738.91
Cyclic trimer	$C_{45}H_{57}N_9O_{12}S_6$	1108.36
Cyclic tetramer	$C_{60}H_{76}N_{12}O_{16}S_8$	1477.82
Cyclic pentamer	$C_{75}H_{95}N_{15}O_{20}S_{10}$	1847.27
Cyclic pentamer methyl ester	$C_{80}H_{105}N_{15}O_{20}S_{10}$	1917.41

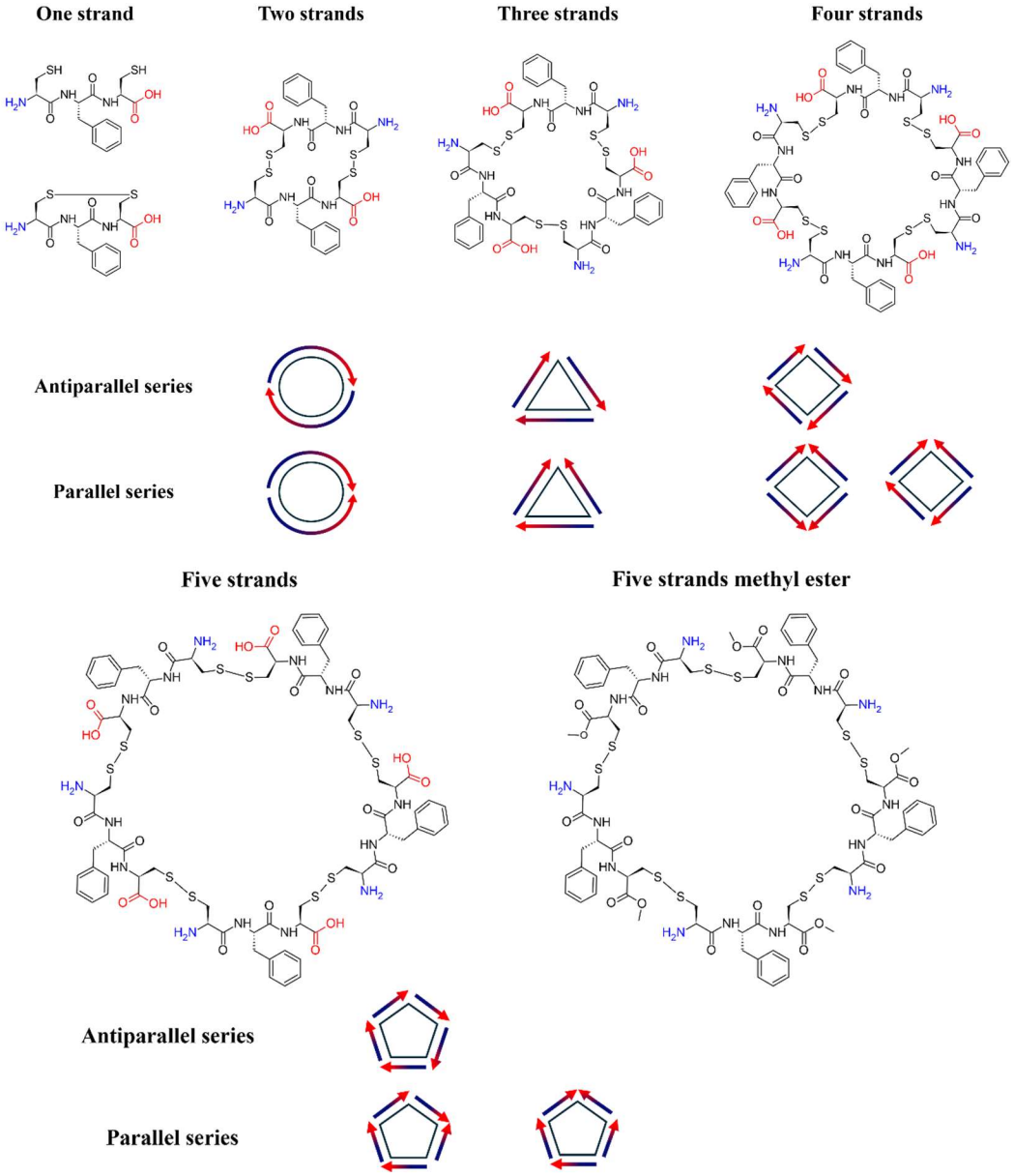

Figure 61: Example of a possible LLL tripeptide library, only the antiparallel products are displayed as molecular structures. The parallel series is represented in cartoon. Arrows point from N- to C-terminus of the strand.

A.2 – Tripeptide spectroscopic data

A.2.1 – L-Cys-L-Phe-L-Cys

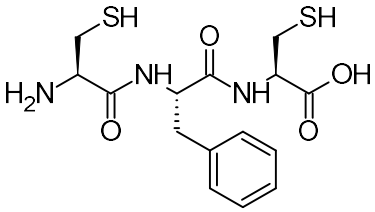

^{1}H-NMR (400 MHz, DMSO-*d*$_6$, TMS), δ (ppm): **8.63** (d, *J*= 8.0 Hz, 1, NH Phe), **8.58** (d, *J*= 8.0 Hz, 1, NH, Cys C), **7.34-7.18** (m, 5H, Ar), **4.68** (ddd, *J* = 4.0 Hz, *J* = 8.0 Hz, *J* = 14.0 Hz, 1, CH_α Phe), **4.43** (ddd, *J* = 4.8 Hz, *J* = 7.6 Hz, *J* = 8.0 Hz, 1, CH_α Cys C), **3.92** (dd, *J* = 4.8 Hz, *J* = 5.6 Hz, 1, CH_α N), **3.09** (dd, *J* = 4.0 Hz, *J* = 14.0 Hz, 1, CH_β Phe), **3.01** (dd, *J* = 5.6 Hz, *J* = 14.0 Hz, 1, CH_β Cys N), **2.90** (dd, *J* = 4.8 Hz, *J* = 13.6 Hz, 1, CH_β Cys C), **2.86** (dd, *J* = 4.8 Hz, *J* = 14.0 Hz, 1, CH_β Cys N), **2.83** (dd, *J* = 4.0 Hz, *J* = 14.0 Hz, 1, CH_β Phe), **2.78** (dd, *J* = 7.6 Hz, *J* = 14.0 Hz, 1, CH_β Cys C).

MS (ESI): calculated mass **371.10,** observed mass m/z $[M+H]^+$ 372.0, m/z $[M-H]^-$ 369.9.

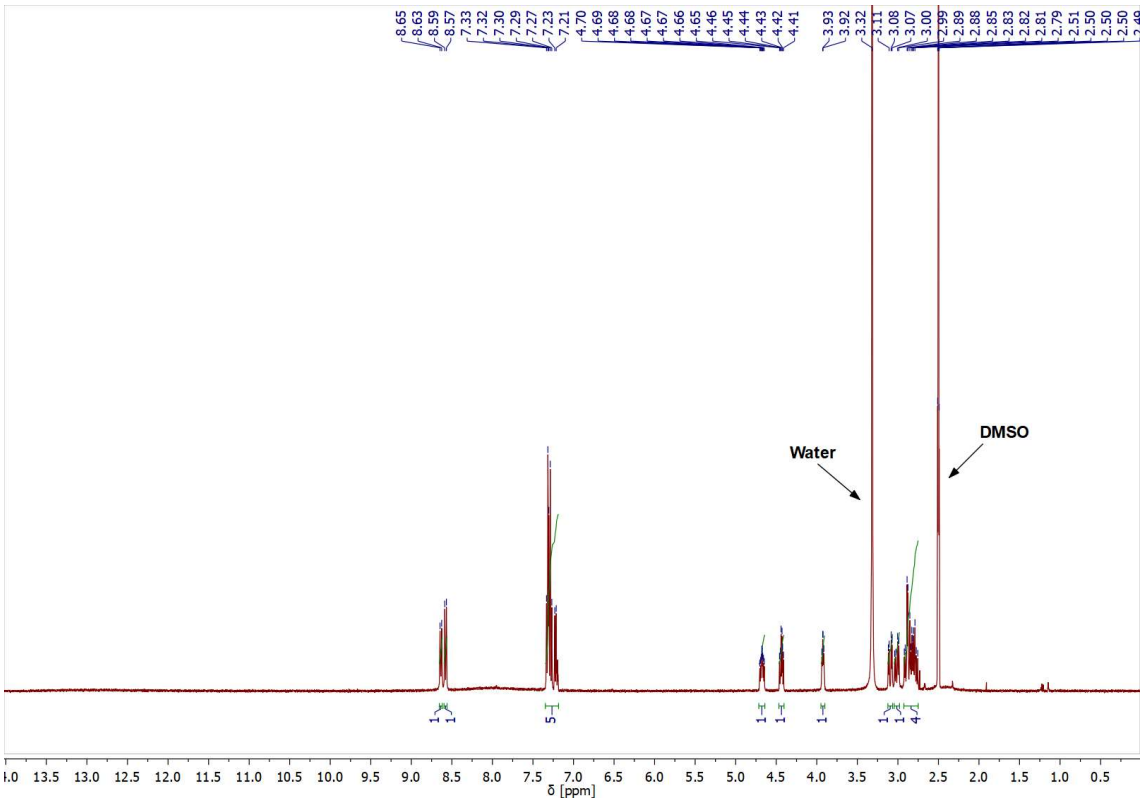

Figure 62: ^{1}H-NMR (400 MHz, DMSO-*d*$_6$) of L-Cys-L-Phe-L-Cys tripeptide. Protons were assigned with the aid of the H-H COSY (400 MHz) spectrum.

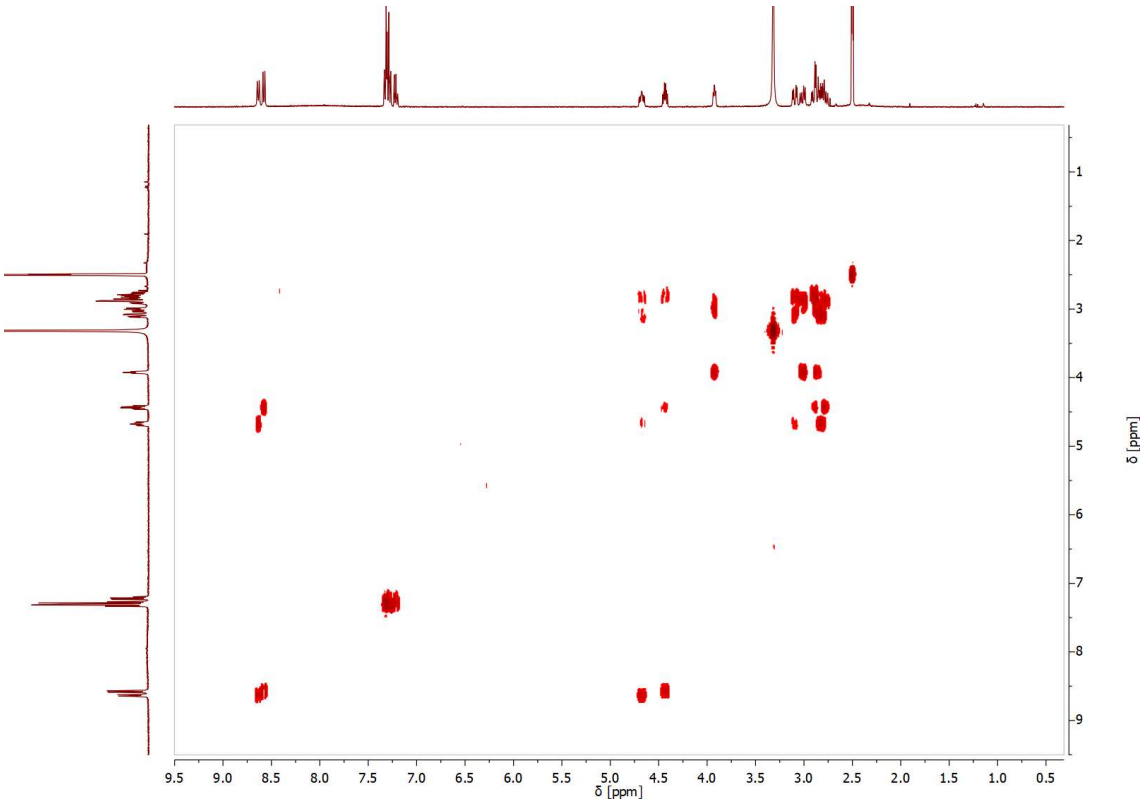

Figure 63: H-H COSY (400 MHz, DMSO-d_6) of L-Cys-L-Phe-L-Cys tripeptide.

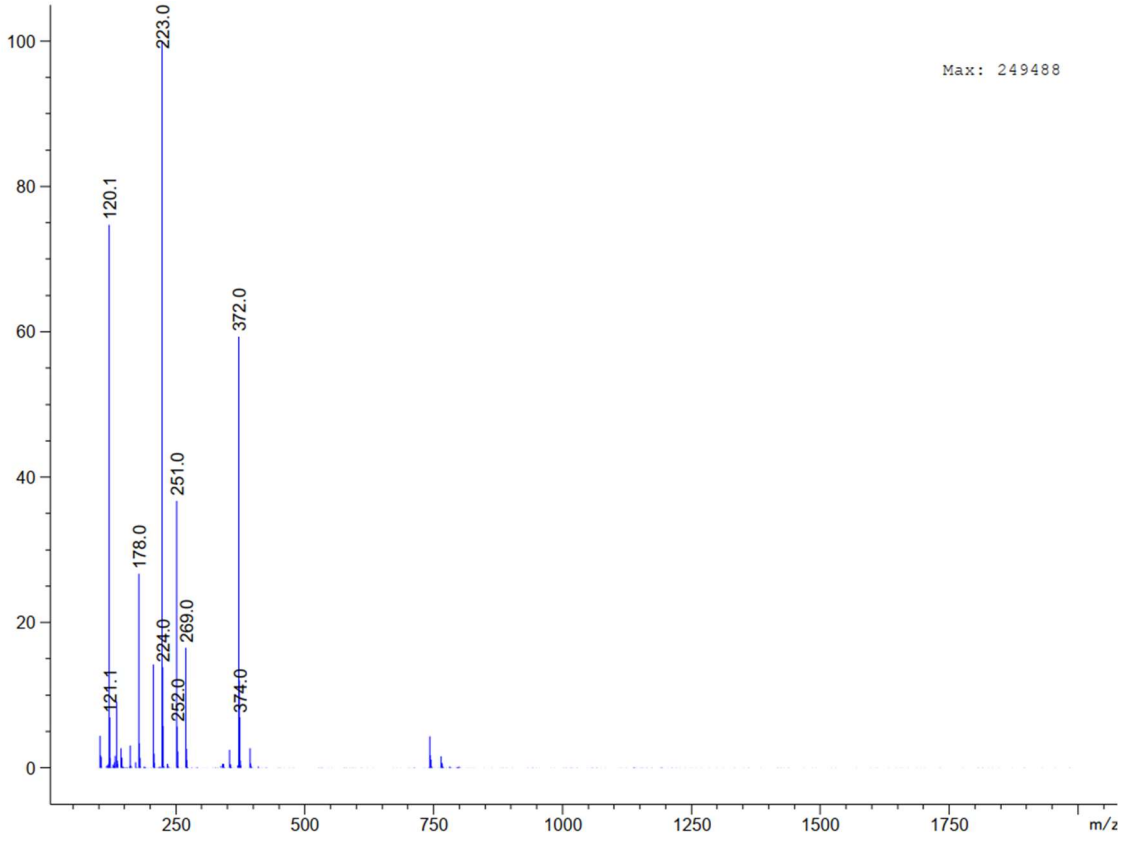

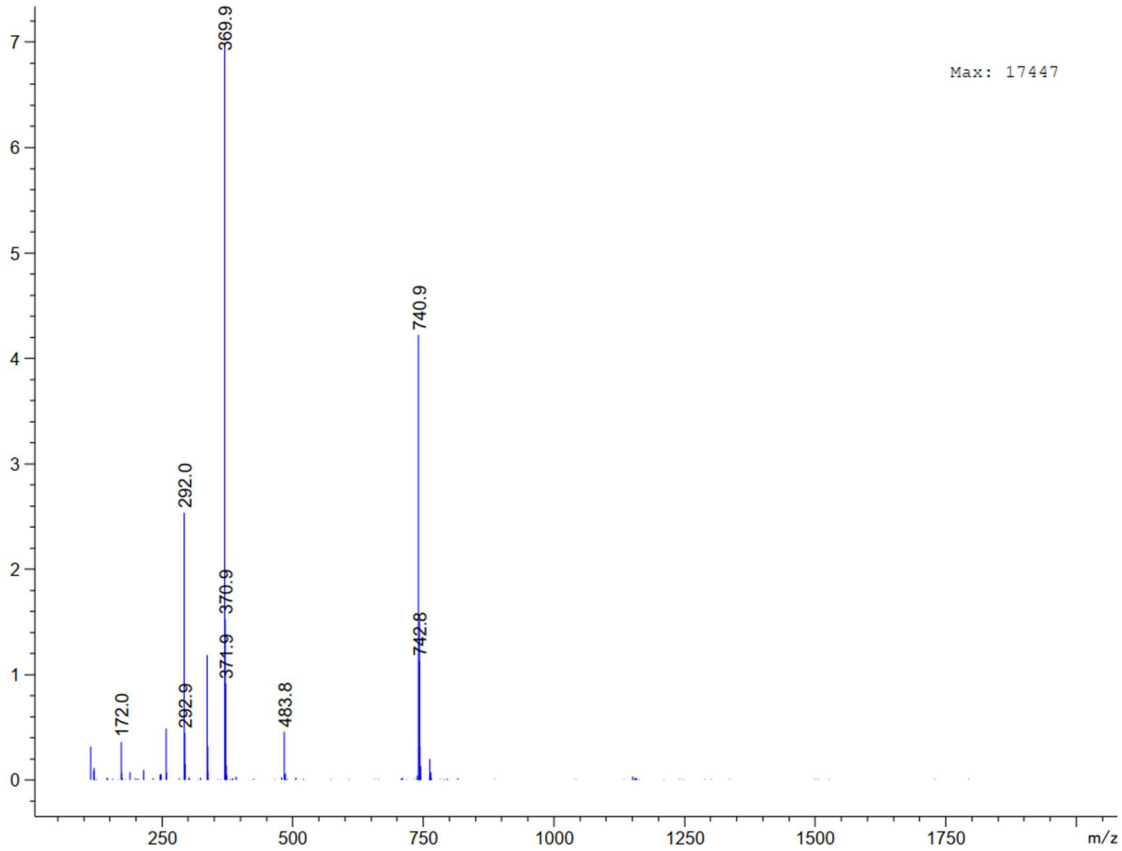

Figure 64: ESI-MS spectrum of L-Cys-L-Phe-L-Cys in positive (top) and negative (bottom) mode.

A.2.2 – D-Cys-L-Phe-L-Cys

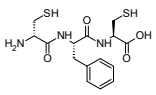

^{1}H-NMR (400 MHz, DMSO-*d*$_6$, TMS), δ (ppm): **8.68** (d, *J* = 8.8 Hz, 1, NH Phe), **8.61** (d, *J* = 8.0 Hz, 1, NH Cys C), **7.31-7.17** (m, 5, Ar), **4.80** (ddd, *J* = 4.0 Hz, *J* = 8.8 Hz, *J* = 10.4 Hz, 1, CH_α Phe), **4.41** (ddd, *J* = 4.4 Hz, *J* = 7.6 Hz, *J* = 8.0 Hz, 1, CH_α Cys C), **3.83** (dd, *J* = 6.4 Hz, *J* = 4.0 Hz, 1, CH_α Cys N), **3.11** (dd, *J* = 4.8 Hz, *J* = 14.0 Hz, 1, CH_β Phe), **2.91** (dd, *J* = 4.4 Hz, *J* = 14.0 Hz, 1, CH_β Cys C), **2.80** (dd, *J* = 7.6 Hz, *J* = 14.0 Hz, 1, CH_β Cys C), **2.75** (dd, *J* = 10.4 Hz, *J* = 14.0 Hz, 1, CH_β Phe), **2.63** (dd, *J* = 4.4 Hz, *J* = 14.4 Hz, 1,CH_β Cys N), **2.55** (dd, *J* = 6.4 Hz, *J* = 14.4 Hz, 1, CH_β Cys N)

MS (ESI): calculated mass **371.10,** observed mass m/z $[M+H]^+$ 372.0, m/z $[2M+H]^+$ 743.1, m/z $[M-H]^-$ 370.0, m/z $[2M-H]^-$ 741.1.

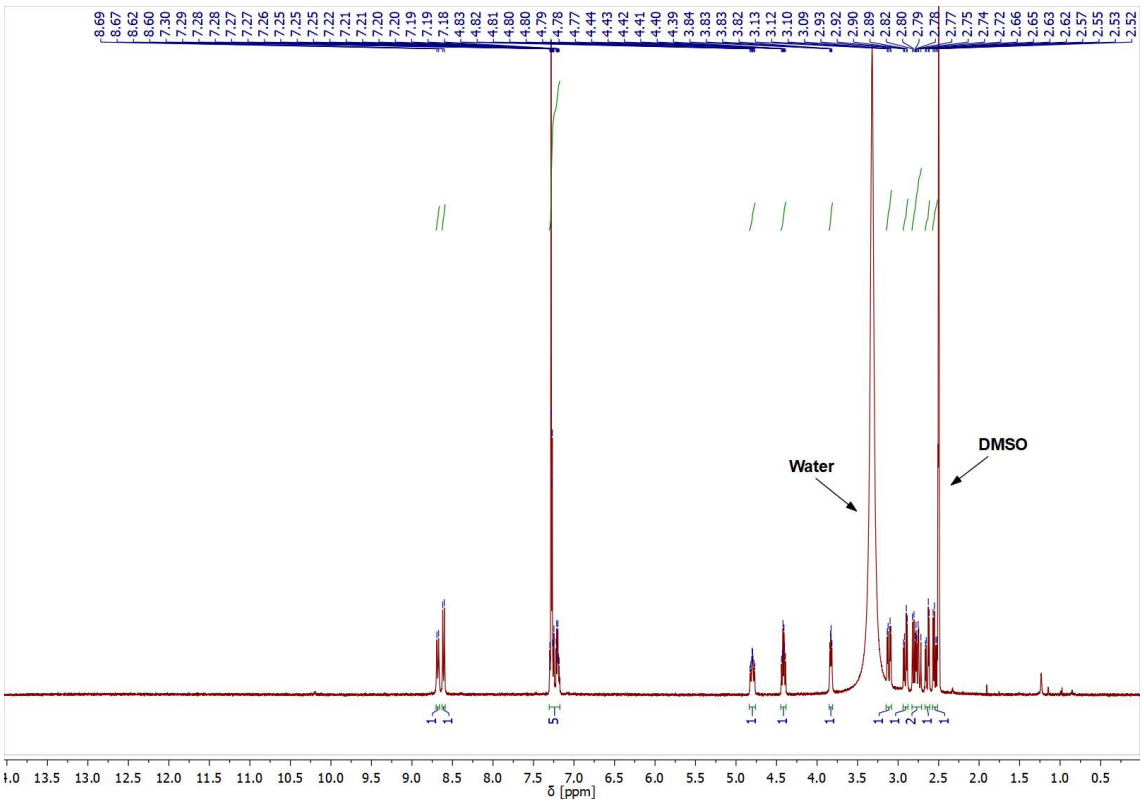

Figure 65: [1]H-NMR (400 MHz, DMSO-d_6) of D-Cys-L-Phe-L-Cys tripeptide. Protons were assigned with the aid of the H-H COSY (400 MHz) spectrum.

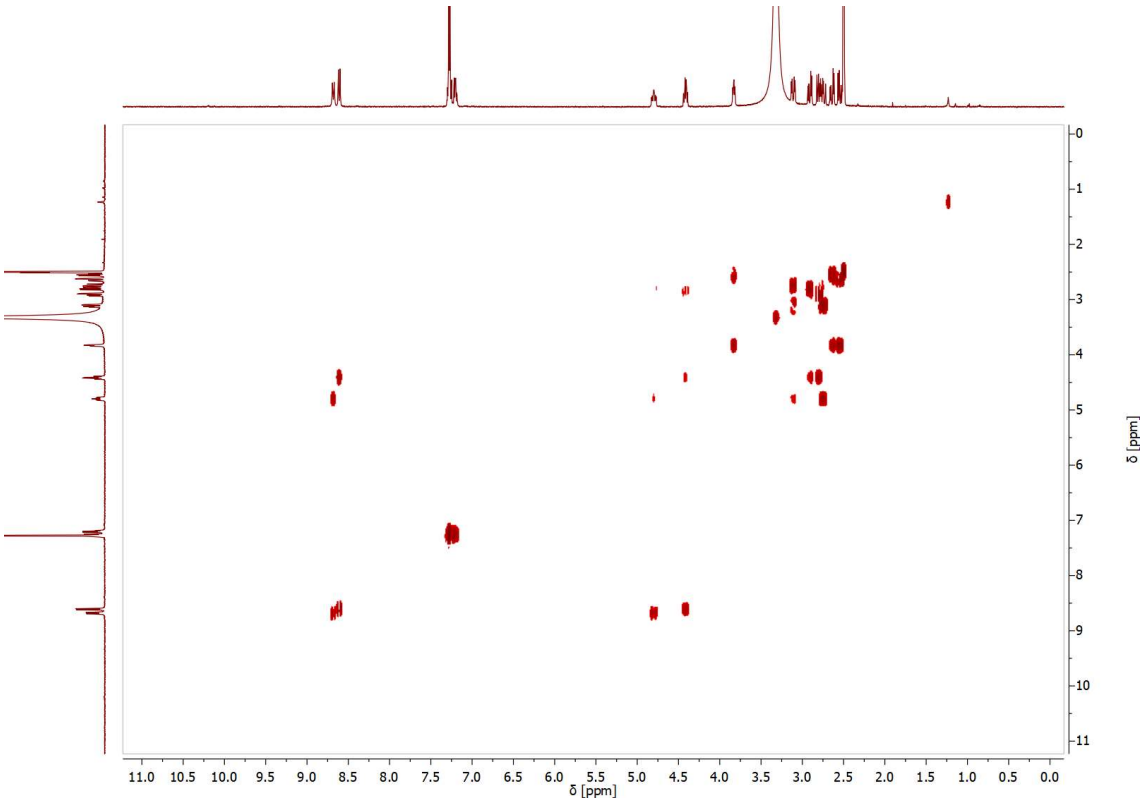

Figure 66: H-H COSY (400 MHz, DMSO-d_6) of D-Cys-L-Phe-L-Cys tripeptide.

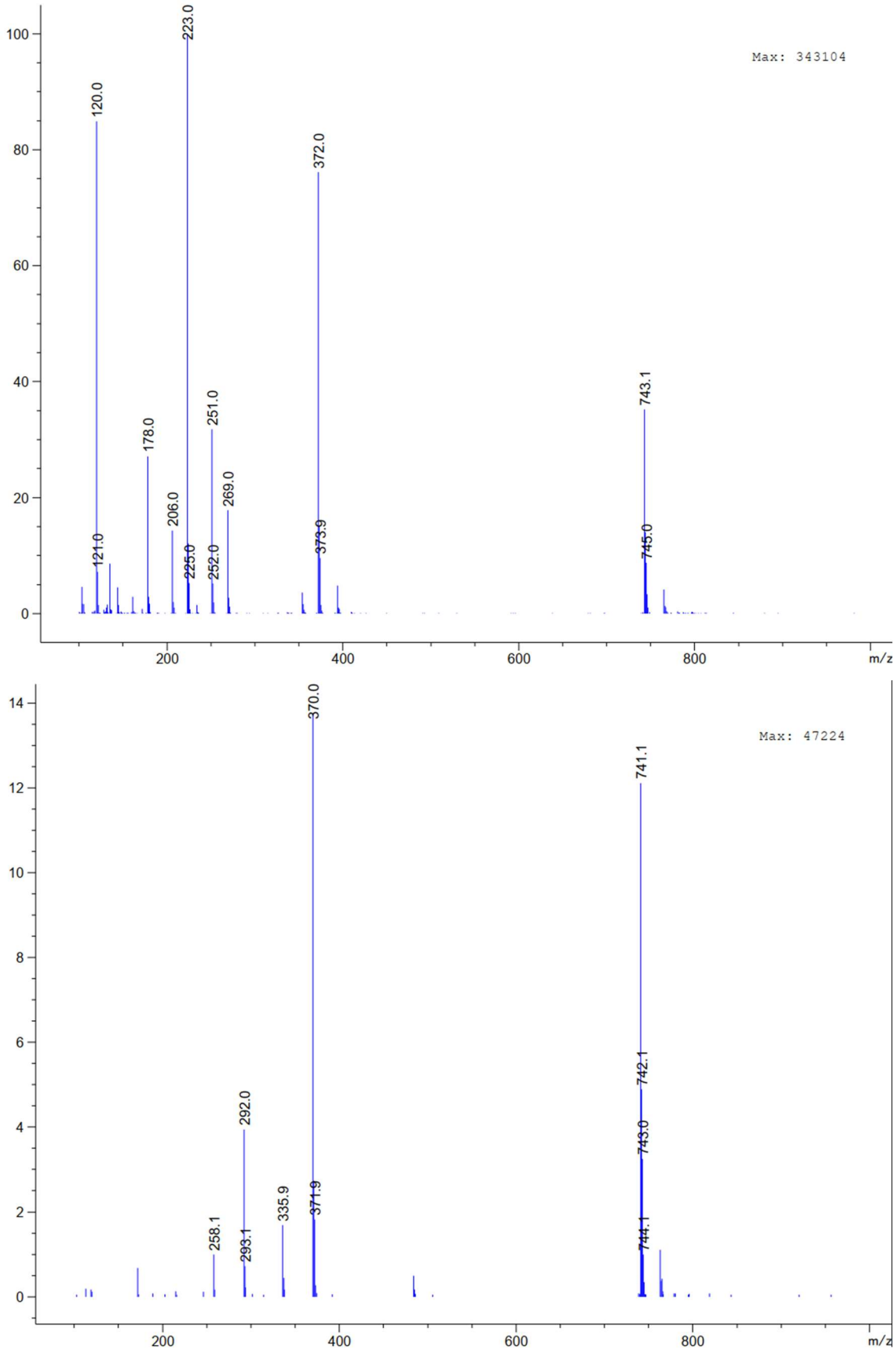

Figure 67: ESI-MS spectrum of of D-Cys-L-Phe-L-Cys in positive (top) and negative (bottom) mode.

A.2.3 - L-Cys-D-Phe-L-Cys

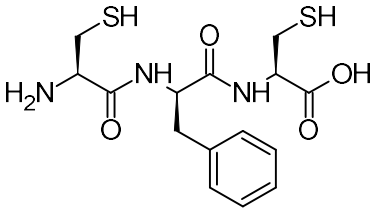

^{1}H-NMR (400 MHz, DMSO-*d*$_6$, TMS), δ (ppm): **8.76** (d, *J* = 8.8 Hz, 1, NH Phe), **8.69** (d, *J* = 8.0 Hz, 1, NH Cys C), **7.31-7.17** (m, 5, Ar), **4.85** (ddd, *J* = 4.8 Hz, *J* = 8.8 Hz, *J* = 10.4 Hz, 1, CH_α Phe), **4.43** (ddd, *J* = 4.8 Hz, *J* = 7.2 Hz, *J* = 8.0 Hz, 1, CH_α Cys C), **3.86** (dd, *J* = 4.0 Hz, *J* = 6.4 Hz, 1, CH_α Cys N), **3.09** (dd, *J* = 4.8 Hz, *J* = 14.0 Hz, 1, CH_β Phe), **2.83** (dd, *J* = 4.8 Hz, *J* = 13.6 Hz, 1, CH_β Cys C), **2.77** (dd, *J* = 10.8 Hz, *J* = 14.0 Hz, 1, CH_β Phe), **2.74** (dd, *J* = 7.2 Hz, *J* = 13.6 Hz, 1, CH_β Cys C), **2.66** (dd, *J* = 4.0 Hz, *J* = 14.4 Hz, 1, CH_β Cys N), **2.57** (dd, *J* = 6.4 Hz, *J* = 14.4 Hz, 1, CH_β Cys N)

MS (ESI): calculated mass **371.10,** observed mass m/z $[M+H]^+$ 371.9, m/z $[2M+H]^+$ 743.0, m/z $[M-H]^-$ 370.0, m/z $[2M-H]^-$ 741.1.

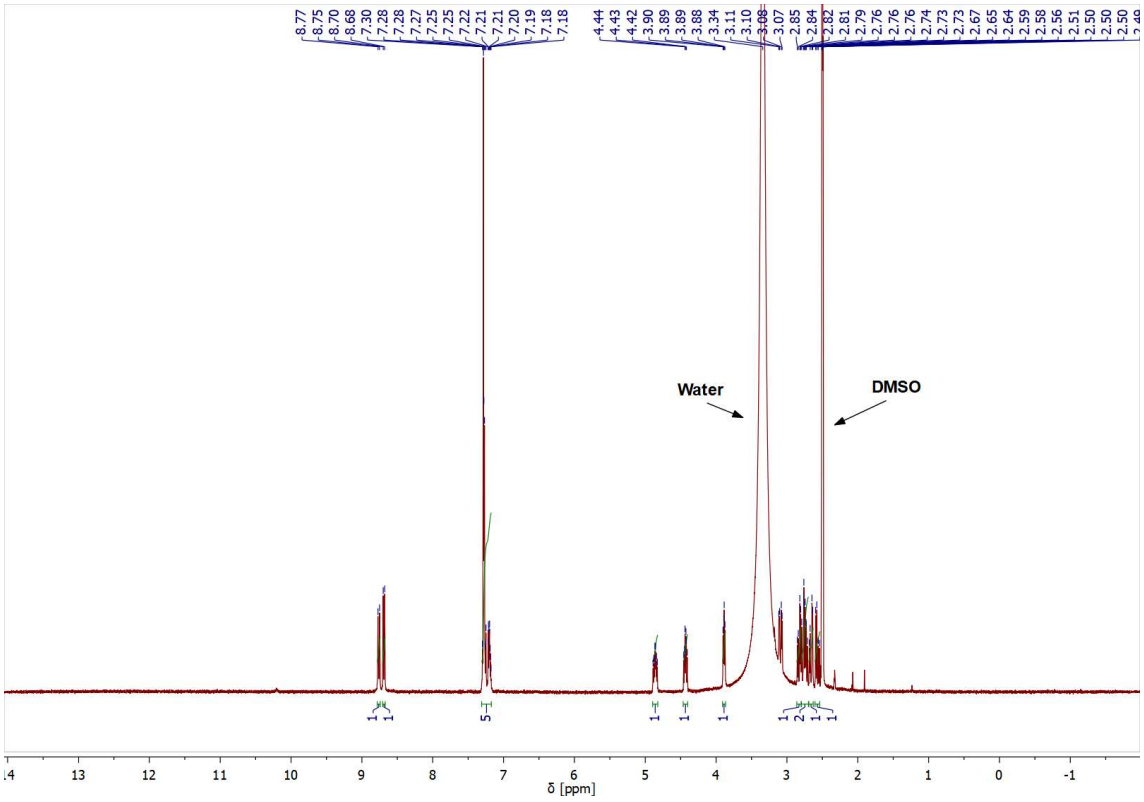

Figure 68: ^{1}H-NMR (400 MHz, DMSO-*d*$_6$) of L-Cys-D-Phe-L-Cys tripeptide. Protons were assigned with the aid of the H-H COSY (400 MHz) spectrum.

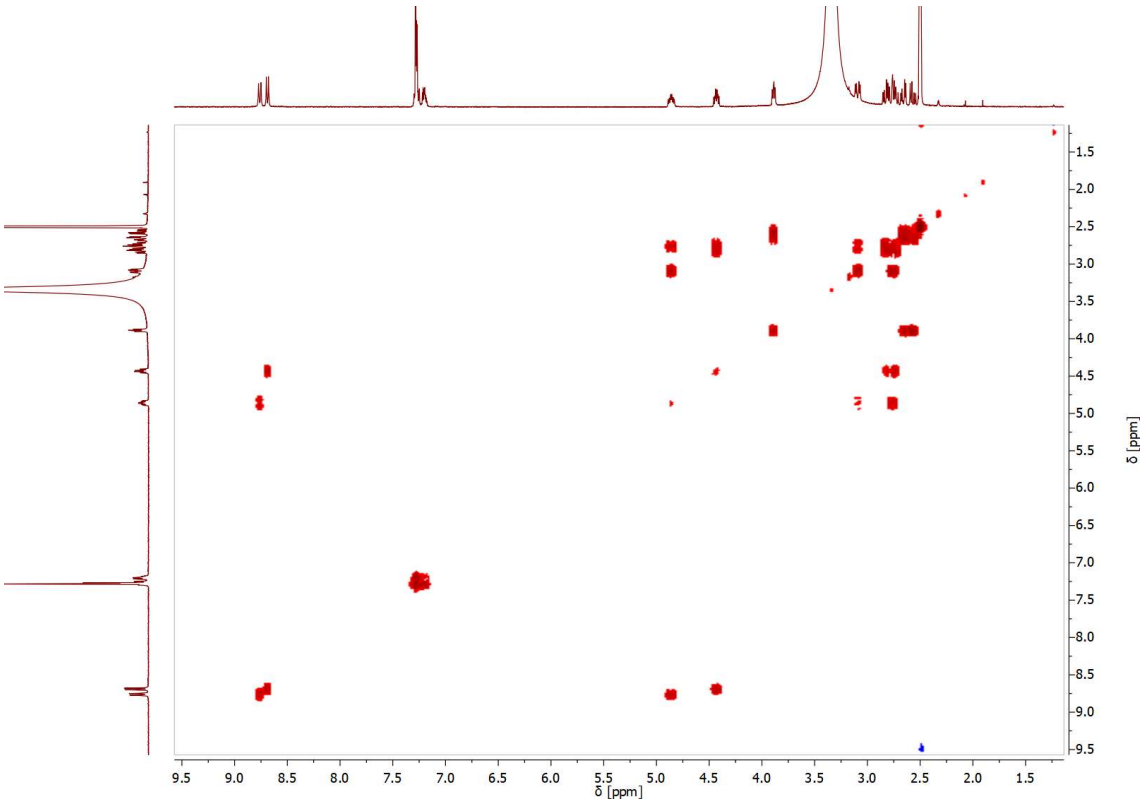

Figure 69: H-H COSY (400 MHz, DMSO-d_6) of L-Cys-D-Phe-L-Cys tripeptide.

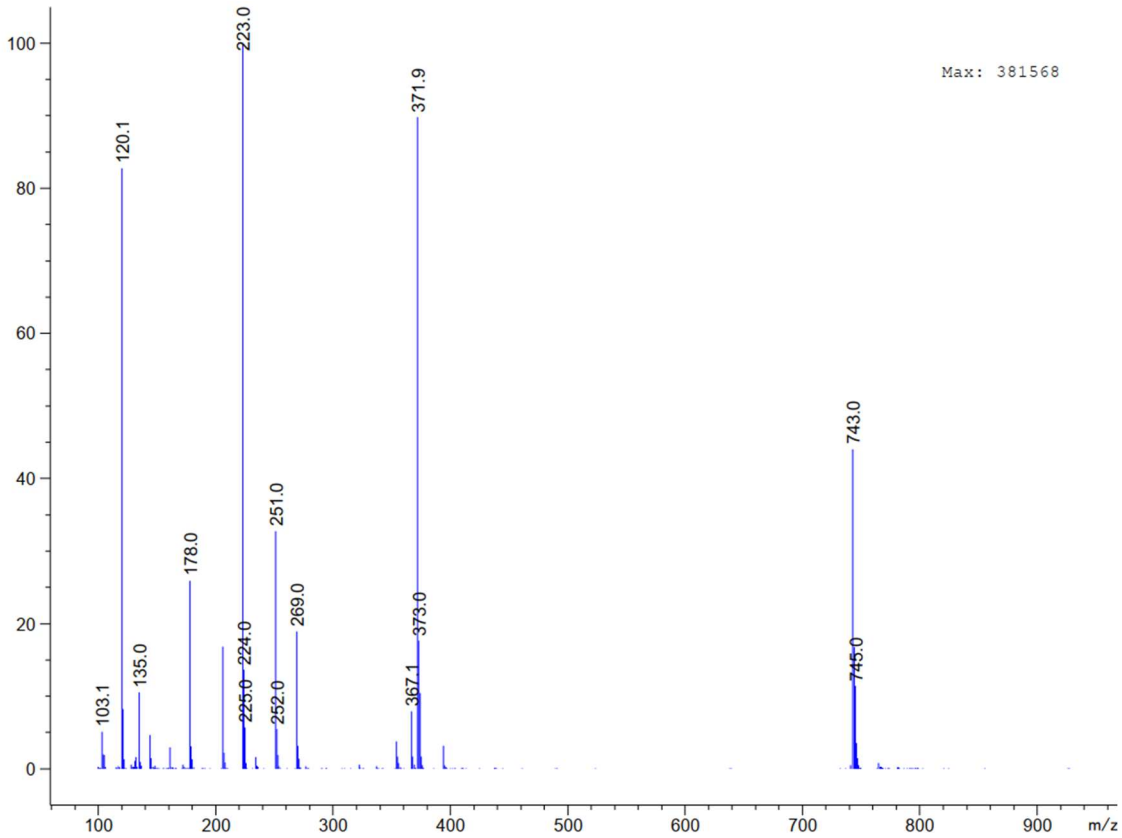

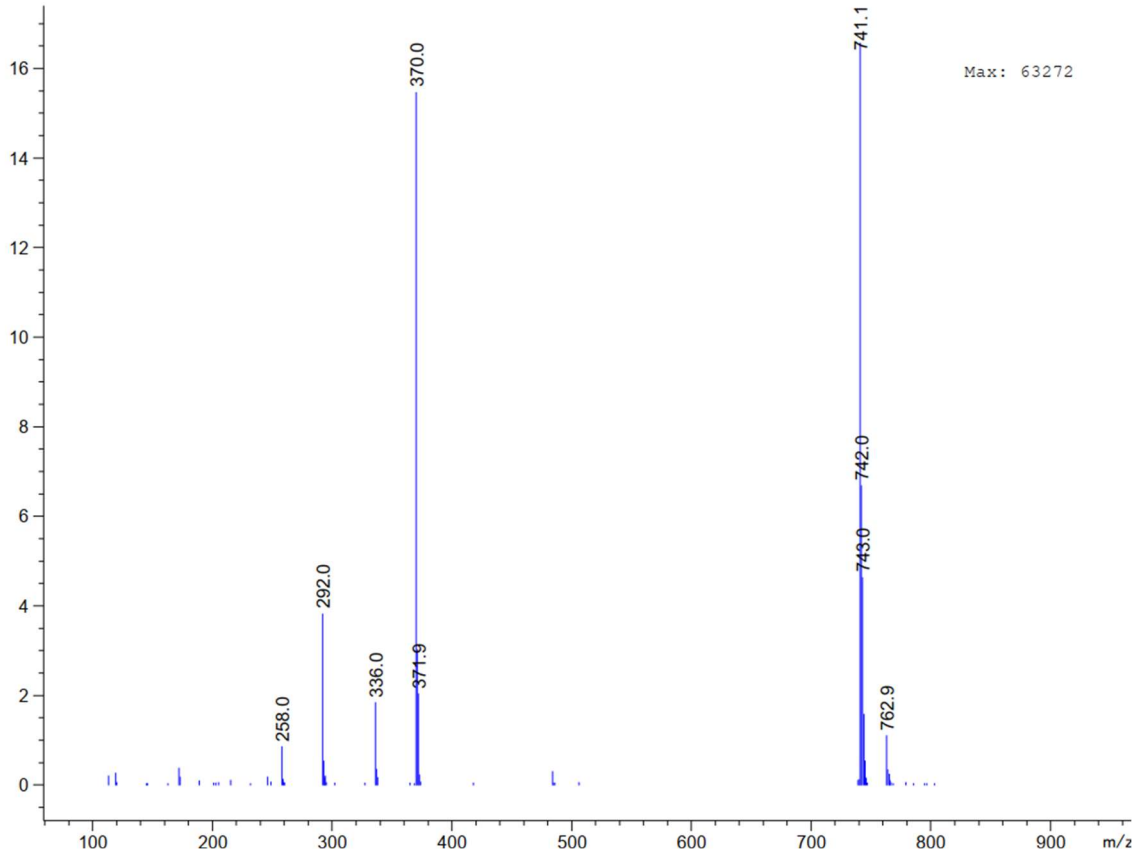

Figure 70: ESI-MS spectrum of L-Cys-D-Phe-L-Cys tripeptide in positive (top) and negative (bottom) mode.

A.2.4 – L-Cys-L-Phe-D-Cys

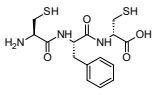

^{1}H-NMR (400 MHz, DMSO-*d*$_6$, TMS), δ (ppm): **13.00** (b, 1, COOH), **8.70** (d, *J* = 8.0 Hz, 1, NH Phe), **8.61** (d, *J* = 8.0 Hz, 1, NH Cys C), **8.15** (b, 3, NH_3^+), **7.33-7.18** (m, 5, Ar), **4.72** (ddd, *J* = 4.8 Hz, *J* = 9.2 Hz, *J* =8.0 Hz, 1, CH_α Phe), **4.41** (ddd, *J* = 4.4 Hz, *J* = 7.6 Hz, *J* = 8.0 Hz, 1, Cys C), **3.96** (dd, *J* = 6.0 Hz, *J* = 4.4 Hz, 1, CH_α Cys N), **3.07** (dd, *J* = 4.8 Hz, *J* = 14.0 Hz, 1, CH_β Phe), **3.02** (*J* = 6.0 Hz, *J* = 14.4 Hz, 1, CH_β Cys N), **2.88** (dd, *J* = 4.4 Hz, *J* = 14.0 Hz, 1, CH_β Cys N), **2.84** (dd, *J* = 9.2 Hz, *J* = 14.0 Hz, 1, CH_β Phe), **2.79** (ddd, *J* = 4.4 Hz, *J* = 8.4 Hz, *J* = 14.0 Hz, 1, CH_β Cys C), **2.71** (ddd, *J* = 7.6 Hz, *J* = 8.4 Hz, *J* = 14.0 Hz, 1, CH_β Cys C), **2.22** (t, *J* = 8.4 Hz, 1, SH Cys C)

MS (ESI): calculated mass **371.10,** observed mass m/z $[M+H]^+$ 372.0, m/z $[M-H]^-$ 370.0, m/z $[2M-H]^-$ 741.0.

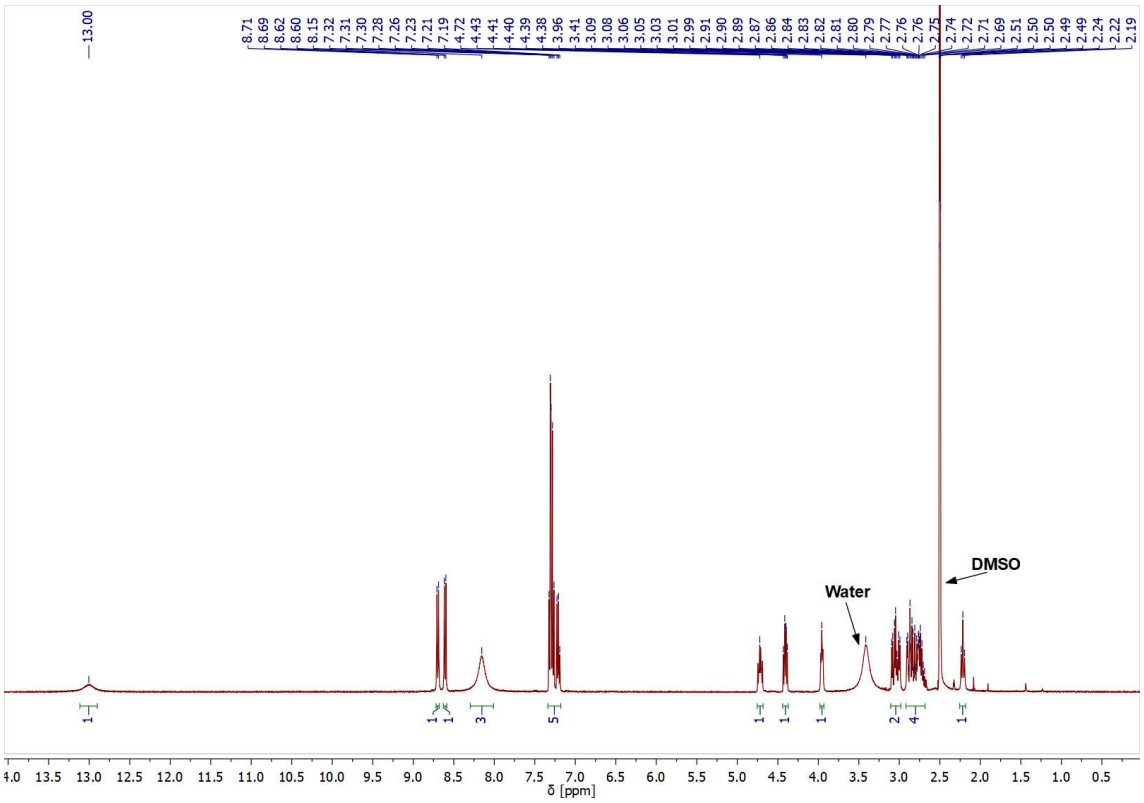

Figure 71: [1]H-NMR (400 MHz, DMSO-*d*$_6$) of L-Cys-L-Phe-D-Cys tripeptide. Protons were assigned with the aid of the H-H COSY (400 MHz) spectrum.

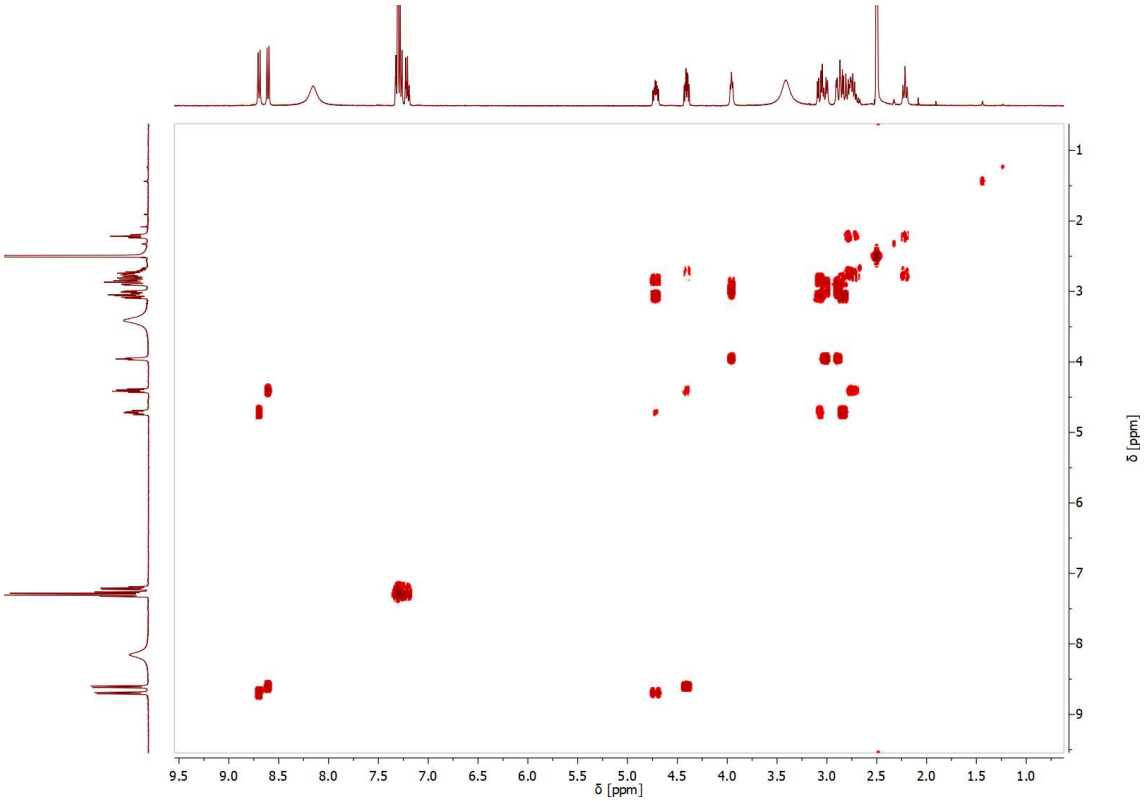

Figure 72: H-H COSY (400 MHz, DMSO-*d*$_6$) of L-Cys-L-Phe-D-Cys tripeptide.

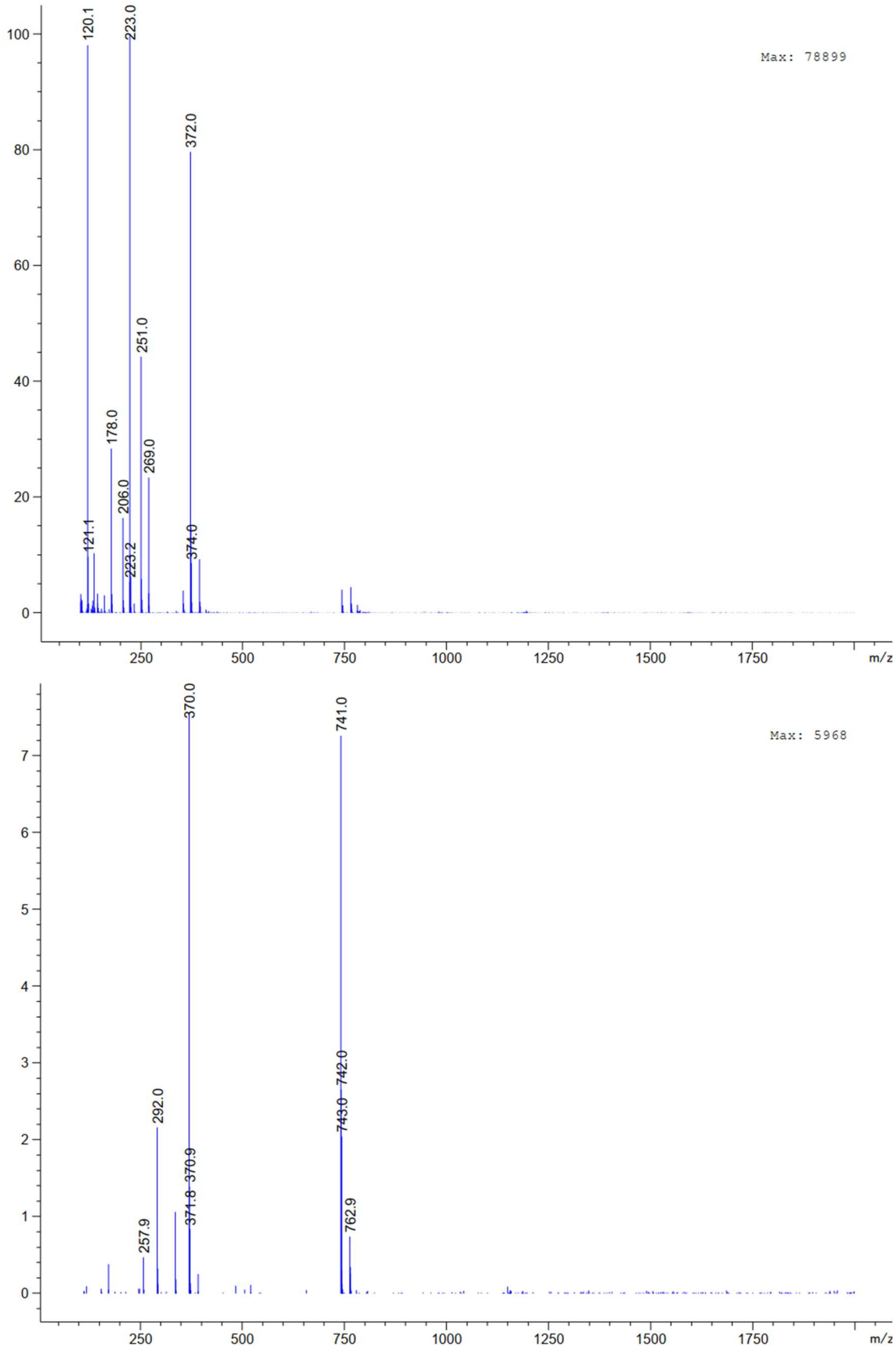

Figure 73: ESI-MS spectrum of L-Cys-L-Phe-D-Cys tripeptide in positive (top) and negative (bottom) mode.

A.3 – Tripeptide HPLC traces

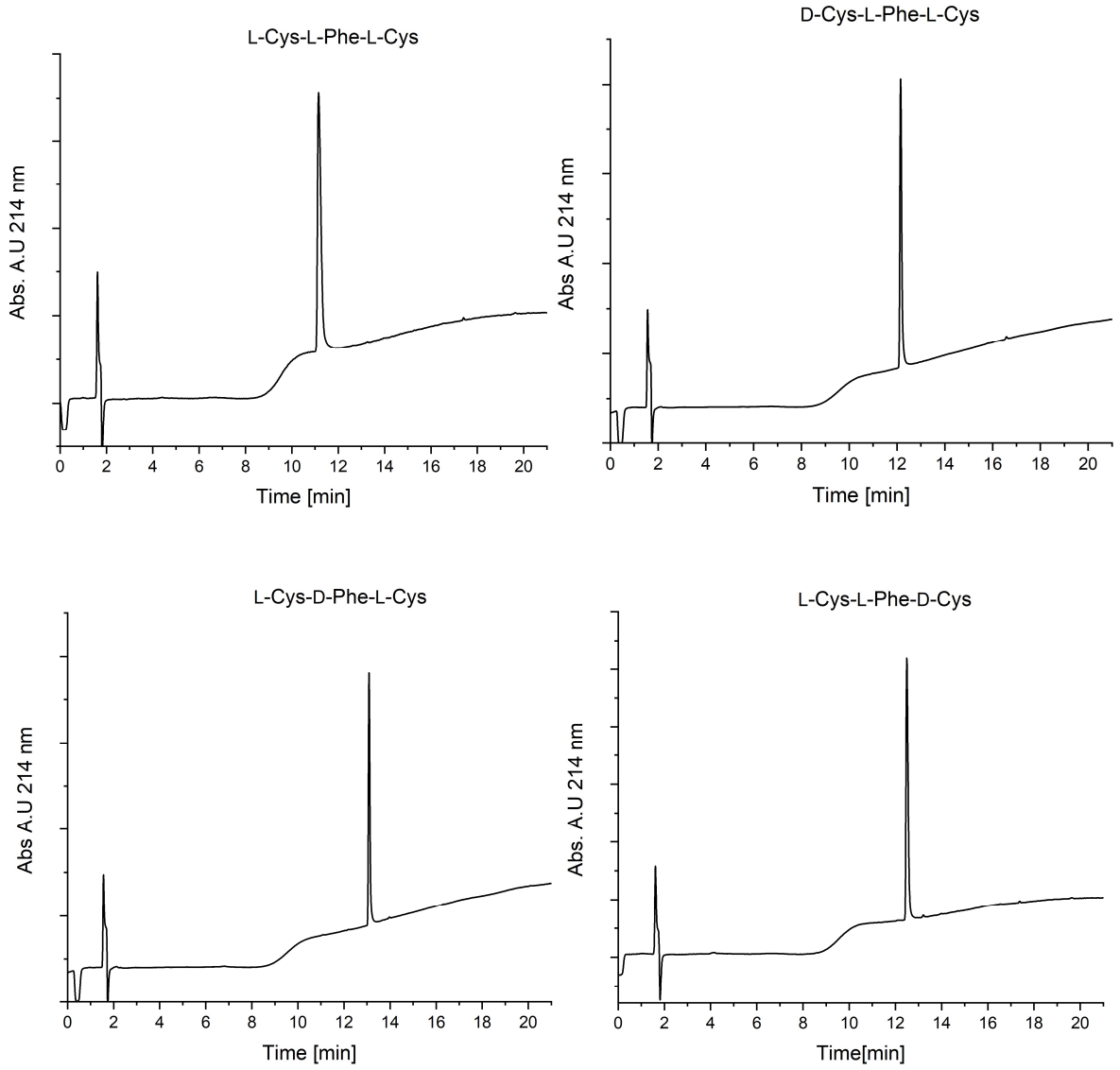

Peptide sequence	Retention time [min]
L-Cys-L-Phe-L-Cys	11.2
D-Cys-L-Phe-L-Cys	12.2
L-Cys-**D-Phe**-L-Cys	13.1
L-Cys-L-Phe-**D-Cys**	12.5

Figure 74: Analytical chromatograms for the four tripeptides (L-Cys-L-Phe-L-Cys, D-Cys-L-Phe-L-Cys, L-Cys-D-Phe-L-Cys, L-Cys-L-Phe-D-Cys). All the spectra were acquired according to **section 7.3.1**

A.4 – LCMS kinetic studies data

		m/z $[M+H]^+$			
	Monoisotopical mass	Z = 1	Z = 2	Z = 3	Z = 4
Monomer	371.10	372.10	/	/	/
Cyclic monomer	369.10	370.10	/	/	/
Linear dimer	740.18	741.18	371.09	/	/
Cyclic Dimer	738.16	739.16	370.08	/	/
Cyclic Trimer	1107.25	1108.25	554.63	370.08	/
Cyclic Tetramer	1476.33	1477.33	739.17	493.11	370.08
Cyclic Pentamer	1845.41	1846.41	923.71	616.14	462.35
Cyclic Hexamer	2214.49	2215.49	1108.25	739.16	554.62

Table 3: Calculated monoisotopical mass for all the studied compounds. $[M+H]^+$ ions are calculated with different values of z.

		m/z $[M-H]^-$			
	Monoisotopical mass	Z = 1	Z = 2	Z = 3	Z = 4
Monomer	371.10	370.10	/	/	/
Cyclic monomer	369.10	368.10	/	/	/
Linear dimer	740.18	739.18	369.09	/	/
Cyclic Dimer	738.16	737.16	368.08	/	/
Cyclic Trimer	1107.25	1106.25	552.63	368.08	/
Cyclic Tetramer	1476.33	1475.33	737.17	491.11	368.08
Cyclic Pentamer	1845.41	1844.41	921.71	614.14	460.35
Cyclic Hexamer	2214.49	2213.49	1106.25	737.16	552.62

Table 4: Calculated monoisotopical mass for all the studied compounds. $[M-H]^-$ ions are calculated with different values of z.

A.4.1 – L-Cys-L-Phe-L-Cys kinetic in H_2O

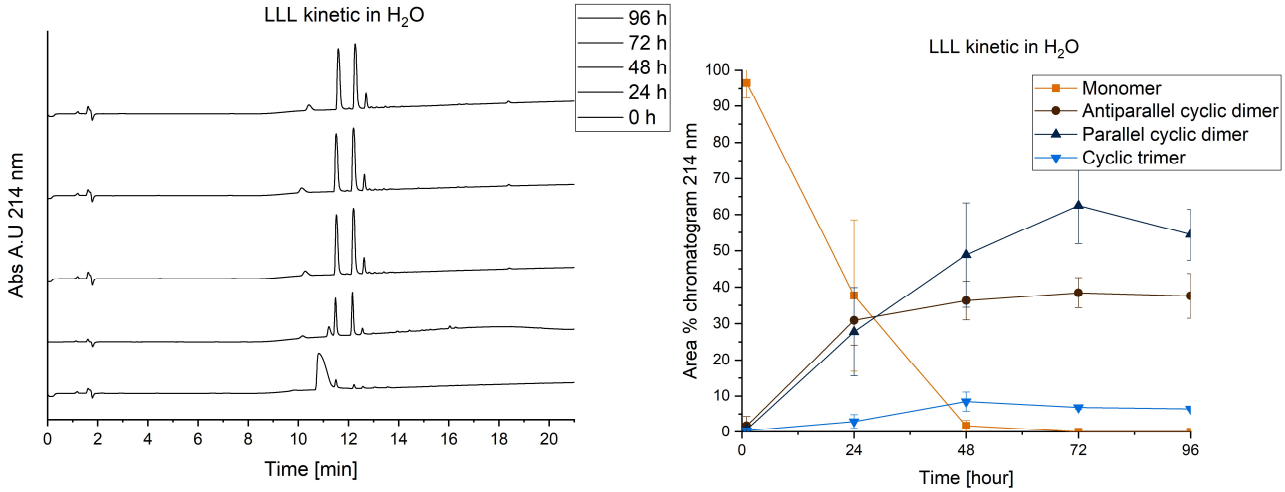

Figure 75: LCMS kinetic study of L-Cys-L-Phe-L-Cys tripeptide in alkaline water (BB 100 mM, pH 8.5) at 20 mM over 96 hours.

		Average chromatogram area %					m/z, z = 1,2	
Compound	**Rt**	**0 h**	**24 h**	**48 h**	**72 h**	**96 h**	**$[M+H]^+$**	**$[M-H]^-$**
Monomer	11.2	96.5	37.7	1.7	0.0	0.0	372.0	369.9
A. Cyclic dimer	11.5	1.7	30.9	36.3	38.5	37.6	739.0	736.8
P. Cyclic dimer	12.2	0.7	27.8	48.9	62.5	54.4	739.0	736.8
Cyclic trimer	12.6	0.4	2.9	8.4	6.8	6.4	1109.9/554.6	1105.8/553.6

		SD chromatogram area %					m/z, z = 1,2	
Compound	**Rt**	**0 h**	**24 h**	**48 h**	**72 h**	**96 h**	**$[M+H]^+$**	**$[M-H]^-$**
Monomer	11.2	4.3	20.8	1.5	0.0	0.0	372.0	369.9
A. Cyclic dimer	11.5	2.6	6.8	5.3	4.1	6.1	739.0	736.8
P. Cyclic dimer	12.2	0.9	12.2	14.4	10.5	7.0	739.0	736.8
Cyclic trimer	12.6	0.5	1.9	2.7	0.5	0.3	1109.9/554.6	1105.8/553.6

Table 5: Compounds identified by LCMS analysis. Average chromatogram area and standard deviation are calculated from triplicates of the kinetic study from **Figure 75**.

A.4.2 – D-Cys-L-Phe-L-Cys kinetic in H_2O

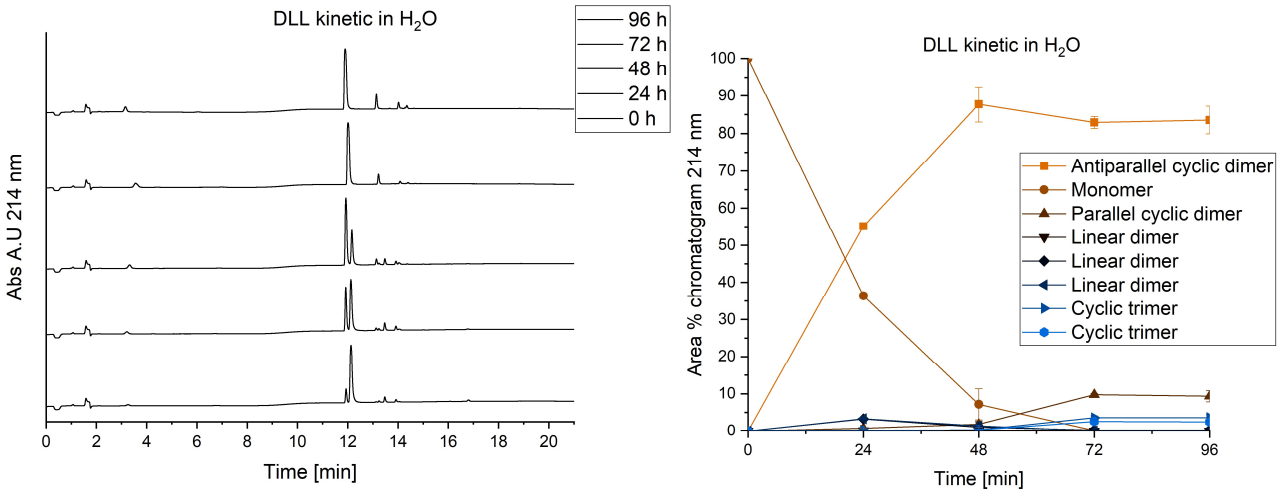

Figure 76: LCMS kinetic study of D-Cys-L-Phe-L-Cys tripeptide in alkaline water (BB 100 mM, pH 8.5) at 20 mM over 96 hours.

		Average chromatogram area %					m/z, z = 1,2	
Compound	**Rt**	**0 h**	**24 h**	**48 h**	**72 h**	**96 h**	**$[M+H]^+$**	**$[M-H]^-$**
A. Cyclic dimer	12.0	0.0	55.1	87.7	82.9	83.6	739.0	736.8
Monomer	12.2	100.0	36.4	7.2	0.1	0.1	372.0	369.9
P. Cyclic dimer	13.2	0.0	0.7	1.8	9.7	9.4	739.0	736.8
Linear dimer	13.2	0.0	0.1	0.0	0.0	0.0	741.2	739.4
Linear dimer	13.5	0.0	3.2	1.0	0.0	0.0	741.2	739.4
Linear dimer	13.9	0.0	3.3	1.4	0.0	0.0	741.2	739.4
Cyclic trimer	14.0	0.0	0.2	0.3	3.6	3.6	1109.9/554.6	1105.8/553.6
Cyclic trimer	14.3	0.0	0.0	0.3	2.6	2.5	1109.9/554.6	1105.8/553.6

		SD chromatogram area %					m/z, z = 1,2	
Compound	**Rt**	**0 h**	**24 h**	**48 h**	**72 h**	**96 h**	**$[M+H]^+$**	**$[M-H]^-$**
A. Cyclic dimer	12.0	0.0	0.5	4.7	1.6	3.6	739.0	736.8
Monomer	12.2	0.0	0.7	4.2	0.0	0.0	372.0	369.9
P. Cyclic dimer	13.2	0.0	0.2	0.9	0.3	1.5	739.0	736.8
Linear dimer	13.2	0.0	0.1	0.0	0.0	0.0	741.2	739.4
Linear dimer	13.5	0.0	0.4	0.3	0.0	0.0	741.2	739.4
Linear dimer	13.9	0.0	0.3	1.1	0.0	0.0	741.2	739.4
Cyclic trimer	14.0	0.0	0.2	0.2	0.5	0.9	1109.9/554.6	1105.8/553.6
Cyclic trimer	14.3	0.0	0.0	0.1	0.4	0.7	1109.9/554.6	1105.8/553.6

Table 6: Compounds identified by LCMS analysis. Average chromatogram area and standard deviation are calculated from triplicates of the kinetic study from **Figure 76**

A.4.3 – L-Cys-D-Phe-L-Cys kinetic in H_2O

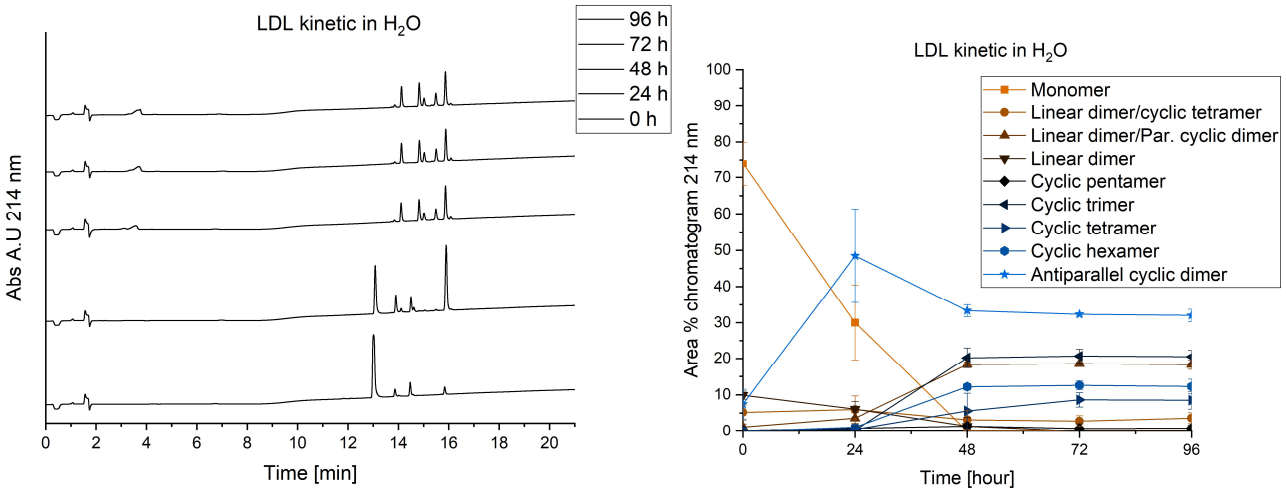

Figure 77: LCMS kinetic study of L-Cys-D-Phe-L-Cys tripeptide in alkaline water (BB 100 mM, pH 8.5) at 20 mM over 96 hours.

		Average chromatogram area %					m/z, z = 1,2,3	
Compound	**Rt**	**0 h**	**24 h**	**48 h**	**72 h**	**96 h**	**$[M+H]^+$**	**$[M-H]^-$**
Monomer	13.1	73.9	30.0	0.0	0.0	0.0	372.0	370.0
Linear dimer	13.9*	5.2	5.9	3.1	0.0	0.0	741.0	738.9
Cyclic tetramer	13.9*	0.0	0.0	3.1	2.8	3.6	739.2	1475.6/737.0
Linear dimer	14.1*	1.1	3.6	0.0	0.0	0.0	741.0	738.9
P. Cyclic dimer	14.1*	0.0	0.0	18.3	18.5	18.3	739.0	737.0
Linear dimer	14.5	9.9	6.1	1.4	0.0	0.0	741.0	738.9
Cyclic pentamer	14.6	0.2	0.8	1.4	0.7	0.8	924.0/616.2	922.6
A. Cyclic trimer	14.8	0.0	0.3	20.2	20.7	20.5	1109.9/554.6	1105.8/553.6
Cyclic tetramer	15.1	0.0	0.5	5.6	8.6	8.5	1476.8/739.2/493.0	1474.4/737.0
Cyclic hexamer	15.5	0.0	1.1	12.2	12.6	12.3	1109.8/739.2	1106.0/738.0
A. Cyclic dimer	15.9	7.4	48.5	33.4	32.3	32.0	739.0	737.0
Cyclic trimer	16.1	0.0	0.0	2.3	1.7	1.4	1109.9/554.6	1105.8/553.6

	SD chromatogram area %						m/z, z = 1,2,3	
Compound	**Rt**	**0 h**	**24 h**	**48 h**	**72 h**	**96 h**	**$[M+H]^+$**	**$[M-H]^-$**
Monomer	13.1	6.0	10.4	0.0	0.0	0.0	372.0	370.0
Linear dimer	13.9*	2.1	3.8	0.0	0.0	0.0	741.0	738.9
Cyclic tetramer	13.9*	0.0	0.0	2.6	1.5	1.5	739.2	1475.6/737.0
Linear dimer	14.1*	0.9	1.5	0.0	0.0	0.0	741.0	738.9
P. Cyclic dimer	14.1*	0.0	0.0	0.8	0.4	1.3	739.0	737.0
Linear dimer	14.5	1.1	2.1	2.4	0.0	0.0	741.0	738.9

Cyclic pentamer	14.6	0.3	0.7	2.4	1.3	0.8	924.0/616.2	922.6
Cyclic trimer	14.8	0.0	0.4	2.7	1.9	1.8	1109.9/554.6	1105.8/553.6
Cyclic tetramer	15.1	0.0	0.5	4.9	2.0	2.4	1476.8/739.2/493.0	1474.4/737.0
Cyclic hexamer	15.5	0.0	0.6	0.9	1.2	2.0	1109.8/739.2	1106.0/738.0
A. Cyclic dimer	15.9	4.1	12.8	1.7	0.5	1.7	739.0	737.0
Cyclic trimer	16.1	0.0	0.1	0.4	0.7	0.6	1109.9/554.6	1105.8/553.6

Table 7: Compounds identified by LCMS analysis. Average chromatogram area and standard deviation are calculated from triplicates of the kinetic study from **Figure 77**. *Overlapped peaks.

A.4.4 – L-Cys-L-Phe-D-Cys kinetic in H_2O

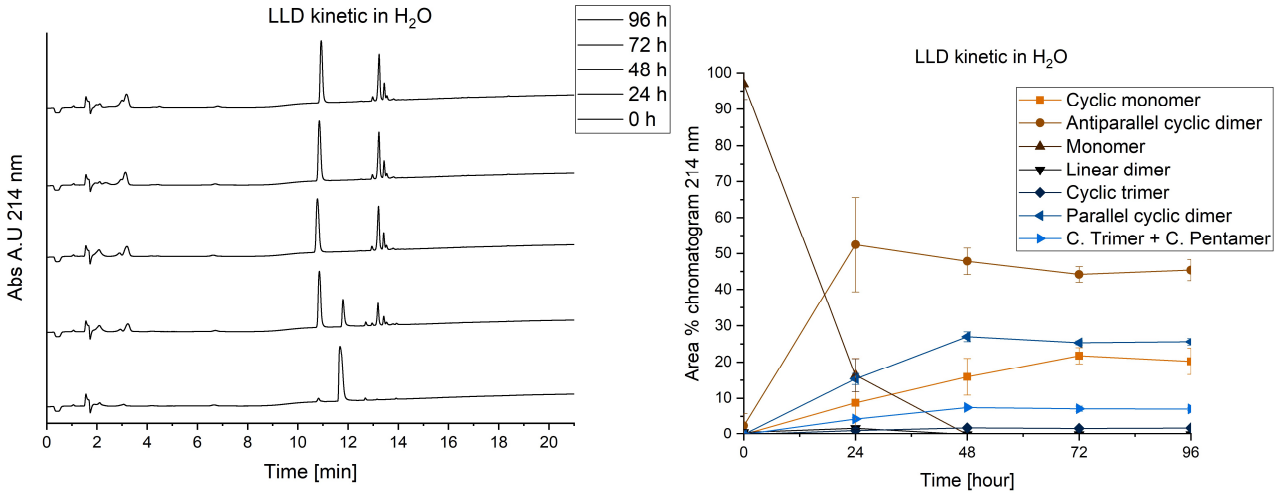

Figure 78: LCMS kinetic study of L-Cys-L-Phe-D-Cys tripeptide in alkaline water (BB 100 mM, pH 8.5) at 20 mM over 96 hours.

		Average chromatogram area %					m/z, z = 1,2,3	
Compound	**Rt**	**0 h**	**24 h**	**48 h**	**72 h**	**96 h**	**$[M+H]^+$**	**$[M-H]^-$**
Cyclic monomer	3.2	0.0	8.7	15.9	21.7	20.2	370.0	367.7
A. Cyclic dimer	10.9	2.4	52.4	47.8	44.2	45.4	739.0	737.0
Monomer	11.7	97.0	16.4	0.0	0.0	0.0	372.0	371.0
Linear dimer	12.7	0.6	1.7	0.0	0.0	0.0	741.0	739.0
Cyclic dimer	13.0	0.0	1.1	1.8	1.7	1.8	554.6	1105.8
P. Cyclic dimer	13.2	0.0	15.3	27.0	25.3	25.6	739.0	737.0
Cyclic trimer	13.4*	0.0	4.3	7.4	7.1	7.0	554.7/1109.2	1106.0
Cyclic pentamer	13.4*	0.0	4.3	7.4	7.1	7.0	923.2/615.8	921.6

	SD chromatogram area %						m/z, z = 1,2,3	
Compound	**Rt**	**0 h**	**24 h**	**48 h**	**72 h**	**96 h**	**$[M+H]^+$**	**$[M-H]^-$**
Cyclic monomer	3.2	0.0	12.3	5.1	2.2	3.6	370.0	367.7
A. Cyclic dimer	10.9	3.4	13.1	3.7	2.2	2.9	739.0	737.0
Monomer	11.7	4.3	4.6	0.0	0.0	0.0	372.0	371.0
Linear dimer	12.7	0.9	0.4	0.0	0.0	0.0	741.0	739.0
Cyclic dimer	13.0	0.0	0.1	0.2	0.1	0.1	554.6	1105.8
P. Cyclic dimer	13.2	0.0	1.5	1.3	0.5	0.9	739.0	737.0
Cyclic trimer	13.4*	0.0	0.3	0.2	0.7	0.5	554.7/1109.2	1106.0
Cyclic pentamer	13.4*	0.0	0.3	0.2	0.7	0.5	923.2/615.8	921.6

Table 8: Compounds identified by LCMS analysis. Average chromatogram area and standard deviation are calculated from triplicates of the kinetic study from **Figure 78**. *Overlapped peaks.

A.5 – Cyclic peptides HPLC traces

A.5.1 – LLL dynamic library

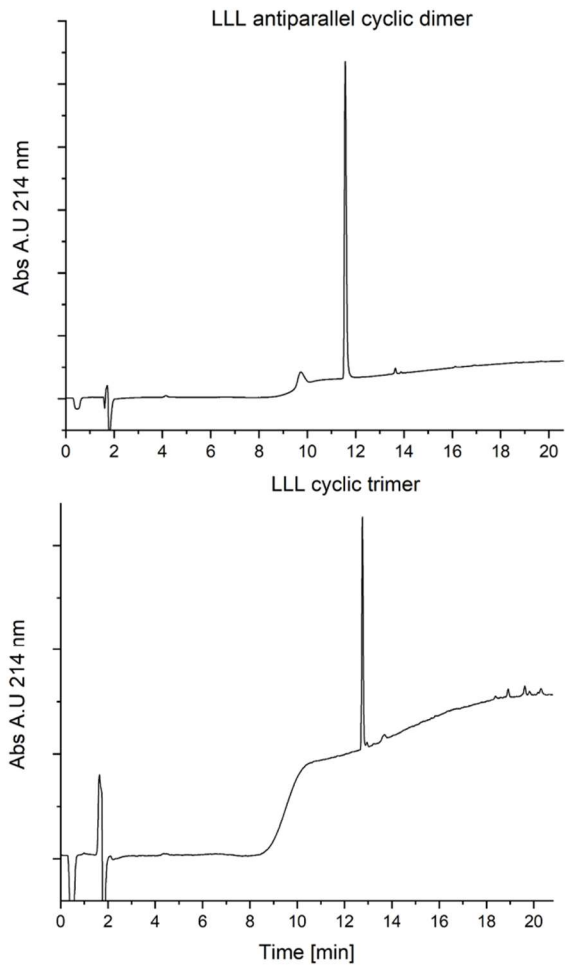

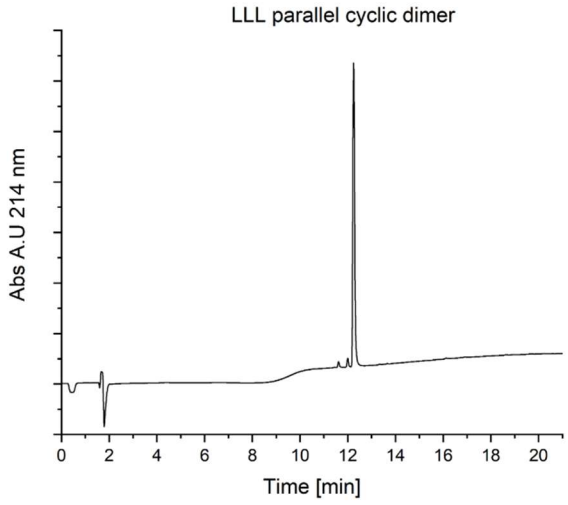

Compound	Rt [min]	$[M+H]^+$	$[M-H]^-$
A. Cyclic dimer	11.6	739.0	736.8
P. Cyclic dimer	12.2	739.0	736.8
Cyclic Trimer	12.7	1109.9/554.6	1105.8/553.6

Figure 79: Analytical chromatograms of the purified compounds from the large-scale LLL dynamic library. The retention time and the ESI-MS analysis confirmed the identity of the products.

A.5.2 – DLL dynamic library

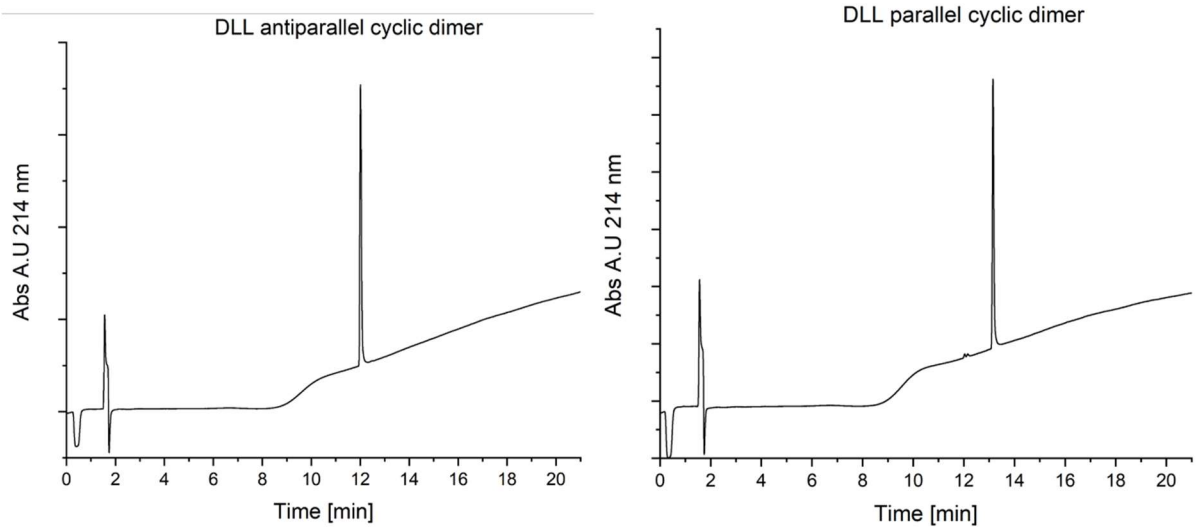

Compound	Rt [min]	$[M+H]^+$	$[M-H]^-$
A. Cyclic dimer	12.0	739.0	736.8
P. Cyclic dimer	13.2	739.0	736.8

Figure 80: Analytical chromatograms of the purified compounds from the large-scale DLL dynamic library. The retention time and the ESI-MS analysis confirmed the identity of the products.

A.5.3 – LDL dynamic library

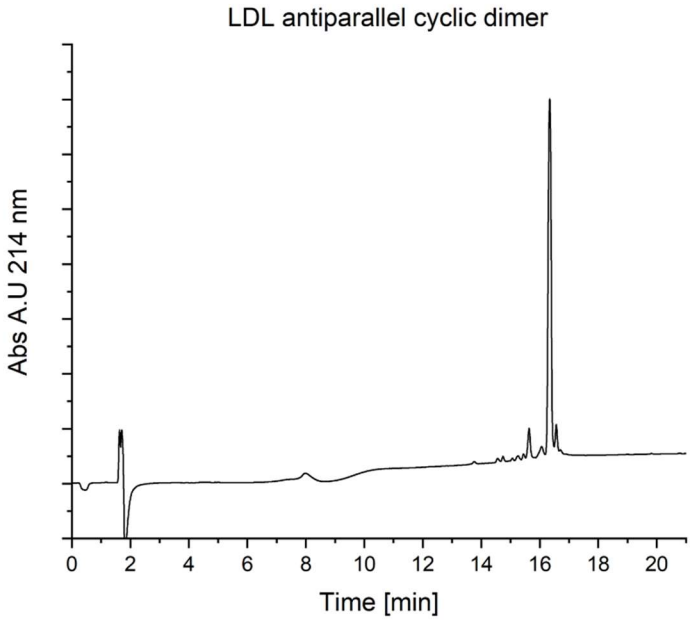

Compound	Rt [min]	$[M+H]^+$	$[M-H]^-$
A. Cyclic dimer	16.3	739.0	736.8

Figure 81: Analytical chromatograms of the purified compounds from the large-scale LDL dynamic library. The retention time and the ESI-MS analysis confirmed the identity of the products.

A.5.4 – LLD dynamic library

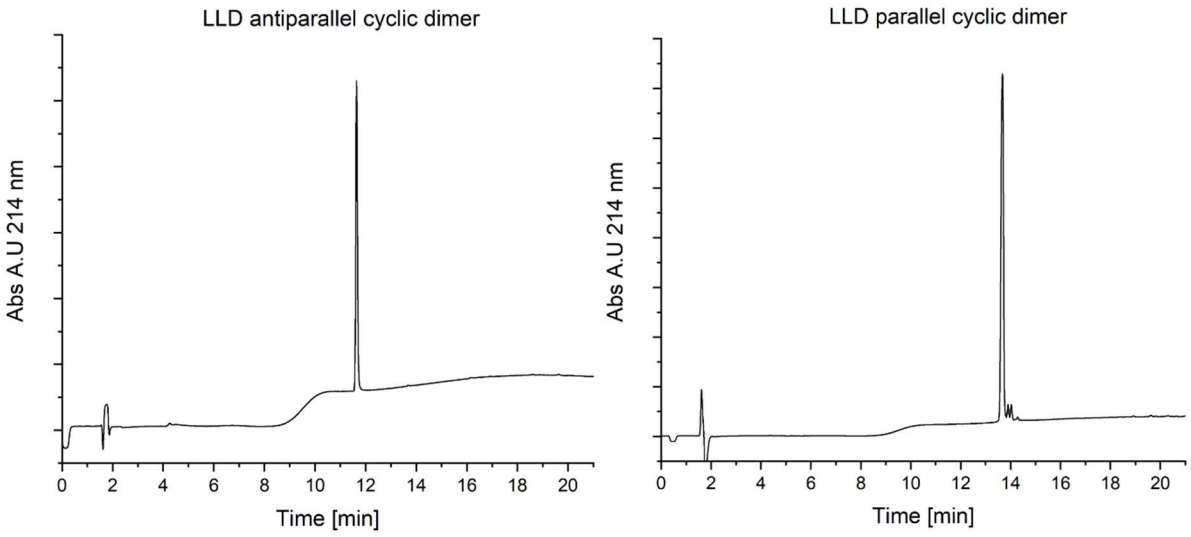

Compound	Rt [min]	$[M+H]^+$	$[M-H]^-$
A. Cyclic dimer	11.6	739.0	736.8
P. Cyclic dimer	13.7	739.0	736.8

Figure 82: Analytical chromatograms of the purified compounds from the large-scale LLD dynamic library. The retention time and the ESI-MS analysis confirmed the identity of the products.

A.6 – Cyclic dimers NMR characterisation

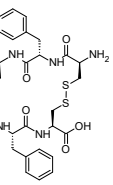

A.6.1 – LLL antiparallel cyclic dimer

^{1}H-NMR (400 MHz, D_2O, TMS), δ (ppm): **7.25-7.12** (m, 5, Ar), **4.65** (m, 1, CH_α Phe), **4.36** (m, 1, CH_α Cys C), **3.49** (m, 1, CH_α Cys N), **3.09** (m, CH_β Phe), **3.07** (m, 1, CH_β Cys C), **2.82** (m, 1, CH_β Phe), **2.76** (m, 1, CH_β Cys C), **2.67** (m, 2, CH_β Cys N)

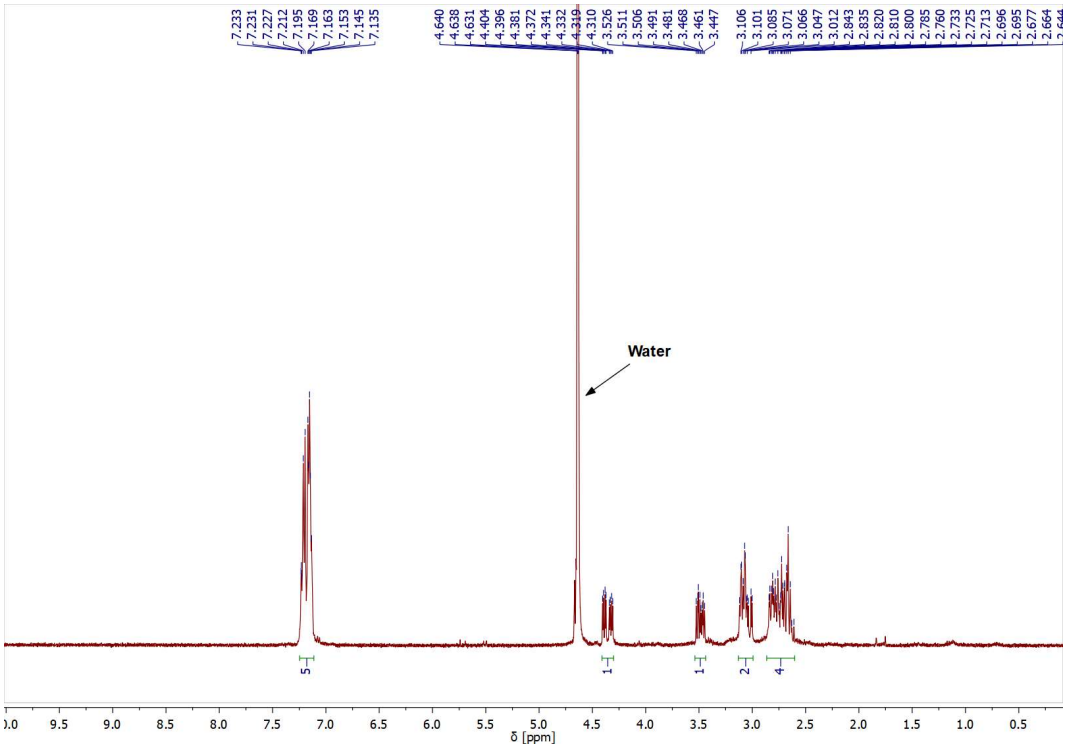

Figure 83: ^{1}H-NMR (400 MHz, D_2O) of LLL antiparallel cyclic dimer. The correct assignation of chemical shift has been done with the aid of the TOCSY and ROESY analysis.

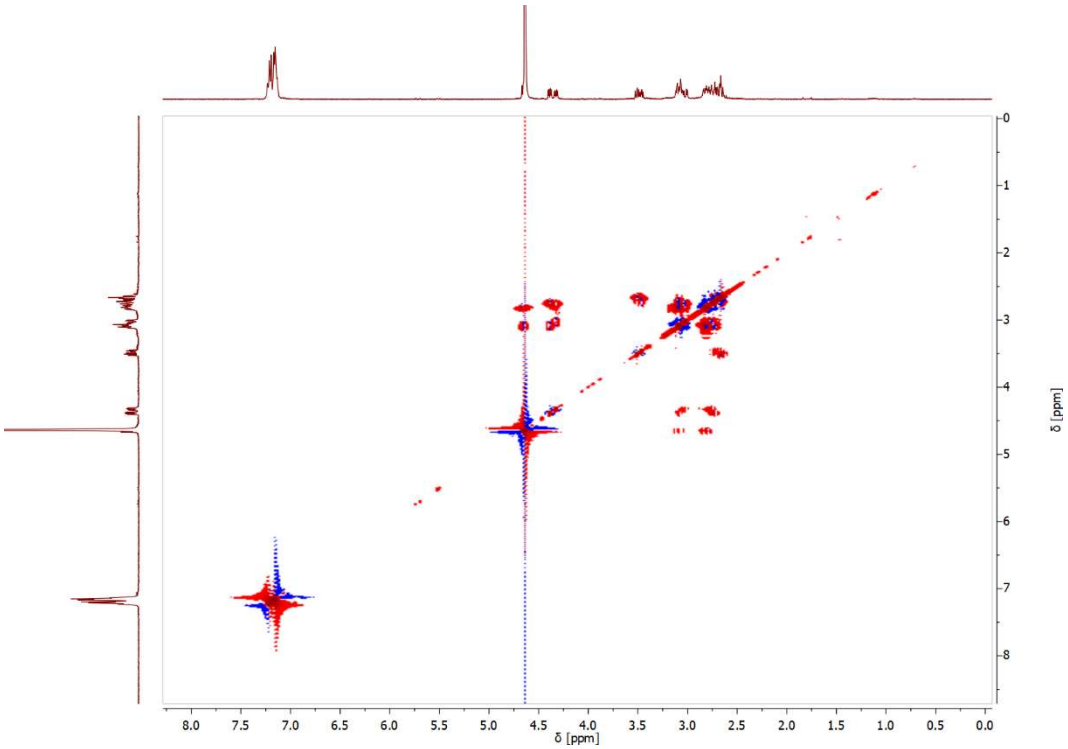

Figure 84: H-H TOCSY (400 MHz, D_2O) of LLL antiparallel cyclic dimer.

A.6.2 – LLL parallel cyclic dimer

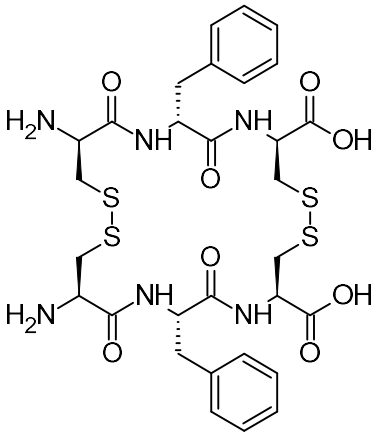

^{1}H-NMR (400 MHz, DMSO-*d*$_6$, TMS), δ (ppm): **9.65** (d, *J* = 10.0 Hz, 1, NH Phe), **7.88** (d, *J* = 6.4 Hz, 1, NH Cys C), **7.39** (m, J_o = 8.4 Hz, J_m = 1.2 Hz, 2, Ar), **7.24** (m, J_o = 7.6 Hz, J_m = 1.2 Hz, 2, Ar), **7.20** (m, J_o = 7.6 Hz, J_m = 1.2 Hz, 1, Ar), **4.38** (dd, *J* = 4.4 Hz, *J* = 10.4 Hz, 1, CH_α Phe), **4.05** (dd, *J* = 4.0 Hz, *J* = 6.4 Hz, 1, CH_α Cys C), **3.57** (dd, *J* = 4.0 Hz, *J* = 10.0 Hz, 1, CH_β Cys N), **3.38** (dd, *J* = 4.0 Hz, *J* = 13.0 Hz, 1, CH_α Cys N), **3.27** (dd, *J* = 6.4 Hz, *J* = 13.6 Hz, 1, CH_β Cys C), **3.19** (dd, *J* = 4.0 Hz, *J* = 14.0 Hz, 1, CH_β Cys C), **3.07** (dd, *J* = 10.4 Hz, *J* = 13.6 Hz, 1, CH_β Phe), **3.01** (dd, *J* = 4.4 Hz, *J* = 13.6 Hz, 1, CH_β Phe), **2.44** (dd, *J* = 10.4 Hz, *J* = 13.0 Hz, 1, CH_β Cys N)

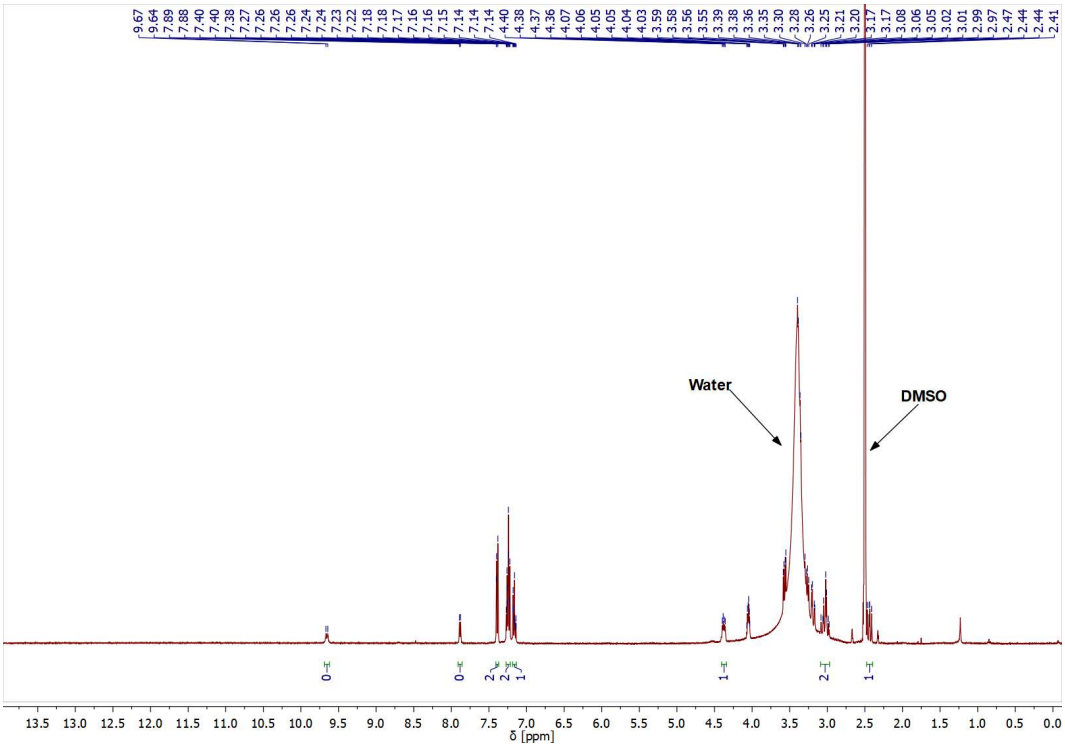

Figure 85: ^{1}H-NMR (400 MHz, DMSO-*d*$_6$) of LLL parallel cyclic dimer. The correct assignation of chemical shift has been done with the aid of the TOCSY and ROESY analysis. Water peak does not allow to integrate correctly most of the peaks relative to CH_α and CH_β it was possible to determine the coupling constants. Amide protons exchange with the solvent and their integrals are around 0.4.

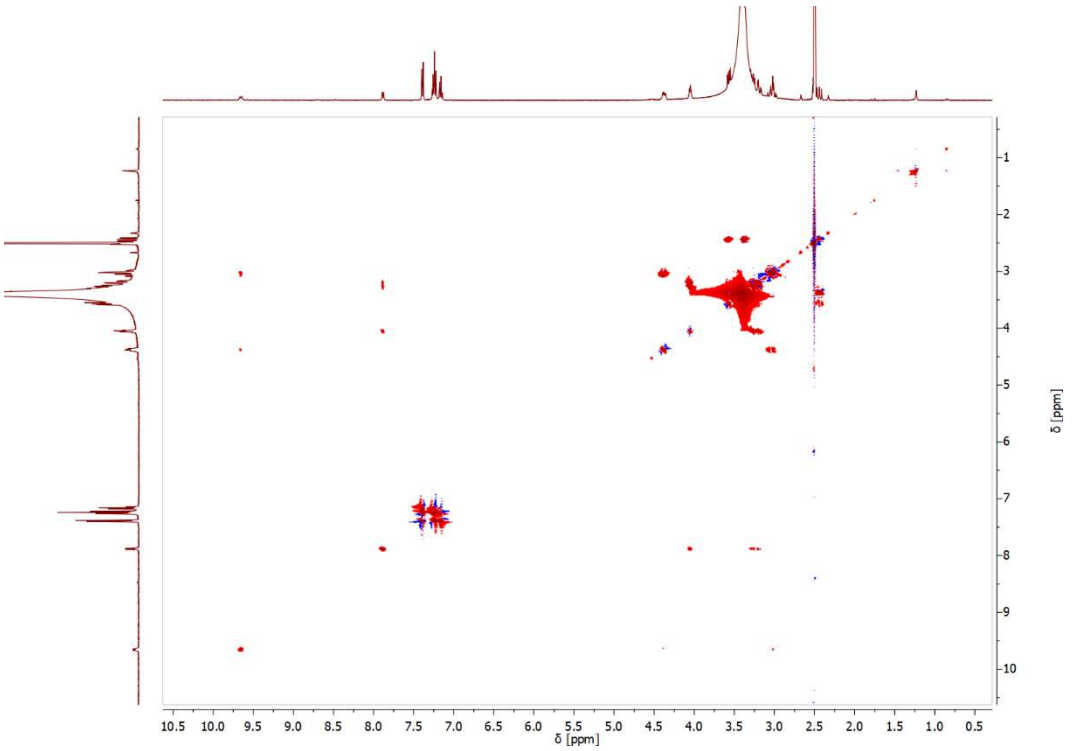

Figure 86: H-H TOCSY (400 MHz, DMSO-*d*$_6$) of LLL parallel cyclic dimer.

A.6.3 – DLL antiparallel cyclic dimer

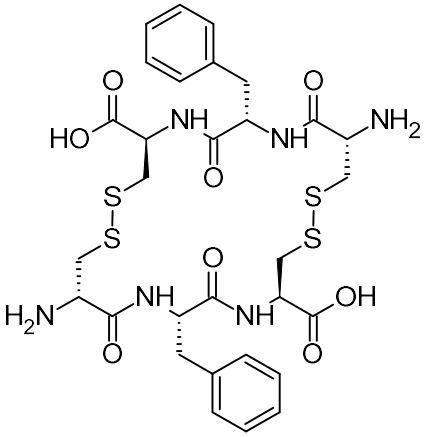

^{1}H-NMR (400 MHz, DMSO-*d*$_6$, TMS), δ (ppm): **9.35** (d, *J* = 9.2 Hz, 1, NH Cys C), **9.09** (d, *J* = 9.6 Hz, 1, NH Phe), **7.28-7.15** (m, 5, Ar), **5.11** (ddd, *J* = 4.4 Hz, *J* = 9.2 Hz, *J* = 9.2 Hz, 1, CH$_\alpha$ Phe), **4.78** (ddd, *J* = 2.4 Hz, *J* = 9.2 Hz, *J* = 11.6 Hz, 1, CH$_\alpha$ Cys C), **3.51** (dd, *J* = 2.4 Hz, *J* = 14.0 Hz, 1, CH$_\alpha$ Cys N), **3.51** (dd, *J* = 2.4 Hz, *J* = 14.0 Hz, 1, CH$_\beta$ Cys N), **3.35** (dd, *J* = 2.4 Hz, *J* = 14.8 Hz, 1, CH$_\beta$ Cys C), **3.03** (dd, *J* = 4.4 Hz, *J* = 14.0 Hz, 1, CH$_\beta$ Phe), **2.90** (dd, *J* = 11.6 Hz, *J* = 14.8 Hz, 1, CH$_\beta$ Cys C), **2.62** (dd, *J* = 8.8 Hz, *J* = 13.6 Hz, 1, CH$_\beta$ Phe), **2.20** (dd, *J* = 14.0 Hz, *J* = 14.0 Hz, 1, CH$_\beta$ Cys N)

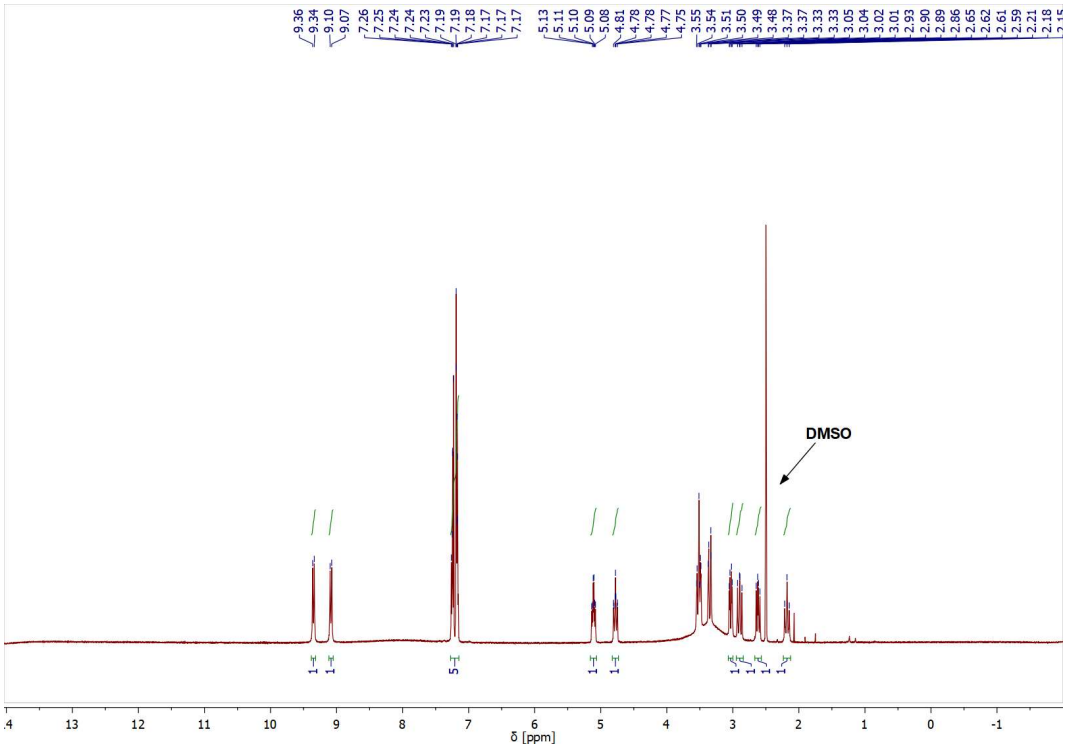

Figure 87: ^{1}H-NMR (400 MHz, DMSO-d_6) of DLL antiparallel cyclic dimer. CH_α of Cys N and CH_β of Cys N and Cys C are not integrated. In their chemical shift region, the presence of water alters the overall integer number. The correct assignation of chemical shift has been done with the aid of the TOCSY and ROESY analysis.

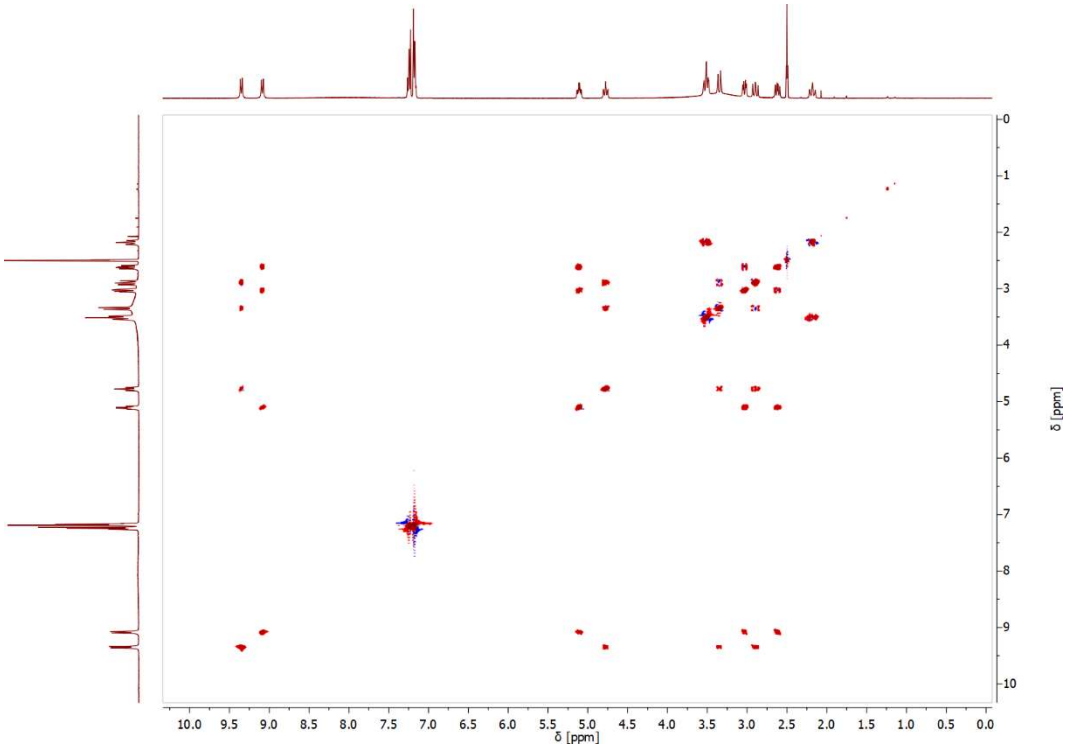

Figure 88: H-H TOCSY (400 MHz, DMSO-d_6) of DLL antiparallel cyclic dimer.

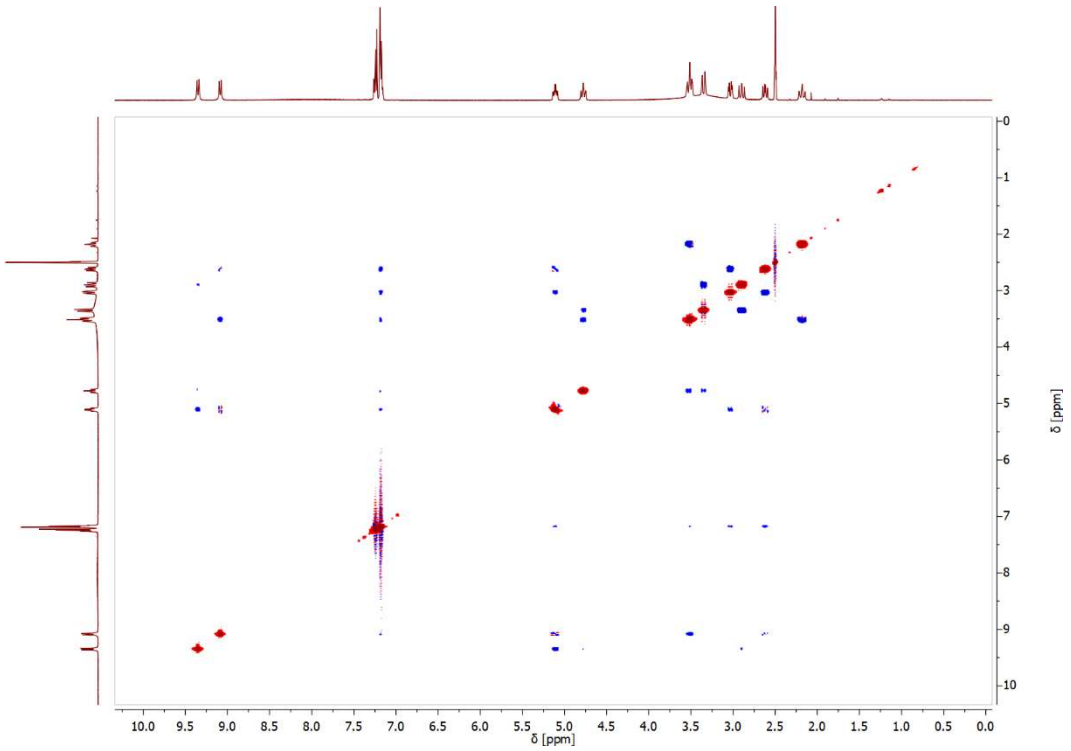

Figure 89: NMR ROESY (400 MHz, DMSO-*d*$_6$) of DLL antiparallel cyclic dimer.

A.6.4 – LLD antiparallel cyclic dimer

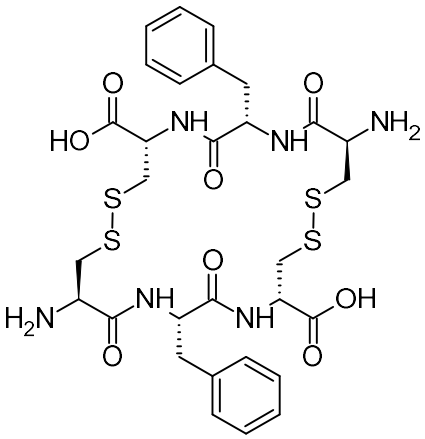

^{1}H-NMR (400 MHz, DMSO-*d*$_6$, TMS), δ (ppm): **9.12** (d, *J* = 8.8 Hz, 1, NH Cys C), **8.68** (d, *J* = 6.8 Hz, 1, NH Phe), **8.52** (dt, *J* = 5.2 Hz, *J* = 20.4 Hz, 3, NH_3^+), **7.35** (m, J_o = 8.4 Hz, J_m = 1.6 Hz, 2, Ar), **7.29** (m, J_o = 7.6 Hz, J_m = 1.6 Hz, 2, Ar), **7.22** (m, J_o = 6.8 Hz, J_m = 2.4 Hz, 1, Ar), **4.81** (ddd, *J* = 6.8 Hz, *J* = 5.2 Hz, *J* = 4.0 Hz, 1, CH_α Phe), **4.62** (ddd, *J* = 2.4 Hz, *J* = 8.8 Hz, *J* = 12.0 Hz, 1, CH_α Cys C), **3.73** (ddd, *J* = 2.4 Hz, *J* = 5.2 Hz, *J* = 14.0 Hz, 1, CH_α Cys N), **3.67** (dd, *J* = 2.4 Hz, *J* = 10.8 Hz, 1, CH_β Cys N), **3.21** (dd, *J* = 2.4 Hz, *J* = 14.0 Hz, 1, CH_β Cys C), **2.92** (dd, *J* = 5.2 Hz, *J* = 14.0 Hz, 1, CH_β Phe), **2.84** (dd, *J* = 7.2 Hz, *J* = 14.0 Hz, 1, CH_β Phe), **2.78** (dd, *J* = 2.4 Hz, *J* = 12.0 Hz, 1, CH_β Cys C), **2.61** (dd, *J* = 10.8 Hz, *J* = 14.0 Hz, 1, CH_α Cys N)

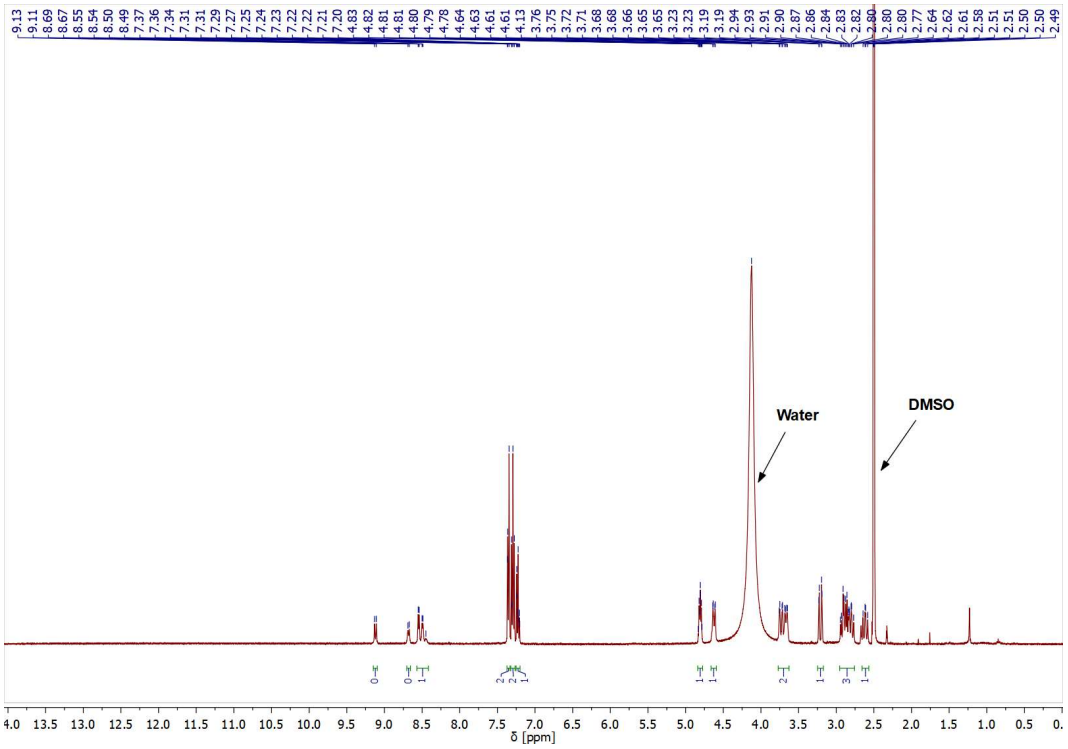

Figure 90: ^{1}H-NMR (400 MHz, DMSO-d_6) of LLD antiparallel cyclic dimer. The correct assignation of chemical shift has been done with the aid of the TOCSY and ROESY analysis.

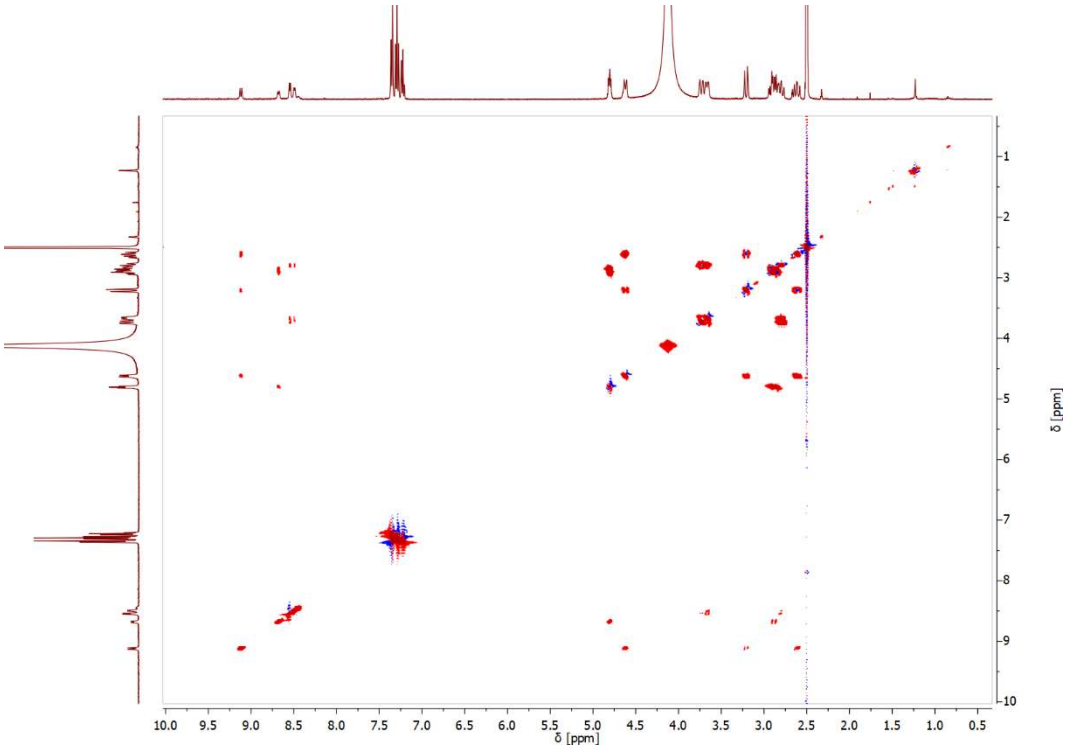

Figure 91: H-H TOCSY (400 MHz, DMSO-d_6) of LLD antiparallel cyclic dimer.

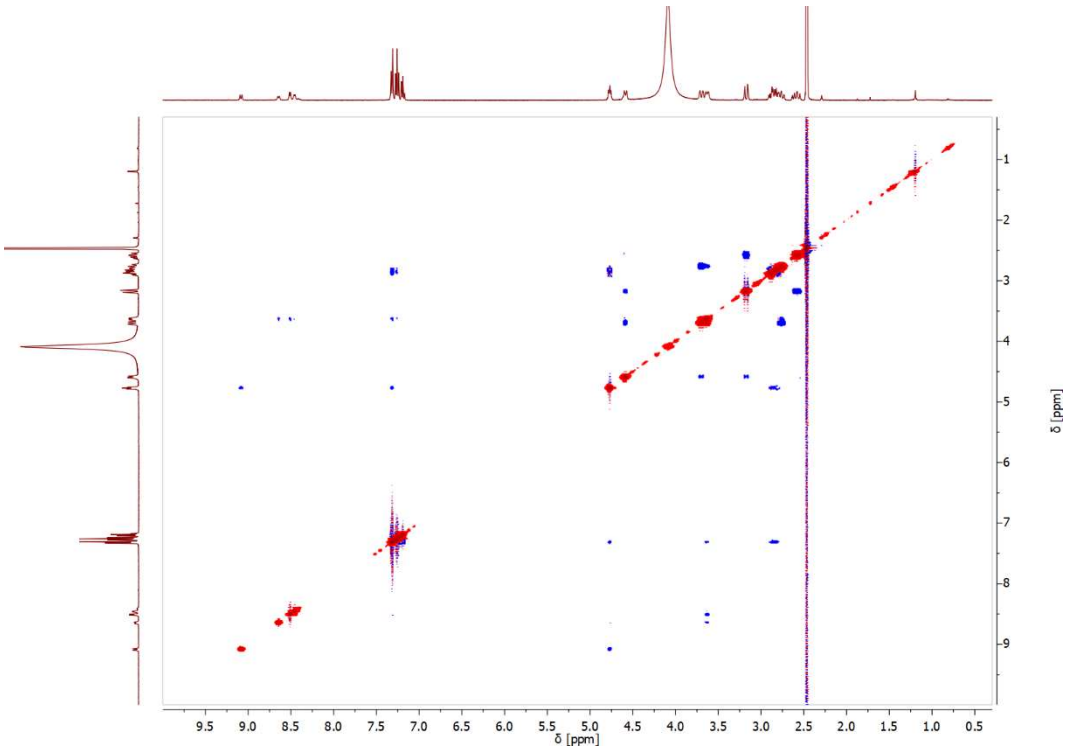

Figure 92: NMR ROESY (400 MHz, DMSO-*d*$_6$) of LLD antiparallel cyclic dimer

A.6.5 – LLD parallel cyclic dimer

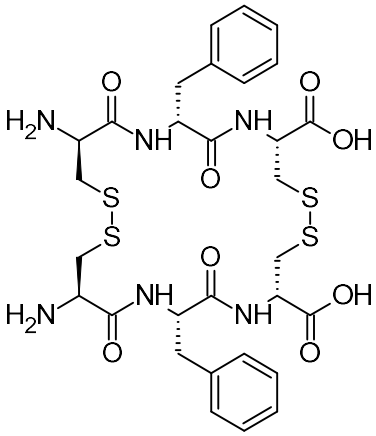

^{1}H-NMR (400 MHz, DMSO-*d*$_6$, TMS), δ (ppm): **9.92-8.62** (b, 2, NH Phe, Cys C), **7.34-7.21** (m, 5, Ar), **4.68** (b, 1, CH$_\alpha$ Phe), **4.52** (b, 1, CH$_\alpha$ Cys C), **4.19** (b, 1, CH$_\alpha$ Cys N), **3.26** (b, 1, CH$_\beta$ Cys N), **3.13** (dd, *J* = 6.0 Hz, *J* = 14.0 Hz, 1, CH$_\beta$ Phe), **2.97** (dd, *J* = 7.6 Hz, *J* = 14.0 Hz, CH$_\beta$ Cys N), **2.91** (b, 2, CH$_\beta$ Cys C), **2.83** (dd, *J* = 9.2 Hz, *J* = 14.0 Hz, 1, CH$_\beta$ Phe)

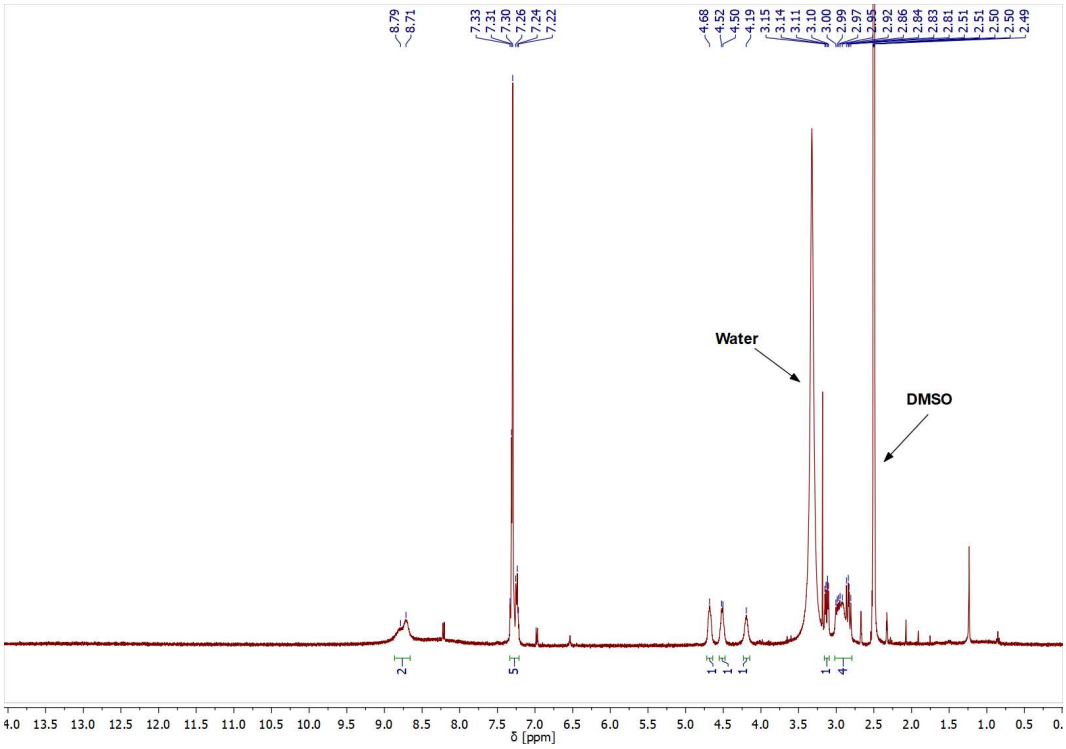

Figure 93: ^{1}H-NMR (400 MHz, DMSO-d_6) of LLD parallel cyclic dimer. The correct assignation of chemical shift has been done with the aid of the TOCSY and ROESY analysis.

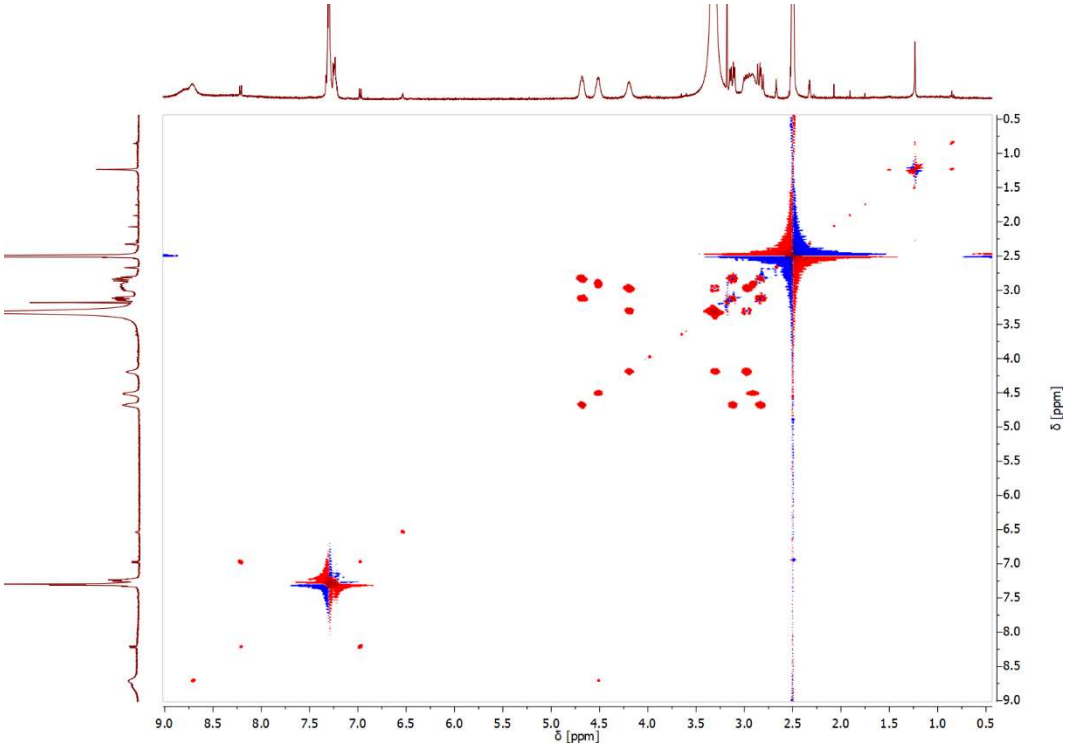

Figure 94: H-H TOCSY (400 MHz, DMSO-d_6) of LLD parallel cyclic dimer.

A.7 – LDL Cyclic pentamer methyl ester mass spectrometry

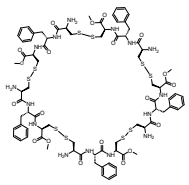

		m/z $[M+H]^+$			
	Monoisotopical mass	**Z = 1**	**Z = 2**	**Z =3**	**Z =4**
Cyclic pentamer OMe	1915.49	1916.49	958.75	639.50	479.87
		m/z $[M-H]^-$			
		1914.49	956.75	637.50	477.87

A.7.1 – LCMS characterisation

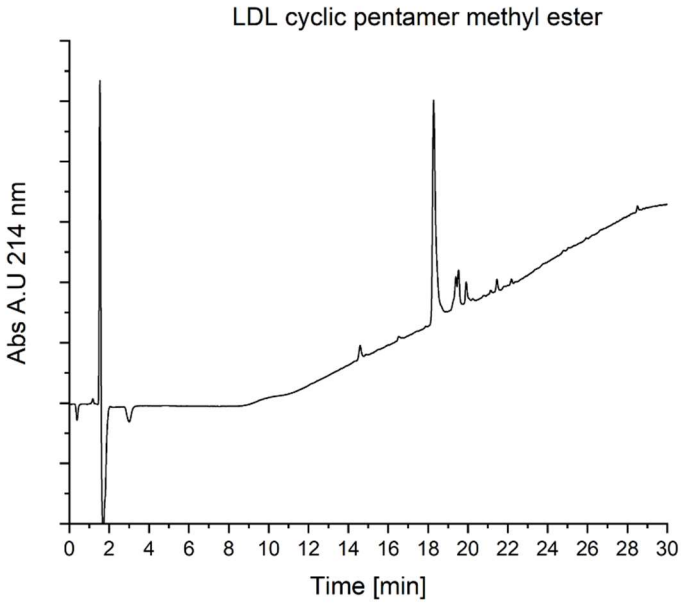

Compound	Rt [min]	$[M+H]^+$	$[M-H]^-$
Cyclic pentamer OMe	18.3	959.2/639.6	993.7

Figure 95: Analytical chromatogram of cyclic pentamer methyl ester. The main peak at Rt 18.3 min represents the fully esterified compound whereas all the following small peaks are tetra ester isomers. This is due to a non-complete esterification reaction.

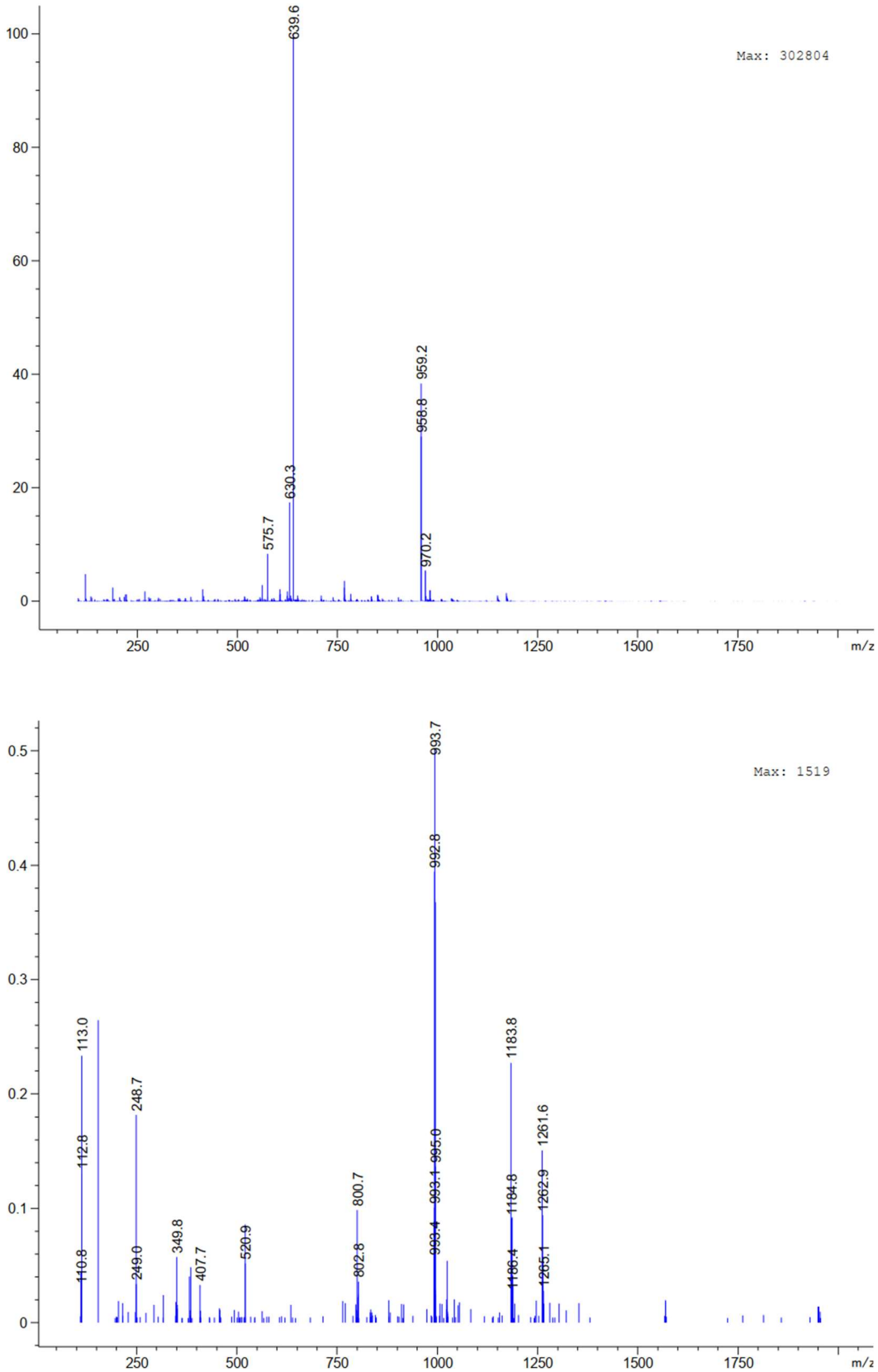

Figure 96: ESI-MS spectrum of cyclic pentamer methyl ester in positive (top) and negative (bottom) mode.

A.7.2 – ESI-TOF characterisation

The same sample was then characterised by ESI-TOF in order to get a precise mass spectrum.

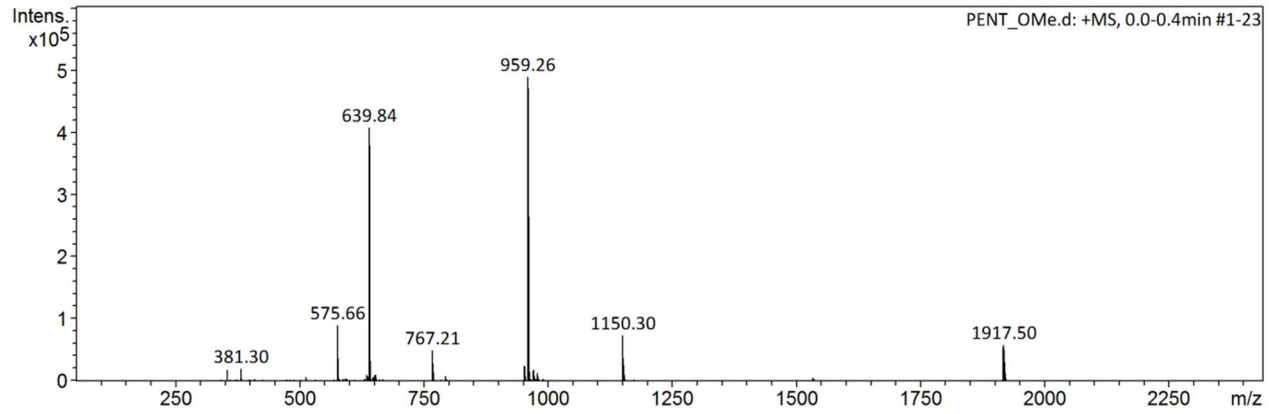

Figure 97: ESI-microTOF spectrum of LDL cyclic pentamer methyl ester.

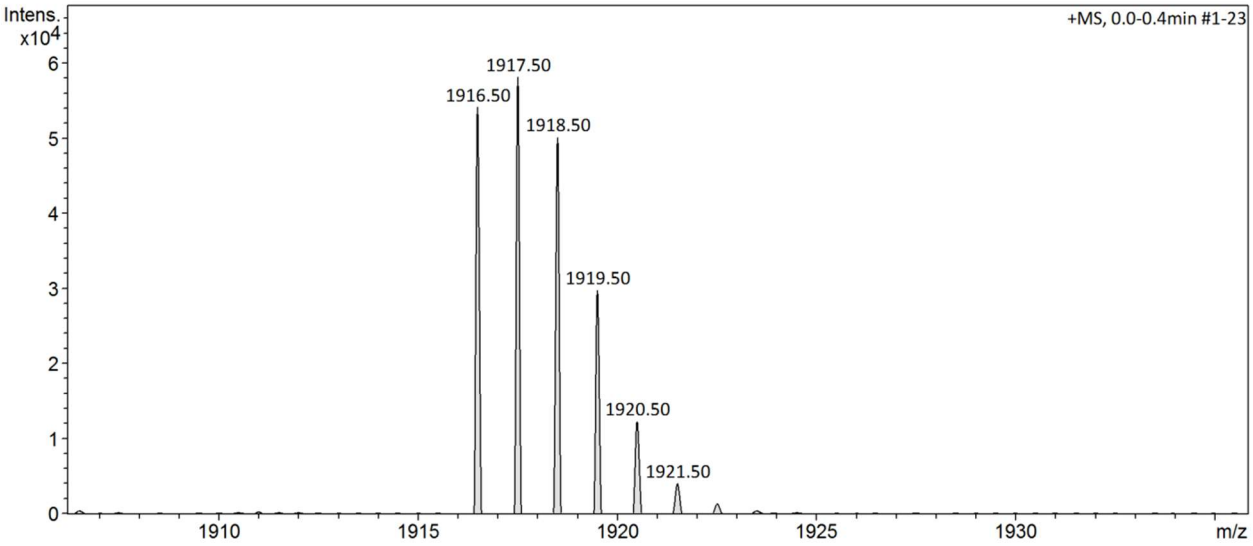

Figure 98: Isotopical pattern of the peak at 1917.50 of **Figure 97**.

The isotopical pattern was confirmed by a theoretical calculation from the online tool *Prot-Pi*, a free tool for peptide and proteins.

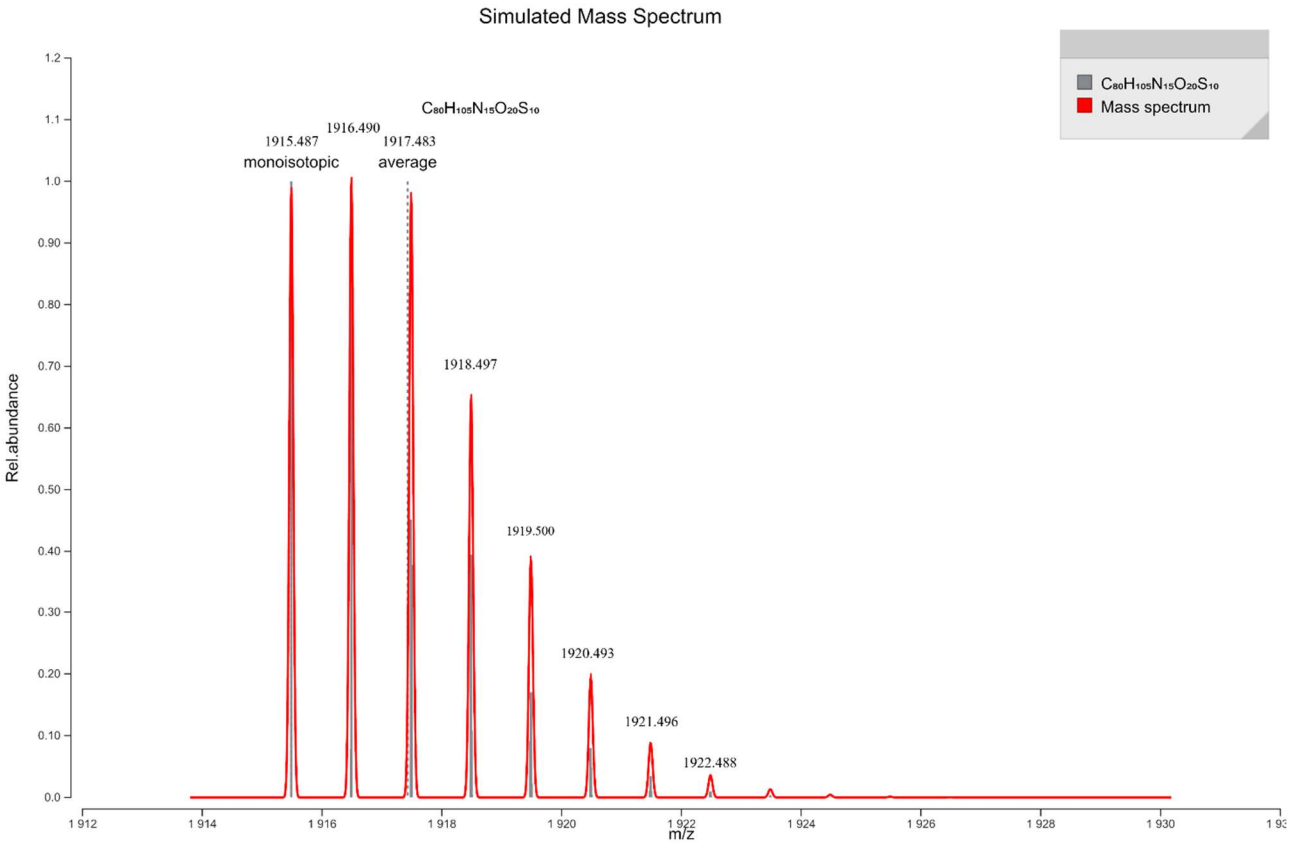

Figure 99: Calculated mass spectrum of cyclic pentamer methyl ester by the free online tool *Prot-Pi*.

A.8 – Circular dichroism

A.8.1 Cyclic dimers

Samples were dissolved in milli-Q water and the pH was tuned with NaOH 1 M. The spectra were collected in the range of 185-280 nm in a 0.1 mm quartz cuvette at 25 °C.

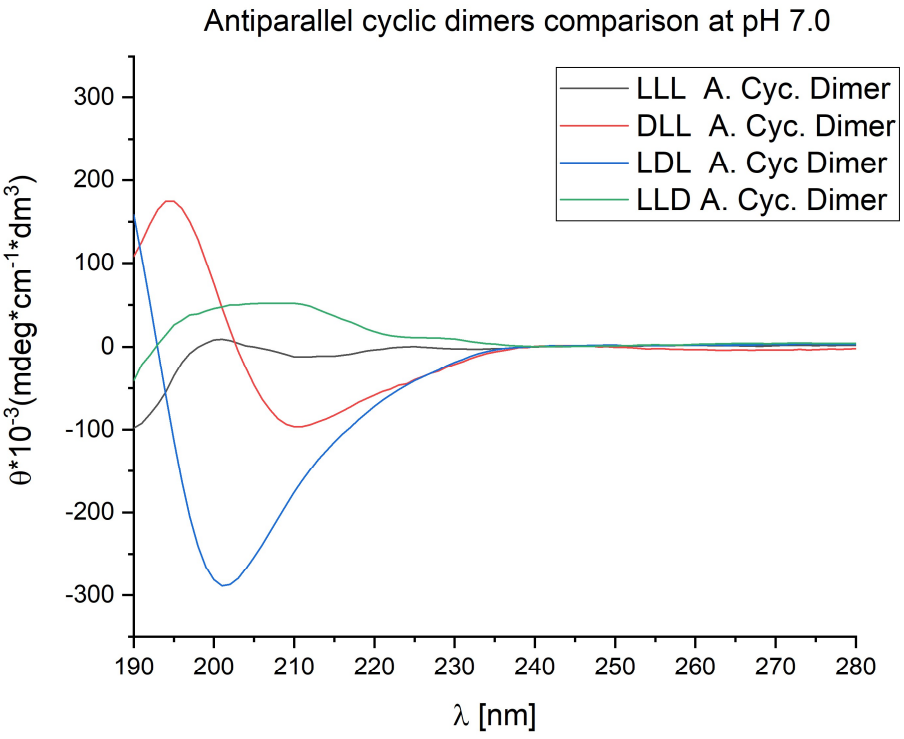

Figure 100: Antiparallel cyclic dimers circular dichroism comparison at pH 7.0. Optical path 0.1 mm.

A.8.2 Cyclic pentamer

Samples were prepared diluting 1:2 the DCL after TCEP amplification and tuning the pH with NaOH and HCl 1.0 M.

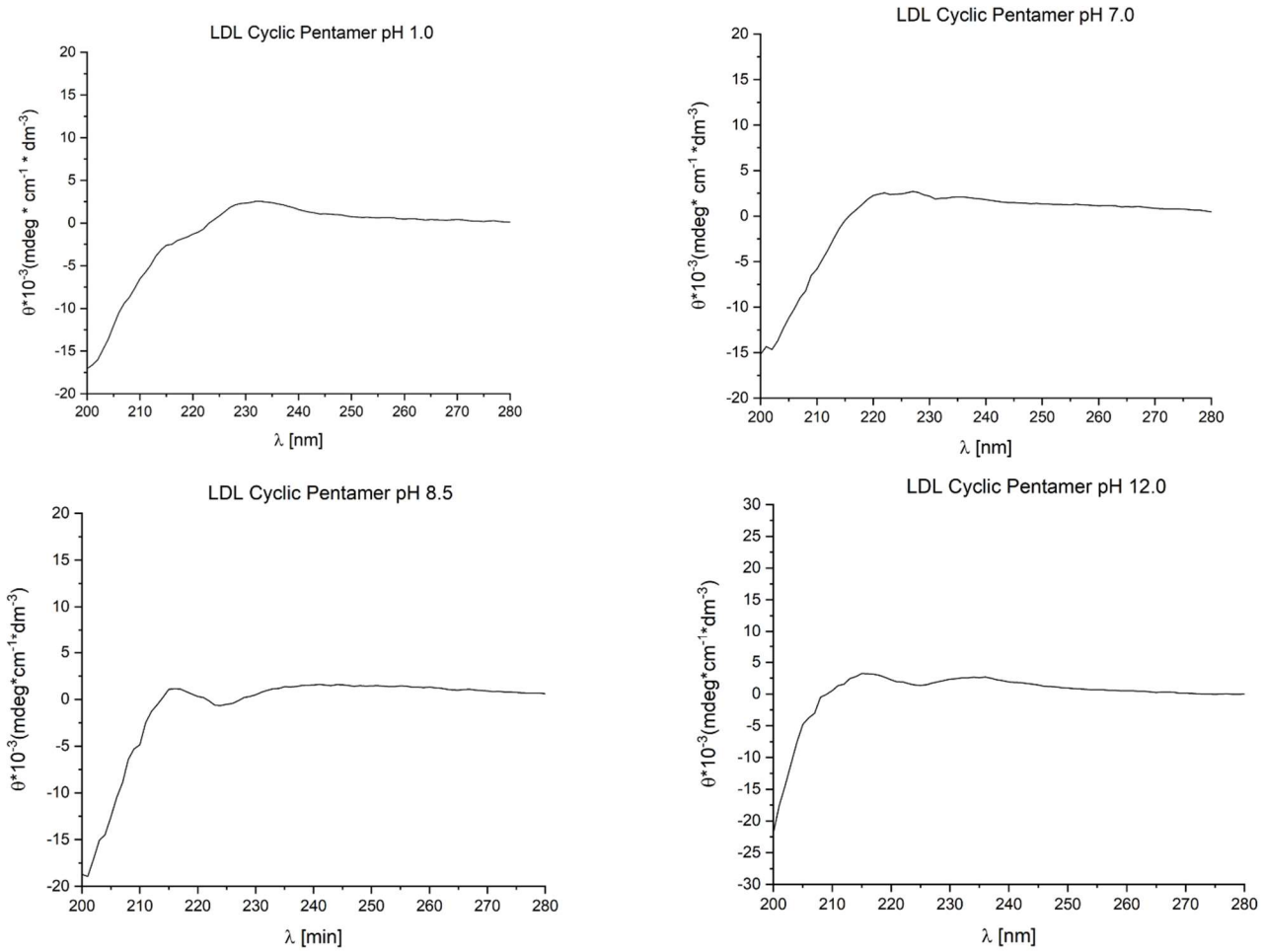

Figure 101: Cyclic pentamer circular dichroism spectra at 25 °C. Optical path 0.1 mm.

A.9 – Crystallisation experiments

A.9.1 – LLL stereoisomers

All compounds were crystallised in water with the hanging drop technique. Peptides were dissolved in milli-Q water at the desired concentration and then the pH value was tuned with HCl 1.0 M or NaOH 1.0 M to reach the final value. NaCl solutions were used as crystallising agent.

LLL antiparallel dimer 8.0 mM					
pH	**NaCl 0.5 M**	**NaCl 1 M**	**NaCl 2 M**	**NaCl 3 M**	**NaCl 4 M**
1.1	/	P	G	G	G
7.2	F	F	F	G	G
12.1	/	/	/	/	/

LLL antiparallel dimer 5.5 mM					
pH	**NaCl 0.1 M**	**NaCl 0.25 M**	**NaCl 0.5 M**	**NaCl 0.75 M**	**NaCl 1 M**
1.2	/	/	/	/	C
6.8	C	C	C	C	C

LLL parallel dimer 2.7 mM					
pH	**NaCl 0.5 M**	**NaCl 1 M**	**NaCl 2 M**	**NaCl 3 M**	**NaCl 4 M**
3.8	C	F	F	F	F
7.3	/	/	/	F	F
12.1	/	/	/	/	/

LLL parallel dimer 5.5 mM					
pH	**NaCl 0.5 M**	**NaCl 1 M**	**NaCl 2 M**	**NaCl 3 M**	**NaCl 4 M**
2.3	/	|	C	C	G
6.8	P	P	P	P	P

Table 9: Hanging drop schemes for LLL antiparallel and parallel cyclic dimer. P: precipitate, G: gel, F: fibre, C: crystals. In yellow are highlighted the selected batches for the single-crystal XRD data collection.

A.9.2 – DLL antiparallel cyclic dimer

The compound was crystallised in batch after a qualitative essay under optical microscope. The compound was solubilised in water at pH 7.1 (20 mM) and the solution was mixed with an equal amount of organic solvent.

Solvent	**MeOH**	**EtOH**	***i*PrOH**	***n*BuOH**
Result	Solution	Solution	Precipitate	Crystals

A.9.3 – LDL antiparallel cyclic dimer

The compound was dissolved in MeOH at 4 mM, and the vial was closed inside a cylinder with a solution composed by MeOH/H_2O 50/50. The system was left equilibrate, and crystals formed after 1 week.

A.9.4 – LLD antiparallel cyclic dimer

All compounds were crystallised in water with the hanging drop technique. Peptides were dissolved in milli-Q water at the desired concentration and then the pH value was tuned with HCl 1.0 M or NaOH 1.0 M to reach the final value. NaCl solutions were used as crystallising agent.

	LLD antiparallel dimer 10.0 mM					
pH	**NaCl 0.1 M**	**NaCl 0.5 M**	**NaCl 1.0 M**	**NaCl 2.0 M**	**NaCl 3.0 M**	**NaCl 4.0 M**
2.0	C	C	G	G	C	C
7.2	C	P	P	P	P	C
12.0	/	/	/	/	/	/

Table 10: Hanging drop schemes for LLD antiparallel cyclic dimer. P: precipitate, G: gel, C: crystal. In yellow are highlighted the selected batches for the single-crystal XRD data collection.

A.9.5 – LDL antiparallel cyclic trimer

	LDL gel 20 mM (monomer), pH 7.0, BB 100 mM					
Guest (10-60 mM)	**NaCl 0.2 M**	**NaCl 0.4 M**	**NaCl 0.6 M**	**NaCl 0.8 M**	**NaCl 1.0 M**	**NaCl 1.2 M**
Urea	G	G	G	G	G	G
NH_4^+	G	G	G	G	G	G
$ZnSO_4$	G	G	G	G + C	G + C	G + C
$AuCl_3$	G	G	G	C*	C*	C*

Table 11: Hanging drop schemes for LDL gel. P: precipitate, G: gel, C: crystal. In yellow are highlighted the selected batches for the single-crystal XRD data collection. *Gold borate crystals.

A.10 – XRD data

A.10.1 – LLL stereoisomers

	LLL antiparallel dimer zwitterion	**LLL parallel dimer zwitterion**
Formula	$C_{30}H_{38}N_6O_8S_4$, 8(H_2O)	$C_{30}H_{38}N_6O_8S_4$, 1.5(H2O)
Temperature (K)	100	100
Wavelength (Å)	0.7	0.7
Crystal system	Monoclinic	Orthorhombic
Space group	*C 2*	*P 2_1 2_1 2_1*
a (Å)	24.277(9)	4.941(4)
b (Å)	4.923(2)	22.182(10)
c (Å)	20.832(7)	32.294(14)
α (°)	90	90
β (°)	120.86(3)	90
γ (°)	90	90
V (Å^3)	2137.3(16)	3539(4)
Z, ρcalc (g/cm^3)	2, 1.372	4, 1.437
μ (mm^{-1})	0.279	0.313
F (000)	936	1612
Data collection θ range	1.121 – 22.865	1.097 – 21.609
Refl. Collected / unique	10302 / 3056	16941 / 4300
Rint	0.1761	0.1641
Completeness (%)	99.6	99.4
Data/Restraints/Parameters	3056 / 1 / 266	4300 / 0 / 456
GooF	0.991	0.997
R1, wR2 [I>2σ(I)]	0.0744 / 0.1762	0.0670 / 0.1428
R1, wR2 all data	0.1557 / 0.2201	0.1337 / 0.1730

Table 12: Crystallographic data for LLL stereoisomers.

A.10.2 – DLL antiparallel cyclic dimer

	DLL Antiparallel cyclic dimer zwitterion
Formula	3 $C_{30}H_{38}N_6O_8S_4$ · 15.5 H_2O
Temperature (K)	100
Wavelength (Å)	0.7
Crystal system	Monoclinic
Space group	*C 2*
a (Å)	37.237(7)
b (Å)	19.396(4)
c (Å)	20.373(4)
α (°)	90
β (°)	114.24(3)
γ (°)	90
V (Å^3)	13417(5)
Z, ρcalc (g/cm^3)	4, 1.459
μ (mm^{-1})	0.282
F (000)	6176
Data collection θ range	1.181 - 24.835
Refl. Collected / unique	97400 / 39476
Rint	0.0727
Completeness (%)	99.7
Data/Restraints/Parameters	39476 / 1 / 1436
GooF	1.064
R1, wR2 [I>2σ(I)]	0.0912 / 0.2506
R1, wR2 all data	0.1394 / 0.2982

Table 13: Crystallographic details for DLL antiparallel dimer.

A.10.3 – LDL antiparallel cyclic dimer

	LDL antiparallel cyclic dimer zwitterion
Formula	2($C_{30}H_{38}N_6O_8S_4$)·10.5(H_2O)·0.5(CH_4O)
Temperature (K)	100
Wavelength (Å)	0.7
Crystal system	Monoclinic
Space group	*C 2*
a (Å)	25.156(5)
b (Å)	11.326(2)
c (Å)	30.693(6)
α (°)	90
β (°)	100.37(3)
γ (°)	90
V (Å^3)	8602(3)
Z, ρcalc (g/cm^3)	4, 1.147
μ (mm^{-1})	0.22
F (000)	3136
Data collection θ range	1.329 – 28.216

Refl. Collected / unique	19817 / 35181
Rint	0.0589
Completeness (%)	97.6
Data/Restraints/Parameters	19817 / 88 / 1031
GooF	1.348
R1, wR2 [I>2σ(I)]	0.1124 / 0.2848
R1, wR2 all data	0.1408 / 0.3023

Table 14: Crystallographic details for LDL antiparallel dimer.

A.10.4 – LLD antiparallel cyclic dimer

	DLL antiparallel dimer zwitterion	**DLL antiparallel dimer cation**
Formula	$C_{30}H_{38}N_6O_8S_4$, 3.15 H_2O	$C_{30}H_{39}N_6O_8S_4^{+1}$, 0.9 Cl^{-1}, 0.1 ($C_2F_3O_2^{-1}$), 2.8(H_2O)
Temperature (K)	100	100
Wavelength (Å)	0.7	0.7
Crystal system	Trigonal	Monoclinic
Space group	*P* 3_2	*P* 2_1
a (Å)	13.9670(16)	12.592(19)
b (Å)	13.9670(16)	22.396(14)
c (Å)	33.742(7)	14.313(8)
α (°)	90	90
β (°)	90	110.77(2)
γ (°)	120	90
V (Å^3)	5700.4(18)	3774(7)
Z, ρcalc (g/cm^3)	6, 1.389	4, 1.467
μ (mm^{-1})	0.297	0.361
F (000)	2512	1751
Data collection θ range	1.658 - 29.893	1.499 - 29.900
Refl. Collected / unique	102297 / 22601	72120 / 22471
Rint	0.0471	0.0477
Completeness (%)	98.4	99.5
Data/Restraints/Parameters	22601 / 1 / 937	22471 / 16 / 990
GooF	1.114	1.054
R1, wR2 [I>2σ(I)]	0.0707 / 0.2057	0.0387 / 0.1061
R1, wR2 all data	0.0740 / 0.2274	0.0402 / 0.1074

Table 15: Crystallographic details for LLD antiparallel cyclic dimer.

A.10.5 – LDL antiparallel cyclic trimer

	LDL antiparallel cyclic trimer
Formula	$C_{15}H_{18}N_3O_4S_2^-$, 0.66 Zn^{2+}, 0.33 Cl^{-1}, 2.1(H_2O)
Temperature (K)	100
Wavelength (Å)	0.7
Crystal system	Trigonal
Space group	*R 3*
a (Å)	14.600(5)
b (Å)	14.600(5)
c (Å)	24.649(14)
α (°)	90
β (°)	90
γ (°)	120
V (Å^3)	4550(4)
Z, ρcalc (g/cm^3)	3, 1.516
μ (mm^{-1})	1.066
F (000)	2155
Data collection θ range	1.783 - 29.748
Refl. Collected / unique	14159 / 5730
Rint	0.1124
Completeness (%)	99.9
Data/Restraints/Parameters	5730 / 1 / 252
GooF	0.94
R1, wR2 [I>2σ(I)]	0.0795 / 0.1932
R1, wR2 all data	0.1160 / 0.2191

Table 16: Crystallographic details for LDL antiparallel cyclic trimer.

References

(1) Ramberg, P. J. The Death of Vitalism and The Birth of Organic Chemistry: Wohler's Urea Synthesis and the Disciplinary Identity of Organic Chemistry. *Ambix* **2000**. https://doi.org/10.1179/amb.2000.47.3.170.

(2) Crick, F. The Double Helix: A Personal View. *Nature* **1974**, *248* (5451), 766–769. https://doi.org/10.1038/248766a0.

(3) Klug, A. The Discovery of the DNA Double Helix. *J. Mol. Biol.* **2004**, *335* (1), 3–26. https://doi.org/10.1016/j.jmb.2003.11.015.

(4) Cram, D. J. The Design of Molecular Hosts, Guests, and Their Complexes (Nobel Lecture). *Angew. Chem. Int. Ed. Engl.* **1988**, *27* (8), 1009–1020. https://doi.org/10.1002/anie.198810093.

(5) Whitesides, G. M.; Simanek, E. E.; Mathias, J. P.; Seto, C. T.; Chin, D.; Mammen, M.; Gordon, D. M. Noncovalent Synthesis: Using Physical-Organic Chemistry To Make Aggregates. *Acc. Chem. Res.* **1995**, *28* (1), 37–44. https://doi.org/10.1021/ar00049a006.

(6) Lehn, J.-M. Supramolecular Chemistry. *Science* **1993**, *260* (5115), 1762–1763. https://doi.org/10.1126/science.8511582.

(7) Evans, N. H.; Beer, P. D. Advances in Anion Supramolecular Chemistry: From Recognition to Chemical Applications. *Angew. Chem. Int. Ed.* **2014**, *53* (44), 11716–11754. https://doi.org/10.1002/anie.201309937.

(8) Chen, H.; Fraser Stoddart, J. From Molecular to Supramolecular Electronics. *Nat. Rev. Mater.* **2021**, *6* (9), 804–828. https://doi.org/10.1038/s41578-021-00302-2.

(9) Kolesnichenko, I. V.; Anslyn, E. V. Practical Applications of Supramolecular Chemistry. *Chem. Soc. Rev.* **2017**, *46* (9), 2385–2390. https://doi.org/10.1039/C7CS00078B.

(10) Mann, S. Self-Assembly and Transformation of Hybrid Nano-Objects and Nanostructures under Equilibrium and Non-Equilibrium Conditions. *Nat. Mater.* **2009**, *8* (10), 781–792. https://doi.org/10.1038/nmat2496.

(11) Yan, Y.; Huang, J.; Zhong Tang, B. Kinetic Trapping – a Strategy for Directing the Self-Assembly of Unique Functional Nanostructures. *Chem. Commun.* **2016**, *52* (80), 11870–11884. https://doi.org/10.1039/C6CC03620A.

(12) Lehn, J.-M. Towards Complex Matter: Supramolecular Chemistry and Self-Organization. *Eur. Rev.* **2009**, *17* (2), 263–280. https://doi.org/10.1017/S1062798709000805.

(13) Grzybowski, B. A.; Wilmer, C. E.; Kim, J.; Browne, K. P.; Bishop, K. J. M. Self-Assembly: From Crystals to Cells. *Soft Matter* **2009**, *5* (6), 1110–1128. https://doi.org/10.1039/B819321P.

(14) Northrop, B. H.; Zheng, Y.-R.; Chi, K.-W.; Stang, P. J. Self-Organization in Coordination-Driven Self-Assembly. *Acc. Chem. Res.* **2009**, *42* (10), 1554–1563. https://doi.org/10.1021/ar900077c.

(15) Chen, L.; Chen, Q.; Wu, M.; Jiang, F.; Hong, M. Controllable Coordination-Driven Self-Assembly: From Discrete Metallocages to Infinite Cage-Based Frameworks. *Acc. Chem. Res.* **2015**, *48* (2), 201–210. https://doi.org/10.1021/ar5003076.

(16) Sherrington, D. C.; Taskinen, K. A. Self-Assembly in Synthetic Macromolecular Systems via Multiple Hydrogen Bonding Interactions. *Chem. Soc. Rev.* **2001**, *30* (2), 83–93. https://doi.org/10.1039/B008033K.

(17) Sijbesma, R. P.; Meijer, E. Self-Assembly of Well-Defined Structures by Hydrogen Bonding. *Curr. Opin. Colloid Interface Sci.* **1999**, *4* (1), 24–32. https://doi.org/10.1016/S1359-0294(99)00011-4.

(18) Conn, M. M.; Rebek, J. Self-Assembling Capsules. *Chem. Rev.* **1997**, *97* (5), 1647–1668. https://doi.org/10.1021/cr9603800.

(19) Cox, C. J. T.; Hale, J.; Molinska, P.; Lewis, J. E. M. Supramolecular and Molecular Capsules, Cages and Containers. *Chem. Soc. Rev.* **2024**. https://doi.org/10.1039/D4CS00761A.

(20) Oshovsky, G. V.; Reinhoudt, D. N.; Verboom, W. Supramolecular Chemistry in Water. *Angew. Chem. Int. Ed.* **2007**, *46* (14), 2366–2393. https://doi.org/10.1002/anie.200602815.

(21) Kronberg, B. The Hydrophobic Effect. *Curr. Opin. Colloid Interface Sci.* **2016**, *22*, 14–22. https://doi.org/10.1016/j.cocis.2016.02.001.

(22) Biedermann, F.; Nau, W. M.; Schneider, H.-J. The Hydrophobic Effect Revisited—Studies with Supramolecular Complexes Imply High-Energy Water as a Noncovalent Driving Force. *Angew. Chem. Int. Ed.* **2014**, *53* (42), 11158–11171. https://doi.org/10.1002/anie.201310958.

(23) Lombardo, D.; Kiselev, M. A.; Magazù, S.; Calandra, P. Amphiphiles Self-Assembly: Basic Concepts and Future Perspectives of Supramolecular Approaches. *Adv. Condens. Matter Phys.* **2015**, *2015* (1), 151683. https://doi.org/10.1155/2015/151683.

(24) Zhao, X.; Pan, F.; Xu, H.; Yaseen, M.; Shan, H.; Hauser, C. A. E.; Zhang, S.; Lu, J. R. Molecular Self-Assembly and Applications of Designer Peptide Amphiphiles. *Chem. Soc. Rev.* **2010**, *39* (9), 3480–3498. https://doi.org/10.1039/B915923C.

(25) Kokkoli, E.; Mardilovich, A.; Wedekind, A.; Rexeisen, E. L.; Garg, A.; Craig, J. A. Self-Assembly and Applications of Biomimetic and Bioactive Peptide-Amphiphiles. *Soft Matter* **2006**, *2* (12), 1015–1024. https://doi.org/10.1039/B608929A.

(26) Wang, T.; Ménard-Moyon, C.; Bianco, A. Self-Assembly of Amphiphilic Amino Acid Derivatives for Biomedical Applications. *Chem. Soc. Rev.* **2022**, *51* (9), 3535–3560. https://doi.org/10.1039/D1CS01064F.

(27) Then, A.; Mácha, K.; Ibrahim, B.; Schuster, S. A Novel Method for Achieving an Optimal Classification of the Proteinogenic Amino Acids. *Sci. Rep.* **2020**, *10* (1), 15321. https://doi.org/10.1038/s41598-020-72174-5.

(28) Baker, E. G.; Bartlett, G. J.; Crump, M. P.; Sessions, R. B.; Linden, N.; Faul, C. F. J.; Woolfson, D. N. Local and Macroscopic Electrostatic Interactions in Single α-Helices. *Nat. Chem. Biol.* **2015**, *11* (3), 221–228. https://doi.org/10.1038/nchembio.1739.

(29) Fujiwara, K.; Toda, H.; Ikeguchi, M. Dependence of α-Helical and β-Sheet Amino Acid Propensities on the Overall Protein Fold Type. *BMC Struct. Biol.* **2012**, *12* (1), 18. https://doi.org/10.1186/1472-6807-12-18.

(30) Minor, D. L.; Kim, P. S. Measurement of the β-Sheet-Forming Propensities of Amino Acids. *Nature* **1994**, *367* (6464), 660–663. https://doi.org/10.1038/367660a0.

(31) Löwik, D. W. P. M.; Hest, J. C. M. van. Peptide Based Amphiphiles. *Chem. Soc. Rev.* **2004**, *33* (4), 234–245. https://doi.org/10.1039/B212638A.

(32) Makhatadze, G. I. Thermodynamics Of α-Helix Formation. In *Advances in Protein Chemistry*; Peptide Solvation and HBonds; Academic Press, 2005; Vol. 72, pp 199–226. https://doi.org/10.1016/S0065-3233(05)72008-8.

(33) Nesloney, C. L.; Kelly, J. W. Progress towards Understanding β-Sheet Structure. *Bioorg. Med. Chem.* **1996**, *4* (6), 739–766. https://doi.org/10.1016/0968-0896(96)00051-X.

(34) Cheng, P.-N.; Pham, J. D.; Nowick, J. S. The Supramolecular Chemistry of β-Sheets. *J. Am. Chem. Soc.* **2013**, *135* (15), 5477–5492. https://doi.org/10.1021/ja3088407.

(35) Gilead, S.; Gazit, E. Self-Organization of Short Peptide Fragments: From Amyloid Fibrils to Nanoscale Supramolecular Assemblies. *Supramol. Chem.* **2005**, *17* (1–2), 87–92. https://doi.org/10.1080/10610270412331328943.

(36) Blackmond, D. G. The Origin of Biological Homochirality. *Philos. Trans. R. Soc. B Biol. Sci.* **2011**, *366* (1580), 2878–2884. https://doi.org/10.1098/rstb.2011.0130.

(37) Deng, M.; Yu, J.; Blackmond, D. G. Symmetry Breaking and Chiral Amplification in Prebiotic Ligation Reactions. *Nature* **2024**, *626* (8001), 1019–1024. https://doi.org/10.1038/s41586-024-07059-y.

(38) Noorduin, W. L.; Bode, A. A. C.; van der Meijden, M.; Meekes, H.; van Etteger, A. F.; van Enckevort, W. J. P.; Christianen, P. C. M.; Kaptein, B.; Kellogg, R. M.; Rasing, T.; Vlieg, E.

Complete Chiral Symmetry Breaking of an Amino Acid Derivative Directed by Circularly Polarized Light. *Nat. Chem.* **2009**, *1* (9), 729–732. https://doi.org/10.1038/nchem.416.

(39) Hendricks, M. P.; Sato, K.; Palmer, L. C.; Stupp, S. I. Supramolecular Assembly of Peptide Amphiphiles. *Acc. Chem. Res.* **2017**, *50* (10), 2440–2448. https://doi.org/10.1021/acs.accounts.7b00297.

(40) Panda, J. J.; Chauhan, V. S. Short Peptide Based Self-Assembled Nanostructures: Implications in Drug Delivery and Tissue Engineering. *Polym. Chem.* **2014**, *5* (15), 4418–4436. https://doi.org/10.1039/C4PY00173G.

(41) Yadav, N.; Chauhan, M. K.; Chauhan, V. S. Short to Ultrashort Peptide-Based Hydrogels as a Platform for Biomedical Applications. *Biomater. Sci.* **2019**, *8* (1), 84–100. https://doi.org/10.1039/C9BM01304K.

(42) Wang, H.; Yang, Z. Short-Peptide-Based Molecular Hydrogels: Novel Gelation Strategies and Applications for Tissue Engineering and Drug Delivery. *Nanoscale* **2012**, *4* (17), 5259–5267. https://doi.org/10.1039/C2NR31149F.

(43) Ardoña, H. A. M.; Tovar, J. D. Peptide π-Electron Conjugates: Organic Electronics for Biology? *Bioconjug. Chem.* **2015**, *26* (12), 2290–2302. https://doi.org/10.1021/acs.bioconjchem.5b00497.

(44) Frederix, P. W. J. M.; Scott, G. G.; Abul-Haija, Y. M.; Kalafatovic, D.; Pappas, C. G.; Javid, N.; Hunt, N. T.; Ulijn, R. V.; Tuttle, T. Exploring the Sequence Space for (Tri-)Peptide Self-Assembly to Design and Discover New Hydrogels. *Nat. Chem.* **2015**, *7* (1), 30–37. https://doi.org/10.1038/nchem.2122.

(45) Garcia, A. M.; Iglesias, D.; Parisi, E.; Styan, K. E.; Waddington, L. J.; Deganutti, C.; De Zorzi, R.; Grassi, M.; Melchionna, M.; Vargiu, A. V.; Marchesan, S. Chirality Effects on Peptide Self-Assembly Unraveled from Molecules to Materials. *Chem* **2018**, *4* (8), 1862–1876. https://doi.org/10.1016/j.chempr.2018.05.016.

(46) Bellotto, O.; Kralj, S.; Zorzi, R. D.; Geremia, S.; Marchesan, S. Supramolecular Hydrogels from Unprotected Dipeptides: A Comparative Study on Stereoisomers and Structural Isomers. *Soft Matter* **2020**, *16* (44), 10151–10157. https://doi.org/10.1039/D0SM01191F.

(47) Bellotto, O.; Pierri, G.; Rozhin, P.; Polentarutti, M.; Kralj, S.; D'Andrea, P.; Tedesco, C.; Marchesan, S. Dipeptide Self-Assembly into Water-Channels and Gel Biomaterial. *Org. Biomol. Chem.* **2022**, *20* (31), 6211–6218. https://doi.org/10.1039/D2OB00622G.

(48) Bellotto, O.; Kralj, S.; Melchionna, M.; Pengo, P.; Kisovec, M.; Podobnik, M.; De Zorzi, R.; Marchesan, S. Self-Assembly of Unprotected Dipeptides into Hydrogels: Water-Channels Make

the Difference. *ChemBioChem* **2022**, *23* (2), e202100518. https://doi.org/10.1002/cbic.202100518.

(49) Bellotto, O.; Scarel, E.; Pierri, G.; Rozhin, P.; Kralj, S.; Polentarutti, M.; Bandiera, A.; Rossi, B.; Vargiu, A. V.; Tedesco, C.; Marchesan, S. Supramolecular Hydrogels and Water Channels of Differing Diameters from Dipeptide Isomers. *Biomacromolecules* **2024**, *25* (4), 2476–2485. https://doi.org/10.1021/acs.biomac.3c01439.

(50) Scarel, E.; Pierri, G.; Rozhin, P.; Adorinni, S.; Polentarutti, M.; Tedesco, C.; Marchesan, S. Self-Assembly and Gelation Study of Dipeptide Isomers with Norvaline and Phenylalanine. *Chemistry* **2022**, *4* (4), 1417–1428. https://doi.org/10.3390/chemistry4040093.

(51) Monti, M.; Scarel, E.; Hassanali, A.; Stener, M.; Marchesan, S. Diverging Conformations Guide Dipeptide Self-Assembly into Crystals or Hydrogels. *Chem. Commun.* **2023**, *59* (73), 10948–10951. https://doi.org/10.1039/D3CC02682E.

(52) Scarel, E.; De Corti, M.; Polentarutti, M.; Pierri, G.; Tedesco, C.; Marchesan, S. Self-Assembly of Heterochiral, Aliphatic Dipeptides with Leu. *J. Pept. Sci.* **2024**, *30* (5), e3559. https://doi.org/10.1002/psc.3559.

(53) Reches, M.; Gazit, E. Casting Metal Nanowires Within Discrete Self-Assembled Peptide Nanotubes. *Science* **2003**, *300* (5619), 625–627. https://doi.org/10.1126/science.1082387.

(54) Yan, X.; Zhu, P.; Li, J. Self-Assembly and Application of Diphenylalanine-Based Nanostructures. *Chem. Soc. Rev.* **2010**, *39* (6), 1877–1890. https://doi.org/10.1039/B915765B.

(55) Tao, K.; Levin, A.; Adler-Abramovich, L.; Gazit, E. Fmoc-Modified Amino Acids and Short Peptides: Simple Bio-Inspired Building Blocks for the Fabrication of Functional Materials. *Chem. Soc. Rev.* **2016**, *45* (14), 3935–3953. https://doi.org/10.1039/C5CS00889A.

(56) Rajbhandary, A.; Raymond, D. M.; Nilsson, B. L. Self-Assembly, Hydrogelation, and Nanotube Formation by Cation-Modified Phenylalanine Derivatives. *Langmuir* **2017**, *33* (23), 5803–5813. https://doi.org/10.1021/acs.langmuir.7b00686.

(57) Kralj, S.; Bellotto, O.; Parisi, E.; Garcia, A. M.; Iglesias, D.; Semeraro, S.; Deganutti, C.; D'Andrea, P.; Vargiu, A. V.; Geremia, S.; De Zorzi, R.; Marchesan, S. Heterochirality and Halogenation Control Phe-Phe Hierarchical Assembly. *ACS Nano* **2020**, *14* (12), 16951–16961. https://doi.org/10.1021/acsnano.0c06041.

(58) Scarel, E.; Bellotto, O.; Rozhin, P.; Kralj, S.; Tortora, M.; Vargiu, A. V.; Zorzi, R. D.; Rossi, B.; Marchesan, S. Single-Atom Substitution Enables Supramolecular Diversity from Dipeptide Building Blocks. *Soft Matter* **2022**, *18* (11), 2129–2136. https://doi.org/10.1039/D1SM01824H.

(59) Liyanage, W.; Nilsson, B. L. Substituent Effects on the Self-Assembly/Coassembly and Hydrogelation of Phenylalanine Derivatives. *Langmuir* **2016**, *32* (3), 787–799. https://doi.org/10.1021/acs.langmuir.5b03227.

(60) *Molecular Self-Assembly and Supramolecular Chemistry of Cyclic Peptides | Chemical Reviews*. https://pubs.acs.org/doi/full/10.1021/acs.chemrev.0c01291 (accessed 2024-10-08).

(61) Tomasic, L.; Lorenzi, G. P. Some Cyclic Oligopeptide with S2 Symmetry. *Helv. Chim. Acta* **1987**, *70* (4), 1012–1016. https://doi.org/10.1002/hlca.19870700413.

(62) Ghadiri, M. R.; Granja, J. R.; Milligan, R. A.; McRee, D. E.; Khazanovich, N. Self-Assembling Organic Nanotubes Based on a Cyclic Peptide Architecture. *Nature* **1993**, *366* (6453), 324–327. https://doi.org/10.1038/366324a0.

(63) Hartgerink, J. D.; Granja, J. R.; Milligan, R. A.; Ghadiri, M. R. Self-Assembling Peptide Nanotubes. *J. Am. Chem. Soc.* **1996**, *118* (1), 43–50. https://doi.org/10.1021/ja953070s.

(64) Khazanovich, N.; Granja, J. R.; McRee, D. E.; Milligan, R. A.; Ghadiri, M. R. Nanoscale Tubular Ensembles with Specified Internal Diameters. Design of a Self-Assembled Nanotube with a 13-.ANG. Pore. *J. Am. Chem. Soc.* **1994**, *116* (13), 6011–6012. https://doi.org/10.1021/ja00092a079.

(65) Saviano, M.; Zaccaro, L.; Lombardi, A.; Pedone, C.; Di Blasio, B.; Sun, X.; Lorenzi, G. P. A Structural Two-Ring Version of a Tubular Stack Ofβ-Rings in Crystals of a Cyclic D,L-Hexapeptide. *J. Incl. Phenom. Mol. Recognit. Chem.* **1994**, *18* (1), 27–36. https://doi.org/10.1007/BF00706936.

(66) Sun, X.; Lorenzi, G. P. On the Stacking of β -Rings: The Solution Self-Association Behavior of Two Partially N-Methylated Cyclo(Hexaleucines). *Helv. Chim. Acta* **1994**, *77* (6), 1520–1526. https://doi.org/10.1002/hlca.19940770607.

(67) Clark, T. D.; Buriak, J. M.; Kobayashi, K.; Isler, M. P.; McRee, D. E.; Ghadiri, M. R. Cylindrical β-Sheet Peptide Assemblies. *J. Am. Chem. Soc.* **1998**, *120* (35), 8949–8962. https://doi.org/10.1021/ja981485i.

(68) Silk, M. R.; Newman, J.; Ratcliffe, J. C.; White, J. F.; Caradoc-Davies, T.; Price, J. R.; Perrier, S.; Thompson, P. E.; Chalmers, D. K. Parallel and Antiparallel Cyclic D/L Peptide Nanotubes. *Chem. Commun.* **2017**, *53* (49), 6613–6616. https://doi.org/10.1039/C7CC00846E.

(69) Rosenthal-Aizman, K.; Svensson, G.; Undén, A. Self-Assembling Peptide Nanotubes from Enantiomeric Pairs of Cyclic Peptides with Alternating d and l Amino Acid Residues. *J. Am. Chem. Soc.* **2004**, *126* (11), 3372–3373. https://doi.org/10.1021/ja0372659.

(70) Kobayashi, K.; Granja, J. R.; Ghadiri, M. R. β-Sheet Peptide Architecture: Measuring the Relative Stability of Parallel vs. Antiparallel β-Sheets. *Angew. Chem. Int. Ed. Engl.* **1995**, *34* (1), 95–98. https://doi.org/10.1002/anie.199500951.

(71) Shaikh, H.; Rho, J. Y.; Macdougall, L. J.; Gurnani, P.; Lunn, A. M.; Yang, J.; Huband, S.; Mansfield, E. D. H.; Peltier, R.; Perrier, S. Hydrogel and Organogel Formation by Hierarchical Self-Assembly of Cyclic Peptides Nanotubes. *Chem. – Eur. J.* **2018**, *24* (71), 19066–19074. https://doi.org/10.1002/chem.201804576.

(72) Seebach, D.; Matthews, J. L.; Meden, A.; Wessels, T.; Baerlocher, C.; McCusker, L. B. Cyclo-β-Peptides: Structure and Tubular Stacking of Cyclic Tetramers of 3-Aminobutanoic Acid as Determined from Powder Diffraction Data. *Helv. Chim. Acta* **1997**, *80* (1), 173–182. https://doi.org/10.1002/hlca.19970800116.

(73) Amorín, M.; Castedo, L.; Granja, J. R. New Cyclic Peptide Assemblies with Hydrophobic Cavities: The Structural and Thermodynamic Basis of a New Class of Peptide Nanotubes. *J. Am. Chem. Soc.* **2003**, *125* (10), 2844–2845. https://doi.org/10.1021/ja0296273.

(74) Brea, R. J.; Castedo, L.; Granja, J. R. Large-Diameter Self-Assembled Dimers of α,γ-Cyclic Peptides, with the Nanotubular Solid-State Structure of Cyclo-[(L-Leu-D-MeN-γ-Acp)4-]·4CHCl2COOH. *Chem. Commun.* **2007**, No. 31, 3267–3269. https://doi.org/10.1039/B703659K.

(75) Reiriz, C.; Amorín, M.; García-Fandiño, R.; Castedo, L.; Granja, J. R. α,γ-Cyclic Peptide Ensembles with a Hydroxylated Cavity. *Org. Biomol. Chem.* **2009**, *7* (21), 4358–4361. https://doi.org/10.1039/B911247M.

(76) Rodríguez-Vázquez, N.; García-Fandiño, R.; Amorín, M.; Granja, J. R. Self-Assembling α,γ-Cyclic Peptides That Generate Cavities with Tunable Properties. *Chem. Sci.* **2015**, *7* (1), 183–187. https://doi.org/10.1039/C5SC03187G.

(77) Rovero, P.; Quartara, L.; Fabbri, G. Synthesis of Cyclic Peptides on Solid Support. *Tetrahedron Lett.* **1991**, *32* (23), 2639–2642. https://doi.org/10.1016/S0040-4039(00)78806-X.

(78) Chen, J.; Zhang, B.; Xie, C.; Lu, Y.; Wu, W. Synthesis of a Highly Hydrophobic Cyclic Decapeptide by Solid-Phase Synthesis of Linear Peptide and Cyclization in Solution. *Chin. Chem. Lett.* **2010**, *21* (4), 391–394. https://doi.org/10.1016/j.cclet.2009.11.026.

(79) Rowan, S. J.; Cantrill, S. J.; Cousins, G. R. L.; Sanders, J. K. M.; Stoddart, J. F. Dynamic Covalent Chemistry. *Angew. Chem. Int. Ed.* **2002**, *41* (6), 898–952. https://doi.org/10.1002/1521-3773(20020315)41:6<898::AID-ANIE898>3.0.CO;2-E.

(80) Jin, Y.; Yu, C.; Denman, R. J.; Zhang, W. Recent Advances in Dynamic Covalent Chemistry. *Chem. Soc. Rev.* **2013**, *42* (16), 6634–6654. https://doi.org/10.1039/C3CS60044K.

(81) Belowich, M. E.; Stoddart, J. F. Dynamic Imine Chemistry. *Chem. Soc. Rev.* **2012**, *41* (6), 2003–2024. https://doi.org/10.1039/C2CS15305J.

(82) Benchimol, E.; Nguyen, B.-N. T.; Ronson, T. K.; Nitschke, J. R. Transformation Networks of Metal–Organic Cages Controlled by Chemical Stimuli. *Chem. Soc. Rev.* **2022**, *51* (12), 5101–5135. https://doi.org/10.1039/D0CS00801J.

(83) Jin, Y.; Wang, Q.; Taynton, P.; Zhang, W. Dynamic Covalent Chemistry Approaches Toward Macrocycles, Molecular Cages, and Polymers. *Acc. Chem. Res.* **2014**, *47* (5), 1575–1586. https://doi.org/10.1021/ar500037v.

(84) Orrillo, A. G.; Furlan, R. L. E. Sulfur in Dynamic Covalent Chemistry. *Angew. Chem.* **2022**, *134* (26), e202201168. https://doi.org/10.1002/ange.202201168.

(85) Li, J.; Nowak, P.; Otto, S. Dynamic Combinatorial Libraries: From Exploring Molecular Recognition to Systems Chemistry. *J. Am. Chem. Soc.* **2013**, *135* (25), 9222–9239. https://doi.org/10.1021/ja402586c.

(86) Ashkenasy, G.; Hermans, T. M.; Otto, S.; Taylor, A. F. Systems Chemistry. *Chem. Soc. Rev.* **2017**, *46* (9), 2543–2554. https://doi.org/10.1039/C7CS00117G.

(87) Kaiser, D.; Klose, I.; Oost, R.; Neuhaus, J.; Maulide, N. Bond-Forming and -Breaking Reactions at Sulfur(IV): Sulfoxides, Sulfonium Salts, Sulfur Ylides, and Sulfinate Salts. *Chem. Rev.* **2019**, *119* (14), 8701–8780. https://doi.org/10.1021/acs.chemrev.9b00111.

(88) Field, L. Some Recent Developments in Synthetic Organic Sulfur Chemistry. *Synthesis* **2002**, *1972*, 101–133. https://doi.org/10.1055/s-1972-21838.

(89) Mamathambika, B. S.; Bardwell, J. C. Disulfide-Linked Protein Folding Pathways. *Annu. Rev. Cell Dev. Biol.* **2008**, *24* (Volume 24, 2008), 211–235. https://doi.org/10.1146/annurev.cellbio.24.110707.175333.

(90) Bulaj, G. Formation of Disulfide Bonds in Proteins and Peptides. *Biotechnol. Adv.* **2005**, *23* (1), 87–92. https://doi.org/10.1016/j.biotechadv.2004.09.002.

(91) Zheng, Y.; Zheng, W.; Zhu, D.; Chang, H. Theoretical Modeling of pKa's of Thiol Compounds in Aqueous Solution. *New J. Chem.* **2019**, *43* (13), 5239–5254. https://doi.org/10.1039/C8NJ06259E.

(92) Bagiyan, G. A.; Koroleva, I. K.; Soroka, N. V.; Ufimtsev, A. V. Oxidation of Thiol Compounds by Molecular Oxygen in Aqueous Solutions. *Russ. Chem. Bull.* **2003**, *52* (5), 1135–1141. https://doi.org/10.1023/A:1024761324710.

(93) Mthembu, S. N.; Sharma, A.; Albericio, F.; de la Torre, B. G. Breaking a Couple: Disulfide Reducing Agents. *ChemBioChem* **2020**, *21* (14), 1947–1954. https://doi.org/10.1002/cbic.202000092.

(94) Paranjothy, M.; Siebert, M. R.; Hase, W. L.; Bachrach, S. M. Mechanism of Thiolate-Disulfide Exchange: Addition–Elimination or Effectively SN2? Effect of a Shallow Intermediate in Gas-Phase Direct Dynamics Simulations. *J. Phys. Chem. A* **2012**, *116* (47), 11492–11499. https://doi.org/10.1021/jp307795j.

(95) Putzu, M.; Gräter, F.; Elstner, M.; Kubař, T. On the Mechanism of Spontaneous Thiol–Disulfide Exchange in Proteins. *Phys. Chem. Chem. Phys.* **2018**, *20* (23), 16222–16230. https://doi.org/10.1039/C8CP01325J.

(96) Black, S. P.; Sanders, J. K. M.; Stefankiewicz, A. R. Disulfide Exchange: Exposing Supramolecular Reactivity through Dynamic Covalent Chemistry. *Chem. Soc. Rev.* **2014**, *43* (6), 1861–1872. https://doi.org/10.1039/C3CS60326A.

(97) Otto, S.; Furlan, R. L. E.; Sanders, J. K. M. Selection and Amplification of Hosts From Dynamic Combinatorial Libraries of Macrocyclic Disulfides. *Science* **2002**, *297* (5581), 590–593. https://doi.org/10.1126/science.1072361.

(98) Ponnuswamy, N.; Cougnon, F. B. L.; Clough, J. M.; Pantoş, G. D.; Sanders, J. K. M. Discovery of an Organic Trefoil Knot. *Science* **2012**, *338* (6108), 783–785. https://doi.org/10.1126/science.1227032.

(99) Carnall, J. M. A.; Waudby, C. A.; Belenguer, A. M.; Stuart, M. C. A.; Peyralans, J. J.-P.; Otto, S. Mechanosensitive Self-Replication Driven by Self-Organization. *Science* **2010**, *327* (5972), 1502–1506. https://doi.org/10.1126/science.1182767.

(100) Pappas, C. G.; Mandal, P. K.; Liu, B.; Kauffmann, B.; Miao, X.; Komáromy, D.; Hoffmann, W.; Manz, C.; Chang, R.; Liu, K.; Pagel, K.; Huc, I.; Otto, S. Emergence of Low-Symmetry Foldamers from Single Monomers. *Nat. Chem.* **2020**, *12* (12), 1180–1186. https://doi.org/10.1038/s41557-020-00565-2.

(101) Das, K.; Gabrielli, L.; Prins, L. J. Chemically Fueled Self-Assembly in Biology and Chemistry. *Angew. Chem. Int. Ed.* **2021**, *60* (37), 20120–20143. https://doi.org/10.1002/anie.202100274.

(102) Yang, S.; Schaeffer, G.; Mattia, E.; Markovitch, O.; Liu, K.; Hussain, A. S.; Ottelé, J.; Sood, A.; Otto, S. Chemical Fueling Enables Molecular Complexification of Self-Replicators. *Angew. Chem. Int. Ed.* **2021**, *60* (20), 11344–11349. https://doi.org/10.1002/anie.202016196.

(103) Liu, B.; Wu, J.; Geerts, M.; Markovitch, O.; Pappas, C. G.; Liu, K.; Otto, S. Out-of-Equilibrium Self-Replication Allows Selection for Dynamic Kinetic Stability in a System of Competing Replicators. *Angew. Chem.* **2022**, *134* (18), e202117605. https://doi.org/10.1002/ange.202117605.

(104) Marić, I.; Yang, L.; Li, X.; Santiago, G. M.; Pappas, C. G.; Qiu, X.; Dijksman, J. A.; Mikhailov, K.; van Rijn, P.; Otto, S. Tailorable and Biocompatible Supramolecular-Based Hydrogels Featuring Two Dynamic Covalent Chemistries. *Angew. Chem. Int. Ed.* **2023**, *62* (14), e202216475. https://doi.org/10.1002/anie.202216475.

(105) Mthembu, S. N.; Chakraborty, A.; Schönleber, R.; Albericio, F.; de la Torre, B. G. Solid-Phase Synthesis of C-Terminus Cysteine Peptide Acids. *Org. Process Res. Dev.* **2022**, *26* (12), 3323–3335. https://doi.org/10.1021/acs.oprd.2c00321.

(106) Whitmore, L.; Wallace, B. A. Protein Secondary Structure Analyses from Circular Dichroism Spectroscopy: Methods and Reference Databases. *Biopolymers* **2008**, *89* (5), 392–400. https://doi.org/10.1002/bip.20853.

(107) Kuril, A. K.; Vashi, A.; Subbappa, P. K. A Comprehensive Guide for Secondary Structure and Tertiary Structure Determination in Peptides and Proteins by Circular Dichroism Spectrometer. *J. Pept. Sci. n/a* (n/a), e3648. https://doi.org/10.1002/psc.3648.

(108) Vogel, E. R.; Jackson, W.; Masterson, D. S. Efficient Esterification of Oxidized L-Glutathione and Other Small Peptides. *Molecules* **2015**, *20* (6), 10487–10495. https://doi.org/10.3390/molecules200610487.

(109) Boros, S.; Gáspári, Z.; Batta, G. Chapter One - Accurate NMR Determinations of Proton–Proton Distances. In *Annual Reports on NMR Spectroscopy*; Webb, G. A., Ed.; Academic Press, 2018; Vol. 94, pp 1–39. https://doi.org/10.1016/bs.arnmr.2017.12.002.

(110) Sedaghat Doost, A.; Akbari, M.; Stevens, C. V.; Setiowati, A. D.; Van der Meeren, P. A Review on Nuclear Overhauser Enhancement (NOE) and Rotating-Frame Overhauser Effect (ROE) NMR Techniques in Food Science: Basic Principles and Applications. *Trends Food Sci. Technol.* **2019**, *86*, 16–24. https://doi.org/10.1016/j.tifs.2019.02.001.

(111) Chayen, N. E. Turning Protein Crystallisation from an Art into a Science. *Curr. Opin. Struct. Biol.* **2004**, *14* (5), 577–583. https://doi.org/10.1016/j.sbi.2004.08.002.

(112) Krishna Kumar, D.; W. Steed, J. Supramolecular Gel Phase Crystallization: Orthogonal Self-Assembly under Non-Equilibrium Conditions. *Chem. Soc. Rev.* **2014**, *43* (7), 2080–2088. https://doi.org/10.1039/C3CS60224A.

(113) Amblard, M.; Fehrentz, J.-A.; Martinez, J.; Subra, G. Methods and Protocols of Modern Solid Phase Peptide Synthesis. *Mol. Biotechnol.* **2006**, *33* (3), 239–254. https://doi.org/10.1385/MB:33:3:239.

(114) Chakraborty, A.; Mthembu, S. N.; de la Torre, B. G.; Albericio, F. Ready to Use Cysteine Thiol Protecting Groups in SPPS, A Practical Overview. *Org. Process Res. Dev.* **2024**, *28* (1), 26–45. https://doi.org/10.1021/acs.oprd.3c00425.

(115) Eissler, S.; Kley, M.; Bächle, D.; Loidl, G.; Meier, T.; Samson, D. Substitution Determination of Fmoc-Substituted Resins at Different Wavelengths. *J. Pept. Sci.* **2017**, *23* (10), 757–762. https://doi.org/10.1002/psc.3021.

(116) Sabatino, G.; Chelli, M.; Brandi, A.; Papini, A. M. Analytical Methods for Solid Phase Peptide Synthesis. *Curr. Org. Chem. 8* (4), 291–301. https://doi.org/10.2174/1385272043485954.

(117) Shalaby, A. A.; Mohamed, A. A. Determination of Acid Dissociation Constants of Alizarin Red S, Methyl Orange, Bromothymol Blue and Bromophenol Blue Using a Digital Camera. *RSC Adv.* **2020**, *10* (19), 11311–11316. https://doi.org/10.1039/C9RA10568A.

(118) Monzó, I. S.; Palou, J.; Roca, J.; Valero, R. Kinetics and Mechanism of the Reactions between Chloranil and N-Butylamine in Cyclohexane Solution. *J. Chem. Soc. Perkin Trans. 2* **1988**, No. 12, 1995–1998. https://doi.org/10.1039/P29880001995.

(119) Vázquez, J.; Qushair, G.; Albericio, F. Qualitative Colorimetric Tests for Solid Phase Synthesis. In *Methods in Enzymology*; Combinatorial Chemistry, Part B; Academic Press, 2003; Vol. 369, pp 21–35. https://doi.org/10.1016/S0076-6879(03)69002-6.

(120) Kabsch, W. XDS. *Acta Crystallogr. D Biol. Crystallogr.* **2010**, *66* (2), 125–132. https://doi.org/10.1107/S0907444909047337.

(121) Evans, P. Scaling and Assessment of Data Quality. *Acta Crystallogr. D Biol. Crystallogr.* **2006**, *62* (1), 72–82. https://doi.org/10.1107/S0907444905036693.

(122) Sheldrick, G. M. SHELXT – Integrated Space-Group and Crystal-Structure Determination. *Acta Crystallogr. Sect. Found. Adv.* **2015**, *71* (1), 3–8. https://doi.org/10.1107/S2053273314026370.

(123) Sheldrick, G. M. Crystal Structure Refinement with SHELXL. *Acta Crystallogr. Sect. C Struct. Chem.* **2015**, *71* (1), 3–8. https://doi.org/10.1107/S2053229614024218.

(124) Hübschle, C. B.; Sheldrick, G. M.; Dittrich, B. ShelXle: A Qt Graphical User Interface for SHELXL. *J. Appl. Crystallogr.* **2011**, *44* (6), 1281–1284. https://doi.org/10.1107/S0021889811043202.

(125) Emsley, P.; Cowtan, K. Coot: Model-Building Tools for Molecular Graphics. *Acta Crystallogr. D Biol. Crystallogr.* **2004**, *60* (12), 2126–2132. https://doi.org/10.1107/S0907444904019158.

(126) Spek, A. L. Single-Crystal Structure Validation with the Program PLATON. *J. Appl. Crystallogr.* **2003**, *36* (1), 7–13. https://doi.org/10.1107/S0021889802022112.